An Investigation of the Crystallization of 7-hydroxynaphthalene-1,3-disulphonic acid dipotassium salt monohydrate from Aqueous Sulphuric Acid Solution

A thesis submitted to
The University of Manchester
for the degree of
Doctor of Philosophy
in the Faculty of Technology

by

Christopher John Price, B.Sc. M.Sc.

Department of Chemical Engineering
University of Manchester Institute of Science and Technology

January 1990

To my wife and my daughter

Acknowledgements

I would like to express my thanks to Professor J. Garside and Mr. W. M. L. Wood for their supervision and helpful advice throughout this work. I would also like to thank Professor R. J. Davey and Mr. G. Taylor for their advice and assistance.

I would also set on record my gratitude to my colleagues in the Crystallization Research Group who were first rate companions throughout my studies at UMIST, in particular I would thank Dr. N. S. Tavare and Dr. G. Webster.

I gratefully acknowledge the financial assistance I have received from the Science and Engineering Research Council and Imperial Chemical Industries Plc. during the course of this work.

I would also like to express my thanks to my wife who has encouraged me throughout the writing of this thesis.

Finally I would like to thank my colleagues at Harwell who have spurred on me in the later stages of writing up.

Declaration

The work reported on the solubility of G-acid dipotassium salt monohydrate in sulphuric acid solution supplements earlier work reported in an M.Sc. thesis submitted by the same author to this University in January 1985. In order to describe adequately the work reported in this thesis it has been necessary to restate some of the introductory comments concerning G-acid dipotassium salt monohydrate and the descriptions of some of the experimental procedures employed for solubility measurement.

No other part of the work included in this thesis has been submitted in support of an application for another degree or qualification of this or any other university or other institute of learning.

C. J. Price

About the author

I graduated from York University in 1982 with a B.Sc. degree in Chemistry, after which I worked for Draeger Safety Ltd for almost a year. I entered the Department of Chemical Engineering at UMIST as a postgraduate research student in October 1983. I gained an M.Sc. for a thesis submitted in January 1985 which was entitled, "The Solubility and Phase Characterisation of Hydroxynaphthalene Sulphonic Acids". I continued my research at UMIST undertaking the work reported in this thesis until December 1986. In January 1987 I began work for the Separation Processes Service at Harwell Laboratory, joining a team of scientists and engineers undertaking research in industrial crystallization.

Abstract

G-acid is a typical member of an important class of compounds, the aromatic sulphonic acids, which are widely used as chemical intermediates in the dyestuffs industry. There are comparatively few published investigations of the industrial crystallization of organic acids by salting out and it is probable that the industrial isolation of such compounds by crystallization could be improved if procedures were available to acquire the information necessary to optimise the processes. The principle reason for not addressing these problems has been the difficulty of obtaining the necessary information to perform such optimisations. In this study an attempt has been made to characterise one crystallizing system in order to determine to what extent these objectives could be achieved. The study serves to identify the problems which are likely to be encountered in such systems and suggests solutions where these have been identified.

The solubility of G-acid dipotassium salt monohydrate in aqueous sulphuric acid in the presence of potassium ion has been determined over a range of temperatures, sulphuric acid concentrations and potassium ion concentrations which span the conditions used during the industrial crystallization of this material. A solubility expression has been developed which can be used to predict the solubility of G-acid dipotassium salt monohydrate over the range of conditions investigated:

$$\ln[G-acid^{2-}]_{Eq} = -1.9736\ln[K^{+}]_{Eq} - 1.1873\ln[H_2SO_4]_{Eq} - \frac{5287}{T} + 5.5957$$

The metastable zone width of G-acid dipotassium salt monohydrate in aqueous sulphuric acid solution has been determined for supersaturation generated by cooling and salting out by addition of excess potassium ion, the supersaturation

ratios were 1.44 and 1.04 respectively. An attempt was made to assess interfacial tension between the G-acid dipotassium salt monohydrate crystals and the solution phase.

The kinetics of the crystallization of G-acid dipotassium salt monohydrate from aqueous sulphuric acid solution were measured under conditions similar to those used industrially. The experimental procedures employed were complex and a number of practical obstacles were encountered, many of which were overcome.

The principle difficulties lay in the measurement of crystal size distributions during the crystallization process. The experimental error associated with the measured size distributions was almost as great as the differences between size distributions from which the kinetic expressions were derived.

The growth kinetics derived using a moments based procedure were approximately twice those predicted for the same conditions using the graphical procedure. There was evidence of growth rate size dependency in the early stages of the experiments although the screening procedure required prior to crystal sizing masked growth rate size dependence during the later stages of the experiment.

The moments based procedure substantially underestimated the nucleation rate whereas a graphical procedure based on extrapolation of the cumulative number oversize distribution to zero size yielded more plausible nucleation kinetics.

A simulation procedure was developed and used to compare the kinetics derived from the experimental data with the experimental data. The differences between the experimentally measured values and the ones predicted by the two sets of kinetics reveal the shortcomings of both the experimental data and the kinetics derived from them.

Contents

1 Introduction

G-acid is a typical member of an important class of compounds, the aromatic sulphonic acids, which are widely used as chemical intermediates in the dyestuffs industry. The sulphonic acids may also be considered to share some of the characteristics of a wider group of industrially important compounds, as many organic acids are isolated by crystallization of their metal salts from aqueous solutions.

There are comparatively few published investigations of the industrial crystallization of organic acids by salting out. It is probable that the industrial isolation of such compounds by crystallization could be improved if procedures were available to acquire the information necessary to optimise the process, the most important objectives being to improve product purity and yield and to shorten the crystallization time. A major obstacle to addressing these problems has been the difficulty of obtaining the necessary information to perform such optimisations.

In this study an attempt has been made to characterise one crystallizing system in order to determine to what extent these objectives could be achieved. The study serves to identify the problems which are likely to be encountered in such systems and suggests solutions where these have been identified.

The study is in five main sections:

Section 2 is a literature survey which begins with a review of the published information concerning G-acid. This is followed by discussion of solubility and supersaturation, nucleation, metastability and crystal growth. The final portion of the literature survey deals with experimental procedures for measuring crystallization kinetics.

In Section 3 the solubility of G-acid dipotassium salt monohydrate in aqueous sulphuric acid in the presence of potassium ion is reported. The measurements were made over a range of temperatures, sulphuric acid concentrations and potassium ion concentrations which span the conditions used during the industrial crystallization of this material. A solubility expression was developed to predict the solubility of G-acid dipotassium salt monohydrate over the range of conditions investigated.

In Section 4 the metastable zone width of G-acid dipotassium salt monohydrate in aqueous sulphuric acid solution is reported for supersaturation generated both by cooling and salting out with potassium sulphate.

The measurement of the crystallization kinetics of G-acid dipotassium salt monohydrate is reported in Section 5. A complex experimental procedure was developed and two techniques were employed to extract crystallization kinetics from the experimental data. Both procedures achieved limited success.

In Section 6 a simulation procedure is described. The simulation allowed the derived kinetics to be used to simulate the crystallization of G-acid dipotassium salt monohydrate. This permitted the derived kinetics to be tested against the experimental data.

2 Literature Review

2.1 Industrial manufacture of G-acid dipotassium salt monohydrate.

In the second half of the nineteenth century it was discovered that several substituted naphthalene compounds would couple with diazotized bases to form useful synthetic dyestuffs. Amino-G-acid is one such compound which has probably been manufactured commercially as a dyestuffs intermediate for about 100 years. The synthesis proceeds by amination of G-acid. An alternative route to the synthesis of amino-G-acid involves sulphonation of 2-naphthylamine which is highly carcinogenic.

Most of the 2-hydroxynaphthalene sulphonic acids may be obtained by direct sulphonation of 2-hydroxynaphthalene with sulphuric acid or oleum. The extent of the sulphonation and isomer ratio are influenced by the temperature and duration of the sulphonation and the concentration of sulphuric acid employed. General reaction schemes similar to that in Figure 2.1 have been described by various authors, eg. Bucherer (1914), Thorpe (1922) and Forster and Keyworth (1927). These reaction schemes were formulated from the research studies of chemists working in the latter half of the 19th century and the early part of this century. For a more detailed discussion of this topic see Price (1985).

Forster and Keyworth (1927) attribute Baum with the discovery that sulphonation of 2-hydroxynaphthalene at elevated temperatures with concentrated sulphuric acid yields a mixture of two disulphonic acids. Baum found that after coupling the reaction mass with diazo compounds it was possible to separate two different dyestuffs, one yellow (termed *Gelb*) and the other red (termed *Rot*); hence the trivial names G-acid and R-acid.

G-acid may be produced together with R-acid and Schaeffer's acid over a wide range of reaction conditions. Disulphonic acid formation is favoured by molar ratios of sulphuric acid to 2-hydroxynaphthalene greater than two (Forster and Keyworth 1927). Sulphonation at higher temperatures with more concentrated sulphuric acid

Fig. 2.1 SULPHONATION OF 2-HYDROXYNAPHTHALENE

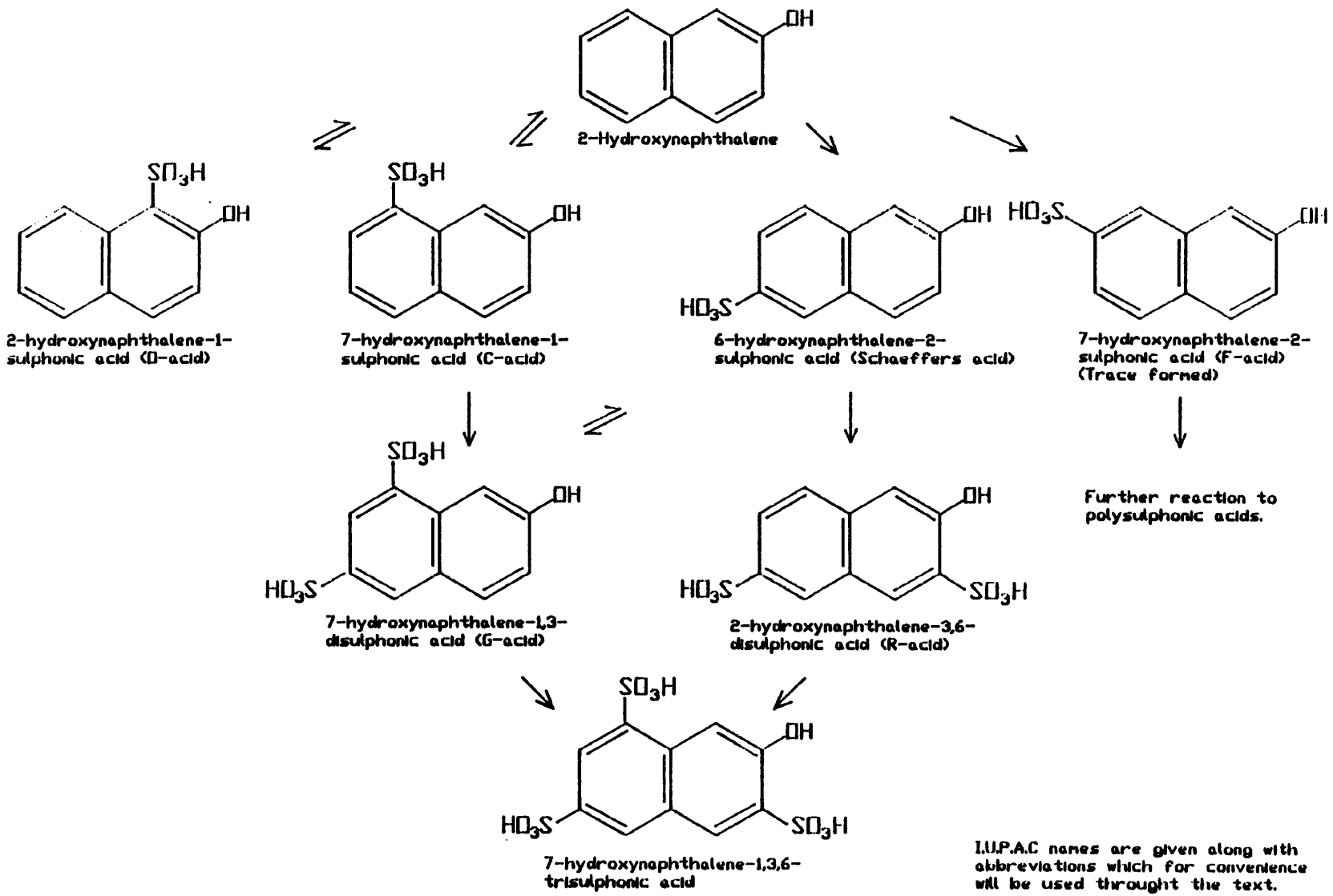

I.U.P.A.C names are given along with abbreviations which for convenience will be used throught the text.

favours R-acid production as the -SO_3 group occupying the 1-position in G-acid is prone to hydrolysis (Donaldson 1958). With continued sulphonation the Schaeffer's acid resulting from this hydrolysis is further sulphonated to a mixture of G-and R-acids, the concentration of R-acid increasing overall, though the yield of G-acid may not be reduced below 20 to 25% in this way (Vorontzov 1951). Lower temperatures coupled with lower sulphuric acid concentrations result in an increase in the proportion of Schaeffer's acid produced. The yield of G- acid may be maximised by optimising the reaction conditions, in particular the ratio of sulphuric acid to 2-hydroxynaphthalene, the sulphuric acid concentration and the sulphonation temperature - time profile. Halting the reaction before equilibrium is reached permits a higher yield of G-acid to be obtained, since its decomposition is slower than the rate of formation. Efforts to improve the manufacturing process have been concentrated mainly in this area. Information relating to such investigations is commercially valuable and is therefore not usually available in the open literature.

The following extract is from a report published shortly after the Second World War (F.I.A.T. 1947). It concerns a process operated by I. G. Farbenindustrie at Leverkusen, Germany:

"1,000kg of 98% sulphuric acid is cooled to 15-17°C and 1,000kg of flaked 2-hydroxynaphthalene is added over 25 to 30 minutes with cooling. The temperature is allowed to rise to 35 to 40°C over 20 minutes when addition of 1,700kg of 20% oleum over 6 to 7 hours is commenced. The temperature is kept below 50°C whilst the first 1,400kg of oleum is added and then allowed to rise to 60°C and is held there for 10 hours, this is followed by 15 hours at 80°C. The sulphonation mass is blown into 6,000 litres of water or wash liquor, the mixture is heated to between 80 and 85°C then 1,000kg of potassium chloride is added. The batch is then allowed to cool for 24 hours with agitation. The potassium salt of G-acid is filtered at 35°C and washed with water at 35 to 40°C until free from R- acid as determined by titration with iodine. The product contains approximately 0.3% R-acid. R-acid is separated from the filtrate by mixing with 6,000 litres of sodium chloride solution. This mixture is heated to 55 to 60°C and allowed to cool over 24 hours to 30°C with agitation. The sodium salt of R-acid is filtered off and sucked dry. The yield is 13% (of R-acid) based on the 2-hydroxynaphthalene starting material; it contains 2 to 3% Schaeffer's acid."

This reference is no more than a brief outline of an industrial process and includes only passing reference to the separation of the crystalline potassium salt of G-acid. The separation of the other compounds from the reaction mixture may be achieved in a number of ways. Griess (1880) and Forster and Keyworth (1927) report that

G-acid and R-acid separation may be based upon the different solubilities of the barium, sodium or potassium salts. Solubility data from the literature are shown in Table 2.1.

From the information in Table 2.1 it appears that isolation of G-acid from the reaction mixture is best performed by crystallization of the potassium salt, as the potassium salts of R- and Schaeffer's acids are likely to remain in solution. Price (1985) has reported the solubility of G-acid dipotassium salt monohydrate, R-acid mono-sodium salt dihydrate and Schaeffer's acid mono-sodium salt dihydrate in aqueous sulphuric acid solutions over the temperature range 20 to 80°C.

Table 2.1 Solubilities of G-, R-, and Schaeffer's acids and their salts.

Compound	Salt	Hydration State	Temperature °C	Solubility g/100gsoln	Reference
G-acid	K^+	Anhydrous	25	7.4	Lange (1979)
G-acid	K^+	Anhydrous	Boiling	28.5	Thorpe (1922)
G-acid	Na^+	Anhydrous	20	25.5	Lange (1979)
G-acid	Free acid	Unspecified	Unspecified	12.7	Thorpe (1922)
R-acid	K^+	Anhydrous	25	22.8	Lange (1979)
R-acid	Na^+	Anhydrous	25	20.1	Lange (1979)
R-acid	Ba^{2+}	Hexahydrate	Boiling	7.7	Donaldson (1958)
R-acid	Free acid	Unspecified	Unspecified	2.7	Thorpe (1922)
S-acid	Na^+	Unspecified	11.5	1.43	(Forster and
S-acid	Na^+	Unspecified	14	1.7	Keyworth (1927)
S-acid	Na^+	Unspecified	80	23.1	Garner (1936)
S-acid	K^+	Unspecified	15	2.0	Thorpe (1922)
S-acid	Ba^{2+}	Anhydrous	20	1.7	Ephraim and Pfister (1925)
S-acid	Free acid	Unspecified	Unspecified	Very Soluble	Garner (1936)

Note; S-acid = Schaeffer's Acid.

An alternative method of separation of the purified G-acid involves coupling reactions with diazo compounds, since R-acid and Schaeffer's acid couple more rapidly than

G-acid. Smith (1906) explained this finding in terms of steric hindrance. The dyes produced by coupling may be recovered from solution by salting out of the sodium salts to leave the purified G-acid solution (Forster and Keyworth, 1927).

The literature contains few references to the crystallization of G-acid or its salts. Garner (1936) describes the free acid crystallizing as dendrites or rods and the sodium salt as needles. Whitmore and Gebhart (1938) describe crystals of the sodium salt as long rectangular plates.

2.2 Solubility and Supersaturation.

Bohm (1985) credits Lowitz with drawing together much of the early work on crystallization in "Crell's Chemical Annals" published in 1795. In this work Lowitz reaffirmed the requirement of supersaturation for crystal growth to take place, this having only been implied by some earlier researchers. He then described many features of supersaturated solutions. He reported that supersaturation may be achieved by evaporation or super-cooling and that the level of supersaturation attainable is dependent upon the solute and the pre-treatment of the solution.

A saturated solution is one in which the solute is in equilibrium with undissolved solute material. Equilibrium may be attained either from under-saturation by dissolution of additional solute or from supersaturation by deposition of excess solute on the solute crystals.

A supersaturated solution is one in which the solute concentration exceeds the equilibrium concentration under the same conditions. Supersaturation is a vital parameter in the crystallization process since it provides the driving force for both crystal growth and nucleation. Solubility and supersaturation may both be expressed in a number of ways (Mullin, 1972). Examples include; mass of solute per unit mass of solution, solvent, or free solvent in the case of a solvated material. Additionally supersaturation may be expressed as a ratio with respect to the saturation concentration or as an undercooling below the saturation temperature. It is clearly important that the form of expression used is unambiguous. Some forms of expression have greater physical significance to the crystallization process than others. This is discussed in detail by Söhnel and Mullin (1978).

In general the solubility of a material is found to depend on a number of parameters. Solvent, temperature and impurity concentration are often of major importance. The solubility of an ionised or partially ionised solute may be reduced by addition of a material with an ion in common with the solute. This effect is referred to as the common ion effect and precipitation or crystallization resulting from the addition of a common ion is termed salting out. An alternative technique to reduce the solubility of a material is the addition of a co-solvent which renders the solute less soluble. This is termed drowning out. Both techniques are frequently employed to generate supersaturation in crystallizing systems, (eg. F.I.A.T., 1947; Jones et al., 1987).

The common ion effect may be expressed in a solubility product. For a sparingly soluble salt, M_nX_m in aqueous solution, the solubility product, K_{sp} is described by the Nernst equation:

$$M_nX_{m(s)} \Leftrightarrow nM^{m+}_{(aq)} + mX^{n-}_{(aq)} \qquad 2.1$$

$$K_{sp} = [M^{m+}]^n.[X^{n-}]^m \qquad 2.2$$

$[M^{m+}]$ and $[X^{n-}]$ are the equilibrium concentrations of the two ionic species. At a given temperature K_{sp} remains constant irrespective of solution composition. Thus if M^{m+} ions are added to the system above X^{n-} ions must leave the solution as crystalline M_nX_m salt in-order to re-establish equilibrium. Strictly the activities of the two species should be employed rather than their concentrations, though the use of concentrations is a widely accepted approximation for sparingly soluble salts. At high concentrations there may be deviations from ideality and as a consequence the relationship no longer holds. There is however evidence to suggest that this approach may be extended beyond the limits of sparingly soluble salts, eg. Davey and Richards (1986).

2.2.1 Techniques used to Measure Solubility and Supersaturation.

In order to measure solubility it is necessary to prepare a saturated solution and perform an accurate determination of the solute concentration. The level of supersaturation may be determined using the same analysis technique used for the

solubility measurement. A knowledge of the solubility under the same experimental conditions is also required. The measured supersaturation is often very sensitive to inaccuracies in concentration measurement because the supersaturation is usually small compared with the solubility.

2.2.1.1 Preparation of saturated solutions. Mullin (1972) describes the basic method employed by many researchers, eg Chianese et al. (1986a), to prepare saturated solutions. The technique involves agitation of excess solute material with the solvent in a closed vessel at a constant temperature. Samples of particle free solution are removed at suitable time intervals and the solution concentration is determined. Saturation is presumed to have been achieved when successive concentration determinations show no variations outside the accuracy of the concentration analysis technique.

2.2.1.2 Concentration analysis techniques applicable to the G-acid system. Several commonly used concentration measurement techniques are not applicable to the system under investigation because of the number and nature of the solution components. In addition to G-acid the solutions contain sulphuric acid, potassium sulphate and a range of sulphonic acid impurities. The situation is further complicated by variations in the relative concentrations of these components. Techniques based on measurement of physical properties of the solution such as density, conductivity and refractive index are not applicable because variation of the concentration of the other components may influence the measured parameter. Evaporation to dryness is unlikely to produce accurate results as evaporation of a solution containing sulphuric acid is likely to be incomplete, and all non-volatile components present would be assayed as G-acid.

2.2.1.3 Chemical analysis techniques. There are several qualitative analysis techniques reported in the literature which permit identification of G-acid and a range of similar sulphonic acids based on their relative rates of coupling with compounds such as diazotised amines. For example Forster and Keyworth (1924a, 1924b) describe a procedure to identify naphthalene sulphonic acids as their arylamine salts. Forrester and Bain (1930a, 1930b) and Smith-Harland et al. (1931) described a bromopotentiometric analysis technique which enables G- acid, R-acid

and Schaeffer's acid to be determined quantitatively in a mixture containing other interfering impurities. Accuracies as high as ±1% are claimed for the technique which demands a high degree of experimental accuracy and is rather time consuming. Care has to be taken to ensure complete monobromination of the un-reactive G-acid at elevated temperatures.

Traditionally in the dyestuffs industry a titration technique has been employed to quantify G-acid and its associated sulphonic acids. This technique is described by Fierz-David and Blangey (1949) who performed a series of three titrations in order to determine the concentration of a mixture of G-, R- and Schaeffer's acids. In the first titration a highly reactive coupling reagent, diazotised p-nitroaniline, is used, which couples with all three acids. A second titration is performed with a less reactive coupling reagent, diazotised p-toluidine, in order to determine the combined concentration of R- and Schaeffer's acids. Reaction with formaldehyde to eliminate Schaeffer's acid followed by titration with diazotised p-toluidine permits R-acid to be assayed in isolation. The sample composition is then calculated from these measurements.

Lee and Yeh (1983) compared the accuracy of this method with an HPLC technique. They report that the chemical technique was inacurate, especially when it was used to determine a low concentration of one of the materials in the presence of a high concentration of one of the others. In some cases the error exceeded 200%. They suggest that these inaccuracies stem from several factors, chiefly the instability of the diazotised coupling reagents when exposed to light, the influence of pH on the reactions and the ambiguity of the end point.

2.2.1.4 Spectrophotometric techniques. During the course of attempts to correlate uv absorption spectra with molecular structure Daglish (1950) determined absorption coefficients for a range of substances including G-acid, R-acid and Schaeffer's acid. The absorption maxima were located at wavelengths of 237, 237 and 233nm respectively. Koepernik and Borsdorf (1984) reported similar values for absorption coefficients and wavelengths of maximum absorption. Christen and Zollinger (1962) employed a spectrophotometric technique to follow the bromination of G-acid. Price (1985) investigated the use of a spectrophotometric technique for

the present system measuring the molar absorption coefficients and wavelengths of maximum absorption for each of the sulphonic acids known to be present. These results showed good agreement with the available literature values. However the overlapping wavelengths of the absorption maxima reported in these studies impose significant limitations on the use of spectrophotometry for the G-acid system. Price (1985) reported that if the composition of a batch of material containing predominantly G-acid was determined by another technique and was known to be constant then spectrophotometry could be employed to determine the concentration of a solution by using small correction factors to account for the absorption of impurities.

2.2.1.5 High performance liquid chromatography. A number of HPLC analysis methods have been developed for the quantitative determination of sulphonic acids. Separation is usually achieved using reversed phase ion pairing techniques. The detection technique usually employed is uv absorption. Key research in this field includes the work of Kraak and Huber (1974), Knox and Laird (1976), Rossinelli et al (1979), Prandi and Venturini (1981) and Lee and Yeh (1983). For further discussion of their individual contributions see Price (1985).

The work of Lee and Yeh (1983) is especially relevant to the present investigation. They developed an HPLC method which gave good separation of G-acid, R-acid and Schaeffer's acid and a linear response to concentration over a wide range of compositions. Their reversed phase ion pairing technique is similar to that employed by ICI Organics Division for routine analysis of G-acid and is the method employed in this study. Using a more sophisticated technique with amino G-acid as an internal standard Lee and Yeh report accuracies of ±2% in the determination of G-acid. They report lower accuracies of around ±5% for trace impurity concentration measurement.

HPLC appears to be the most suitable technique for determination of the impurity composition of a G-acid sample. However this is time consuming, especially for the routine analysis of large numbers of samples. As discussed in the previous section dealing with spectrophotometry once the impurity distribution of a particular batch

of material is known a spectrophotometric technique may be employed. This offers advantages in both time and cost of analysis with little reduction in accuracy compared with the HPLC technique.

2.2.1.6 Atomic absorption. In addition to accurate measurement of G-acid concentration it has been necessary to determine the potassium ion concentration in order to investigate the salting-out of G-acid dipotassium salt monohydrate. Atomic absorption was considered a suitable technique. Detailed descriptions of the procedures involved are given in most texts dealing with instrumental analytical chemistry, eg. Willard et al. (1981). The technique was employed by Price (1985) for phase characterisation and by Davey and Richards (1986) in metastable zone width measurements.

2.3 Nucleation.

The two most important processes in crystallization are nucleation and crystal growth. Nucleation is the process by which new crystals are formed. Mullin (1972) draws a distinction between nuclei formed in the presence and in the absence of crystals of the nucleating phase; the former is termed secondary nucleation and the latter primary nucleation. Primary nucleation is further subdivided into homogeneous and heterogeneous nucleation. Heterogeneous nucleation involves the participation of material other than the nucleating phase in the nucleation process. The foreign material may take the form of small particulate matter (often termed hetero nuclei) present even in carefully filtered solutions. Alternatively other materials in contact with the solution, for example the vessel walls, may be involved in primary heterogeneous nucleation. As a consequence of the difficulties encountered in preparation and storage of an entirely particle free solution true primary homogeneous nucleation only occurs in highly contrived situations. Very small volumes of highly purified solutions dispersed as droplets (Wojciechowski and Kibalczyc, 1986) probably make the closest approach to true primary homogeneous nucleation. In most situations the dominant form of nucleation is either primary heterogeneous or secondary (Hulbert, 1983). Mullin (1972) suggests that the likelihood of primary heterogeneous nucleation occurring is reduced in many circumstances because of

the presence of small particles of the nucleating phase in the work area. The presence of such "dust" particles is inevitable in many locations, especially in industrial plant. Clearly in a seeded system the nucleation process is secondary.

2.3.1 Primary Nucleation

The principal requirement for the occurrence of nucleation is supersaturation. In the case of secondary nucleation any level of supersaturation is adequate although the rate of nucleation increases with increasing supersaturation. In the case of primary nucleation there is a minimum supersaturation level below which the nucleation rate is so slow as to be imperceptible; above this minimum the nucleation rate increases very rapidly with increasing supersaturation. This leads to a phenomenon referred to as metastability which (according to Bohm, 1985) was first reported by Lowitz (1795). This is illustrated in Figure 2.2. A metastable solution is one which is supersaturated and yet in which no nucleation appears to occur. As the level of supersaturation is increased a value is reached at which nucleation appears to be instantaneous. Unlike the solubility curve the limit of the metastable zone is not well defined, there being no absolute limiting supersaturation level but rather a continuum (Söhnel, 1983). The "edge" of the metastable zone is found to depend on a number of factors including; rate of supersaturation generation, agitation, impurity concentration and solution history; (eg. Mullin and Gaska, 1969; Janse and de Jong, 1978). The level of supersaturation at which nucleation occurs may be expressed in absolute terms or as a ratio with respect to the saturation concentration. Alternatively it may be expressed as an undercooling if supersaturation is generated by cooling a saturated solution (Nyvlt, 1972).

The early development of classical nucleation theory has been reviewed by La Mer (1952). It is accepted that the formation of nuclei in pure particle-free solution (primary homogeneous nucleation) requires individual growth units (atoms, molecules or ions) to congregate together forming ordered or semi-ordered clusters. (eg. Larson and Garside, 1986). Initially as these clusters increase in size (number of growth units) their Gibbs' free energy increases, see Figure 2.3. The energy

Figure 2.2 An illustration of the concept of metastability. (After Söhnel, 1983).

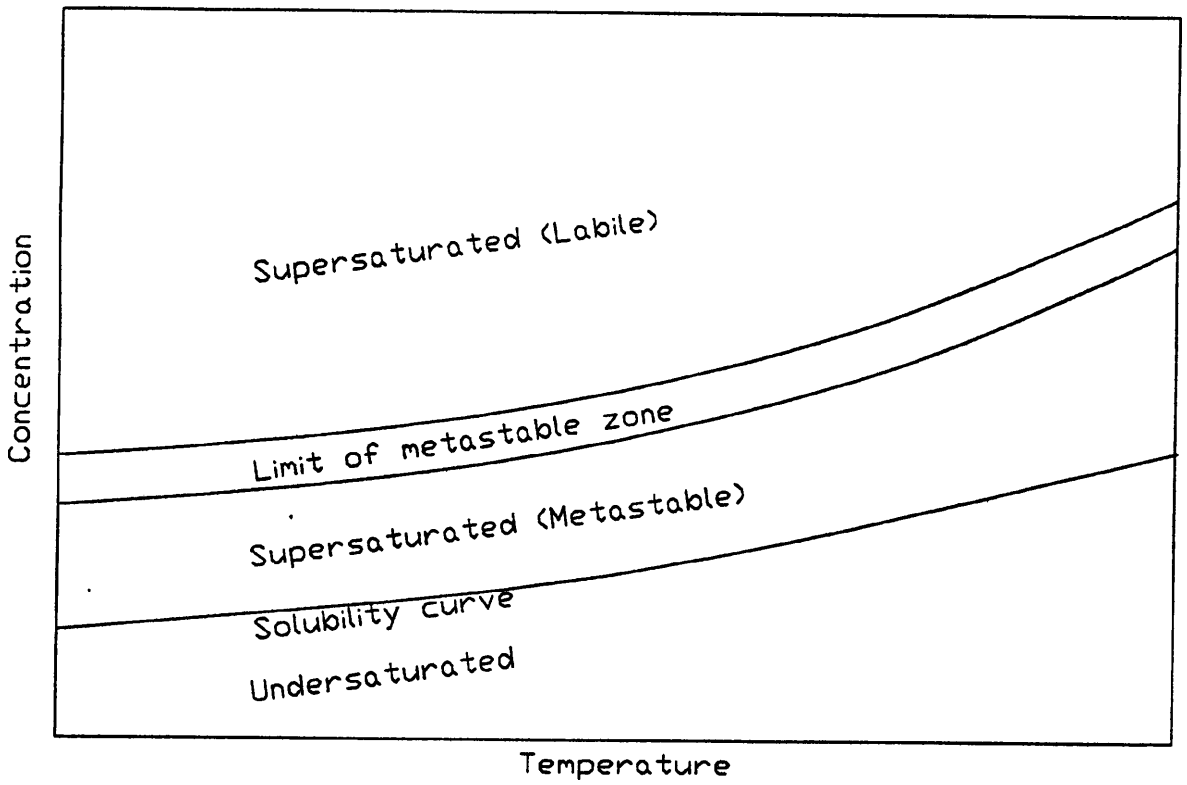

requirement to form the cluster surface (interfacial tension, σ) increases with the cluster surface area but this is offset by a decrease in free energy associated with the formation of the new phase which is proportional to cluster volume.

The maximum in Gibbs' free energy, ΔG^*, indicated in Figure 2.3 occurs at a particular cluster radius, the critical size r_c. Once this size has been exceeded it is energetically favourable for the cluster to grow and a nucleus is formed. Walton (1969) demonstrated that the critical cluster size is inversely proportional to the logarithm of the supersaturation.

$$r_c = \frac{4\sigma\Omega}{RT \ln S} \qquad 2.3$$

Much of the development of classical nucleation theory was based on liquid droplet formation from the vapour where the interfacial tension is the surface tension of the droplet. Application of the theory to the nucleation of crystals requires a conceptually similar interfacial tension between the crystal nucleus and the surrounding supersaturated solution. The boundary of the cluster is not so readily defined as in

Figure 2.3 The Free Energy of Formation of a Critical Cluster (After Larson and Garside, 1986).

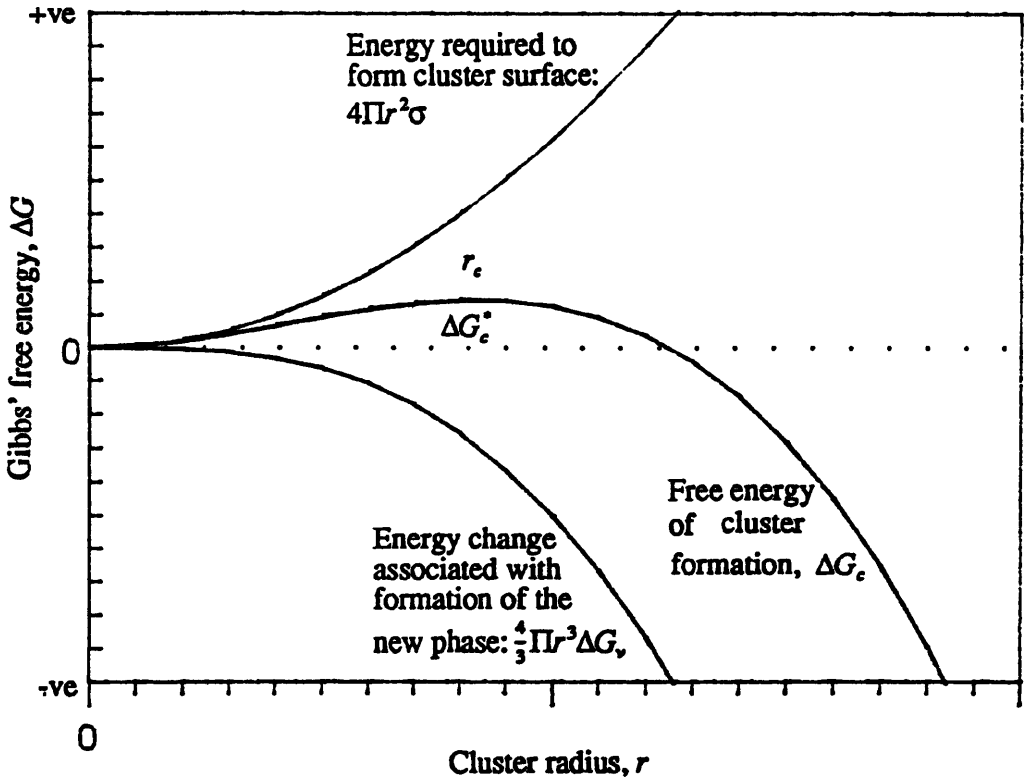

the case of a droplet and the physical significance of the term is open to question (Nyvlt, 1972; Mullin, 1972). The role of a foreign surface in reducing the metastable zone width may be considered in terms of a reduction of the energy required to form a critical sized nucleus. Nielsen (1964) incorporated a term in the classical nucleation equation to account for the effect of a foreign surface. Its value lay between 1 (no effect on metastability) and 0 (effect identical to a crystal of the nucleating phase). A more mathematical treatment of nucleation theory is given in Section 4.2.

2.3.1.1 Determination of metastable zone width. Amongst the approaches adopted by the many researchers who have investigated primary nucleation there appear to be two that are preferred. In the first supersaturation is generated at a constant rate until nucleation is detected. This permits measurement of the maximum supersaturation attainable at various rates of supersaturation generation. A logarithmic plot of the measured (critical) supersaturation against the rate of supersaturation generation yields a straight line, the slope of which Nyvlt (1968) interpreted as the order of the nucleation process. Nyvlt's initial interpretation took no account of the growth period required for the nuclei to attain detectable size. Several attempts have been made subsequently to refine this approach by taking the

growth period into account, eg. Söhnel and Nyvlt (1975). In spite of these refinements Janse and de Jong (1978) take the view that attempts to evaluate nucleation kinetics using this approach should be treated with great caution.

The second approach to the determination of metastable zone width involves measuring induction time, (occasionally referred to as waiting time), at various constant levels of supersaturation. This approach permits estimation of the interfacial tension of the crystal nucleus, although the physical significance of this parameter is uncertain (Nyvlt, 1972). In most of the metastable zone width determinations reported in the literature, supersaturation was generated by cooling, although there are a few references to supersaturation generation by salting out eg. Davey and Richards (1986).

2.3.1.2 Experimental Techniques. The determination of metastable zone widths and induction periods requires techniques to generate and measure supersaturation and to detect nucleation. In the case of supersaturation generated by cooling an accurate knowledge of the dependence of the solubility on temperature and accurate temperature measurement are required. In the case of supersaturation generated by salting out a knowledge of the variation of solubility with change in common ion concentration is required. This usually necessitates measurement of the equilibrium concentration of both the solute and the common ion over the whole of the required experimental range. This is particularly important for solutes with relatively high solubilities where the behaviour of the system may deviate significantly from that implied by the Nernst equation unless solute activities are known.

A range of techniques has been employed for detection of nucleation. Examples include visual detection, optical methods based on light scattering or turbidity measurement, conductivity and selective ion metering. Prostakov et al. (1982) examined the detection limit for several techniques and reported that optical techniques are generally the most sensitive. Mullin and Jancic (1979) compared the limits for detection by eye and electrical zone sensing. Wojociechowski and Kibalczyc (1986) successfully employed a laser light scattering technique. For each technique there

is a minimum size below which the nuclei cannot be detected. It is necessary to calculate the time required for a nucleus to reach this in order to evaluate the induction time accurately.

The methods employed by Davey and Richards (1986) are similar to those used in the current metastable zone width measurements. They precipitated the sodium salt of a reactive dye by salting out. However unlike the present study the common ion took several hours to dissolve. Both dissolution and crystal growth were monitored using a Coulter Counter periodically to obtain crystal size distributions.

2.3.1.3 Metastable zone width measurements. As discussed above the two approaches to the determination of metastable zone width and the subsequent use of the data may be subject to significant errors. Metastable zone width measurements are clearly valuable in indicating the level of supersaturation a system can attain before primary nucleation occurs and as such gives a useful indication of the supersaturation needed in the operation of an unseeded crystallizer. The measurements also indicate the maximum supersaturation which could be tolerated in a seeded crystallizer, although in practice this maximum value would often result in excessive secondary nucleation. The usefulness of metastable zone width and induction time data to determine other parameters is more doubtful. Nucleation orders obtained in this way may be misleadingly high (Janse and de Jong, 1978) and the concept of interfacial tension in solution crystallization is of doubtful physical significance (Nyvlt, 1972).

2.3.2 Secondary Nucleation.

Botsaris (1976) defines secondary nucleation as; "that nucleation which occurs irrespective of the mechanism, only because of the presence of crystals of the nucleating phase. If these crystals were absent no nucleation would occur." The process of secondary nucleation permits the formation of nuclei at much lower supersaturations than either of the primary mechanisms discussed earlier. Mason and Strictland-Constable (1966) identify three main sources of secondary nuclei:

i) Spurious "dusting" from the surface of dry seed crystals, sometimes called apparent nucleation. Often this is important in seeded batch crystallizers.

ii) The breaking off of dendritic growths which form on crystal surfaces exposed to high levels of supersaturation.

iii) Micro-attrition (often referred to as contact nucleation or collision breeding) arising from crystal collisions, for example in a magma suspension.

The last of these mechanisms is the most widely investigated and according to Hulburt (1983) and Garside (1985) it is the dominant form of nucleation where crystallization takes place in a stirred suspension.

Several experimental approaches have been used to investigate contact nucleation. Lal et al. (1969) investigated the nucleation resulting from sliding a crystal along a surface. Colntz and McCabe (1971) investigated crystal - crystal impacts in a moving stream directing nuclei downstream of the contact. Rusli et al (1980) demonstrated the importance of attrition in secondary nucleation in a stirred tank crystallizer. Garside and Larson (1978) and Garside et al. (1979) reported the effect of striking crystals in supersaturated solution and observed nuclei generated at different sizes. They also noted the importance of imperfections such as solvent inclusions in the crystal structure in determining the size and number of crystal fragments and nuclei produced. Botsaris et al. (1974) demonstrated that at supersaturations close to the metastable limit striking a glass "dummy" crystal resulted in the production of nuclei which according to his definition quoted earlier (Botsaris, 1976) was considered primary nucleation.

The effect of fluid shear rather than actual impact has been investigated by a number of researchers including Jagganathan et al. (1980) who have demonstrated that nucleation can occur without contact taking place. The actual mechanism by which this occurs is unclear, although Hulburt (1983) suggests two alternative mechanisms. Either the fluid shear removes fragments from the crystal surface or alternatively the supersaturation level adjacent to the crystal is increased, dendritic growth occurs and some of those dendrites break off.

Another mechanism of secondary nucleation has been proposed (Strictland-Constable, 1979) in which "mosaic" fragments are released from the crystal surface. This is as a result of stresses built up during collisions in which the crystal undergoes

plastic deformation. Evans et al. (1974) suggest that in such an instance the Young's modulus of the crystal may be an important factor in the cleavage of these mosaic fragments from the crystal surface. Denk and Botsaris (1972) employed the optical isomerism of sodium chlorate to distinguish between nuclei formed from seed crystals of a specific enantiomer and the bulk solution where an equal mixture of the two enantiometic froms would be anticipated. They reported that under a wide range of conditions nuclei were formed from the existing crystals rather than the bulk solution. Several researchers, Shah et al. (1973) and Ness and White (1976), have investigated the effect on nucleation rate of using soft coatings on the crystallizer and impeller surfaces. All report substantial reductions in the nucleation rate indicating the importance of the impact energy in determining the number of nuclei generated in crystal - crystallizer collisions.

2.3.3 Empirical kinetic equation.

It has been demonstrated that there are several mechanisms by which secondary nucleation may occur and that their individual importance may vary in different circumstances. Further investigation of the phenomenon is required to produce a unified mathematical approach. Currently in the absence of such a mathematical description of the nucleation process authors seeking to investigate overall nucleation kinetics must employ empirical relationships. According to Garside (1985) such relationships take the general form:

$$B = K_b \Delta C^b M_T^j N^m \exp\frac{-E_b}{RT} \qquad 2.4$$

where B is the nucleation rate, K_b is a constant, ΔC is a measure of the supersaturation level, and M_T is the magma density or solids loading. N is a measure of the system hydrodynamics, (stirrer speed or specific power input are often employed). E_b is a measure of the activation energy for nucleation, R is the universal gas constant and T is the absolute temperature.

2.4 Crystal Growth.

Following nucleation, the other process necessary to achieve crystallization is the growth of the nucleus.

2.4.1 Growth mechanism.

The development of classical crystal growth theory began with the work of Noyes and Whitney (1897) who proposed that the rate of crystal growth was limited by the rate of diffusion through the fluid surrounding the crystal. This assumes that crystallization is the reverse of dissolution. The rate of diffusion is often found to be significantly greater than the growth rate when the two are measured under comparable conditions. This realization that diffusional processes alone could not account for the observed crystallization kinetics lead to the work of Volmer (1939) and his successors. Basing his theory on the thermodynamic reasoning that a growth unit adjacent to the growing crystal has one less degree of freedom than a similar unit in the bulk of the solution Volmer postulated the existence of a layer of adsorbed growth units on the crystal surface. He suggested that growth units from this adsorbed layer would begin to link into the crystal lattice, starting at an "active centre". This process would spread outwards until a complete growth layer had been established. Thus the formation of an active site was similar to primary nucleation occurring on a two-dimensional surface. Kossel (1934) developed a similar theory by considering the relative binding energies of a growth unit at different locations on the crystal surface. He proposed that most growth occurred by growth units moving across the crystal surface until they arrived at a kink site on a step growing across the crystal surface where they are incorporated in to the crystal lattice. This mechanism is often referred to as the birth and spread model (see Figure 2.4).

The theories of Volmer and Kossel both require new crystal nuclei to form on a smooth crystal surface for the growth of each successive layer. This would lead to discontinuities in growth especially at low supersaturation where the probability of surface nucleation is relatively low. Experimental evidence that many crystals do grow even at low supersaturation levels indicates that this theory based on the formation of perfect crystals is incomplete.

Figure 2.4 The Presence of a Kink in a Step on a Crystal Surface (after Burton et al. 1951).

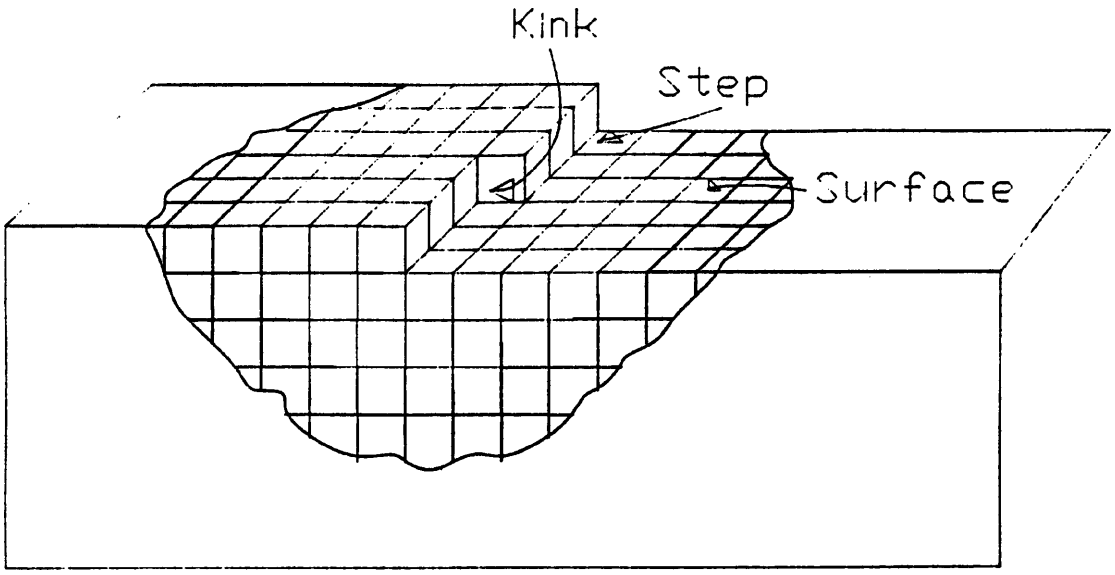

2.4.1.1 The role of the crystal surface and imperfections. Frank (1949) was the first to highlight the important role that imperfections in the crystal structure have in the process of crystal growth. Most crystals contain significant numbers of imperfections, indeed considerable difficulty is encountered in growing near perfect crystals (McArdle and Sherwood, 1986). Screw dislocations are particularly important in the context of crystal growth because they enable a crystal to grow continuously without the need for surface nucleation (see Figure 2.5).

Figure 2.5 Development of a growth spiral from a single screw dislocation (after Mullin 1972).

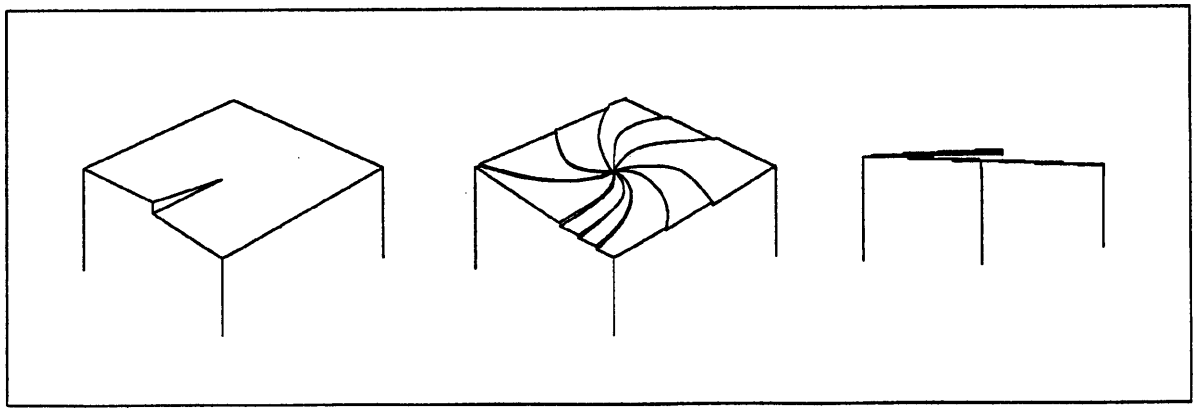

Burton Cabrera and Frank (1951) were the first to produce a mathematical description of how growth may arise from a screw dislocation. The significance of dislocations in the crystal growth process has been demonstrated by a number of authors, such as Hampton et al (1974) who attempted to relate the dislocation structures revealed by X-ray topography to face growth rates.

Further examination of the role of the crystal surface in the growth process has resulted in two limiting conditions being identified. In the first the crystal surface is rough on a molecular scale and there are sufficiently many kink sites that all growth units arriving at the crystal surface can be rapidly incorporated in to the lattice. The second condition arises when the crystal surface is smooth and growth may only take place at kink sites on steps resulting from dislocations. Between these two limiting conditions there is a region where surface nucleation is possible and growth may proceed by the birth and spread mechanism unaided by the intervention of screw dislocations. Jackson (1958) introduced a term to characterise the roughness of the crystal surface which he called the surface entropy factor. As the magnitude of this factor increases the surface becomes smoother. Various authors, such as van der Erden et al. (1978), have developed this approach further using computer simulations to predict the effect of a range of parameters, in particular temperature and solubility, on the surface roughness and in consequence on crystal growth mechanism and hence rate. Bourne and Davey (1976, 1978) have demonstrated the value of this approach. They compared estimates of the surface entropy factor with measurements of growth kinetics determined under conditions where the growth mechanisms differed. Good agreement was found between the estimated surface entropy factor, the growth mechanism and the growth rate.

The importance of dislocations in governing crystal growth rate, especially at relatively low supersaturations, leads to a phenomenon known as growth rate dispersion. Observation of single crystals grown under identical conditions reveals considerable variations in growth rates both between crystals and with time for an individual crystal (eg White and Wright, 1970). The theoretical basis for this is considered by Bennema (1976). The variations in growth rate may be accounted for by differences in the dislocation structures of the individual crystals. Additional evidence in support of this argument comes from the observed broadening of initially narrow size

distributions during growth under identical conditions (Janse and de Jong, 1976). In discussing the consequences of growth rate dispersion the same workers note that growth rate dispersion results in an apparent growth rate-size dependency as those crystals which attain large size are those which grow fastest. In an agitated suspension crystallizer the situation is further complicated by apparent growth rate-size dependency arising from variations in the hydrodynamic environment of different sizes of crystals. This effect is widely documented, eg McCabe and Stevens (1951) and Mullin and Gaska (1969). In general large crystals exhibit greater slip velocities with respect to the surrounding solution than smaller ones, which results in a more favourable mass transfer environment and hence more rapid growth.

2.4.1.2 Impurity effects. Mullin (1972) notes that the presence of soluble impurities in a system may have a significant effect on the growth rate. This effect is particularly important in industrial crystallization, where crystallization is used as a purification technique. The effect of impurities usually takes the form of a reduction in overall growth rate and is often accompanied by a change in crystal habit. Quantitatively this effect has been known for many years, however only a few instances have been thoroughly investigated and the reason for the effect explained. Davey et al (1986) for example have investigated the effect of biuret on the crystallization of urea. A number of researchers, including Lahav et al. (1985) have made a considerable contribution in this area by linking the three dimensional structure of habit modifiers with the crystallographic structure of the substances they affect.

2.4.2 Empirical kinetic equation.

In this discussion it has been demonstrated that the growth process is relatively complex. An accurate mathematical description of the process would certainly require accurate knowledge of a number of these parameters which are difficult to measure at an atomic level. As in the case of nucleation in the absence of such a mathematical description most researchers seeking to correlate growth rates of large crystal populations with readily measurable parameters employ empirical correlations. Equation 2.5 is a typical example employed by Pawle et al (1985).

$$G = K_g \Delta C^g N^m L^d \exp\left\{\frac{-E_g}{RT}\right\} \exp\{k.I\} \qquad 2.5$$

It incorporates terms to account for the effect of supersaturation, ΔC^g; temperature, $\exp\frac{-E_g}{RT}$; agitation, N^m; crystal size, L^d; and impurity concentration, $\exp\{k.I\}$, on overall growth rate. G is the growth rate, K_g is the growth rate constant and I is the impurity concentration.

2.5 Experimental Approaches to Determination of Crystallization Kinetics.

There are two distinct experimental approaches to the determination of crystallization kinetics, those based on measurements of individual crystals and those involving measurements of populations of crystals.

2.5.1 Single Crystal Measurements.

In the case of investigations based on single crystals specific face growth rates may be evaluated either in isolation or with respect to other faces. This approach has been widely employed and has proved helpful in examining the effect of parameters such as supersaturation, temperature and impurity concentration on individual face growth rates and crystal habit. Examples of such studies include the work of Tai and Pan (1985), Karpinski et al. (1984) and Aquilano et al. (1984). The technique has also been valuable in investigating the mechanisms of growth and nucleation, and has been used in the investigation of growth rate dispersion by Garside and Ristic (1983) and surface roughening by Elwenspoek et al. (1986). Useful information relating to secondary nucleation mechanisms and kinetics have been obtained from single crystal studies such as the crystal contacting experiments of Garside and Larson (1978) and the fluid shear experiments of Jagganathan et al. (1980) described in Section 2.3.2. Such single crystal based studies are usually performed under well characterised hydrodynamic conditions, and observations are usually made by photo-microscopy.

The single crystal methods have been very valuable in the investigation of growth and secondary nucleation mechanisms. However the technique has several drawbacks which limit its application to the determination of crystallization kinetics for industrial design (Tavare 1987). Firstly it is time consuming to obtain sufficient kinetic data to make statistically reliable predictions, because the behaviour of a

large number of crystals must be evaluated to eliminate crystal - crystal variations. The conditions encountered in bulk crystallization are likely to be somewhat different and far less well defined than those employed in these studies. In bulk crystallization, supersaturation, hydrodynamics, temperature and purity may all vary during the course of an experiment. In particular the magma densities encountered in industrial crystallizers are very high and since the role of collisions in secondary nucleation is considered to be dominant the scale up of any nucleation kinetics measured in single crystal experiments may be unreliable. However Tengler and Mersmann (1984) claim reasonable agreement between kinetic measurements made on single crystals and in fluidised beds. Growth rates measured for individual crystals may be applicable to bulk crystallization although usually overall rather than individual face growth rates are required.

2.5.2 Measurements based on populations of crystals

In the design of an industrial crystallizer it is desirable that measurements of crystallization kinetics are performed under conditions similar to those anticipated in the industrial process (Tavare, 1987b). This has been highlighted in a number of studies, viz Zumstein and Rousseau (1986 and 1987) and Price and Hazell (1987).

As discussed in Sections 2.3 and 2.4 researchers seeking to determine crystallization kinetics for the purposes of plant design and operation usually employ empirical correlations of the form described earlier in Equations 2.4 and 2.5. The variables considered in such an approach usually include temperature, supersaturation, hydrodynamics and magma density; occasionally impurity effects may also be considered. If growth rate is size dependent crystal size will also be considered, (McCabe and Stevens, 1951).

The various experimental approaches that different researchers have developed to measure growth and nucleation rates can be categorised by the degree of constraint exercised over the experimental variables. A highly constrained approach may be employed where the values of all experimental parameters are held constant during the experiment and measurements are then made at steady state. Alternatively a less constrained approach may be employed where one or more of the parameters is allowed to change during the course of the experiment. Kinetic measurements are

then made at non-steady state and correlations performed using the mean values of the time dependent parameters appertaining to the time increment over which the evaluations were performed.

Tavare and Garside (1986a) observed that in the first approach data analysis is relatively straightforward. As the constraints are relaxed and parameters are allowed to vary with time the data analysis becomes more complex.

The practical experimental techniques that may be adopted can be considered to fall into three broad categories; they are the continuous MSMPR type crystallizer, the fluidised bed crystallizer and the batch crystallizer.

The widely used MSMPR (Mixed Suspension Mixed Product Removal) crystallizer was popularised largely as a result of the work of Randolph and Larson (eg Randolph and Larson, 1971). It is an example of the most constrained case; values of key parameters are set and the system is run for a number of residence times to allow a steady state to be achieved. This procedure allows both growth and nucleation kinetics to be established from a plot of the natural log of population density against size. According to Timm and Larson (1968) this should yield a straight line of slope $-1/G\tau$ and intercept n^o where G is the growth rate τ is the residence time and n^o is the population density at zero size. The nucleation rate B_N is then determined from the relation $B_N = G.n^o$. There are several drawbacks associated with the MSMPR and related techniques employing continuous crystallizers. Tavare and Garside (1986b) note that complex experimental apparatus and procedures are usually required. The experiments themselves are time consuming and temperature and flow rates must be maintained accurately for a period in excess of 10 residence times before steady state is achieved and measurements can commence. Each experiment yields growth and nucleation rates for just one set of conditions; consequently many experiments are required to characterise a system. This is in contrast to other techniques where data relating to a range of conditions may be obtained from each experiment. Thus MSMPR experiments are relatively expensive. The solution requirement for such experiments is relatively large compared with other techniques making it unattractive

for scarce and expensive materials. Despite these disadvantages the procedure is widely used and is clearly valuable in those cases where data are required for the design or operation of a continuous crystallizer.

Garside and Shah (1980) reviewed the published data available at that time obtained using MSMPR crystallizers. The results show good agreement between studies for some materials but in a significant number of cases the agreement was found to be rather poor.

Less constrained approaches to kinetics measurement usually employ either a batch agitated vessel or a fluidised bed crystallizer. These approaches may be categorised by the degree of constraint applied to the experimental variables. The key factors which may be employed for such a categorisation are supersaturation, hydrodynamics, temperature and magma density. As the constraints on these variables are relaxed the range of conditions accessed in each experiment widens. As a consequence kinetic information relating to a wider range of conditions becomes available, though this is obtained at the expense of increased analytical complexity.

An example of slight relaxation of these constraints is the isothermal technique described by Jancic et al. (1984) for investigation of growth rate dispersion. A small carefully selected population of near mono-sized seed crystals was suspended in a fluidised bed to give a very dilute slurry. During the course of the experiment the supersaturation remains almost constant as the depletion required to obtain a conveniently measurable increase in the size of the seed crystal population is negligible. Likewise the magma density increases only slightly so the assumption that the experimental conditions are nearly constant is valid.

A more general isothermal approach is that of isothermal desupersaturation, eg Pawle et al. (1985), Jones and Mullin (1973). In general a predetermined level of supersaturation is generated by cooling (although a similar technique is possible employing salting or drowning out). Crystallization takes place and the system is allowed to attain a new equilibrium condition by depletion of the supersaturation. Either seeding may be adopted or a level of supersaturation in excess of the metastable zone width

must be generated (Ang and Mullin, 1979). If the crystal size distribution is determined periodically during the course of the desupersaturation using such techniques as sieving, electrical zone sensing or laser light diffraction, then mean growth and nucleation rates may be evaluated from successive pairs of size distributions.

A number of techniques have been employed to determine crystallization kinetics from successive pairs of crystal size distributions separated by a suitable time interval (Tavare, 1987). In essence these involve measurement of changes in population density. Growth rates may be determined from the increase in the size corresponding to a particular cumulative number oversize. Likewise nucleation rates may be determined from the increase in cumulative number oversize evaluated at or near zero size. Often the population density is not well characterised, especially at both small and large size (Anderssen and White, 1971). For this reason procedures based on moments of the population density weighted towards the well characterised regions of the population have been employed. The "S-plane" analysis procedure developed by Tavare and Garside (1986a) is an example of such a procedure. The growth and nucleation rate data obtained in this manner may then be correlated with the mean values of the experimental parameters (for example supersaturation and magma density) prevailing over the measurement interval.

A series of isothermal desupersaturations performed at different temperatures enables the temperature dependence of the kinetics to be characterised. In separate additional experiments the effect of agitation on the kinetics may be determined in a similar way.

The approaches considered so far do not resemble industrial crystallization processes in one important aspect, that is the magma densities achieved using these procedures are very much lower than those required for commercial operation in industry. This arises from the absence of supersaturation generation during the course of the experiment which limits the maximum magma density to that achieved by supersaturating to the metastable limit. This limitation is overcome by generating supersaturation during the course of the crystallization, for example by cooling, salting-out or drowning-out.

A typical example of such an approach is non-isothermal batch crystallization. This is essentially the same procedure employed in the batch-wise industrial crystallization of many compounds, for example effect chemicals and pharmaceutical materials (Garside, 1984).

The magma densities encountered in such studies are notably higher than those encountered in the studies previously discussed. For eaxmple Mohamed-kheir et al. (1987) report kinetics for potassium sulphate crystallization at magma densities approaching 0.1kg crystal/kg water. Jones et al (1987) have investigated the effect of controlled supersaturation generation on the crystal size distribution of potassium sulphate produced both by cooling and drowning-out with acetone. A number of similar studies have indicated the influence of controlled supersaturation generation on the product size distribution. Examples include the work of Mullin and Nyvlt (1971) and Chianese et al. (1986b).

Clearly a knowledge of crystallization kinetics for a particular system is very valuable in attempts to exercise control over the product crystal size distribution by seeding and profiled supersaturation generation. A number of researchers have developed computer simulations and optimisation programs in order to attempt to use measured crystallization kinetics to improve product quality by adjusting parameters like seed loading supersaturation. Recent work on the simulation of crystallization processes include the work of Wakao et al. (1987) who simulated the isothermal crystallization of copper sulphate; Rodriguez-Hornedo and Carstensen (1986) who attempted to simulate the crystallization of oxalic acid and Mohamed et al. (1987) who developed a general simulation procedure for batch cooling crystallization.

3.0 SOLUBILITY DETERMINATIONS

3.1 Objectives

There is very little solubility data for G-acid dipotassium salt available in the open literature. Lange (1979) and Thorpe (1922) quote point solubilities for the anhydrous salt in water at 25°C and boiling point respectively from uncited sources. Price (1985) reported the solubility of G-acid dipotassium salt monohydrate over the temperature range 20 to 80°C in aqueous sulphuric acid solutions of concentration 0 to 33g H_2SO_4 per 100g of solution.

The aim of the experimental work reported in this chapter was to determine the solubility of G-acid dipotassium salt monohydrate in sulphuric acid solutions containing potassium sulphate. This work supplements the solubility data reported previously (Price 1985) and provides the solution equilibrium data necessary to analyse the crystallisation kinetics of G-acid dipotassium salt monohydrate crystalised from sulphuric acid both by salting out and cooling.

Solubility determinations were made in sulphuric acid solutions within the concentration range 9 to 40g H_2SO_4 per 100g of solution over the temperature range 25 to 80°C. The effect of increasing the potassium ion concentration up to 5g K^+ per 100g of solution was investigated.

3.2 Experimental Procedure.

The apparatus used to prepare saturated solutions consisted of a series of jacketed vessels linked to a thermostated bath and circulator. Agitation was provided by small magnetic stirrers. The apparatus is shown in Figure 3.1 and has been described in detail elsewhere (Price 1985).

In a typical experiment five vessels were taken, each containing 50ml of sulphuric acid solution of the required concentration. The quantity of G-acid dipotassium salt monohydrate required to saturate the sulphuric acid solution at 80°C and leave a small excess was estimated from the reported solubility data (Price 1985) and the quantity of potassium ion contained in this estimated mass of G-acid dipotassium

Figure 3.1 Equilibration apparatus used in this study.

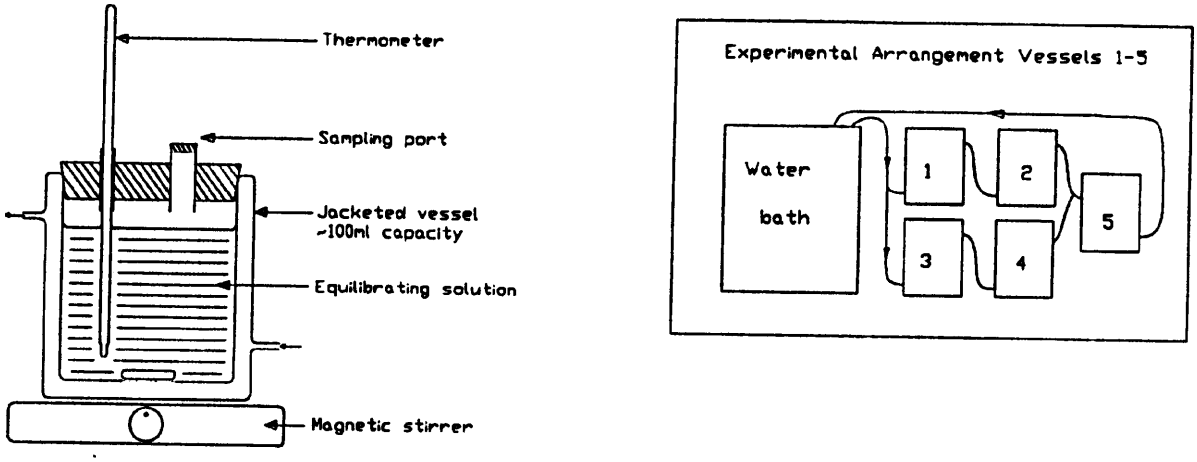

salt monohydrate was calculated. Potassium sulphate was added to the sulphuric acid in vessels 2,3,4 and 5 such that the potassium ion content would exceed the amount present in the estimated quantity of G-acid dipotassium salt monohydrate by 0.25, 0.5, 0.75 and 1.0 times respectively. No potassium sulphate was added to vessel 1. After dissolution of the potassium sulphate at 25°C the calculated mass of G-acid dipotassium salt monohydrate was weighed out accurately and added to each vessel, the vessels were sealed and the solutions left to equilibrate. It had been determined previously (Price 1985) that under similar conditions G-acid dipotassium salt monohydrate solutions usually attain equilibrium within 30 minutes. Thus after three hours agitation at constant temperatures the solutions were considered to be saturated. Agitation was then ceased, the solution temperature was measured with an accuracy greater than ±0.1°C and a solution sample was taken.

The *in situ* sampling technique has been described in detail previously (Price 1985). The sampling apparatus is illustrated in Figure 3.2. It consisted of a grade 3 sintered disk (16-44μm pore size) fused into the end of a glass tube which was connected via a flexible silicone rubber tube to a weighed sample bottle containing a known mass of distilled water. This bottle was connected to vacuum. The sintered disk was immersed in the saturated slurry and a small sample, typically 1g, of the saturated

solution was filtered into the sample bottle which was then sealed and re-weighed. After a sample of saturated solution had been obtained from each vessel in this manner agitation was recommenced and the temperature of the system raised to a higher temperature. This procedure was repeated several times until a temperature of 80°C had been reached.

Figure 3.2 The *in situ* sampling apparatus

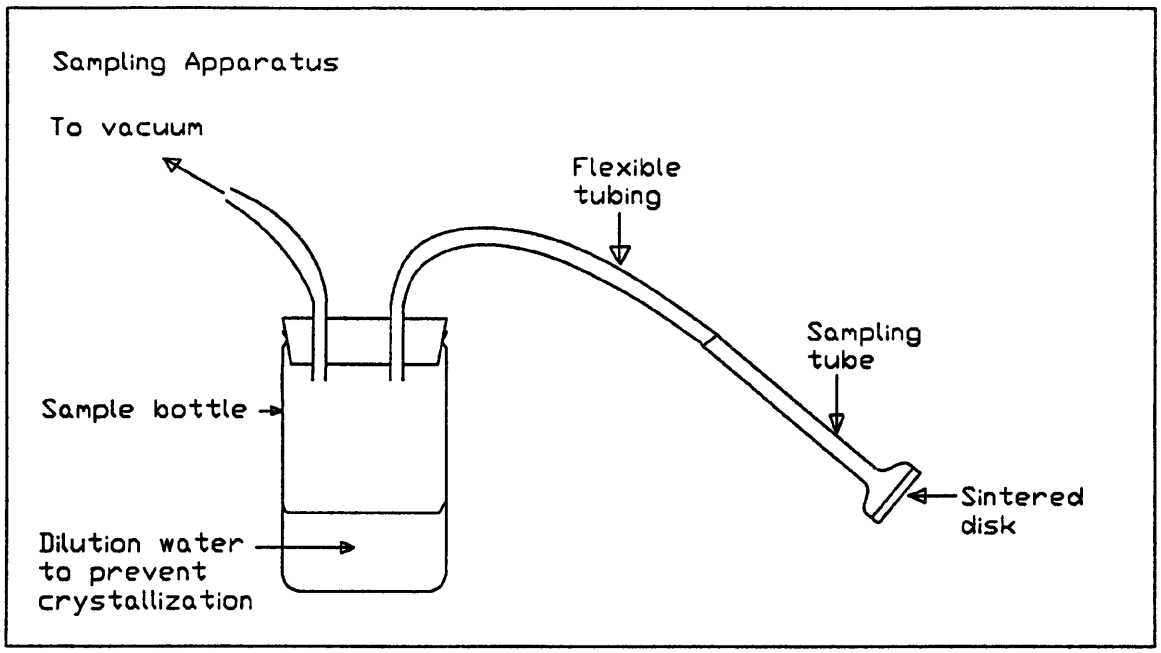

The solutions were analysed for both G-acid^{2-} and potassium ion. The analytical procedure has been described elsewhere (Price 1985) so only the main points are reported here.

The concentration of G-acid^{2-} in the solutions was determined by UV absorption. The wave length of maximum absorption (λ max) for G-acid^{2-} occurs between 236 and 237nm (Daglish 1950, Price 1985), the molar extinction coefficient (ε_v) at 236 nm was found to be 51220 Abs. units (Price 1985). The G-acid dipotassium salt monohydrate used in these experiments was supplied by ICI Organics Division. It contained small traces (<1% by weight) of four other sulphonic acids which also absorb UV light at 236nm and so a correction factor was calculated to account for this. The value of this correction factor reduced the calculated G-acid^{2-} concentration

by 1.10%. Full details of how this correction factor was calculated are given in Appendix 1. The potassium ion concentration in the solutions was determined by atomic absorption at 766.5nm.

Five series of experiments of this type were performed with sulphuric acid concentrations of 9, 18, 26, 33 and 40g H_2SO_4 per 100g of solution).

3.3 Results.

In presenting these results the following nomenclature will be used; concentrations expressed in g per 100g of solution will be signified by { } and concentrations expressed in mole per 100g of solution will be signified by [ ].

The solubility of G-acid dipotassium salt monohydrate expressed as G-acid^{2-} ion, {G-acid^{2-}} was plotted against the potassium ion concentration, {K^+}, for each temperature and sulphuric acid concentration investigated. These plots are shown in Figures 3.3 to 3.7.

Figure 3.3 G-acid solubility in 9% sulphuric acid solution; dependence on potassium ion concentration and temperature.

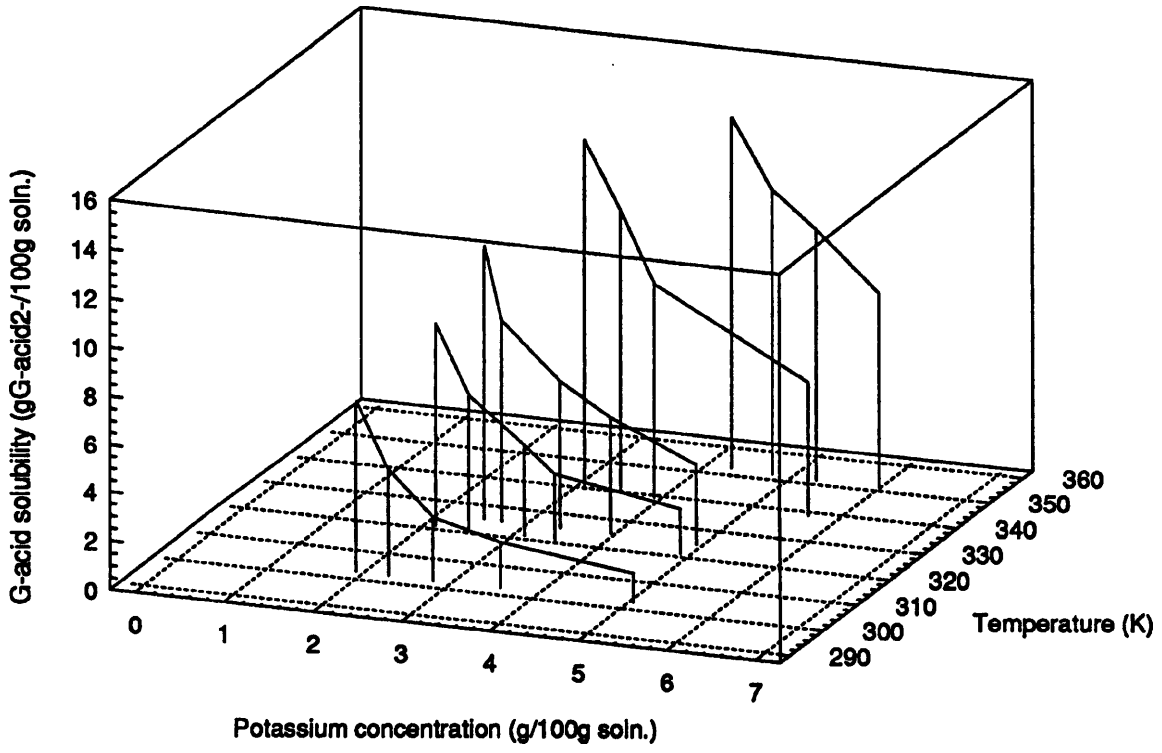

Figure 3.4 G-acid solubility in 18% sulphuric acid solution; dependence on potassium ion concentration and temperature.

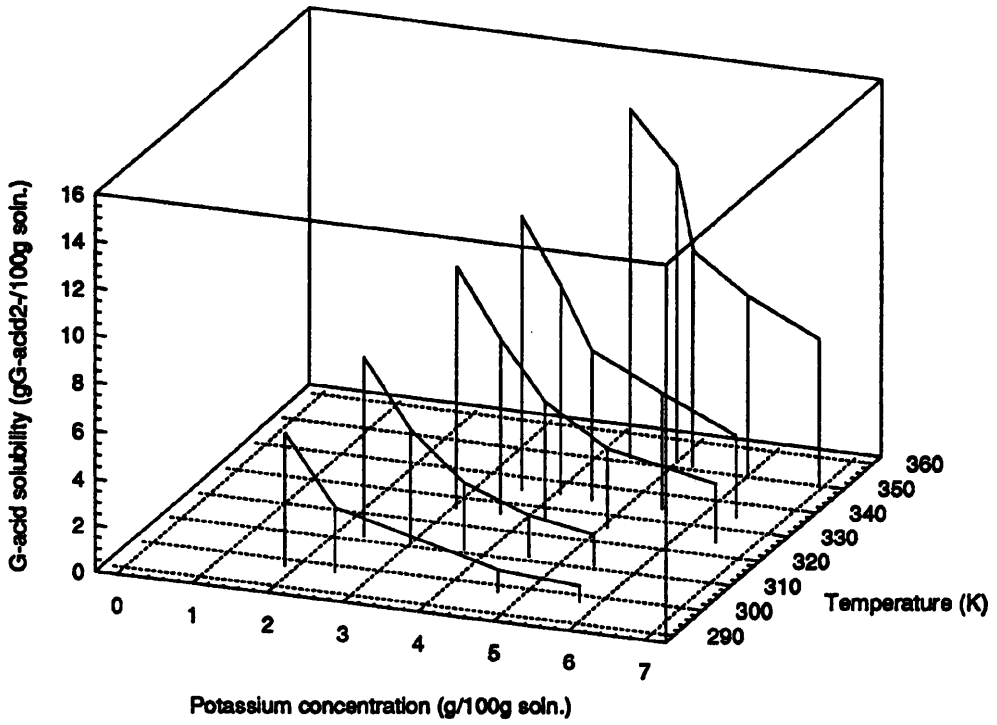

Figure 3.5 G-acid solubility in 26% sulphuric acid solution; dependence on potassium ion concentration and temperature.

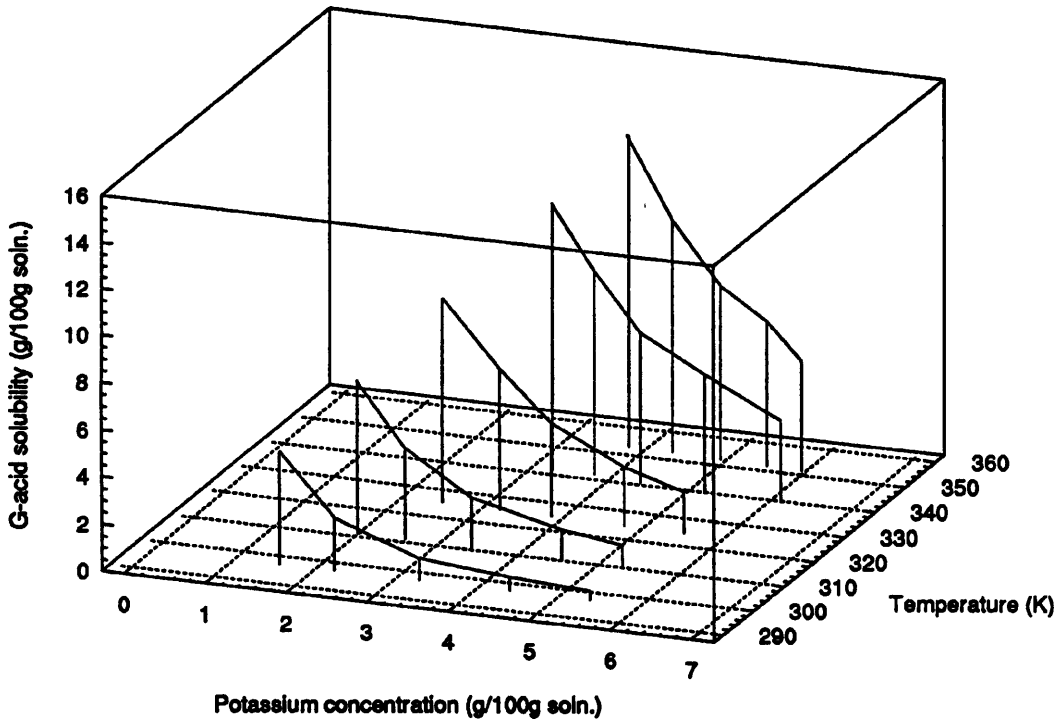

Figure 3.6 G-acid solubility in 33% sulphuric acid solution; dependence on potassium ion concentration and temperature.

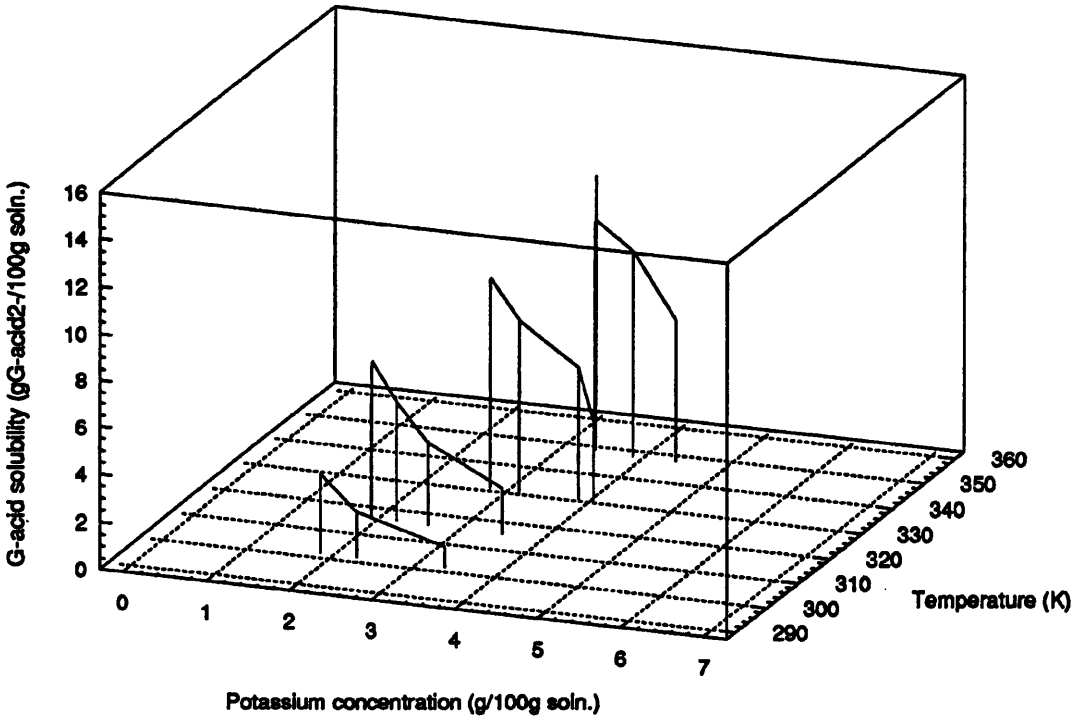

Figure 3.7 G-acid solubility in 40% sulphuric acid solution; dependence on potassium ion concentration and temperature.

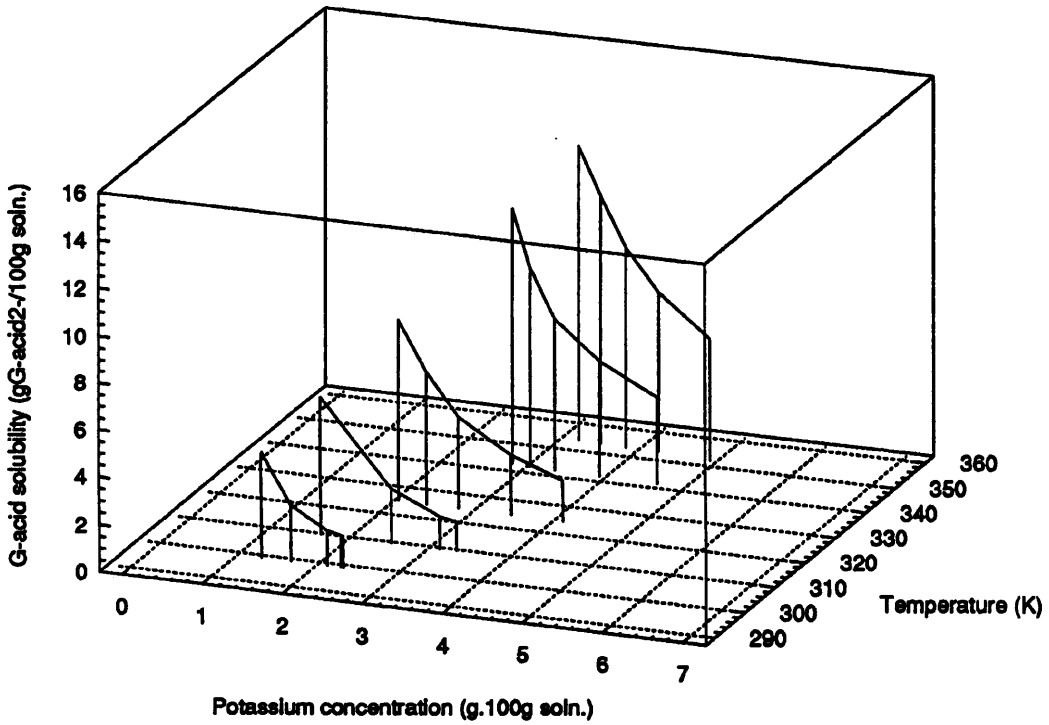

From this data, the solubility product, K_{sp}, has been calculated for each temperature and sulphuric acid concentration.

The solubility product for a saturated solution of a sparingly soluble ionic salt may be defined as follows:

$$M_nX_{m(s)} \Leftrightarrow nM^{m+}_{(aq)} + mX^{n-}_{(aq)} \qquad 3.1$$

$$K_{sp} = [M^{m+}]^n [X^{n-}]^m \qquad 3.2$$

where $[M^{m+}]$ and $[X^{n-}]$ are the equilibrium concentrations of the two ionic species. Equation 3.2 is an approximation since strictly the activities of the ionic species should be used rather than their concentrations. This limits the use of Equation 3.2 to sparingly soluble ionic salts where the activities of the ionic species are approximately equal to their concentrations. At high concentrations values of activity and concentration are frequently found to diverge.

Equation 3.2 can be rearranged and applied to the current system as follows:

$$\ln[G-acid^{2-}]_{Eq} = -n \ln[K^+]_{Eq} + \ln K_{sp} \qquad 3.3$$

Plots of $\ln[G\text{-}acid^{2-}]_{Eq}$ against $\ln[K^+]_{Eq}$ for each temperature and sulphuric acid concentration investigated are recorded in Figures 3.8 to 3.12. Despite the high concentrations encountered in the system the correlations for these plots are found to be good, the correlation coefficient, r, usually exceeding 0.99. The values of n, $\ln K_{sp}$, and r are also given.

The values of n obtained from the plots recorded in Figures 3.9 to 3.12 are found to be close to the expected value of 2.0 since dissolution and ionisation of the G-acid dipotassium salt monohydrate yields two potassium ions for each G-acid^{2-} ion. The values of n recorded in the most dilute sulphuric acid solution (9g H_2SO_4 per 100g of solution), are between about 1.6 and 1.7. This may be taken to indicate either a

change in the dependence of the solubility of G-acid dipotassium salt monohydrate on the potassium ion concentration or a departure from the assumptions described earlier in connection with Equation 3.3.

Figure 3.8 A plot of $\ln[G\text{-}acid^{2-}]_{Eq}$ against $\ln[K^+]_{Eq}$ in 9% sulphuric acid solution over a range of temperatures.

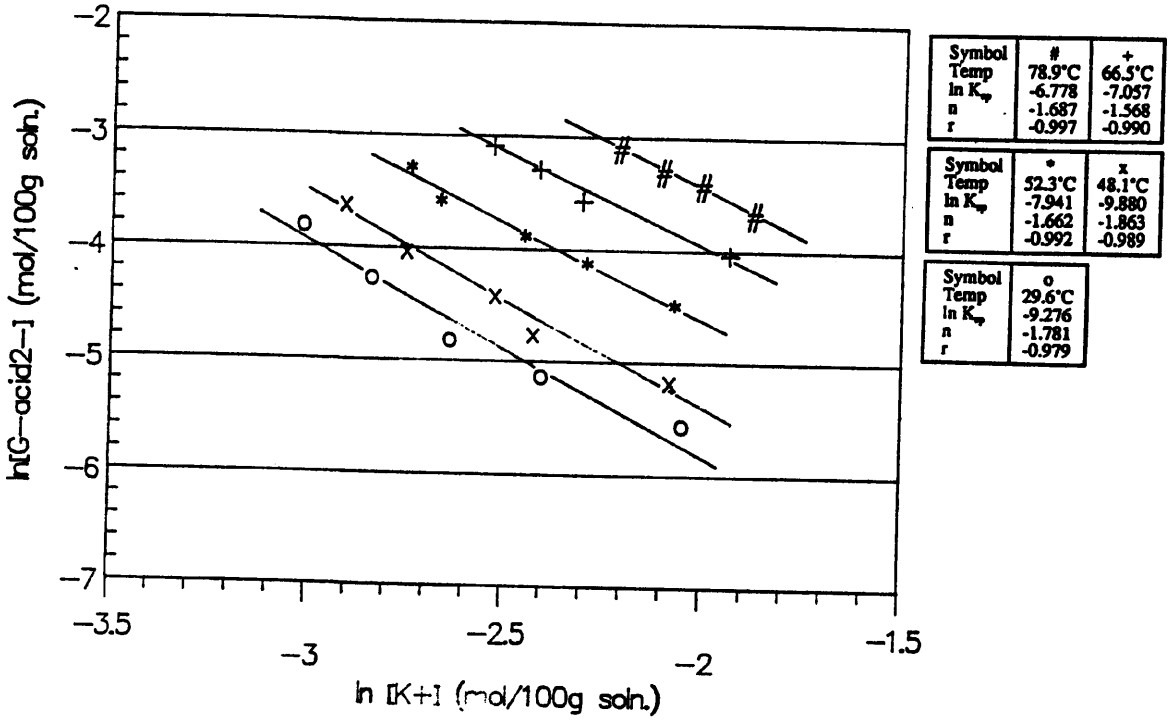

Figure 3.9 A plot of $\ln[G\text{-}acid^{2-}]_{Eq}$ against $\ln[K^+]_{Eq}$ in 18% sulphuric acid solution over a range of temperatures.

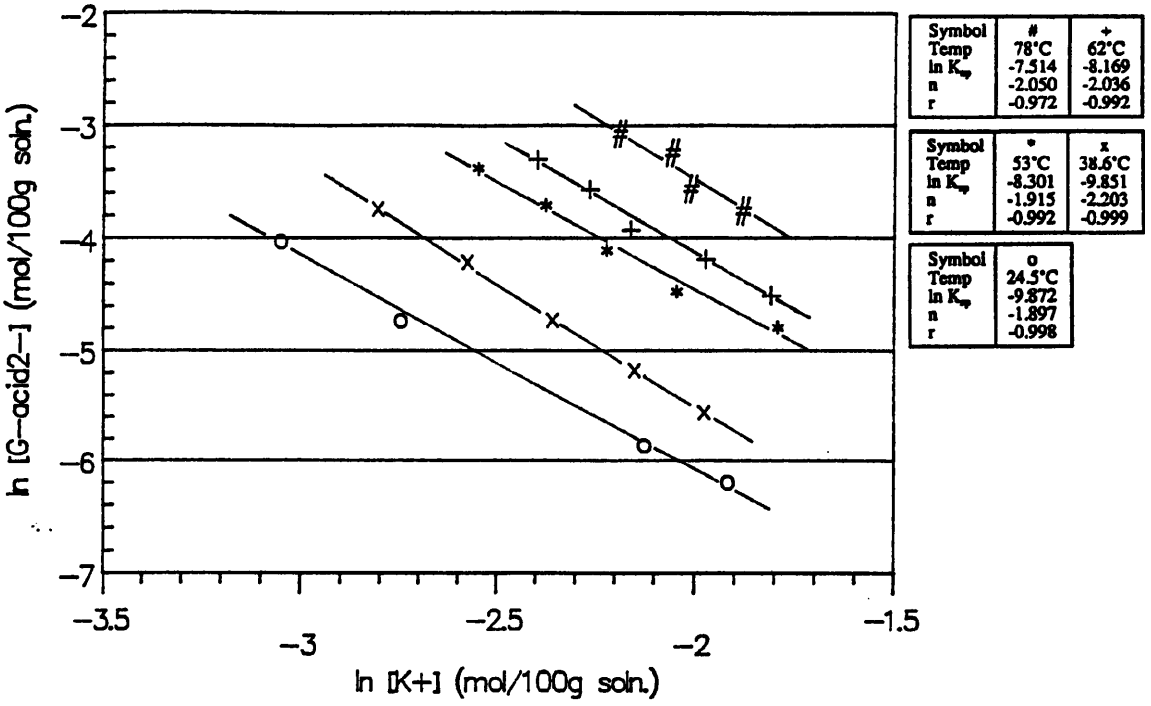

Figure 3.10 A plot of $\ln[G\text{-}acid^{2-}]_{Eq}$ against $\ln[K^+]_{Eq}$ in 26% sulphuric acid solution over a range of temperatures.

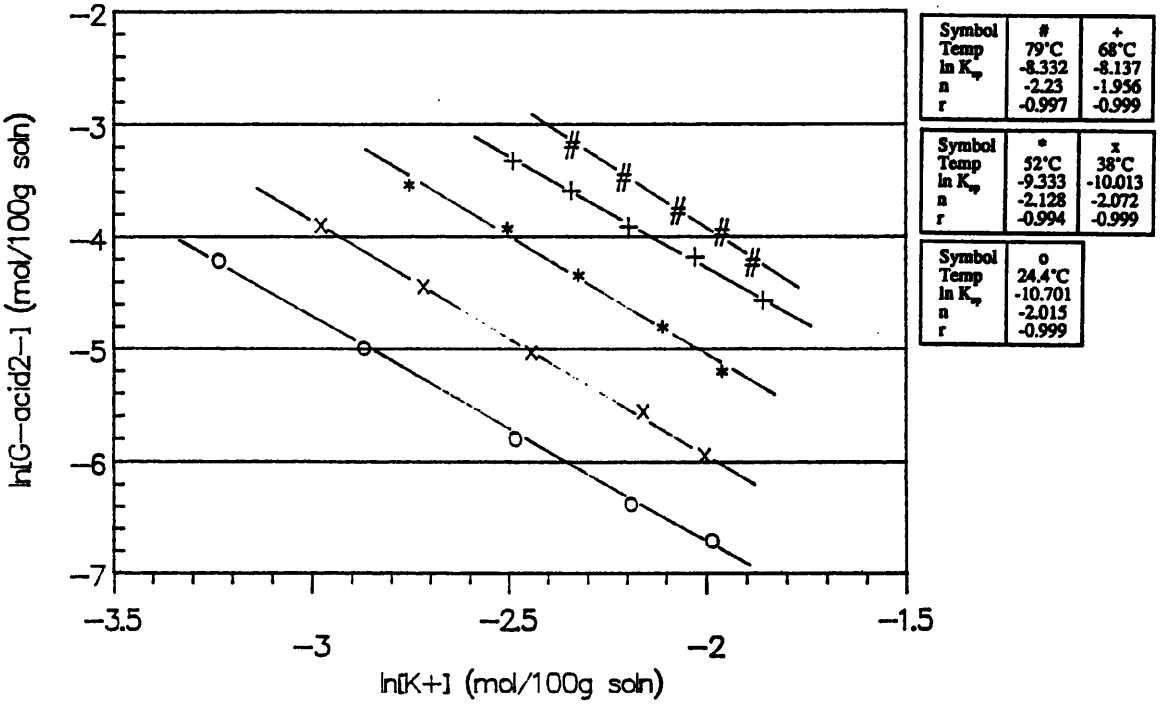

Figure 3.11 A plot of $\ln[G\text{-}acid^{2-}]_{Eq}$ against $\ln[K^+]_{Eq}$ in 33% sulphuric acid solution over a range of temperatures.

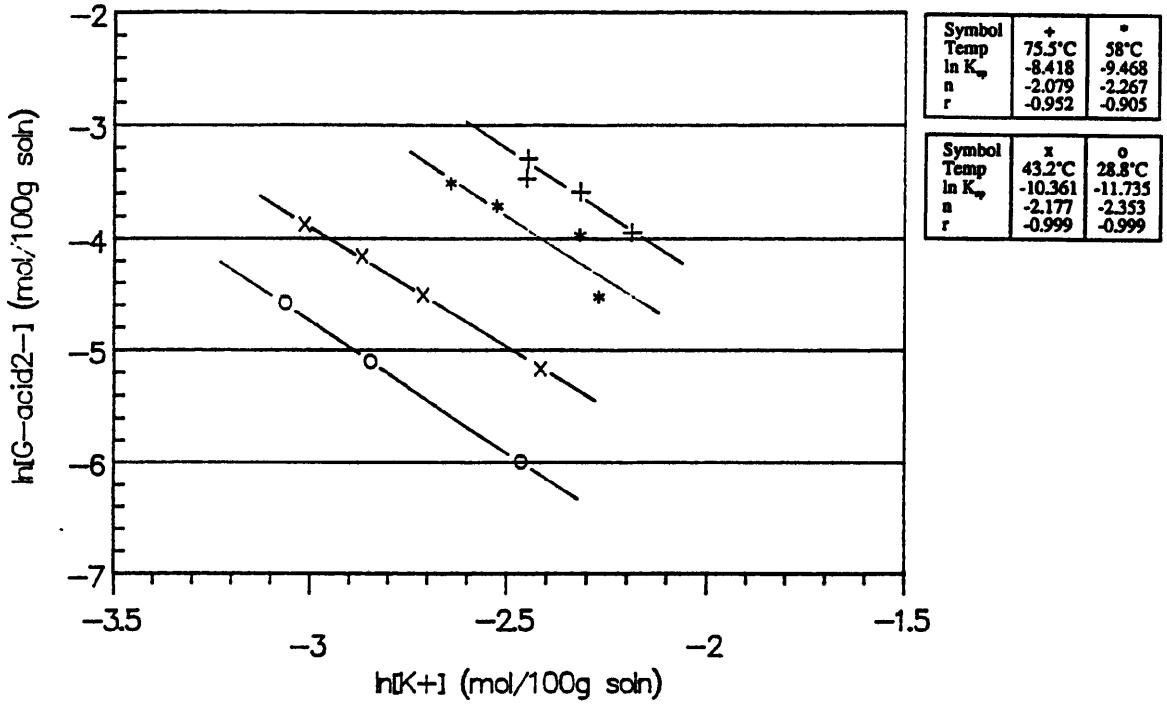

Figure 3.12 A plot of $\ln[G\text{-}acid^{2-}]_{Eq}$ against $\ln[K^+]_{Eq}$ in 40% sulphuric acid solution over a range of temperatures.

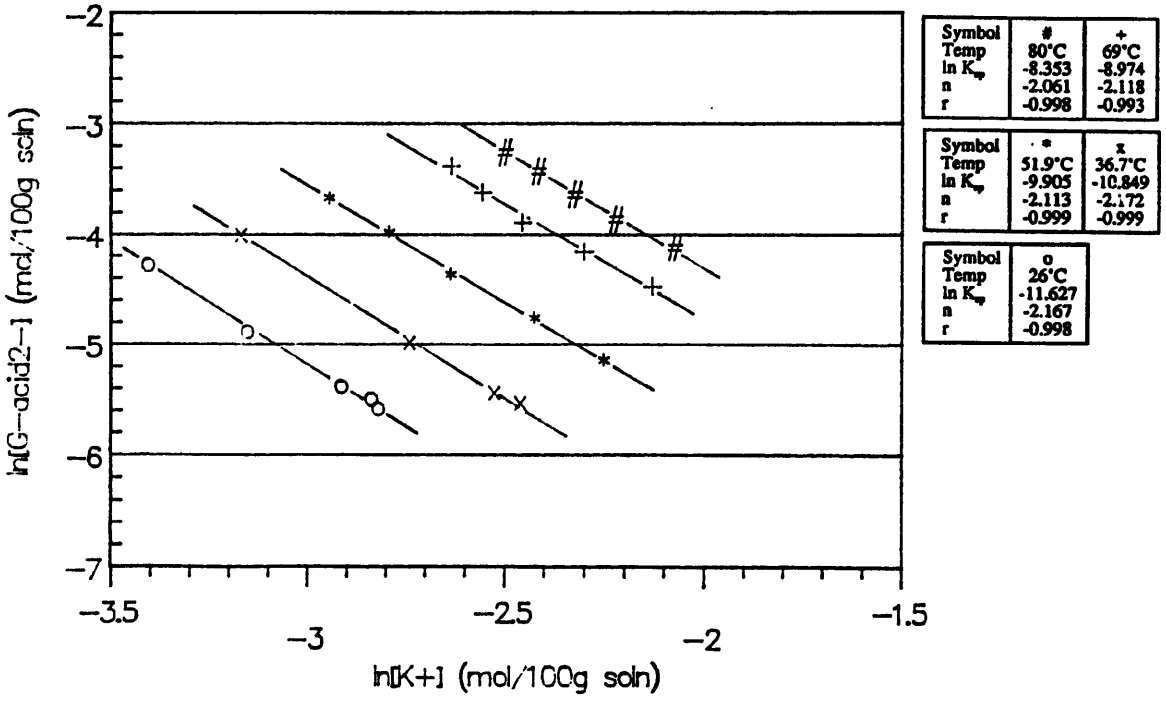

The increasing solubility of G-acid dipotassium salt monohydrate with increasing temperature resulted in the sulphuric acid concentration decreasing. This variation is described by:

$$\{H_2SO_4\}_{Eq} = \frac{100\{H_2SO_4\}_o}{100 + \{DM\}_{Eq}} \qquad 3.4$$

where $\{H_2SO_4\}_{Eq}$ is the equilibrium sulphuric acid concentration at the time of the solubility determination and $\{H_2SO_4\}_o$ is the initial concentration. $\{DM\}_{Eq}$ is the equilibrium concentration of dissolved material. The concentration of dissolved material is calculated as follows:

$$\{DM\}_{Eq} = \{G-acid^{2-}\}_{Eq} + \{K^+\}_{Eq} + \{H_2O\}_{Hyd} + \{SO_4^{2-}\}_{K^+} \qquad 3.5$$

where $\{G\text{-}acid^{2-}\}_{Eq}$ and $\{K^+\}_{Eq}$ are determined experimentally, $\{H_2O\}_{Hyd}$ is the additional concentration of water arising from the release of water of hydration from the dissolved G-acid dipotassium salt monohydrate. $\{SO_4^{2-}\}_{K^+}$ is the additional concentration of sulphate ion arising from the dissolution of potassium sulphate. The values of $\{H_2O\}_{Hyd}$ and $\{SO_4^{2-}\}_{K^+}$ are calculated from the experimentally determined G-acid^{2-} and potassium ion concentrations according to Equations 3.6 and 3.7

$$\{H_2O\}_{Hyd} = \frac{18\{G-acid^{2-}\}_{Eq}}{302} \qquad 3.6$$

$$\{SO_4^{2-}\}_{K^+} = 96\left(\frac{\{K^+\}_{Eq}}{39} - \frac{2\{G-acid^{2-}\}_{Eq}}{302}\right) \qquad 3.7$$

Values of sulphuric acid concentration calculated in this way are shown in Appendix 2, Tables A2.1 to A2.5. The reduction in sulphuric acid concentration was significant, reaching a maximum of 30%. This calculated sulphuric acid concentration was used in all subsequent calculations.

A multi-variable correlation was performed on the solubility data in order to determine the dependence of the solubility of the G-acid dipotassium salt monohydrate on

potassium ion concentration, sulphuric acid concentration and absolute temperature (T). The correlation was based on an extension of Equation 3.3 which took the following form.

$$\ln[G-acid^{2-}]_{Eq} = n\ln[K^{+}]_{Eq} + y\ln[H_2SO_4]_{Eq} + \frac{x}{T} + c \qquad 3.8$$

It has been mentioned previously that the values of n calculated from the solubility data determined with a sulphuric acid concentration of 9g H_2SO_4 per 100g of solution were significantly lower than those calculated for the four higher sulphuric acid concentrations. For this reason it was decided to perform two separate correlations, one including the solubility data obtained in all five sulphuric acid concentrations and a second excluding the data obtained with the lowest sulphuric acid concentration. The respective resulting correlations were as follows.

$$\ln[G-acid^{2-}]_{Eq} = -1.6160\ln[K^{+}]_{Eq} - 0.47284\ln[H_2SO_4]_{Eq} - \frac{4969.9}{T} + 6.3974 \qquad 3.9$$

$$\ln[G-acid^{2-}]_{Eq} = -1.9736\ln[K^{+}]_{Eq} - 1.1873\ln[H_2SO_4]_{Eq} - \frac{5287}{T} + 5.5957 \qquad 3.10$$

The correlation coefficients were 0.95 and 0.994 respectively. The main purpose of obtaining this solubility data and performing the multi-variable correlation was to permit accurate prediction of the solubility of G-acid dipotassium salt monohydrate in the presence of potassium ion in a range of sulphuric acid concentrations. It was decided that the better correlation of the data to Equation 3.10 over Equation 3.9 was desirable although the greater accuracy of solubility prediction from Equation 3.10 was obtained at the cost of reducing the range of sulphuric acid concentrations for which solubility predictions could be made.

The values of $\{G\text{-}acid^{2-}\}_{Eq}$ and $\{K_s\}_{Eq}$ determined experimentally are recorded in Appendix 2 Tables A2.1 to A2.5 together with the calculated values of $\ln[G\text{-}acid^{2-}]_{Eq}$, $\ln[K^{+}]_{Eq}$, $\{H_2SO_4\}_{Eq}$ and $\ln[H_2SO_4]_{Eq}$.

The Tables in Appendix 2 also show the values of $\ln[G\text{-}acid^{2-}]_{Eq}$ and $\{G\text{-}acid^{2-}\}^{Eq}$ predicted using Equations 3.9 and 3.10.

Plots of the predicted values of $\{G\text{-}acid^{2-}\}_{Eq}$ versus the experimentally observed values are shown for both equations in Figures 3.13 and 3.14. The predictions of $\{G\text{-}acid^{2-}\}_{Eq}$ are made by substituting the experimentally observed potassium ion concentrations and temperatures into Equations 3.9 and 3.10 together with the values of sulphuric acid concentration calculated for each determination according to Equation 3.4. All these values are recorded in Appendix 2 Tables A2.1 to A2.5.

Figure 3.13 A plot of G-acid solubility predicted by equation 3.9 against the measured solubility. The ± 10% limit is marked.

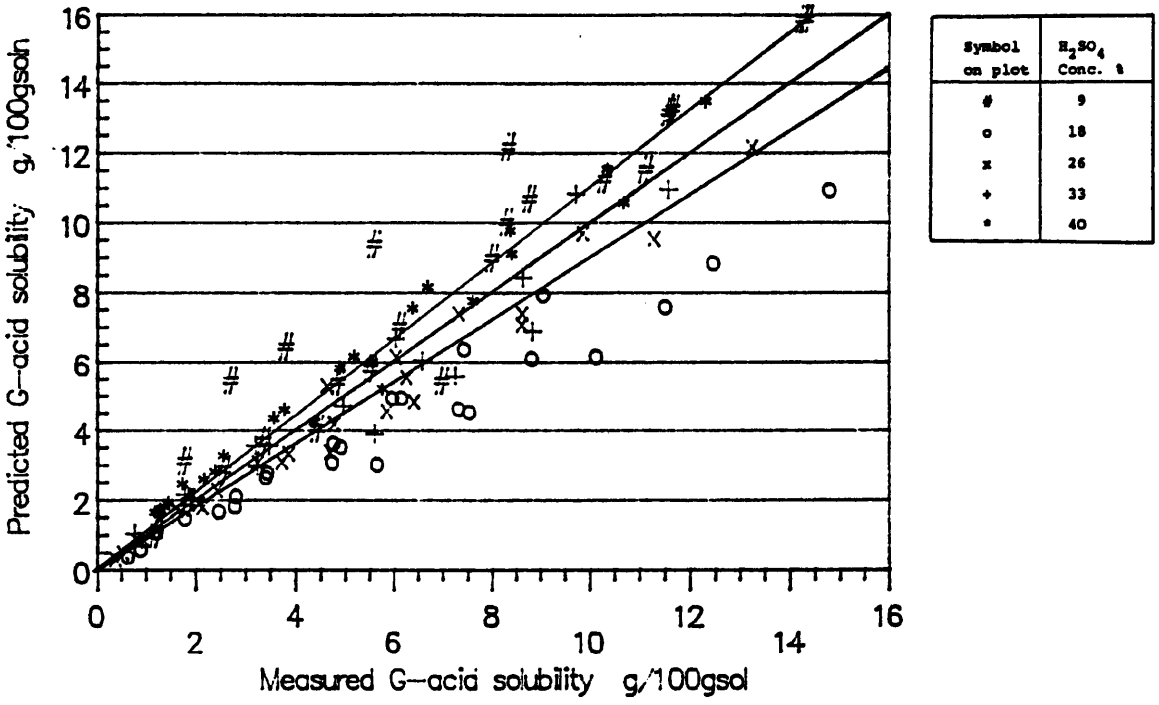

Exclusion of the solubility data for the most dilute sulphuric acid solutions investigated results in a significantly greater percentage of the predicted values of $\{G\text{-}acid^{2-}\}_{Eq}$ falling within ±10% of the experimentally observed value than the values predicted using Equation 3.9. In Figure 3.13 which depicts the values of $\{G\text{-}acid^{2-}\}_{Eq}$ predicted from Equation 3.9 only 29.7% of the predicted values fall within the range ±10% of the experimentally observed values, whereas in Figure 3.14 94.3% of the values of $\{G\text{-}acid^{2-}\}_{Eq}$ predicted from Equation 3.10 fall within the ±10% range.

Figure 3.14 A plot of G-acid solubility predicted by equation 3.10 against the measured solubility. The ± 10% limit is marked.

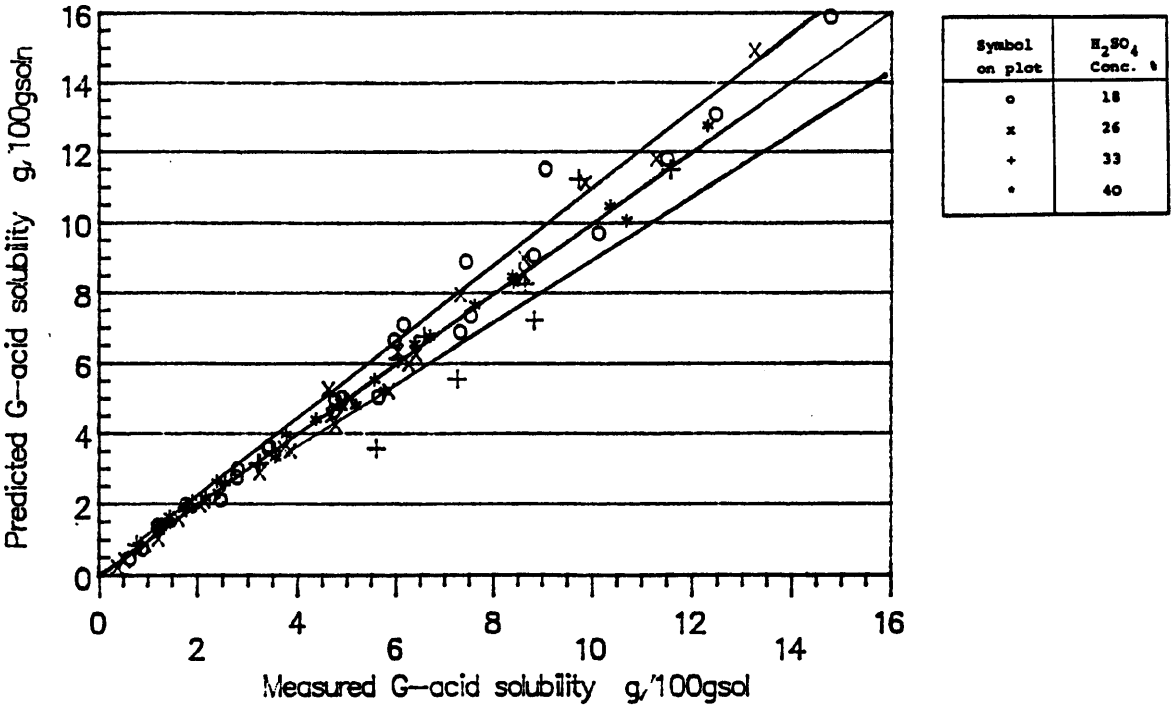

3.4 Discussion.

Examination of Figures 3.3 to 3.6 reveals close agreement between the solubility data determined in the absence of additional potassium ion in the present study and solubilities predicted from comparable data reported in a separate study (Price 1985). No data is available for comparison with the solubilities measured in the presence of added potassium ion.

The low value of *n* calculated from Equation 3.3 for the most dilute sulphuric acid solution may indicate a change in the dependence of the solubility of G-acid dipotassium salt monohydrate on the potassium ion concentration arising from the degree of ionisation of the material. Alternatively this low value of *n* may be due to a departure from the assumptions associated with the assumptions associated with Equation 3.3. No experimental work was undertaken to investigate the cause of this low value

of n as the main purpose of this section of the work was to establish a relationship that was useful in predicting the solubility of G-acid under the experimental conditions, especially at higher sulphuric acid concentrations.

The solubility relationship described by Equation 3.10 provides satisfactory predictions of G-acid dipotassium salt monohydrate solubilities. This is borne out by the high correlation coefficient and the large percentage of predicted solubilities falling within ±10% of the experimentally observed value. Comparison of Figure 3.14 with Figures 3.8 to 3.12 reveals that most of the predicted values which differ from the experimentally observed values by more than ±10% occur where the observed values themselves are in poor agreement with the other observed solubility data in Figures 3.8 to 3.12. This suggests that the poor agreement between these observed and predicted values arises at least in part from experimental errors made in determining $\{G\text{-}acid^{2-}\}_{Eq}$, $\{K^+\}_{Eq}$ and T.

In spite of the generally good agreement with observed solubilities, predicted solubilities may not be accurate enough for use in determining supersaturation where small inaccuracies in determining concentration are magnified in calculation of the supersaturation. For this reason care must be used in making solubility predictions which ideally should be checked against experimentally determined point solubilities.

4.0 Determination of the Metastable Zone Width

4.1 Objectives

Preliminary experiments were undertaken to determine the metastable zone width for the G-acid dipotassium salt monohydrate - sulphuric acid - water system, prior to determining the growth and nucleation kinetics from batch crystallization experiments. Two series of "salting out" experiments were performed in order to determine the dependence of induction time on supersaturation at two temperatures, 52 and 69°C. In addition to estimation of the metastable zone widths from this data the interfacial tension, σ, was determined at each temperature. The metastable zone width was also measured for supersaturation generated by cooling at a constant rate.

4.2 Theory

The historical development of our current understanding of the nucleation process has been discussed in Chapter 2. Only an outline of the theory concerning the determination of interfacial tension from induction time measurements is included in this section. From classical nucleation theory (Volmer and Webber, 1926, Becker and Doring, 1935) the rate of primary homogeneous nucleation per unit volume, J, may be expressed by:

$$J = A.\exp\frac{-\Delta G^*}{k.T} \qquad 4.1$$

where A is a constant, ΔG^* is the Gibbs' free energy for the formation of a critical size nucleus, k is the Boltzmann constant and T is the absolute temperature. The value of the critical Gibbs' free energy is given by:

$$\Delta G^* = \frac{\beta\sigma^3\Omega^2}{kT\ln S^2} \qquad 4.2$$

where β is a shape factor equal to 16π/3 for a spherical nucleus, σ is the interfacial tension, Ω is the molecular volume and S is the supersaturation ratio. Various

authors, eg Turnball (1953), Nielsen (1967), have made the simplifying assumption that the induction period is inversely proportional to the nucleation rate per unit volume, ie.

$$J = K\tau^{-1} \tag{4.3}$$

where K is a constant and τ is the induction period. Combination of Equations 4.1, 4.2 and 4.3 produces:

$$\ln\tau = B + \left(\frac{\beta\sigma^3\Omega^2}{k^3T^3(\ln S)^2}\right) \tag{4.4}$$

where B is a constant. A plot of ln τ against $(\ln S)^{-2}$ should therefore yield a straight line, the slope, m, being given by:

$$m = \frac{\beta\sigma^3\Omega^2}{k^3T^3} \tag{4.5}$$

Making the assumption that the critical nucleus is spherical, ie $\beta = 16\pi/3$, enables the interfacial tension to be determined.

$$\sigma = \left(\frac{mk^3T^3}{\frac{16\Pi}{3}\Omega^2}\right)^{\frac{1}{3}} \tag{4.6}$$

The molecular volume, Ω, may be estimated from the density and molecular weight of the material:

$$\Omega = \frac{MW.10^{-3}}{\rho N} \tag{4.7}$$

where MW is the gram molecular weight, ρ the crystal density and N is Avogadro's number.

4.3 Experimental Procedure

The experimental apparatus is shown in Figures 4.1 and 4.2. Experiments were performed in a jacketed glass vessel of working volume approximately 100ml. Temperature control was achieved by circulating water from a water bath with associated temperature programmer. This permitted the contents of the jacketed vessel to be maintained at a constant temperature or alternatively to be cooled at a controlled rate.

Two quartz light guides were located at windows on opposite sides of the vessel in order to direct a beam of light from a halogen bulb through the solution. The intensity of the transmitted light was monitored together with the intensity at the source using a pair of photoresistive diodes. These diodes and a potentiometric recorder were connected into a resistance bridge so that differences in the light intensities striking the diodes could be recorded. The presence of crystals in the light path caused light to be scattered and resulted in a decrease in the intensity of the transmitted beam. Such a decrease during the course of an experiment was taken to indicate that nucleation followed by crystal growth had occurred. The jacketed vessel was enclosed in a light proof box to prevent interference from external light sources.

The contents of the vessel were agitated using a non-vortexing disk stirrer while the temperature of the vessel contents was measured using both a thermocouple and a mercury in glass thermometer. A small black funnel fitted with a light proof cover was located at the top of the vessel to allow rapid addition of solids to the solution.

Two series of experiments were conducted at temperatures of 52 and 69°C. A solution containing 40g H_2SO_4 per 100g of solution was saturated with G-acid dipotassium salt monohydrate at the chosen temperature. The saturated solution was filtered through a pre-warmed glass microfibre filter of pore size 1.6μm. A sample of the filtrate was taken and analysed for both [G-acid^{2-}] and [K^+] in the manner described in Section 3.2 to confirm that the solution was saturated. A known mass of the saturated solution was transferred to the jacketed vessel which was initially maintained at a temperature a few degrees higher than saturation in order to ensure that any nuclei or micro crystals which may have been present were dissolved. After a few minutes agitation at this elevated temperature the temperature was reduced to

Figure 4.1 The optical measurement cell used to determine metastable zone width.

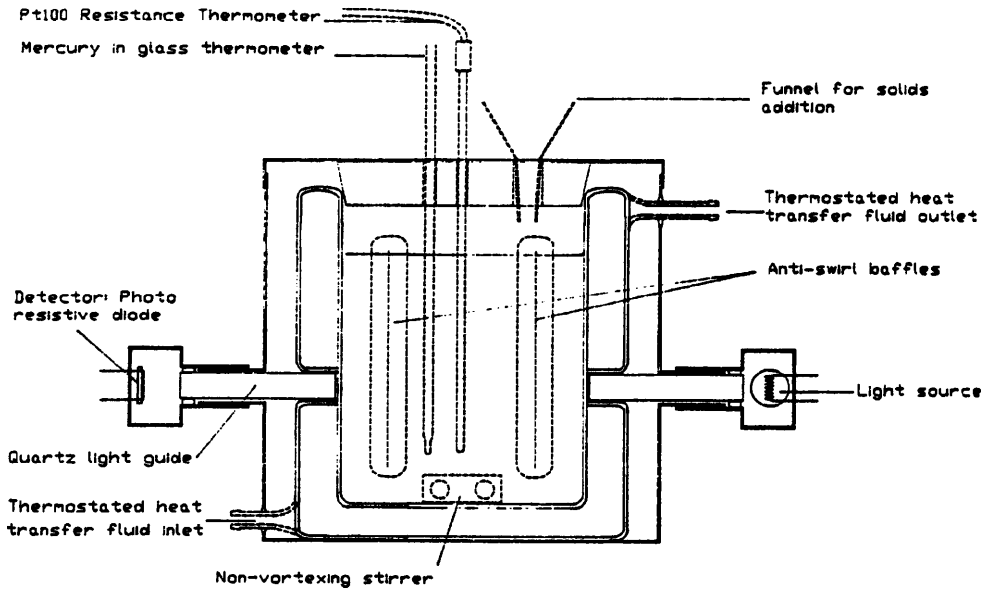

Figure 4.2 The optical cell and associated equipment.

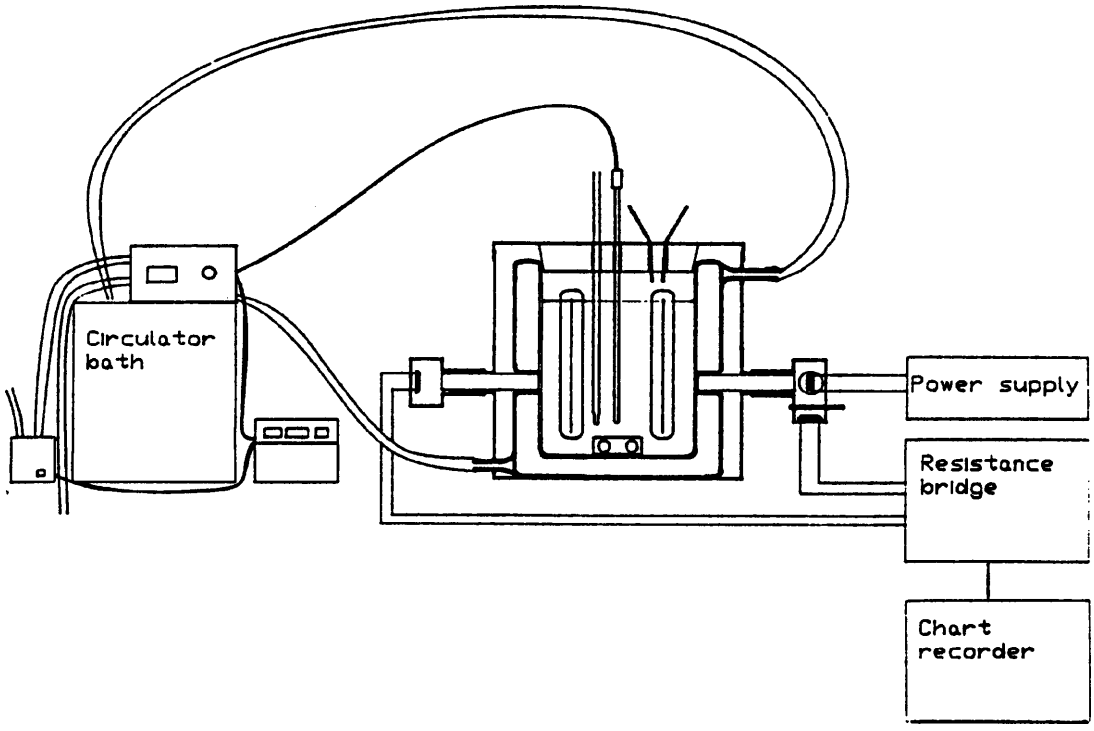

the saturation value and the system allowed to reach thermal equilibrium. The level of agitation was adjusted to a predetermined rate at which the vessel contents were well mixed without any evidence of vortexing. The operation of the optical monitoring system was checked and any necessary adjustments made. After approximately 30 minutes the system was assumed to have reached thermal equilibrium and its temperature was measured. A known mass of potassium sulphate crystals of particle size range 106 to 212μm was then added rapidly to the saturated solution via the funnel and any changes in optical density were recorded.

The mass of potassium sulphate required to generate a particular level of G-acid supersaturation in excess of the metastable zone width which still yielded a measurable induction time was determined experimentally. It had been established previously that the amounts of potassium sulphate added dissolved quite rapidly under the experimental conditions.

A number of experiments were conducted with varying levels of supersaturation at each temperature in order to determine the relationship between induction time and supersaturation. The level of supersaturation attainable by cooling was determined by cooling a solution saturated at 69°C at a constant rate of 1.0°C min^{-1} until the metastable limit was exceeded.

4.4 Results

The outputs from the potentiometric recorder for experiments performed at 52 and 69°C are shown in Figures 4.3 and 4.4 respectively.

For each experiment the supersaturation ratio, S, was calculated from the mass of potassium sulphate added, the initial composition of the solution and the solubility relationship defined by Equation 3.10. The method of calculation was in accordance with the following example.

In experiment 4.1 2.334g of potassium sulphate was dissolved in 100g of solution saturated at 52°C. The concentration of each species present was recalculated. The concentration changes are shown in Table 4.1

Figure 4.3 An optical density trace for the crystallization of G-acid dipotassium salt monohydrate from solution in 40% sulphuric acid at 52°C by salting out with potassium sulphate.

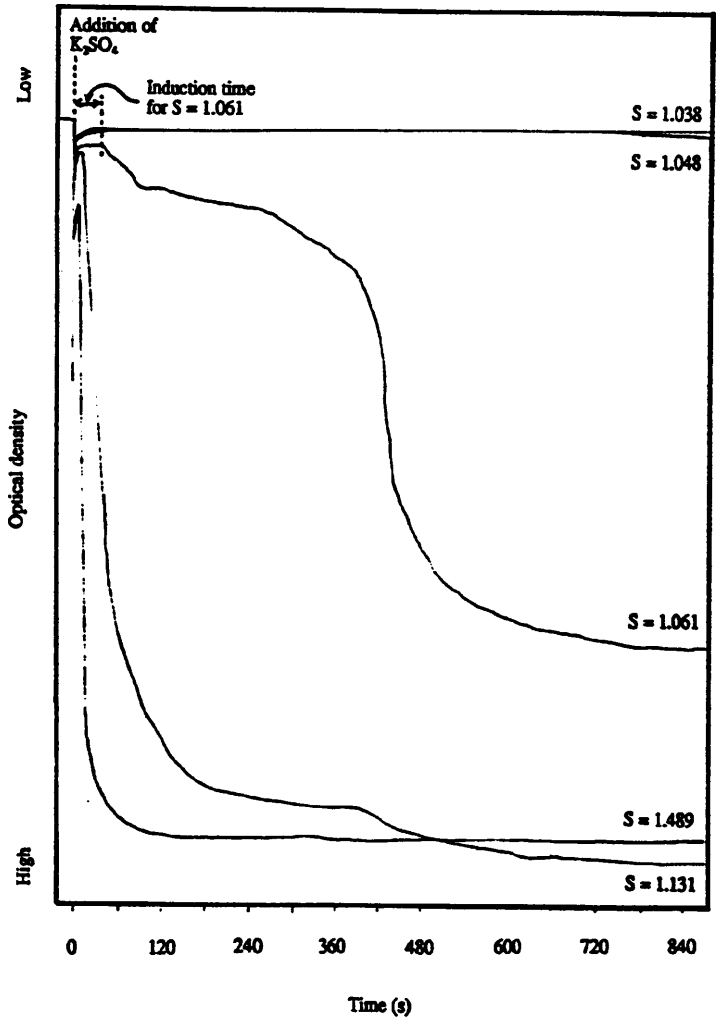

Figure 4.4 An optical density trace for the crystallization of G-acid dipotassium salt monohydrate from solution in 40% sulphuric acid at 69°C by salting out with potassium sulphate.

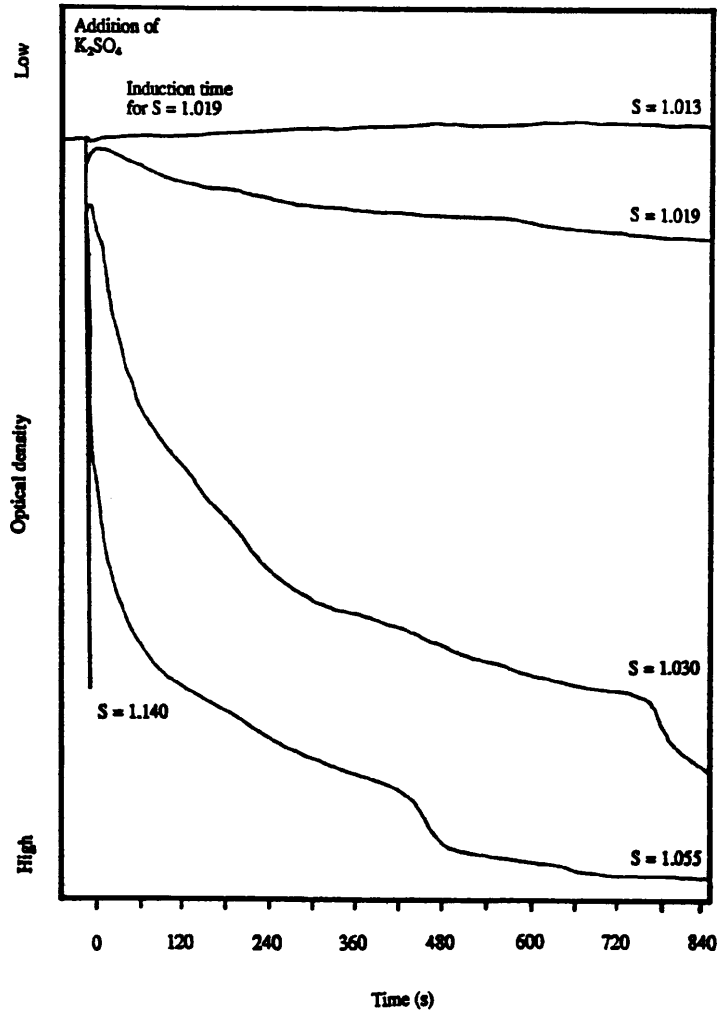

Table 4.1 Concentration changes arising from the addition of 2.334g of K_2SO_4 to a saturated solution at 52°C (Experiment. 4.1)

Species	Initial concentration g(100gsoln)$^{-1}$	Added K_2SO_4 g	Resulting concentration g (in 102.334g of soln)	Dilution factor	Final concentration g(100gsoln)$^{-1}$
{G-acid^{2-}}	7.632	-	7.632	0.977	7.458
{K^+}	2.051	1.046	3.099	0.977	3.028
{H_2O}$_{Hyd}$	0.455	-	0.455	0.977	0.444
{H_2SO_4}	36.28	-	36.28	0.977	35.45
{SO_4^{2-}}$_{K+}$	-	1.288	1.288	0.972	1.258

In order to determine the equilibrium concentrations which correspond to this supersaturated solution it was necessary to consider the mechanism by which supersaturation was relieved. It was assumed that all the supersaturation was relieved by crystallization of G-acid dipotassium salt monohydrate. Formation of 1g of this material would change the solution composition in the manner illustrated in Table 4.2:

Table 4.2 Concentration changes arising from the crystallization of 1g of G-acid dipotassium salt monohydrate from the saturated solution of Table 4.1

Species	Initial concentration g(100gsoln)$^{-1}$	Crystals formed g	Resulting concentration g (in 99g of soln)	Dilution factor	Final concentration g(100gsoln)$^{-1}$
{G-acid^{2-}}	7.458	0.759	6.699	1.010	6.767
{K^+}	3.028	0.196	2.832	1.010	2.861
{H_2O}$_{Hyd}$	0.444	0.045	0.399	1.010	0.403
{H_2SO_4}	35.45	-	35.45	1.010	35.81
{SO_4^{2-}}$_{K+}$	1.258	-	1.258	1.010	1.271

This relief of supersaturation was expressed by the following set of equations in which changes in the concentration of each species are expressed in terms of the change in the potassium ion concentration.

$$\{K^+\} = \frac{100.(\{K^+\}_0 - k)}{100 - (398k/78)} \qquad 4.8$$

$$\{G-acid^{2-}\} = \left(\{G-acid^{2-}\}_o - \left(\frac{302k}{78}\right)\right).\left(100 - \left(\frac{398k}{78}\right)\right) \qquad 4.9$$

$$\{H_2SO_4\} = \{H_2SO_4\}_o.\left(100 - \left(\frac{398k}{78}\right)\right) \qquad 4.10$$

where $\{K^+\}_o$, $\{G\text{-}acid^{2-}\}_o$ and $\{H_2SO_4\}_o$ represent the concentrations of these species following the addition of potassium sulphate and k represents the change in potassium ion concentration due to crystallization. Substitution of equations 4.8, 4.9 and 4.10 into equation 3.10 gives:

$$\ln\left[\frac{\{G-acid^{2-}\}_o - \left(\frac{302k}{78}\right)}{3.02\left(100 - \frac{398k}{78}\right)}\right] = -\left(1.9736\ln\left[\frac{100(\{K^+\}_o - k)}{98\left(100 - \frac{398k}{78}k\right)}\right]\right)\ldots$$

$$\ldots - \left(1.1823\ln\left[\frac{100\{H_2SO_4\}_o}{98\left(100 - \left(\frac{398k}{78}\right)\right)}\right]\right) - \left(\frac{5.287}{T}\right) + 5.5975 \qquad 4.11$$

Which on rearrangement gives:

$$5.5975 - \left(1.9736\ln\left[\frac{(100\{K^+\}_o - k)}{78k\left(100 - \left(\frac{398k}{78}\right)\right)}\right]\right) - \left(1.1823\ln\left[\frac{100\{H_2SO_4\}_o}{98\left(100 - \left(\frac{398k}{78}\right)\right)}\right]\right)\ldots$$

$$\ldots - \left(\frac{5.287}{T}\right) - \left(\ln\left[\frac{100\left(\{G-acid^{2-}\}_o - \left(\frac{302k}{78}\right)\right)}{302\left(100 - \left(\frac{398k}{78}\right)\right)}\right]\right) = 0 \qquad 4.12$$

The value of k was derived from this equation by an iterative technique. For Experiment 1 k was calculated as 0.633. Substitution of this value into Equations 4.8 and 4.9 gave the new equilibrium values of $\{K^+\}_{Eq}$ and $\{G\text{-}acid^{2-}\}_{Eq}$ as 2.475g (100g soln.)$^{-1}$ and 5.174g (100g soln.)$^{-1}$ respectively. The G-acid concentration after the addition of K_2SO_4 was 7.46g (100g soln.)$^{-1}$. Thus the supersaturation ratio prevailing at the time of nucleation in Experiment 1 was:

$$S = \frac{C}{C^*} \quad ie. \quad S = \frac{7.46}{5.174} \qquad 4.13$$

Values of S were calculated in this manner for the remaining experiments and are shown in Table 4.3 together with the induction times determined from Figures 4.3 and 4.4. Calculated values of $\ln\tau$ and $(\ln S)^{-2}$ are also included in Table 4.3

Table 4.3 Values of Induction Time, τ, and Supersaturation Ratio, S, for Experiments 4.1 to 4.10.

Exp N°	Induction time τ(s)	Supersaturation ratio S	$\ln\tau$	$(\ln S)^{-2}$	Temp T (K)
4.1	3	1.489	1.10	6.30	325
4.2	9	1.131	2.20	66.37	325
4.3	40	1.061	3.96	287.05	325
4.4	740	1.048	6.07	456.8	325
4.5	∞	1.038	∞	726.4	325
4.6	3	1.140	1.10	58.2	342
4.7	5	1.055	1.61	349	342
4.8	7	1.030	1.95	1144	342
4.9	15	1.019	2.71	2822	342
4.10	∞	1.013	∞	5994	342

Plots of $\ln\tau$ against $(\ln S)^{-2}$ are shown for both temperatures in Figure 4.5. Values of interfacial tension, σ, were hence calculated for both temperatures from the gradient of the plots using Equation 4.6. The value of molecular volume, Ω, calculated from Equation 4.7 was found to be $5.6*10^{-28}m^3$. The calculated values of interfacial tension were $0.56mJ.m^{-2}$ at 325K and $0.20mJ.m^{-2}$ at 343K.

When a sulphuric acid solution (40g H_2SO_4 per 100g of solution), was saturated with G-acid dipotassium salt monohydrate at 69°C and cooled at a constant rate of $1.0°C.min^{-1}$, nucleation occurred at approximately 50°C, an undercooling of approximately 19°C. An optical trace for such an experiment is shown in Figure 4.6. The supersaturation ratio corresponding to this undercooling was calculated using the technique just outlined and was calculated to be 1.44.

Figure 4.5 A plot of $\ln\tau$ against $(\ln S)^{-2}$ for the nucleation of G-acid dipotassium salt monohydrate from 40% sulphuric acid solution induced by salting out with potassium sulphate at 52 and 69°C.

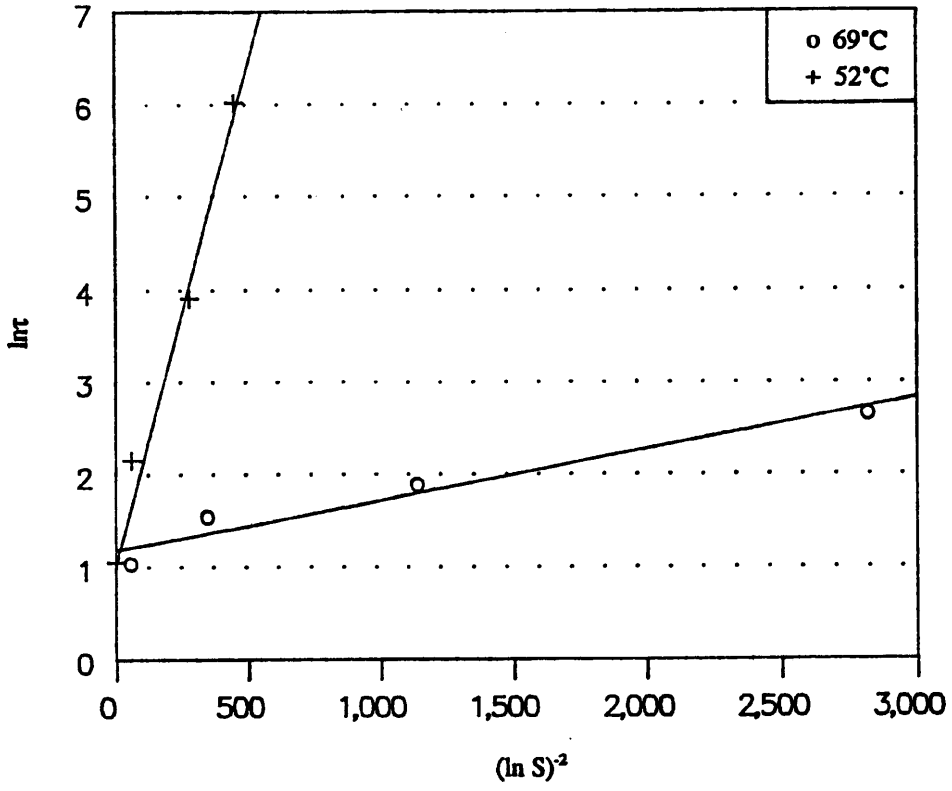

Figure 4.6 An optical density trace for cooling 40% sulphuric acid solution saturated with G-acid dipotassium salt monohydrate at 69°C at a rate of 1.0°C.min^{-1}.

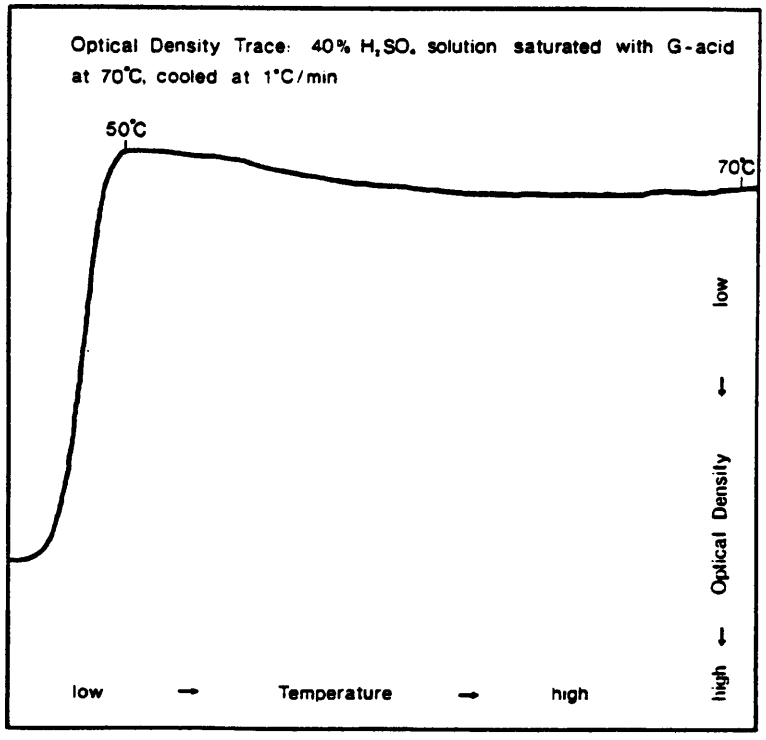

4.5 Discussion

In the case of supersaturation generated by addition of potassium sulphate the limit of the metastable zone was estimated from the lowest supersaturation at which nucleation did occur and the highest supersaturation at which it did not occur. Thus at 52°C the limit of the metastable zone was found to be within the range $S = 1.038$ to 1.048 while at 69°C the range was from $S = 1.013$ to 1.019. The metastable limit for supersaturation generated by cooling at $1.0°C.min^{-1}$ was estimated to be $S = 1.44$ at approximately 50°C. This value of S obtained by cooling was thus significantly greater than the limiting supersaturation, $S = 1.04$ obtained by salting out at 52°C. This difference in metastable zone width could be taken to imply that the presence of potassium sulphate crystals in some way assisted the nucleation process. However it must be noted that the induction time which defined the metastable limit at 52°C was 740s and all the potassium sulphate crystals had dissolved long before any evidence of crystallization was detected. This suggests that the presence of potassium ion reduces the metastable zone width rather than the potassium sulphate crystals acting as favourable nucleation sites. This suggestion could be tested by investigating the effect on the metastable zone width of supersaturation generated by addition of concentrated potassium sulphate solutions.

The role of the crystals may be quite significant however in those experiments where the induction times were quite short. The dissolution of the potassium sulphate crystals results in localised regions of elevated supersaturation in the boundry layer surrounding the crystals where the dissolved potassium sulphate mixes with the G-acid solution. In such regions of localised high supersaturation the critical cluster size for formation of a stable nucleus would be lower than in the bulk solution. In such a region a cluster could grow quite rapidly and if it remained in a region of elevated supersaturation long enough it could attain a size greater than the critical cluster size for the bulk supersaturation level. Such a nucleus would then grow rather more slowly in the bulk of the solution at the bulk supersaturation level. In this case the supersaturation level at the point of nucleation would exceed the bulk supersaturation calculated from the solution composition. Clearly such a process would be very dependent upon the rate of mass transfer to and from the boundry layer around the dissolving crystal. This theory complicates the interpretation of the

metastable zone width data obtained from experiments where supersaturation was generated by salting out with crystalline reagent. A similar effect could be envisaged for salting out with a dissolved reagent or for drowning out. Though in these cases the reagent may be mixed with the bulk solution more quickly and the probability of a nucleus remaining in a region of elevated supersaturation for a significant length of time would be lower.

In the preceding discussion it has been assumed that the measured induction time is the time required for nucleation to occur. However there are two other processes to be considered, one preceding nucleation and one following it. After supersaturation is generated a "relaxation period" is required to achieve a quasi-steady state distribution of molecular clusters before nucleation occurs. Following nucleation a period of growth is necessary before the nuclei reach a detectable size.

Nielsen (1964) estimated the relaxation time (in seconds) to be $10^{-13} * D^{1}$ where D is the diffusivity of the crystallizing species in a saturated solution. In dilute aqueous solution the value of D for low molecular weight electrolytes is approximately $10^{-5}cm^2.s^{-1}$ and therefore the relaxation time was estimated to be $10^{-8}s$. Dunning (1955) reported relaxation times approaching 100 hours for highly viscous sucrose solutions where the diffusivity was much lower.

In the present study Nielsen's value of $10^{-8}s$ was taken to be a suitable approximation for the relaxation period and therefore the relaxation period was considered to have little effect on the measured induction periods.

The time required for nuclei to grow to a detectable size depends on the growth rate and the detection limit. The minimum detectable size is a function of the method of detection and the crystal concentration. Prostakov et al (1982) compared induction times determined from optical density measurements with three techniques based on measurement of the solution parameters; conductivity, concentration and solute activity. They reported induction periods determined from optical densities of approximately half to one third of those determined by the other techniques. Mullin and Jancic (1979) reported that visual detection may be possible for particles as small as 10μm while for particles of approximately 2μm the Coulter Counter was found to be suitable. Janse and de Jong (1978) stated that the visual detection limit

is a function of illumination, agitation and crystal concentration and the minimum limit for visual detection which they reported was approximately 60μm. Wojciechowski and Kibalczyc (1986) gave the detection limit for laser light scattering to be between 1 and 2μm.

Various authors have reported the phenomenon of growth rate size dependency. In some systems small crystals grow more slowly than larger ones under identical conditions. Garside and Jancic (1976) reported the linear growth rate for 70μm potash alum crystals to be twenty times greater than the growth rate for 3μm crystals. It is difficult to measure the growth rate of sub-micron sized crystals but it might be speculated that their growth rate would be very slow.

In Chapter 5 of this study some evidence of growth rate size dependence is reported for the G-acid system. However it was not possible to quantify the extent of the growth rate size dependence. In the absence of any information on the growth rate of sub micron sized crystals of G-acid dipotassium salt monohydrate a growth rate measured for larger crystals has to be assumed, although this assumption may result in an underestimate of the growth period's contribution to the measured induction time. The size independent growth rate at 50°C for a supersaturation ratio of S = 1.05 was estimated from subsequent work reported in Chapter 5 to be between $1.4*10^{-9}ms^{-1}$ and $7.5*10^{-10}ms^{-1}$. On this basis growth from 0 to 1μm would take between 700 and 1320s. This is similar to the measured induction time of 740s.

In view of these considerations, the results of these experiments have been used merely to provide a measure of the metastable zone limits under the experimental conditions. This enables estimation of an upper limit for the level of supersaturation to be used in a seeded crystallizer to avoid catastrophic nucleation, although it is very likely that the limiting value for secondary nucleation may be very much lower.

No values of interfacial tension for G-acid dipotassium salt monohydrate are reported in the literature and so no comparisons can be made with the values calculated here. Interfacial tension values have been reported for two amino acids nucleating from aqueous solution; Walton (1965) quoted a value for the interfacial tension of glycine as 29 mJm^{-2} determined by Lo (1965) and Black and Davey (1988) report the interfacial tension of L-glutamic acid as 6 mJm^{-2}. Nyvlt (1972) compared published

values of several inorganic compounds; where more than one value was available for the same substance interfacial tensions showed wide variations. For example reported values for the interfacial tension of potassium chloride measured under nominally similar conditions ranged from 0.45 to 151 mJm^{-2}. The conclusion drawn by Nyvlt in view of these wide variations was as follows. "The immense spread of these values suggests that interfacial tension has perhaps no physical meaning and thus is only an adjustable parameter in the equations. This concerns nucleation in condensed phases only, since the classical model is perhaps more realistic for nucleation in vapours."

The calculated values for interfacial tension of G-acid dipotassium salt monohydrate in this current work therefore probably have little theoretical significance.

5 Determination of Crystallization Kinetics

5.1 Objectives

A substantial proportion of the crystallization kinetics reported in the literature concern inorganic materials grown in lean slurries. The work reported in this chapter describes an attempt to measure crystallization kinetics of an organic compound grown at high slurry densities under conditions similar to those used industrially.

There are no reports concerning the growth and nucleation kinetics of G-acid dipotassium salt monohydrate in the literature despite its large scale industrial manufacture and its importance as a dyestuffs intermediate. The aim of the experimental work reported in this chapter was to determine the growth and nucleation kinetics of G-acid dipotassium salt monohydrate crystallized from aqueous sulphuric acid solutions under a number of different conditions similar to those encountered in the industrial process. The crystallization conditions investigated were the degree of supersaturation, crystallization temperature and hydrodynamics. The effect of magma density on nucleation kinetics was also investigated. Variations in these parameters were achieved by adjusting the cooling rate and seed loading in a series of batch crystallization experiments. The objective of determining these crystallization kinetics was two fold: firstly to provide data in order to develop a model of the process which suggest ways of improving the industrial crystallization of this material; and secondly to assess the usefulness of this type of technique and to suggest improvements for the crystallization of other materials.

5.2 Theory

There are two procedures commonly used to elucidate crystallization kinetics from a series of measured crystal size distributions, one is a graphical procedure, the other is a mathematical one based on evaluating the moments of the crystal size distributions. Both methods are most useful when the crystal size distribution can be measured accurately to near zero size.

5.2.1 Determination of crystallization kinetics using a graphical procedure

Both growth and nucleation kinetics can be estimated from a series of experimentally measured crystal size distributions using a simple graphical procedure. A sequential series of crystal size distributions, typically expressed as cumulative number oversize or log cumulative number oversize distributions are plotted against size as indicated in Figure 5.1. The growth rate is evaluated by determining the increase in size between successive CSD plots for a suitable cumulative number oversize. The estimated increase in size is then divided by the time interval between the measurement of the two size distributions to get an estimate of the mean growth rate. The nucleation rate is determined from the increase in cumulative number oversize at zero size. As it is not practical to measure the crystal size distribution to zero size the measured distribution must be extrapolated to zero size. This extrapolation can introduce a significant error in the estimate of nucleation rate.

Figure 5.1 Estimation of crystallization kinetics using a graphical procedure from idealised log cumulative number oversize against size plots.

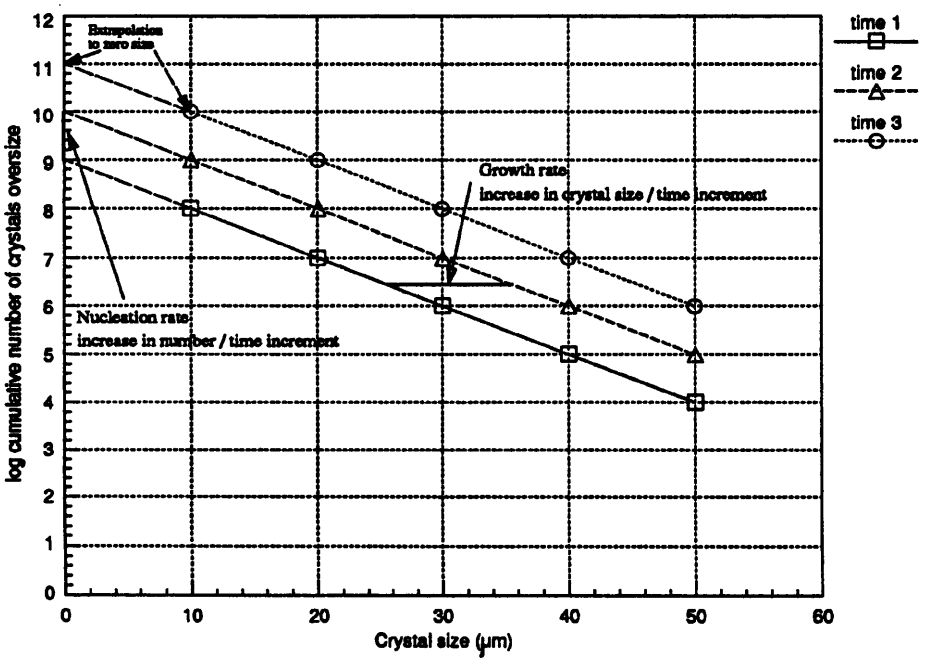

5.2.2 Determination of crystallization kinetics using the moments method

Adequate mathematical representation of a crystallization process requires information concerning both the solution and the crystals suspended within it. The necessary information pertaining to the suspended crystals may be considered in terms of a population balance. Such information, used in conjunction with the mass and energy balances with their associated equilibria and rate equations, permits mathematical representation of the system.

The population density, n is defined as the number of crystals, dN, of characteristic length between L and $L + dL$, per unit volume of solution. ie.

$$n = \frac{dN}{dL} \qquad 5.1$$

A population or number balance requires that, over some time increment, the increase in the number of particles in a particular size range is equal to the difference between the number of particles entering the size range and the number leaving it. For a batch crystallizer in which crystal breakage and agglomeration are considered to be insignificant particles enter and leave a size range solely by growth. Assuming that all nuclei form at zero size and that the growth rate is independent of crystal size the population balance equation according to Randolph and Larson (1971) is:

$$\frac{dn}{dt} + \frac{d(nG)}{dL} = 0 \qquad 5.2$$

where G is the overall change in length per unit time per crystal, ie.

$$G = \frac{d\bar{L}}{\bar{\mathcal{N}}dt} \qquad 5.3$$

$\bar{L}$ is the sum of the characteristic lengths of all the crystals within the distribution averaged over the time increment, dt. $\bar{\mathcal{N}}$ is the average of the total number of crystals in the distribution during the same time increment.

Moment transformation of the population balance equation with respect to size using the general moment transformation equation, Equation 5.4, yields a set of moment equations, Equations 5.5 to 5.8

$$\mu_j = \int_0^\infty f(L) L^j dL \qquad 5.4$$

where μ_j is the jth moment of some function $f(L)$. If $f(L)$ is the population density, n, then;

$$\frac{d\mu_0}{dt} = B \qquad 5.5$$

$$\frac{d\mu_1}{dt} = \mu_0 G \qquad 5.6$$

$$\frac{d\mu_2}{dt} = 2\mu_1 G \qquad 5.7$$

$$\frac{d\mu_3}{dt} = 3\mu_2 G \qquad 5.8$$

These first four moments, μ_0 to μ_3 can be shown to have physical significance as follows:-

$$\mu_0 = \int_0^\infty n dL = \mathcal{N}, \quad \text{the total number of crystals} \qquad 5.9$$

$$\mu_1 = \int_0^\infty nL dL = \mathcal{L}, \quad \text{the sum of the characteristic lengths} \qquad 5.10$$

$$\mu_2 f_A = f_A \int_0^\infty nL^2 dL = \mathcal{A}, \quad \text{the sum of the individual surface areas} \qquad 5.11$$

$$\mu_3 f_V = f_V \int_0^\infty nL^3 dL = \mathcal{V}, \quad \text{the total crystal volume} \qquad 5.12$$

Here f_A and f_V are the area and volume shape factors.

A distinction is drawn between seed crystals and crystals grown from nuclei generated within the crystallizer by using the convention recommended by Jones and Mullin (1974), that is subscripting them *S* and *N* respectively. In this way the crystal size distribution can be considered as two separate distributions, *S* and *N*. The rate of solid deposition on the seed crystals per unit volume of solvent can then be expressed as:

$$\frac{dW_S}{dt} = \frac{3W_{S_0}L_S^2G}{L_{S_0}^3S} \qquad 5.13$$

where W_S is the weight of seed crystals. The rate of solid deposition on the nuclei (*N* crystals) may be determined from Equations 5.8, 5.11 and 5.12;

$$\frac{dW_N}{dt} = \rho_c f_V \frac{d\mu_3}{dt} = \rho_c f_v 3\mu_2 G = \frac{\rho_c f_v 3\mathcal{A}G}{f_A} \qquad 5.14$$

The supersaturation balance equation can be expressed as:

$$\frac{d\Delta C}{dt} = \frac{dC^*}{dt} + \frac{dW_S}{dt} + \frac{dW_N}{dt}$$

$$= \frac{dC^*}{dt} + \frac{3W_{S_0}}{L_{S_0}^3 S} + \frac{\rho_c f_V 3\mathcal{A}G}{f_A} \qquad 5.15$$

The population balance equation, Equation 5.2, coupled with the supersaturation balance equation, Equation 5.15, through the set of moment equations, Equations 5.5 to 5.8, provides a mathematical description of a batch crystallizer operated within the constraints of size independent growth kinetics, and assuming negligible breakage and agglomeration.

If a series of size distributions is measured during the course of a batch crystallization process, simultaneous estimation of growth and nucleation kinetics is possible using this mathematical representation of the system. The zeroth, first and second

moments are calculated for a pair of size distributions separated by a small time interval Δt. The moment equations, Equations 5.5 to 5.7, can be rearranged and the derivatives converted to differentials to give

$$\overline{B} = \frac{\Delta \mu_0}{\Delta t} \qquad 5.16$$

$$\overline{G} = \frac{\Delta \mu_1}{\overline{\mu}_0 \Delta t} \qquad 5.17$$

$$\overline{G} = \frac{\Delta \mu_2}{\overline{\mu}_1 \Delta t} \qquad 5.18$$

where Δ represents the difference between the measured parameters at t and t + Δt. A bar above a quantity indicates the mean value of the quantity over the time interval Δt. In this way the mean overall growth and nucleation rates can be estimated for successive pairs of size distributions measured during a batch crystallization.

Andersen and White (1971) report that weighting of the moments is desirable in order to reduce the contribution of the extremes of the crystal size distribution, where considerable error may be introduced from unrepresentative sampling, especially at the largest sizes. Tavare and Garside (1986a) note that it is advantageous to estimate $\overline{G}$ and $\overline{B}$ in the Laplace transform domain rather than the time domain since the solution of the Laplace transformed differential equations is more straightforward. Experimentally determined population densities may be converted into the Laplace transformed response with respect to size by:

$$\overline{n}(s,t) = \int_0^\infty n(L,t) e^{-sL} dL \qquad 5.19$$

Transformation of the population balance equation, Equation 5.2, gives

$$\frac{d\overline{n}(s,t)}{dt} + G(s\overline{n}(s,t) - n(0,t)) = 0 \qquad 5.20$$

G and $n(0,t)$ are functions of time but, over a small time interval Δt, may be assumed to be constant at the mean values. With the assumption that all nuclei form at zero size Equation 5.20 reduces to:

$$\frac{d\overline{n}(s,t)}{dt}+\overline{G}s\overline{n}(s,t)-\overline{B}=0 \qquad 5.21$$

According to Tavare and Garside (1986a) transforming the derivatives to differentials gives:

$$\frac{\Delta\overline{n}(s,t)}{\Delta t}-G\overline{sn(s,t)}+\overline{B}=0 \qquad 5.22$$

A plot of $\frac{\Delta\overline{n}(s,t)}{\Delta t}$ versus $s\overline{n(s,t)}$ over an optimal range of the Laplace transform variable, s, should yield a straight line with slope $-\overline{G}$ and intercept $\overline{B}$.

5.2.3 Correlation of measured growth and nucleation kinetics with experimental conditions

If mean growth and nucleation rates are obtained, using either of the methods described above, over a range of experimental conditions the dependence of the growth and nucleation kinetics on the experimental variables investigated may be determined by correlation. Palwe et al. (1985) proposed a general growth rate equation which may be expressed as:

$$\overline{G}=K_g\Delta C^g N^{m_g}e^{-E_g/RT} \qquad 5.23$$

This expression allows consideration of the dependence of growth rate on temperature, supersaturation and agitation conditions. A similar empirical power law relationship may be used to correlate the nucleation kinetics.

$$\overline{B}=K_b\Delta C^b M_T^j N^{m_b}e^{-E_b/RT} \qquad 5.24$$

Use of a multivariable correlation technique enables estimates to be made for the dependence of growth and nucleation rates on each of the parameters investigated.

5.3 Experimental Procedures

A series of batch crystallizations was performed at the 1 litre scale over a range of conditions to enable the effects of key parameters to be investigated. During the course of each experiment crystal size distributions were determined periodically to enable kinetic data to be obtained.

5.3.1 The Crystallizer.

A series of batch cooling crystallization experiments was performed in an all-glass crystallizer of 1L capacity shown in Figure 5.2. The experimental arrangement is shown in Figure 5.3 and Plate 5.1. The crystallizer had a concave base and its base and sides were jacketed. Agitation was provided by a glass anchor-shaped agitator which was rotated by a stirrer equipped with a digital tachometer. The geometry was similar to that of the industrial unit employed by I.C.I. Organics Division for the crystallization of this material.

The temperature within the crystallizer was monitored using both a mercury in glass thermometer and a platinum resistance thermometer which was connected to the water bath used for temperature control. The stainless steel clad platinum resistance thermometer was enclosed in a thin walled glass tube to prevent corrosion. The annular space between the thermometer and the glass tube was filled with silicone oil to ensure good thermal contact. The shielded platinum resistance thermometer had a slightly greater time constant than the mercury in glass thermometer. In the subsequent experimental work the temperature indicated by the mercury in glass thermometer was taken to be the crystallizer temperature.

Temperature control was achieved by circulating water from a temperature programmed water bath. The temperature programmer permitted both linear and non-linear cooling rates to be employed.

Figure 5.2 The 1 litre crystallizer vessel used in this study.

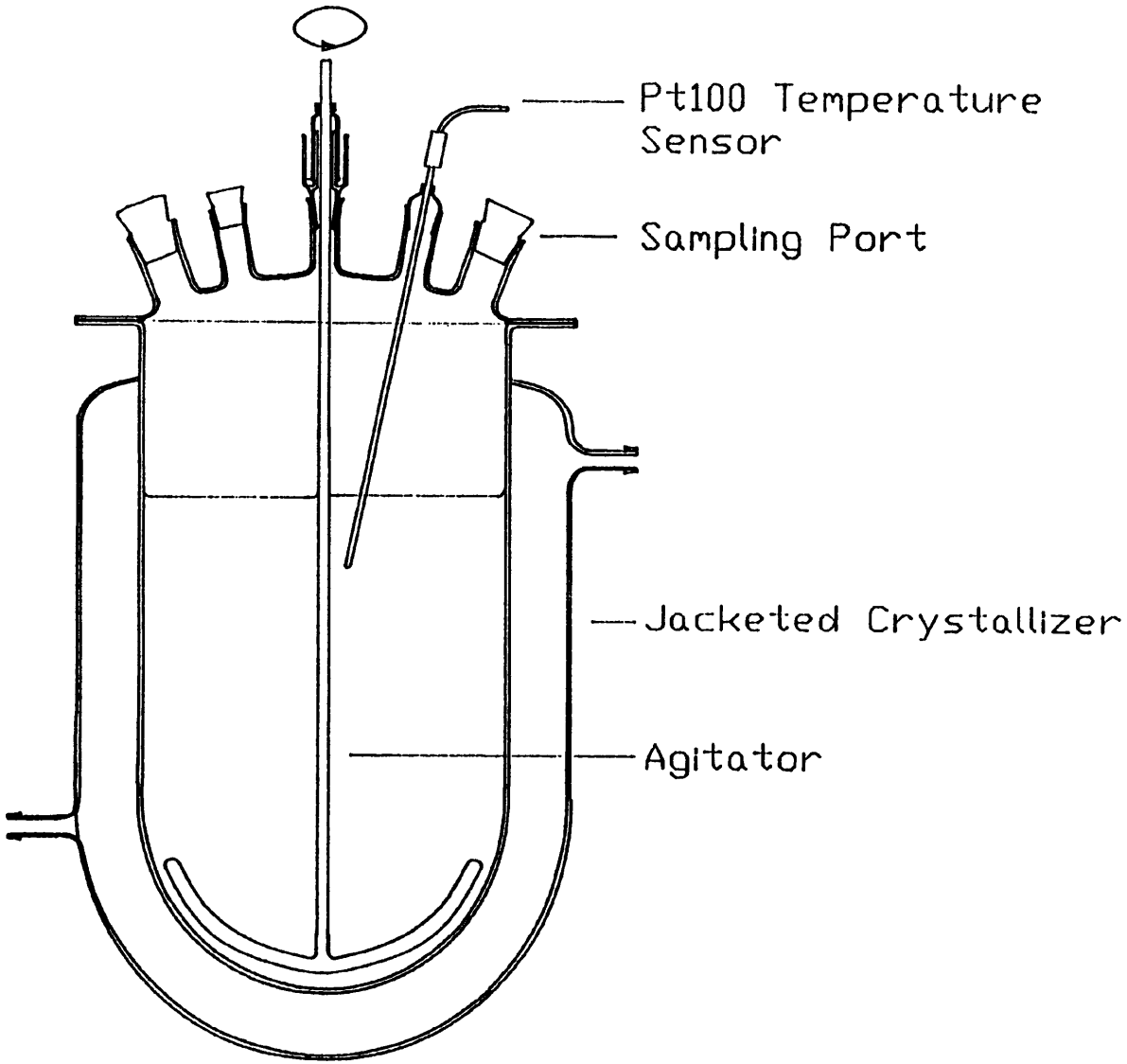

Figure 5.3 A schematic diagram of the crystallizer and associated apparatus.

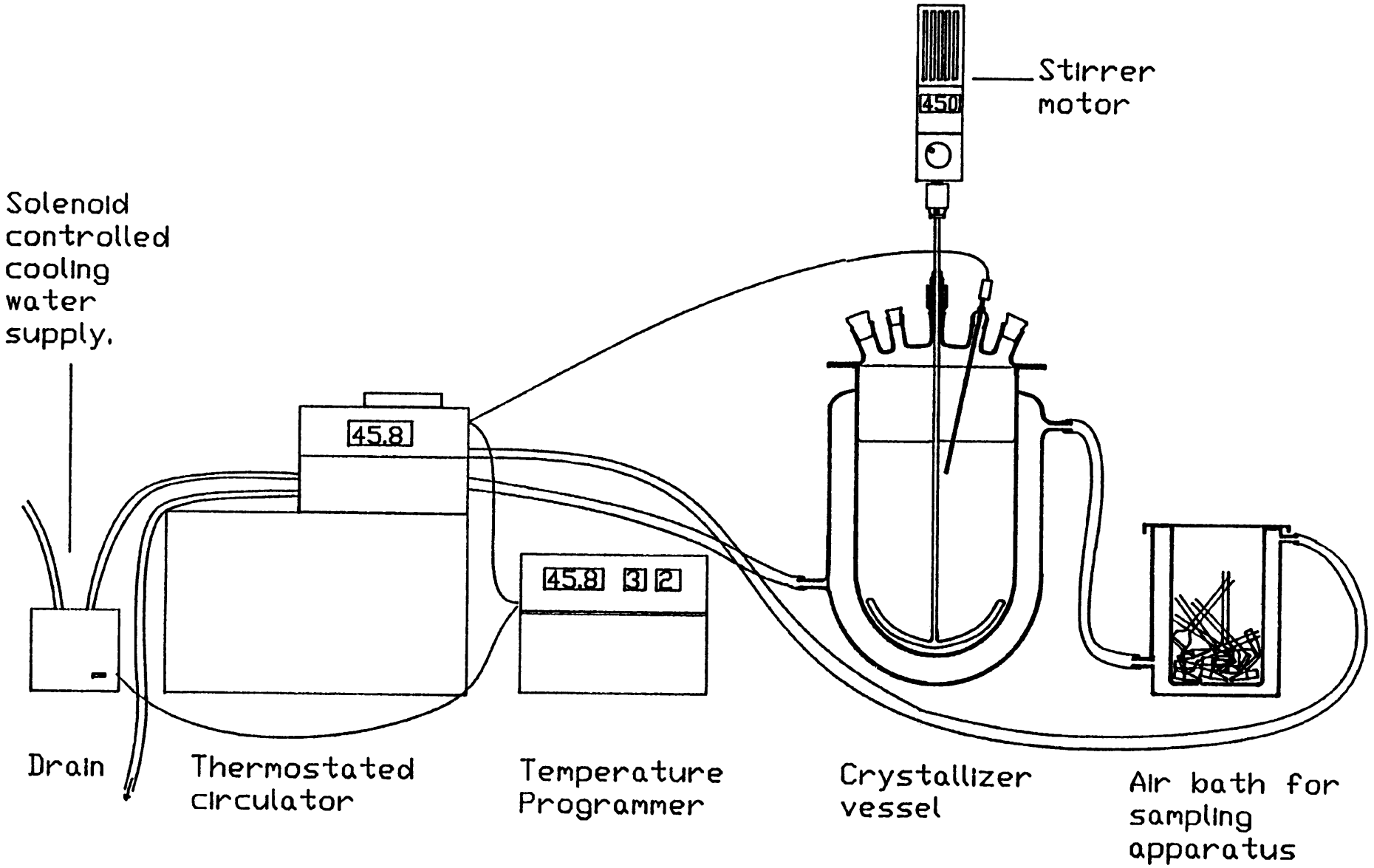

Plate 5.1 The crystalliser and associated apparatus

5.3.2 Operation of the crystallizer.

The equipment used for taking both slurry and solution samples from the crystallizer was pre-heated to the crystallizer temperature in an air bath which consisted of a jacketed beaker situated down stream from the crystallizer in the circulation loop. Addition of material to the crystallizer and sampling from it was achieved via a sampling port in the crystallizer lid.

In a typical experiment a sulphuric acid solution of 40g H_2SO_4 per 100g solution was saturated with G-acid dipotassium salt monohydrate at 80°C. A sample of the saturated solution was taken using the *in-situ* filtration technique described in Chapter 3. The sample was analysed to ensure that the solution was saturated. The remaining saturated solution was filtered through a pre-warmed glass micro-fibre filter of pore size 1.6μm. A known mass of this filtrate was then added to the crystallizer via the sampling port. The temperature of the crystallizer was maintained approximately 5°C higher than the saturation temperature for approximately 15 min in order to dissolve any nuclei or very small crystals which had passed through the micro-fibre filter. Controlled cooling was commenced. A solution sample was taken for concentration analysis. The temperature of the crystallizer was measured at the time of sampling to an accuracy of ±0.1°C. A slurry sample was also taken from the crystallizer and subjected to particle size analysis using an Elzone Particle Size Analyser (see Plate 5.2). These two samples were taken to confirm that the solution in the crystallizer was crystal free and that the G-acid solution was saturated at the required temperature.

Slurry samples were taken using a variable volume micro-pipette. The pipette tips were prepared by cutting off 2mm from the tip in order to enlarge the aperture from 500μm to approximately 1500μm. This was found to be large enough to remove any possibility of blockage during sampling in the later stages of the experiment when the crystal slurry was dense and yet permitted reproducible sampling without dripping. The pipette tips were pre-warmed in the air bath prior to use. The sample was always taken from the same place in the crystallizer, the point being governed by the size and location of the sampling port. The sampling depth was 4cm which represented the maximum depth to which the pipette tips could be safely immersed.

The micro-pipette was allowed to fill at a rate of approximately 200µl.s^{-1} in order to minimise segregation of particles during sampling. This sampling technique was found to be reasonably reproducible. The slurry sample was added to a known volume of electrolyte prior to measurement of the crystal size distribution with an Elzone Particle Size Analyser.

5.3.3 Particle Sizing.

The advantages and disadvantages of different methods of sizing G-acid crystals were assessed and the results are summarised in Table 5.1. Electrical zone sensing was selected as the most acceptable size measurement method with the least shortcomings.

Table 5.1 The advantages and disadvantages of different crystal sizing equipment for sizing G-acid dipotassium salt monohydrate crystals.

Method	Advantages	Disadvantages
Microscopy	Accurate size and shape measurements can be made. Crystals can be photographed.	High magnification needed. Difficult to size a large number of crystals. Subjective crystal selection. Sampling problems.
Sieving	Provides a fraction of crystals below the upper sieve size. Provides a screened product useful for seeding.	Difficult to sieve to completion. Crystals likely to be damaged. Provides no information about crystal numbers. High minimum size (approx 20µm). Crystals must be washed and dried. Crystal shape unfavourable for sieving.
Electrical zone sensing (Elzone or Coulter Counter)	Possible to count and size (by volume) a statistically valid number of crystals. Low minimum size.	Only possible to measure in a dilute suspension. Slurry sample must be diluted.
Laser light diffraction (Malvern)	Rapid sizing possible	Does not provide reliable information on numbers of crystals. May be difficult to relate measured size to the crystal size for plate-like crystals. Can only size a dilute suspension.

5.3.3.1 The Elzone 80XY Particle Size Analyser.

The Elzone Particle Size Analyser measures the volume of individual crystals in a very dilute suspension. A slurry of crystals in an electrolyte is maintained as a

homogeneous suspension by agitation. Crystals are sized as they are sucked through an orifice at a controlled rate. Electrodes on opposite sides of the orifice are used to create a potential difference across the orifice. As crystals pass through the orifice they alter its electrical resistance, these changes in resistance (or other related properties such as capacitance and current) can be monitored and related to the particle size. When a sufficient number of particles have been sized in this way the data may be summed to generate a size distribution. The Elzone Particle Size Analyser is shown schematically in Figure 5.4. Plate 5.2 is a photograph showing the Elzone 80XY and the associated apparatus.

Figure 5.4 A schematic diagram of the Elzone 80XY Particle Size Analyser.

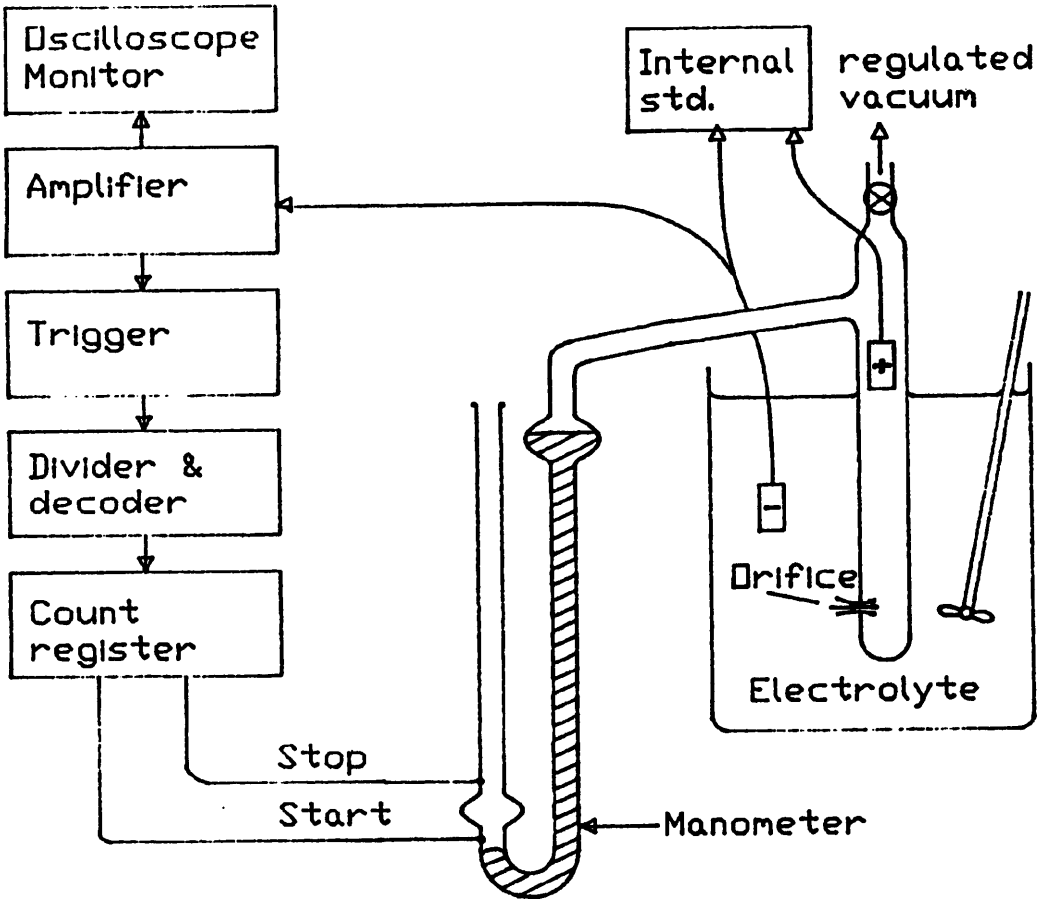

Plate 5.2 The Elsone 80XY Particle Size Analyser and the Kaypro 10 Microcomputer.


PARTICLE SIZE
ANALYSIS (ELZONE)
ELZONE MONITOR
ELZONE
80XY
POWER
MANNESMANN

Plate 5.3 A series of photomicrographs showing typical G-acid dipotassium salt monohydrate crystals. The photographs show crystals grown under different conditions and are taken at different magnifications.

G-acid dipotassium salt monohydrate crystals grown from industrial sulphonation mass by drowning out with potassium sulphate solution and cooling.

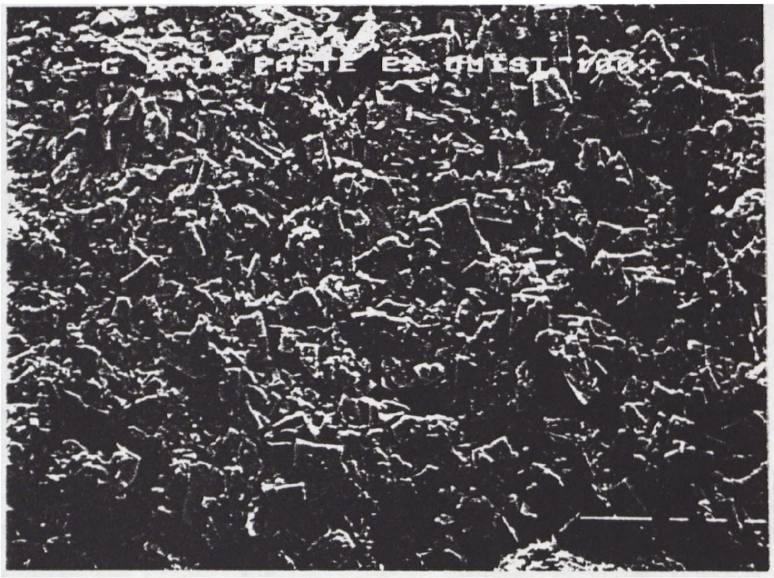

G-acid dipotassium salt monohydrate crystals grown from aqueous sulphuric acid solution by cooling.

G-acid dipotassium salt monohydrate crystals grown from aqueous sulphuric acid solution by cooling and evaporation.

G-acid dipotassium salt monohydrate crystals grown from aqueous solution by slow evaporation.

G-acid dipotassium salt monohydrate crystals grown from aqueous solution by slow cooling. This photograph shows the thickness of the crystal in relation to its length.

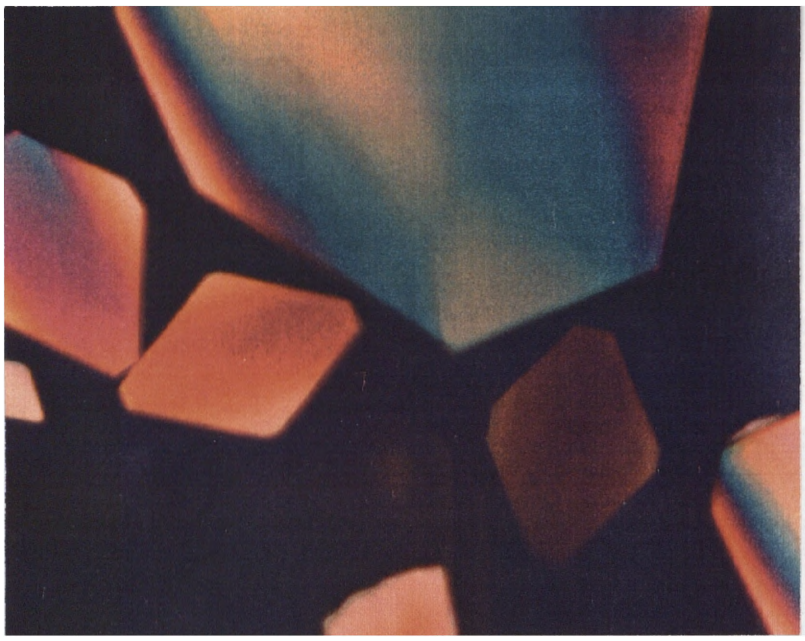

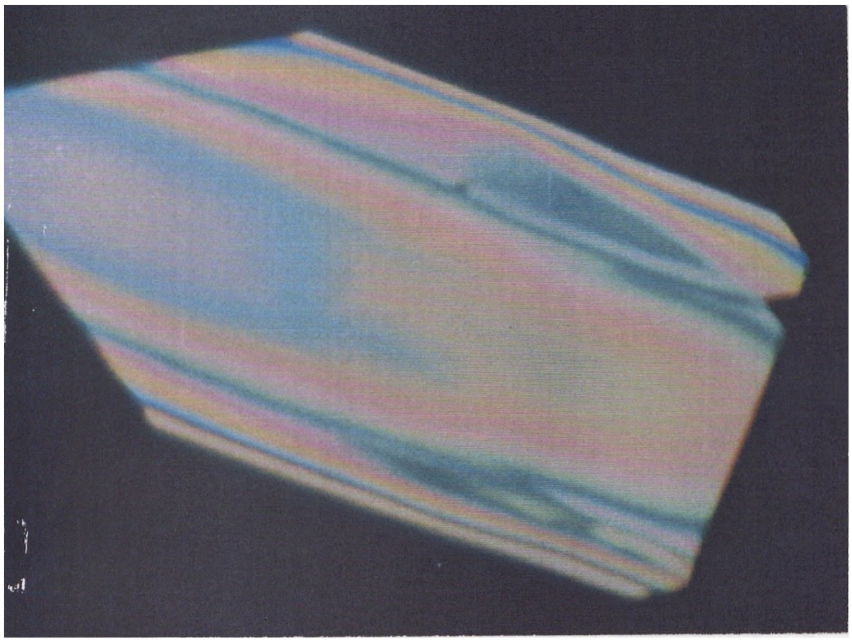

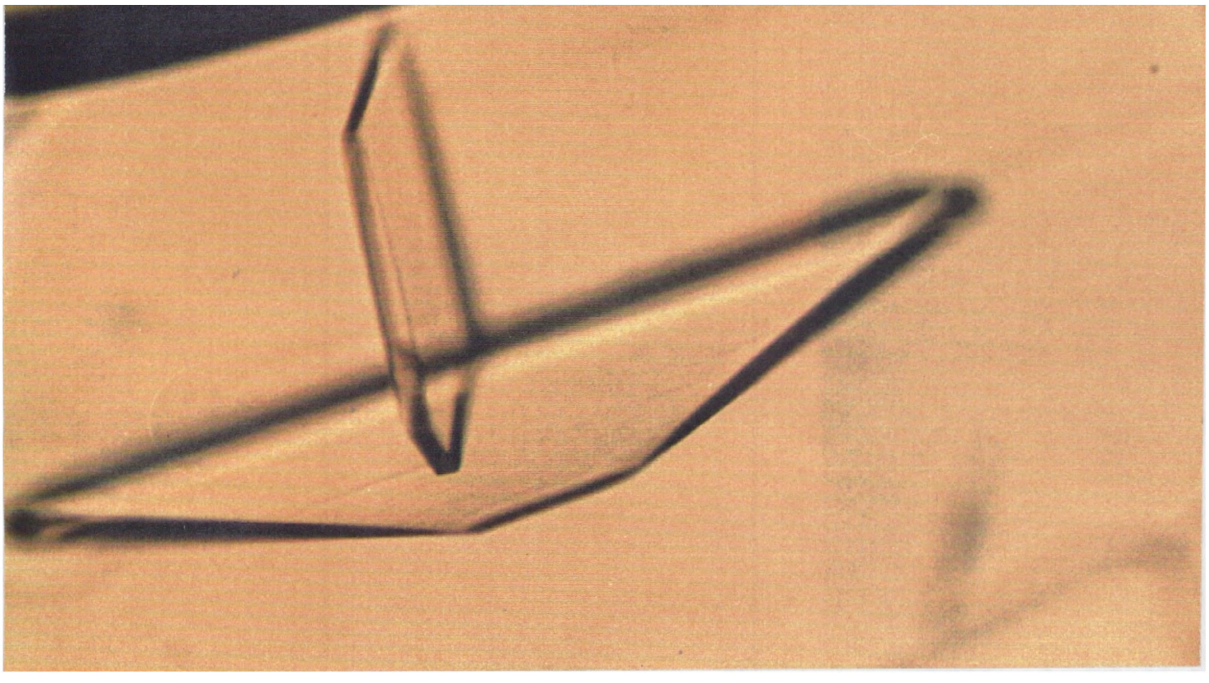

5.3.3.2 The effect of crystal habit in sizing G-acid crystals.

The volumetric size distributions measured by the Elzone are converted to diameter distributions by assuming the crystals are spherical. In the case of G-acid dipotassium salt monohydrate crystals this has been shown not to be the case, microscopic observation of the crystals revealing them to be thin rectangular plates with an aspect ratio of approximately 1:0.8:0.05. A series of photomicrographs of typical crystals is shown in Plate 5.3. As a consequence of the crystal habit the crystal size measured by the Elzone must be related to the crystal size determined by other methods, especially microscopy and sieving. This size relationship is shown in Figure 5.5.

Figure 5.5 A diagram showing the relationship between the crystal size determined by sieving and microscopy and the crystal volume determined using the Elzone 80XY Particle Size Analyser.

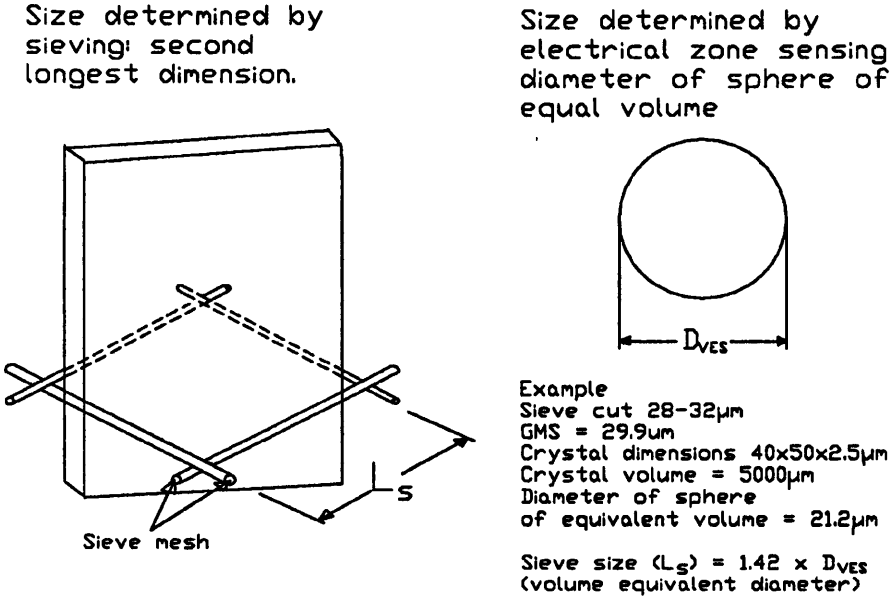

Sieving measures the second largest linear dimension of a crystal perpendicular to the longest axis. The plate-like crystals examined in this study may pass diagonally

through the square of a sieve mesh so the measured geometric mean sieve size is about 0.7 times this second largest dimension. The volume equivalent diameter size measured by the Elzone is around 70% of this geometric mean sieve size.

5.3.3.3 Particle size analysis with the Elzone 80XY particle size analyser

The electrolyte used with the Elzone Particle Size Analyser (model 80XY) was an aqueous solution of G-acid dipotassium salt monohydrate saturated at ambient temperature. This electrolyte was found to have a specific conductivity well within the range required for the Elzone Particle Size Analyser to function effectively (Particle Data 1981). The electrolyte was made up in 2.5L batches by the addition of excess G-acid dipotassium salt monohydrate to distilled water and agitating at ambient temperature without temperature control. This saturated solution was removed immediately prior to use and filtered through a membrane filter of pore size 0.45μm. In this way an electrolyte was produced that was saturated at the working temperature in the laboratory. This was found to be preferable to saturating the solution at some fixed temperature close to ambient as the temperature of the electrolyte tended towards ambient during use, resulting in it becoming either supersaturated or undersaturated. If the electrolyte was supersaturated it was found to be liable to crystallize during use whilst if it were undersaturated the crystals in the slurry sample were found to dissolve rapidly. Attempts to control the temperature of the electrolyte at all stages during its use were found to be impractical.

The Elzone Particle Size Analyser was calibrated in the logarithmic mode in accordance with the instrument manual using standard 13.2μm latex spheres supplied by Coulter Electronics Ltd. Adjustments for any slight variation in electrolyte concentration (and hence specific conductivity) during the course of an experiment were made using the instrument "normalisation" facility. During normalisation, constant amplitude current pulses are generated at the orifice. These current pulses behave as "standard" particles and enable the calibration to be re-validated. The normalisation procedure was performed each time freshly filtered electrolyte was added to the counting cell, prior to determining a background particle size distribution. Normalisation was repeated immediately after the addition of a slurry sample from the crystallizer. This re-normalisation was necessary because the

solution portion of the slurry sample was approximately 40% by weight sulphuric acid which caused the specific conductivity of the electrolyte to increase. Immediately after this second normalisation the crystal size distribution of the slurry sample was determined.

The presence of sufficiently few particles in the freshly filtered electrolyte was confirmed by measuring the crystal size distribution with the Elzone instrument. If fewer than 100 particles per ml greater than 4.5μm in diameter were detected the electrolyte was considered to be satisfactory. Saturation of the electrolyte was established before commencing an experiment by addition of a few mg of crystals of G-acid dipotassium salt monohydrate from the of sub-28μm sieve cut to the electrolyte in the counting cell. The size distribution was determined after approximately 5 s agitation and again after about 3 min. If the two distributions revealed little change during this interval the electrolyte was considered to be saturated.

In order to limit possible changes in the crystal size distribution between withdrawal of a sample from the crystallizer and measurement of its size distribution every effort was made to minimise the interval between sampling and analysis; typically this time was around 30s.

Prior to commencing an experiment the size distribution of a slurry sample from the crystallizer was determined as follows. A known volume of freshly filtered electrolyte was transferred to the Elzone counting vessel and after normalisation a background particle size distribution was measured and stored. A slurry sample was taken from the crystallizer in the manner described earlier and added to the electrolyte in the counting vessel. After a few seconds agitation at a predetermined rate the instrument was re-normalised and the size distribution was measured and stored. The background size distribution was subtracted from the sample size distribution and the resulting distribution stored on a micro-computer. The crystal size distribution in the crystallizer was calculated from this resultant distribution by taking into account the volume dilution used (subtracting the approximately 2ml sample of electrolyte used to determine the background size distribution from the electrolyte volume). This initial size distribution was determined in order to confirm the absence

of particles in the crystallizer. If this size distribution revealed there were very few particles present in the crystallizer then the experiment commenced and controlled cooling was continued until the end of the experiment.

Approximately every 15 min (timed precisely) a solution sample was taken using the technique described earlier, the time and temperature at which the sample was taken being recorded. Immediately following this, a slurry sample was obtained by the method described above, and the time and temperature of sampling were recorded. The sample was immediately transferred to a known mass of freshly filtered electrolyte in the Elzone counting vessel and after approximately 5 s agitation the instrument was re-normalised and the crystal size distribution was measured. The particle size distribution of the fresh electrolyte had been measured just prior to the addition of the slurry sample. This size distribution was subtracted from the sample crystal size distribution and the resulting distribution recorded.

Both sampling procedures were repeated approximately every 15 min whilst the crystallizer was being cooled from 80 to 30°C. In this way a series of solution samples and crystal size distributions were obtained throughout the experiment.

5.3.3.4 Problems encountered sizing G-acid crystals.

During the course of the experiment the magma density in the crystallizer increased as crystals increased in size and new nuclei formed. Eventually the largest crystals became large enough to block the 150μm orifice tube used for the crystal size determination. The use of a larger orifice tube would have prolonged the period of time over which size distributions could have been measured. However information concerning these larger particles would have been obtained at the expense of information on the smallest particles and so increase the interval between nucleation and subsequent detection. An additional problem arising from the use of a larger orifice tube would be a reduction in the maximum permissible particle concentration for which size distributions could be measured. This would have required further dilution of the sample or removal of a smaller sample from the crystallizer.

The problem of the orifice tube blocking was partially overcome by screening the slurry sample prior to analysis. The apparatus used consisted of a 4cm length of 4cm diameter perspex tube. One end of the tube was covered with a piece of nylon sieve cloth of aperture size 100μm held in place with a heavy duty cable tie. The size of the sieve cloth was selected on the basis of the relationship between sieve size, volume equivalent size and the geometry of the crystals discussed in Figure 5.5. The 100μm sieve cloth was expected to retain crystals with a second largest dimension exceeding about 130μm, this corresponds to a volume equivalent diameter of around 70μm. A crystal of this size would have been able to block the sensing orifice only if it were orientated with its large flat faces parallel to the plane of the sampling orifice. The slurry screening process was as follows: A slurry sample was added to a known mass of electrolyte, after brief agitation the resulting suspension was poured through the screen into the counting vessel. In this way particles larger than the screen cut size were removed from the sample. Undoubtedly some smaller particles were also retained, especially towards the end of an experiment when a significant portion of the crystals from the slurry sample were retained on the sieve cloth. An attempt to reduce the retention of smaller crystals was made by washing the residue on the screen with a known mass of electrolyte which was added to that in the counting vessel. The elimination of the largest crystals from the size distribution by screening was found to significantly affect the measured size distributions especially towards the end of the experiments. This limited the usefulness of such data in estimation of crystallization kinetics.

Another problem arose during the course of the experiments as the number of crystals in the crystallizer increased. There is a maximum number concentration of particles for which accurate size distributions may be determined using a particular orifice diameter. (The manufacturers of the instrument report how the accuracy of the instrument decreases with increasing particle concentration (Particle Data 1981)). This maximum permissible particle concentration decreases rapidly with increasing orifice diameter. The limit occurs because of coincidence effects which become significant at high particle concentrations. If successive particles passing through the orifice are separated by an interval which is less than some limiting value the instrument is unable to resolve them as separate particles and so interprets the event

as the passage of a single larger particle; such an event is termed a coincidence. Levels of coincidence of 2, 5, and even 10% may in some circumstances be acceptable (Coulter Electronics, 1979). Coincidence errors were minimised by reducing the volume of the slurry sample taken from the crystallizer during the course of an experiment from an initial value of 1000µl to a minimum of 200µl. In addition the volume of electrolyte into which the sample was dispersed was increased from 100 to 200ml. Use of a larger counting vessel was found to be impractical as uniform agitation was not reliably achievable. Use of a multiple dilution technique was also attempted, but this was found to introduce significant errors, the main cause being an increase in the time interval between obtaining a slurry sample and measuring the crystal size distribution, even very slight undersaturation resulting in a significant alteration in the crystal size distribution prior to its determination.

5.3.4 Investigation of the effect of Seeding

Some experiments were performed to investigate the effect of seeding on the crystallization kinetics. In these experiments a known mass of seed crystals was added to the crystallizer soon after cooling had been commenced and the solution in the crystallizer had become supersaturated. The seeds were prepared from a batch of G-acid dipotassium salt monohydrate recrystallized from water. The seed size chosen was the fraction of crystals retained between 28 and 32µm sieves. This small seed size was selected in order to maximise the growth time before the crystals reached the upper size limit imposed by the screening procedure described above.

Determination of the crystal size distribution of the seeds using the Elzone Particle Size Analyser revealed a wide range of sizes, as seen in Figure 5.6. Figure 5.6a shows the discrete and cumulative number distributions whilst Figure 5.6b shows the discrete and cumulative volume distributions. According to Figure 5.5 the 28-32µm sieve fraction would be expected to have a mean volume equivalent diameter of around 21µm with an upper and lower size limits of 22.6 and 19.8µm respectively. Figure 5.6a, the number distribution, shows about 98% of the crystals are below the upper size limit of 22.6µm but about 96% are below the lower limit of 19.8µm. Figure 5.6b. shows the volume distribution of the seed crystals which indicates that approximately 30% of the crystals have volumes exceeding the upper size limit and about 60% have

volumes lower than the lower limit. Thus only about 10% of the crystal volume falls in the anticipated range. Microscopic examination of the crystals revealed many small crystals, crystal fragments and agglomerates which appeared to be adhering to the larger crystals (see Plate 5.4). Examination of this photomicrograph suggests that as well as the weakly adhering crystals further crystal fragments could probably be released from the surfaces of some of the larger crystals as weakly attached flakes break free as a result of collisions within the crystallizer. Further sieving was found to have little effect in removing the sub size fragments.

Attempts to dissolve the smallest of the crystals by immersing the seeds in a fractionally undersaturated solution were unsuccessful. This was mainly due to the difficulty of attaining a sufficiently small level of undersaturation such that the smallest crystals dissolved without dissolving, or at least very seriously altering, the size of the larger seed crystals. Wet sieving in an organic solvent was found to be unsatisfactory because crystals washed with a range of organic solvents were found to exhibit surface damage. This damage took the form of "crazing" or "frosting" of the originally smooth, transparent crystal faces. Consequently it was decided to use the sieved crystals as seeds despite their wide size distribution.

Plate 5.4 A photomicrograph of typical G-acid dipotassium salt monohydrate crystals seed crystals

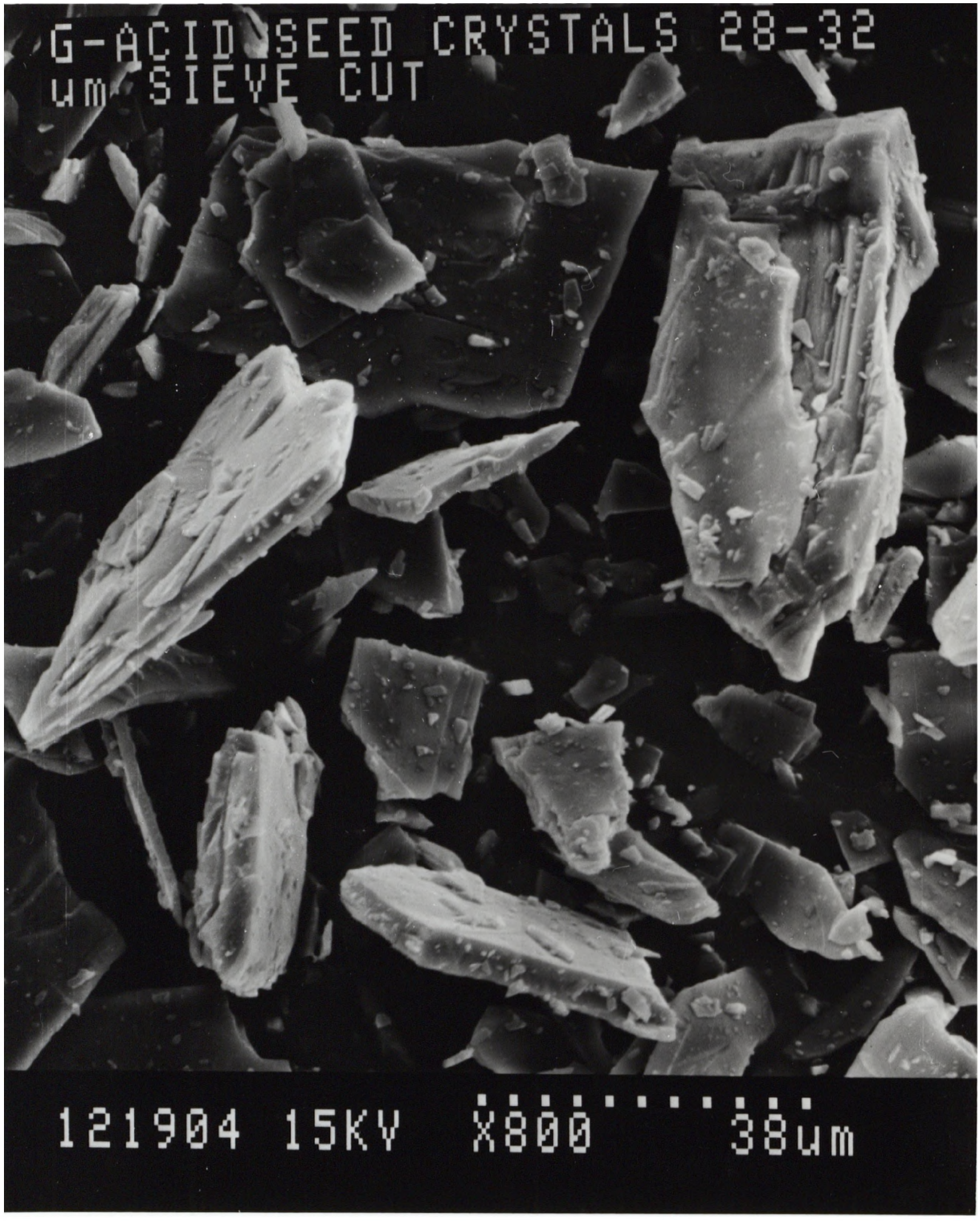
G-ACID SEED CRYSTALS 28-32
um SIEVE CUT
121904 15KV X800 38um

Figure 5.6 Seed crystal size distributions measured using the Elzone 80XY

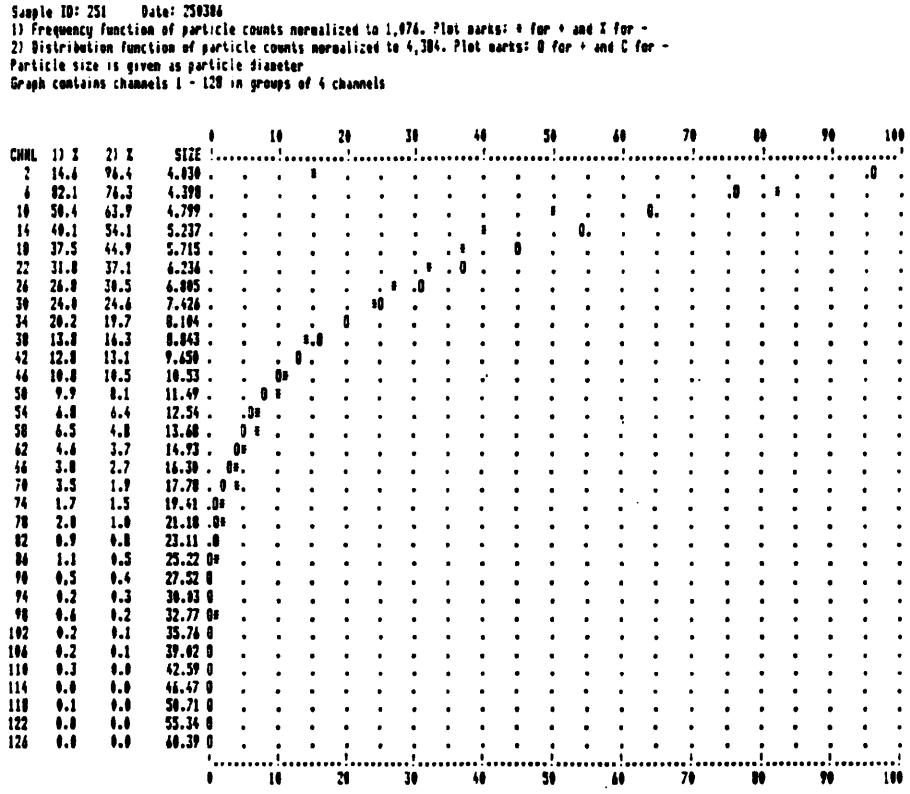

a) Discrete and cumulative number distribution

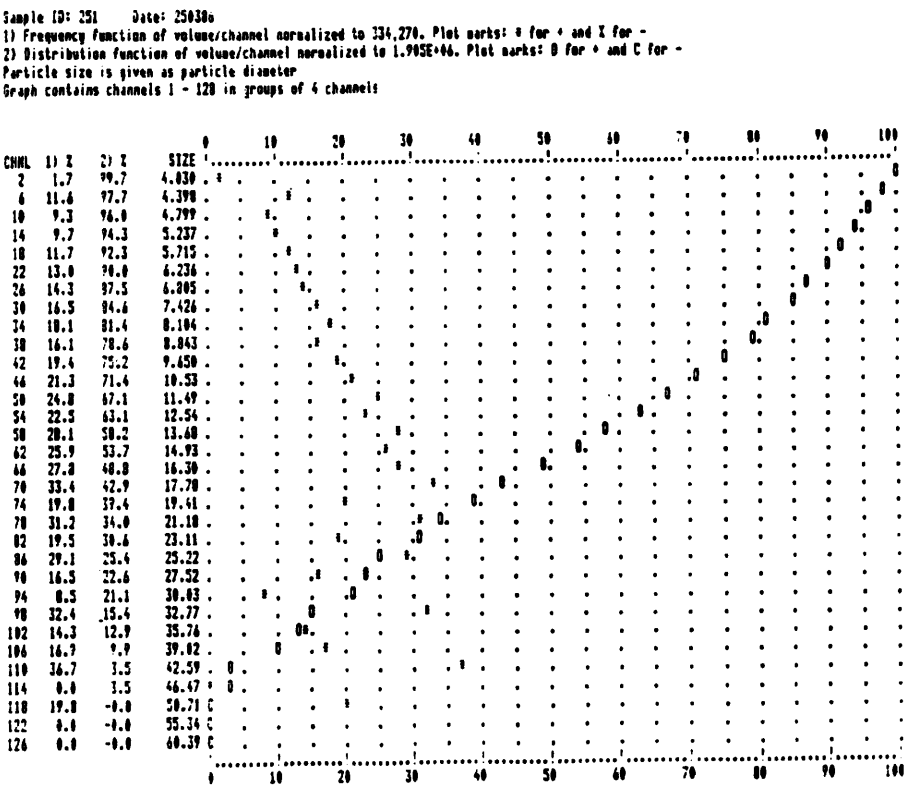

b) Discrete and cumulative volume distribution

5.4 Results

During the course of this series of batch crystallization experiments the effects of cooling rate, seed loading and agitation (and hence supersaturation, temperature, magma density and hydrodynamics) on the growth and nucleation kinetics of G-acid dipotassium salt monohydrate were investigated.

The experimental conditions investigated are listed in Table 5.2. Those highlighted with bold **X**s are considered in more detail and are used as illustrative examples in subsequent discussion of the experimental results.

Table 5.2 Experimental conditions investigated.

Seed loading (kg seed crystals/ kg 40% H_2SO_4 soln)	Cooling Rate (°C/min)		
	0.1	0.2	0.35
0		**X** X	
0.0005		**X** X	
0.0010		X	
0.0025		X	
0.0050	X X	X X X X	X

The results for each experiment included a cooling schedule, a concentration - time profile, a supersaturation - time profile and a series of measured crystal size distributions. Growth and nucleation rates were determined from successive pairs of crystal size distributions. These pairs of growth and nucleation rates were tabulated together with the mean values of the experimental variables pertaining to the time increments over which the rates were determined. The dependence of the kinetics on the values of the experimental parameters was then determined using the growth and nucleation rate equations; Equations 5.23 and 5.24.

5.4.1 Solubility Data.

The G-acid dipotassium salt monohydrate used in the experiments described in this chapter came from a different batch of material to that used in the previous chapters. The supplier's analysis of both batches of material is given in Appendix 1. Though the analyses confirmed that the two batches were similar small changes in composition may have resulted in slight solubility differences between the two

batches. Thus after several of the batch cooling crystallisation experiments the solubility of the slurry remaining in the crystallizer was used to determine the solubility of the new batch of material in the sulphuric acid solution over the working temperature range. The procedure employed was essentially similar to that described in Chapter 3, the main difference being that the potassium ion concentration was not determined. This was unnecessary because the effect of additional potassium ion on the crystallization kinetics was not investigated. The correction factor used to account for the distribution of impurities in the new batch of material was calculated from the analysis of the material in Appendix 1 using the same method as used for the previous batch of material also reported in Appendix 1. The measured solubilities were plotted against temperature and an equation was fitted to the data using a commercial microcomputer based fitting routine.

The solubility data obtained for the G-acid potassium salt monohydrate used in these kinetics experiments (batch BX 5069 A) in sulphuric acid solution of initial concentration 40g H_2SO_4 per 100g solution is recorded in Appendix 2, Table A2.6, and is plotted against temperature in Figure 5.7. The Figure also includes solubility data for batch BX 340366 85 B for comparison. The material from batch BX 5069A used in these experiments was found to be slightly more soluble than that used in the solubility measurement experiments reported in Chapter 3. The dependence of the measured solubility on temperature was fitted with a polynomial equation of the form:

$$C^* = 3.419\text{x}10^{-2} + 9.689\text{x}10^{-4}\,T + 1.259\text{x}10^{-5}\,T^2 \qquad 5.25$$

Figure 5.7 The solubility of G-acid dipotassium salt monohydrate expressed as kg G-acid dipotassium salt monohydrate per kg of solvent (40 % sulphuric acid solution).

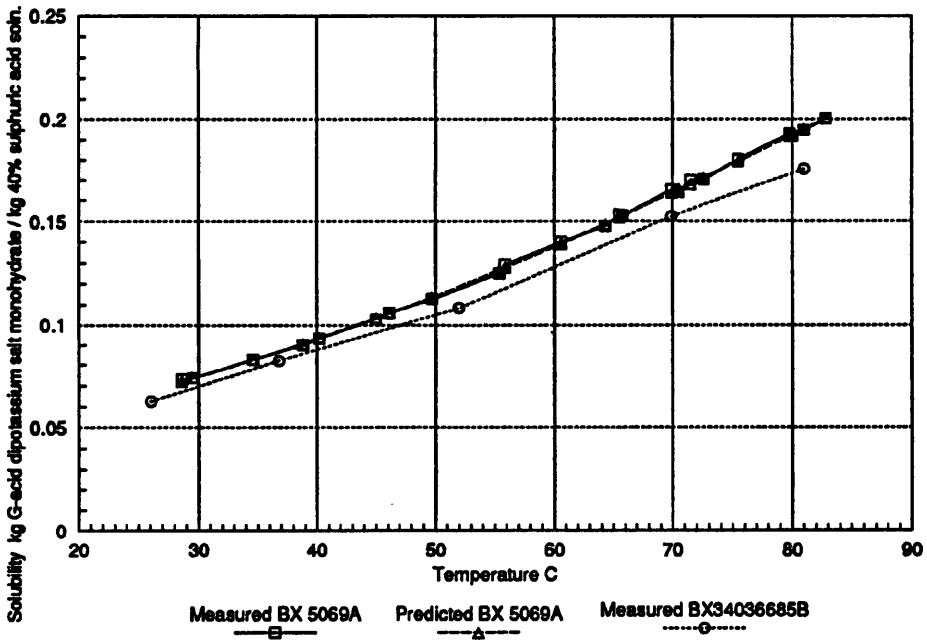

5.4.2 Determination of concentration - time and supersaturation - time profiles

The solution samples taken from the crystallizer during the course of the batch crystallization experiments were analysed for G-acid^{2-} in the manner described earlier. The G-acid concentrations were expressed in terms of kg G-acid dipotassium salt monohydrate per kg of sulphuric acid solution (0.4 kg H_2SO_4 per kg of solution). The level of supersaturation, ΔC, was determined for each measurement using the equilibrium solubility, C^*, calculated from Equation 5.25. For each experiment the concentration - time and supersaturation - time profiles were plotted using this correlation. Typical profiles for seeded and unseeded experiments are shown in Figures 5.8 and 5.9. The temperature time profiles for the seeded and unseeded experiments shown in Figures 5.8 and 5.9 are shown in Figure 5.10

Figure 5.8 A desupersaturation profile typical of those seen in the unseeded batch cooling crystallization experiments. (Unseeded run 2)

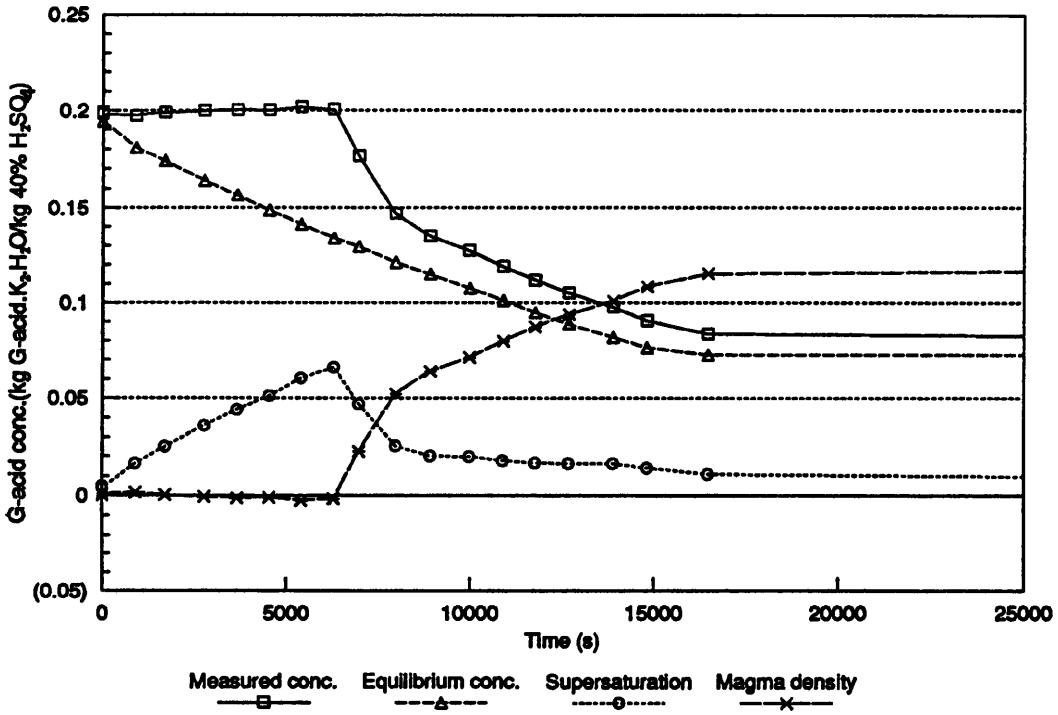

Figure 5.9 A desupersaturation profile typical of those seen in the seeded batch cooling crystallization experiments. (Seeded run 3)

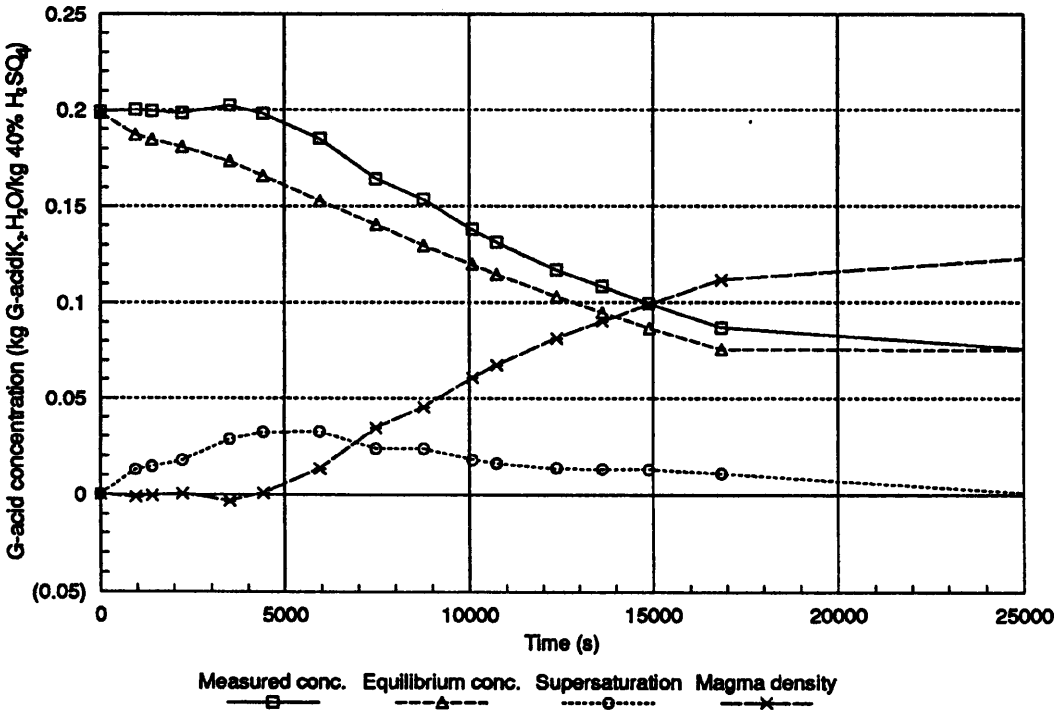

Figure 5.10 Cooling schedules for a typical seeded and unseeded crystallization. (Unseeded run 2 and seeded run 3)

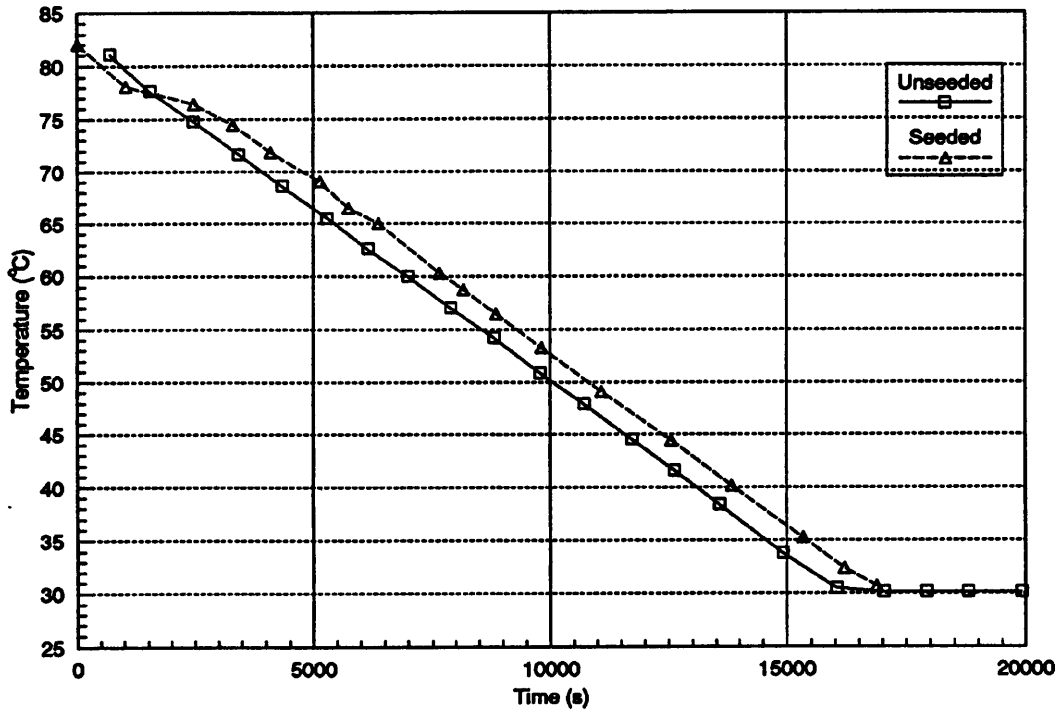

The desupersaturation profiles for the experiments under different conditions provide an indication of the effect of altering the experimental parameters. The maximum level of supersaturation attained and the time and temperature at which it was attained are useful indicators of the effect of changing the seed loading and cooling rate. These are reported in Tables 5.3 and 5.4.

The most significant trend seen from Table 5.3 was that the peak supersaturation decreased as the seed loading was increased. The reduction in peak supersaturation was most pronounced between the unseeded cases and the lowest seed loading. Increasing the seed loading further appeared to reduce the peak supersaturation level; but the rate of reduction appeared to decline with increasing seed loading. The time and temperature at which the supersaturation peaks appears to follow a complex relationship, the limited number of observations prevented this effect being considered in detail.

Table 5.3 The effect of seed loading on peak supersaturation level attained. (in all cases the cooling rate was 0.2°C/min).

Seed loading (kg G-acid seed crystals /kg 40% H_2SO_4 soln)	Peak supersaturation (kg G-acid /kg 40% H_2SO_4 soln)	Time when peak supersaturation was attained (s)	Temperature at which peak supersaturation attained (°C)
0	0.757 0.67[a]	7200 6200	57 57.5
0.0005	0.322[b] 0.392	5000 4300	68 65.5
0.0010	0.320	2880	70.4
0.0025	0.340	3300	67.0
0.0050	0.257 0.210 0.260 0.283	4890 4700 4000 4040	65.1 65.3 65.5 65.8

[a] Initial cooling rate slightly in excess of 0.2°C/min.
[b] Initial cooling rate lower than 0.2°C/min (see Figure 5.10)

Table 5.4 The effect of cooling rate on the peak supersaturation level. (in all cases the seed loading was 0.005kg seed crystals / kg 40% H_2SO_4 solution).

Cooling rate (°C /min)	Peak supersaturation (kg G-acid /kg 40% H_2SO_4 soln)	Time when peak supersaturation was attained (s)	Temperature at which peak supersaturation attained (°C)
0.1	0.202 0.241	4500 5400	72.1 69.2
0.2	0.257 0.210 0.260 0.283	4890 4700 4000 4040	65.1 65.3 65.5 65.8
0.35	0.40	3000	61.9

The data in Table 5.4 indicate that for a seeded crystallization faster cooling results in a higher peak supersaturation level being attained. Increasing the cooling rate also results in the peak supersaturation being achieved at a lower temperature.

5.4.3 Crystal size distributions.

The measured size distributions were transferred directly to computer memory and recorded to disc storage. The data for each size distribution takes the form of the calibration and instrument settings of the Elzone Particle Size Analyser and the number of particles measured in each of the 128 size ranges.

The distributions measured by the Elzone 80XY relate to the diluted crystal slurry from the crystallizer. In order to relate this to the conditions in the crystallizer it is necessary to calculate the crystal size distribution in the crystallizer. This is expressed in terms of number and volume of crystals per kg of 40%w/w sulphuric acid solution saturated with G-acid. This involves converting the number and sizes of crystals per unit volume of crystal slurry sampled by the Elzone instrument to number and size of crystals per unit mass of G-acid saturated sulphuric acid solution over a range of temperatures. This requires the solution density in the crystallizer to be known.

Density measurements were made for 40% sulphuric acid solutions saturated with G-acid dipotassium salt monohydrate at 4 temperatures. The resulting density relationship is shown graphically in Figure 5.11 and can be described by an equation of the form:

$$\rho_s = 1307.4 + 0.273T \qquad 5.26$$

where T is the temperature in °C. This relationship has been used to describe the density of the G-acid solutions encountered in these experiments, the effect of the supersaturation level on solution density has been neglected. It would have been very difficult to obtain an accurate determination of the density of the supersaturated solution at the time of sampling. As the supersaturated solution samples were added to a known mass of water to prevent them crystallizing it was not possible to determine the density of the supersaturated solution after the experiment was completed.

Figure 5.11 The dependence of solution density on temperature for a 40% H_2SO_4 solution saturated with G-acid dipotassium salt monohydrate.

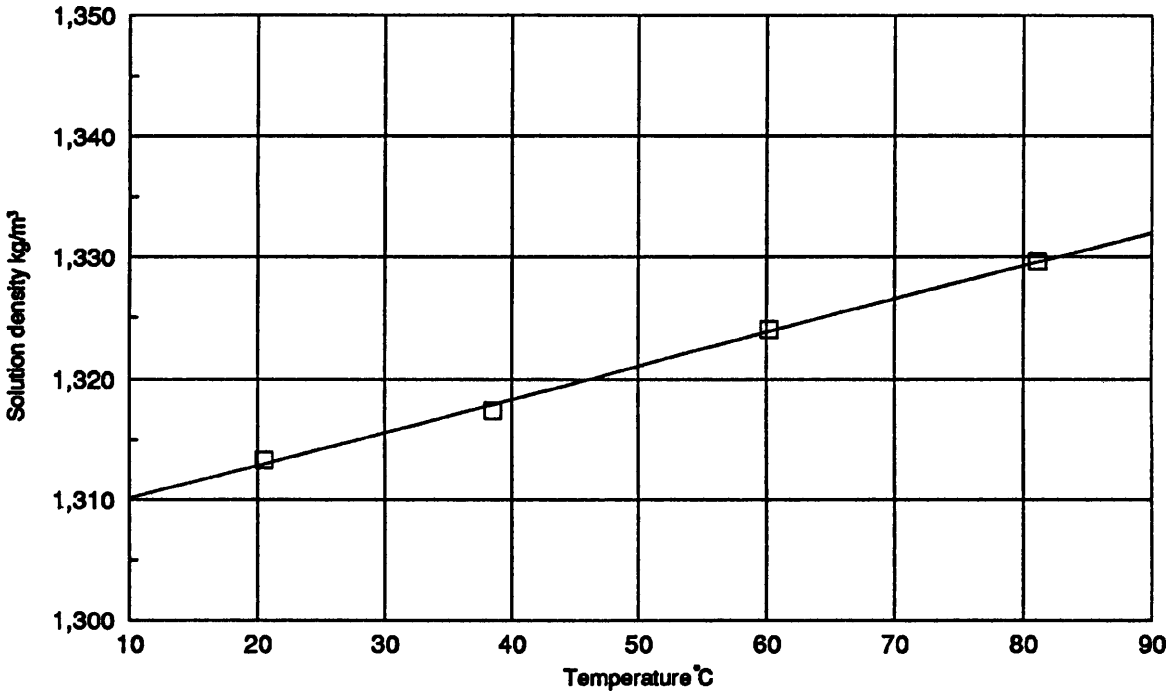

The calculation of the crystal size distribution in the crystallizer from the size distribution of the sample measured using the Elzone instrument took the form indicated in Table 5.5 and discussed below.

The number and volume equivalent diameter of the crystals sampled by the Elzone instrument were used to calculate the total volume of crystals in each size band in the size distribution. These volumes were summed together to get the total crystal volume sampled. This was multiplied by the volume of dilute slurry in the Elzone sampling vessel at the time of sampling and divided by the volume of sample assayed by the Elzone instrument. This gave the volume of crystals removed from the crystallizer in the slurry sample.

Table 5.5 Conversion of size distributions measured by the Elzone 80XY to the size distributions of the samples taken from the crystallizer.

Elzone channel number (grouped in 4s for conve niance)	mean volume equivalent size for channel(μm)	number in channel (sample count minus background count)	number of crystals per kg solvent from crystallizer in the size band	cumulative number of crystals over size per kg solvent	ln cumulative number over size	mass of crystals in cufrent size band kg per kg solvent	cumulative mass of crystals over size (kg)
2	4.03	34.48	12509516	8.9E+08	20.60970	0.000000	0.000611
6	4.398	309.1	1.1E+08	8.8E+08	20.59559	0.000009	0.000610
10	4.799	272.3	98791801	7.7E+08	20.45930	0.000010	0.000601
14	5.237	270.9	98283874	6.7E+08	20.32160	0.000013	0.000591
18	5.715	231.48	83982101	5.7E+08	20.16276	0.000015	0.000577
22	6.236	182.5	66211912	4.9E+08	20.00365	0.000015	0.000562
26	6.805	191.06	69317523	4.2E+08	19.85750	0.000020	0.000547
30	7.426	152	55146360	3.5E+08	19.67747	0.000021	0.000526
34	8.104	152.42	55298738	3.0E+08	19.50677	0.000028	0.000504
38	8.843	138.06	50088858	2.4E+08	19.30017	0.000033	0.000476
42	9.65	111.78	40554342	1.9E+08	19.06715	0.000035	0.000442
46	10.53	90.82	32949950	1.5E+08	18.82830	0.000036	0.000407
50	11.49	63.38	22994580	1.2E+08	18.58088	0.000033	0.000370
--	--	--	--	--	--	--	--

Vol of crystals in sample (m^3)	1.84E-10	Calculated iteratively from mass of crystals in 1kg solvent divided by crystal density and multiplied by mass of solvent in sample.
Mass of crystals in sample (kg)	3.39E-7	Volume of crystals multiplied by crystal density.
Vol of slurry in sample (m^3)	5E-7	Volume of sample taken from crystallizer.
Vol of solution in sample (m^3)	5E-7	Volume of slurry minus volume of crystals.
Mass of solution in sample (kg)	0.000664	Volume of solution multiplied by density of solution saturated at sample temperature.
Soln concentration (kg/kg solvent)	0.1988	Measured concentration.
Mass of solvent in sample (kg)	0.000554	Mass of solution divided by 1 plus solution concentration.
Magma density (kg/kg solvent)	0.000611	Mass of crystals present divided by mass of solvent present.

This calculated volume of crystals was subtracted from the volume of the slurry sample to give the volume of crystal free solution removed from the crystallizer in the sample. The mass of free solvent (40% sulphuric acid solution) in this crystal free solution was calculated using the density correlation for 40% sulphuric acid saturated with G-acid at the temperature of the crystallizer at the time of sampling. As noted earlier it would have been very difficult to measure the density of the supersaturated solution at the time of sampling and it would be difficult to make up a solution with the same level of supersaturation to determine its density later. This approximation was considered to be acceptable, it is likely to yield a slight underestimate of the solution density though the effect is estimated to be small compared with other sources of experimental error. The density was used to calculate the mass of the G-acid supersaturated sulphuric acid solution from the volume of the solution component of the sample taken from the crystallizer. The concentration of G-acid (as the dipotassium salt monohydrate) in the solution was determined by spectrophotometric analysis and so the mass of 40% sulphuric acid could be calculated. In this way a multiplication factor was calculated to relate the number of crystals in the sample analysed by the Elzone 80XY to the number of crystals per kg of 40% sulphuric acid solution in the crystallizer.

The number, cumulative number, volume and cumulative volume distributions measured during a typical seeded experiment (seeded run 3) are plotted against size in Figures 5.12 to 5.15.

Careful examination of Figure 5.13. which shows the evolution of the cumulative number oversize distribution with time reveals some evidence for either growth rate size dependency or growth rate dispersion. The gradient of the ln cumulative number oversize against size plots decreases from the 4th crystal size distribution measured 2880s after seeding to the 8th measured 6960s after seeding. This suggests that the larger crystals were growing faster than the smaller ones causing the fanning out of the ln cumulative number oversize against size plots. Two mechanisms could account for this effect; ether the growth rate is size dependent, larger crystal growing faster than small ones, or crystals of the same size may grow at different rates. If crystals

of the same size grew at different rates eventually the upper size bands would be populated by larger faster growing crystals whilst the lower size ranges would accumulate smaller slower growing crystals.

The ln cumulative number oversize against size plots of the crystal size distributions measured after 6960s turn down at high size. This was due to truncation of the size distributions by the screening procedure required to prevent the Elzone orifice tube blocking. This masks the growth rate dispersion or growth rate size dependency as larger crystals are selectively removed from the size distribution.

Figure 5.12 Evolution of the experimentally measured discrete number distributions over time during a typical seeded batch crystallization.

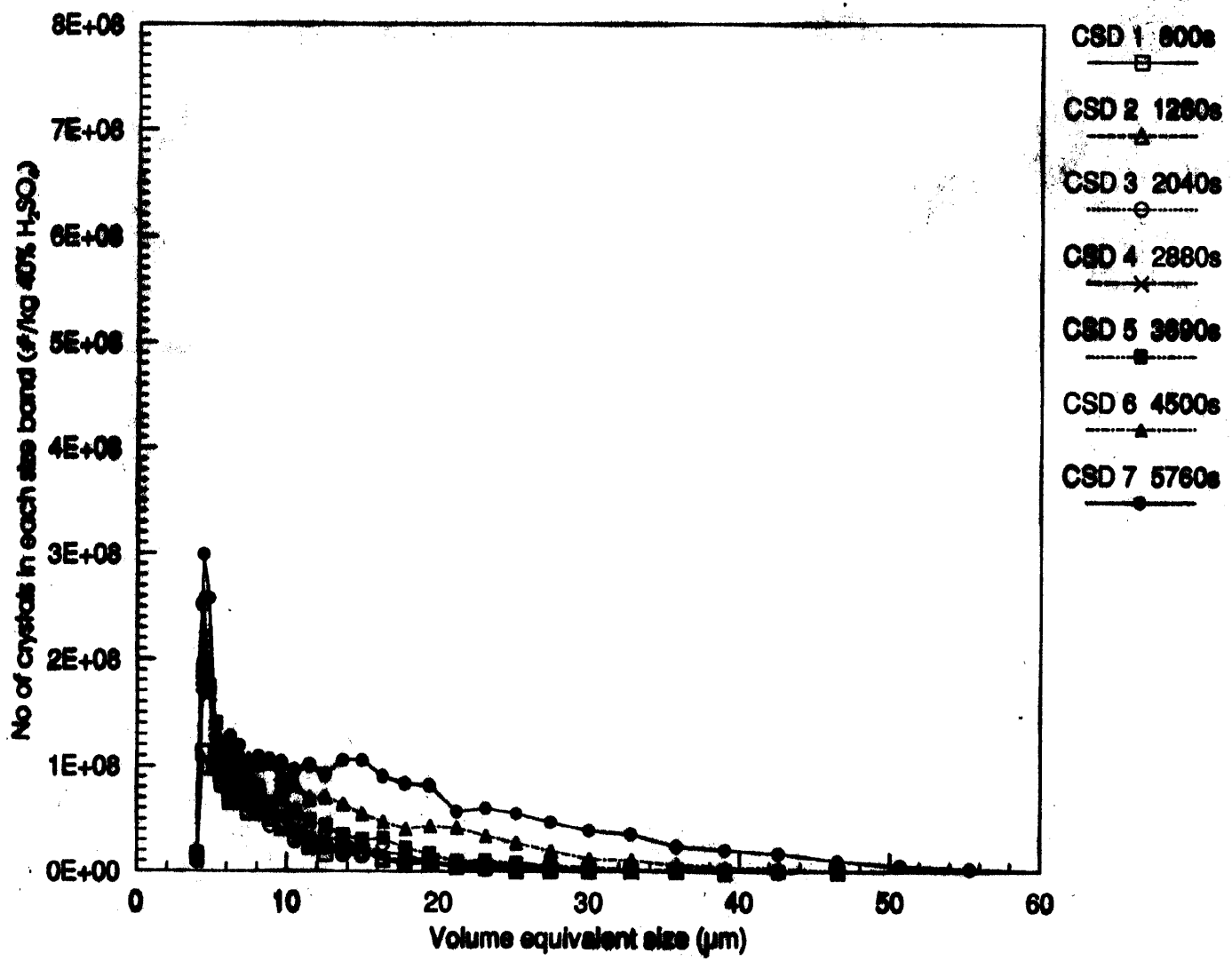

Figure 5.12 Evolution of the experimentally measured discrete number distributions over time during a typical seeded batch crystallization.

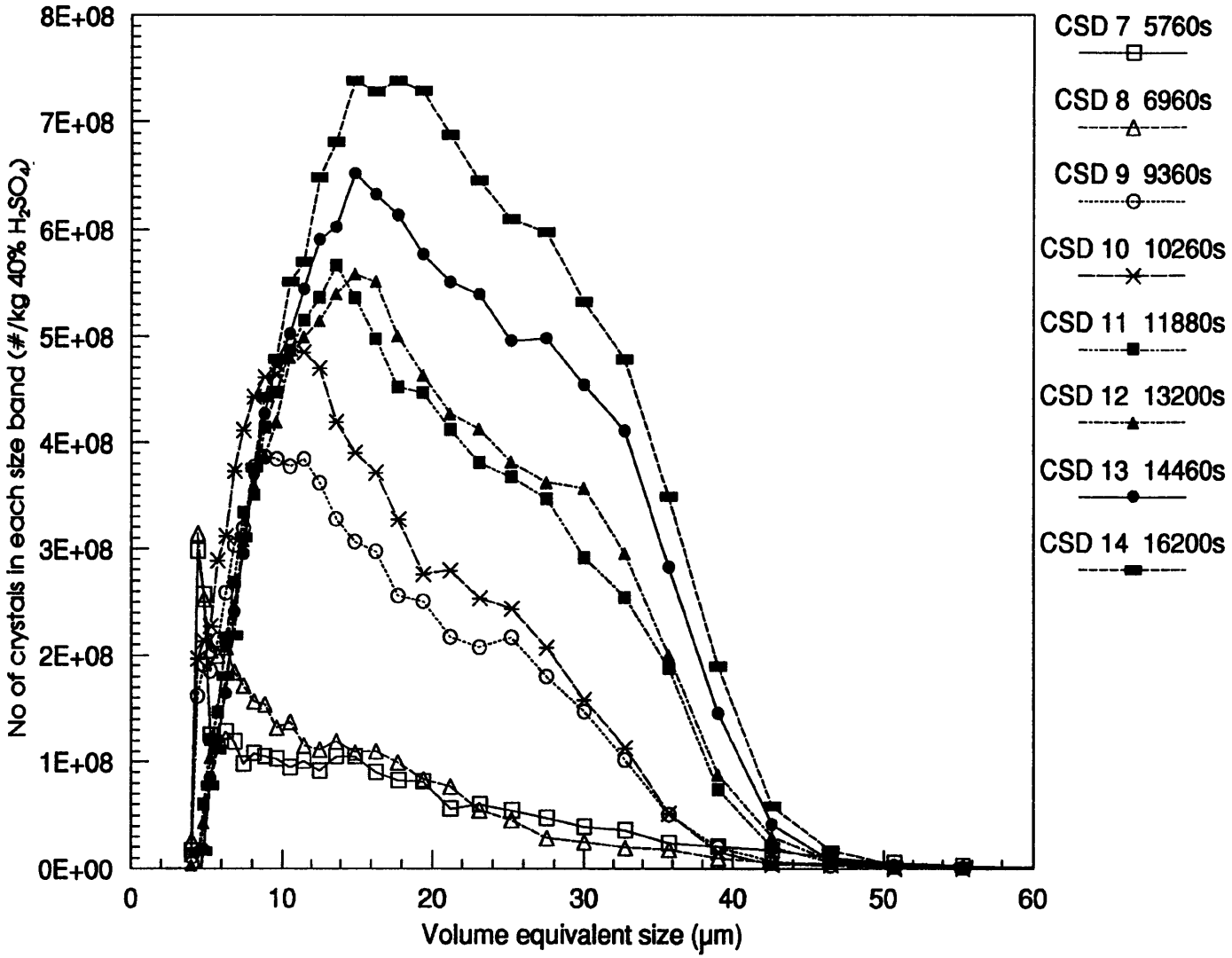

Figure 5.10 Evolution of the cumulative number oversize distribution in a typical seeded batch crystallization experiment.

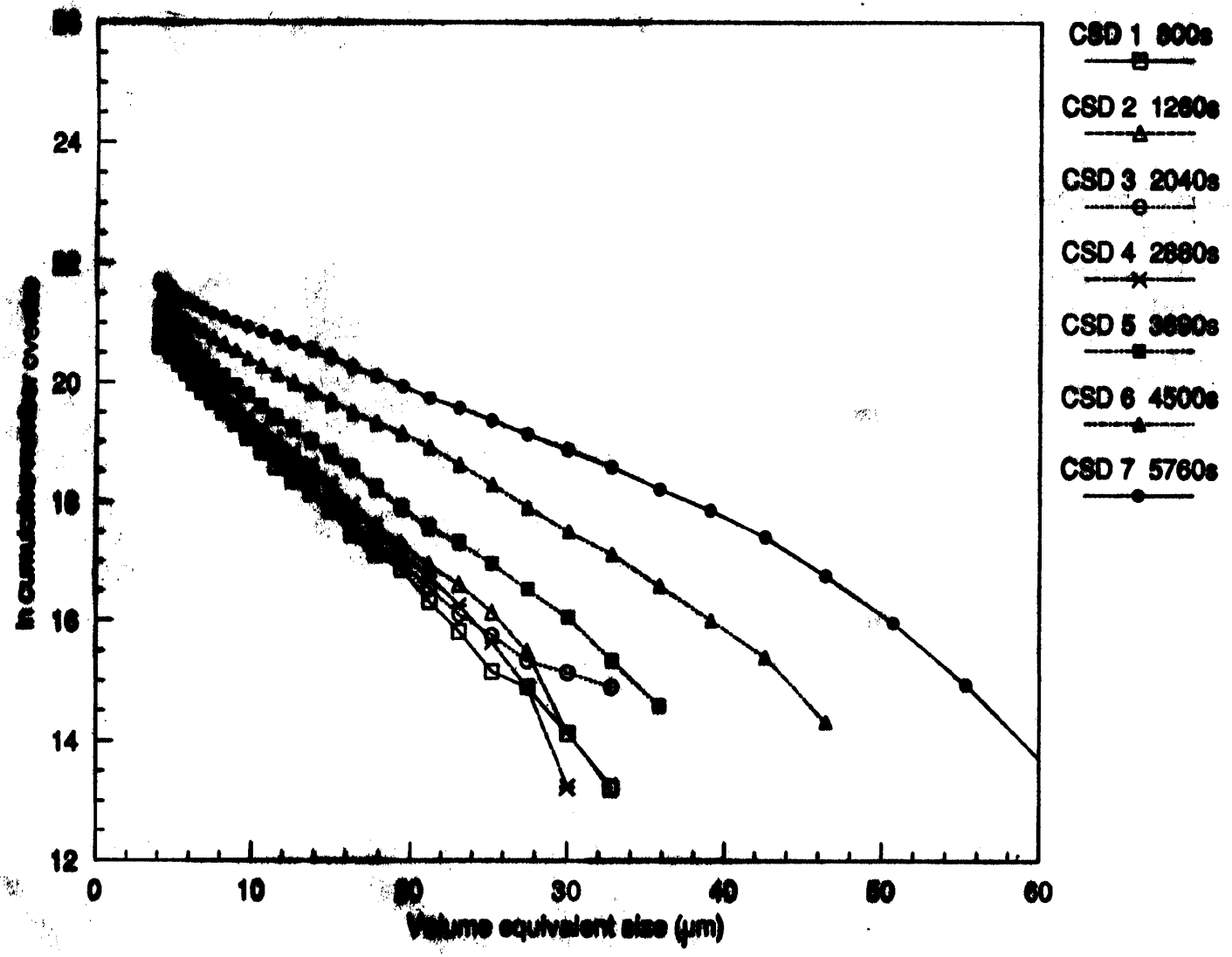

Figure 5.13 Evolution of the cumulative number oversize distribution in a typical seeded batch crystallization experiment.

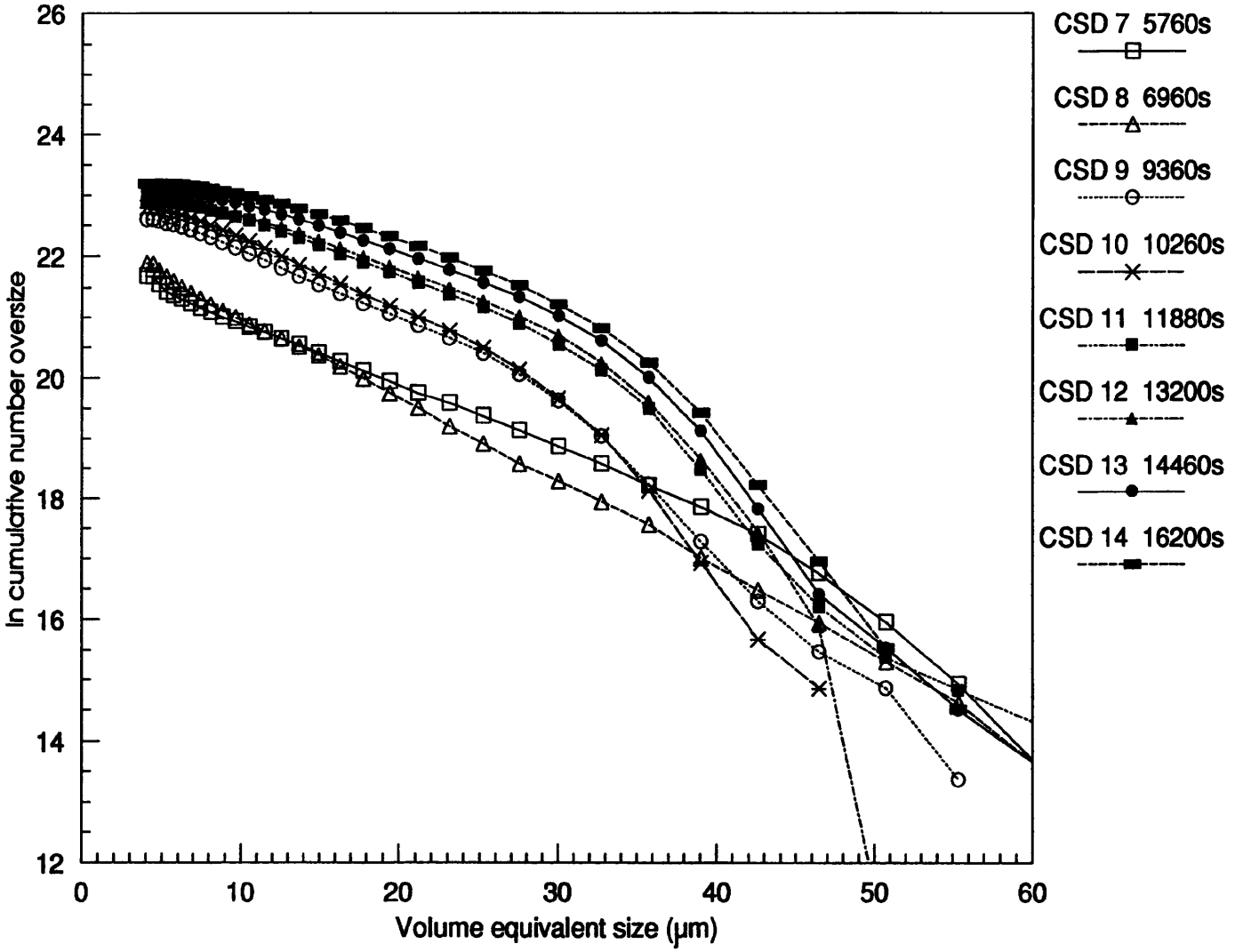

Figure 5.14 Evolution of the discrete mass distributions over time during a typical seeded crystallization.

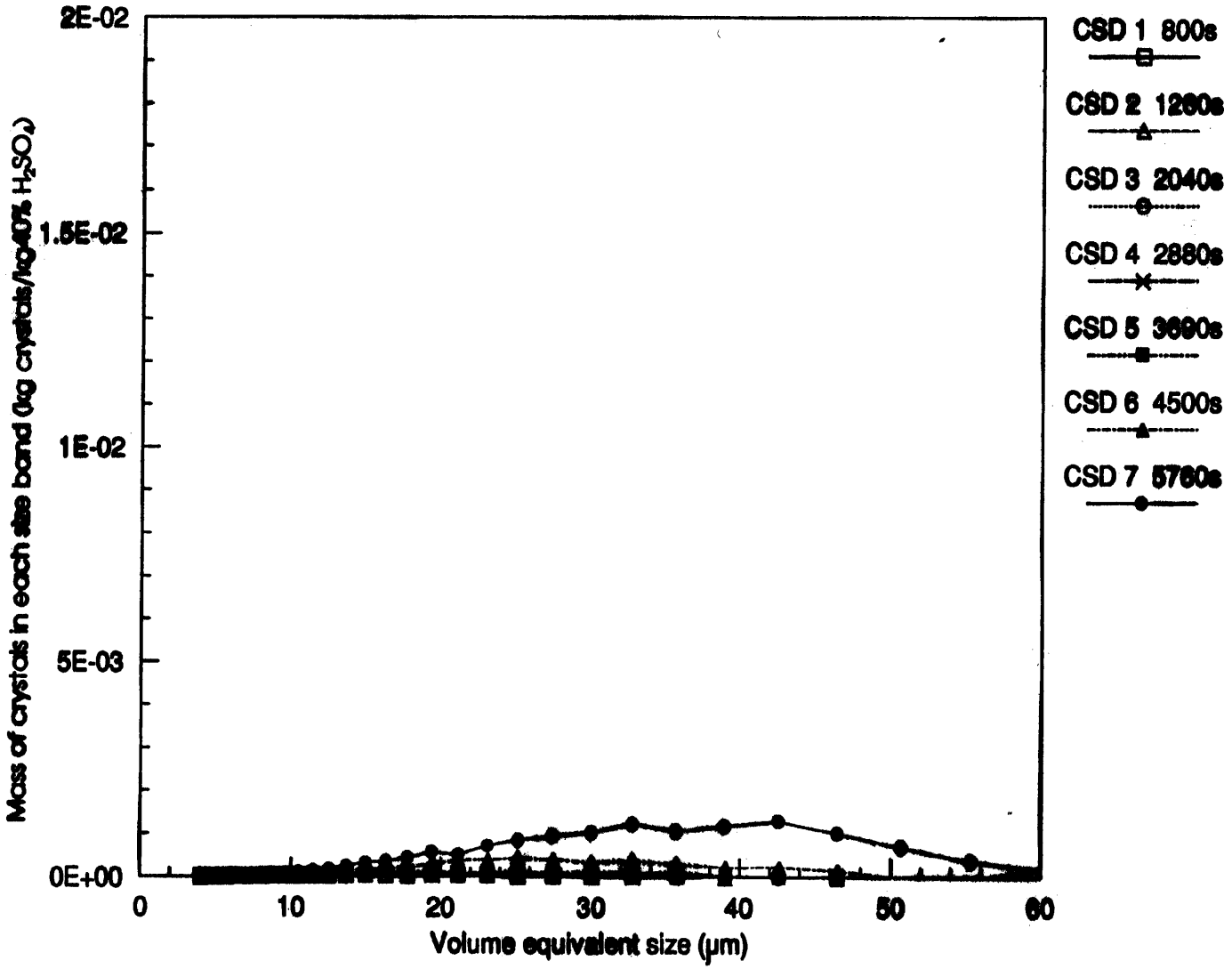

Figure 5.14 Evolution of the discrete mass distributions over time during a typical seeded crystallization.

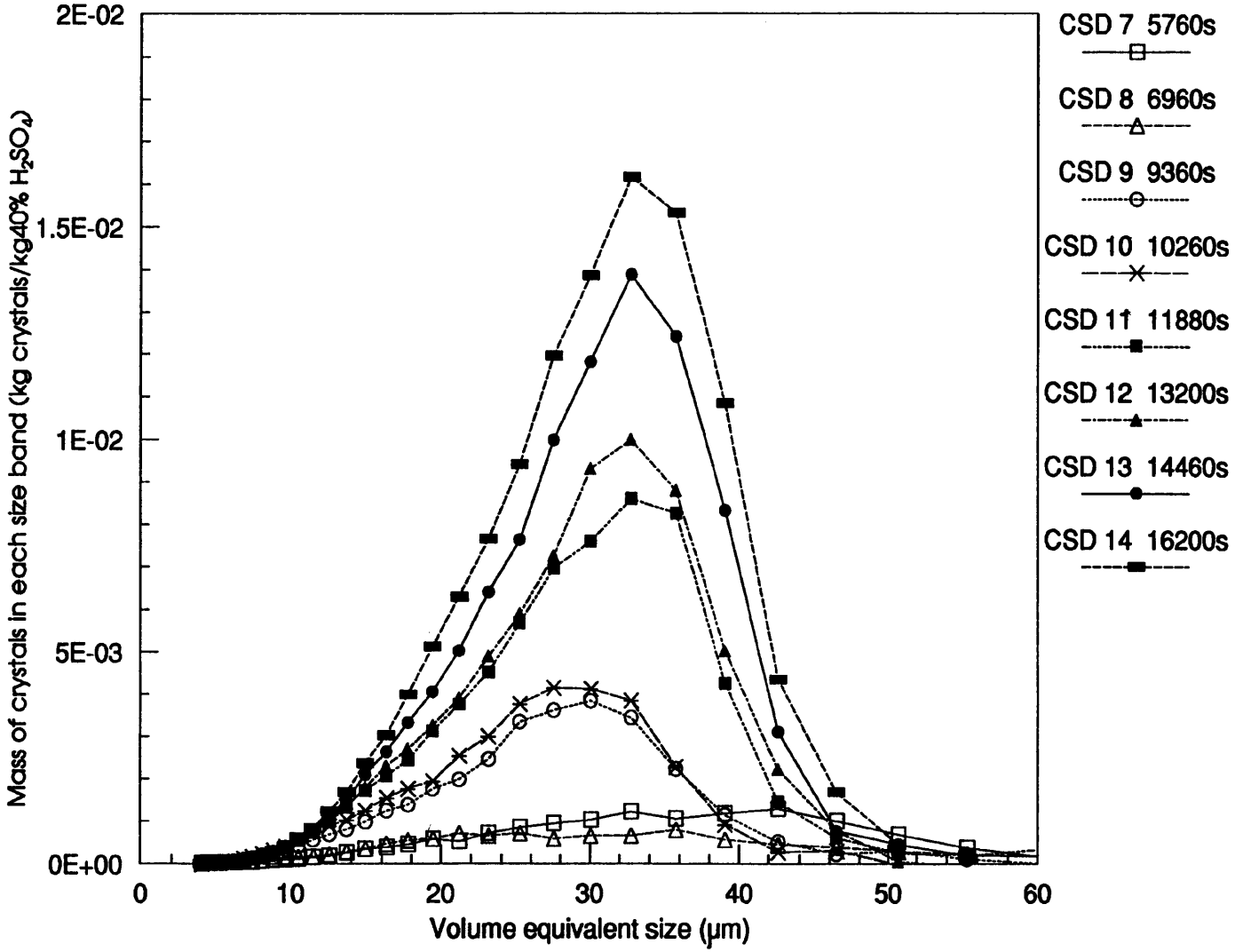

Figure 5.15 A series of cumulative mass distributions measured during a typical seeded crystallisation.

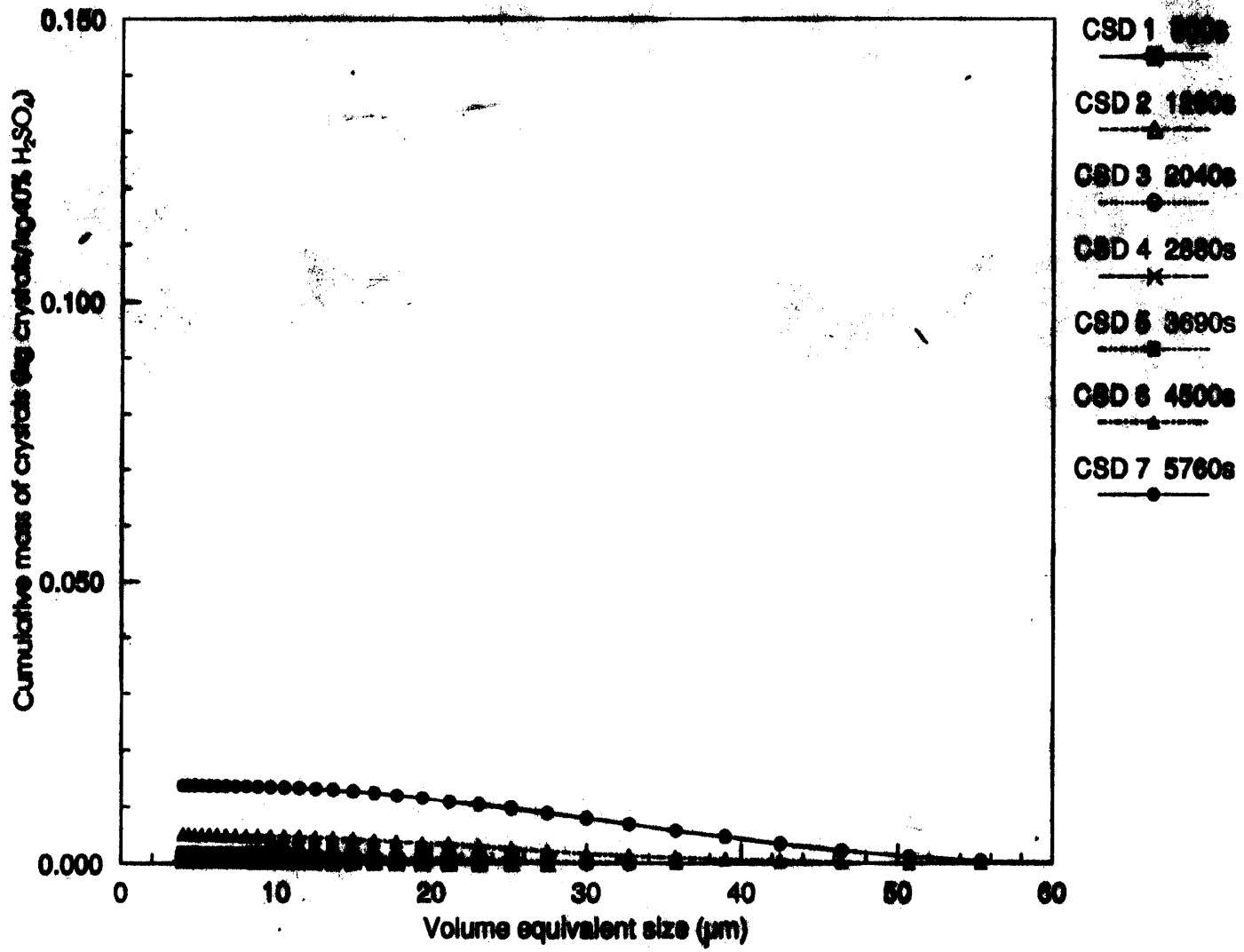

Figure 5.15 A series of cumulative mass distributions measured during a typical seeded crystallization.

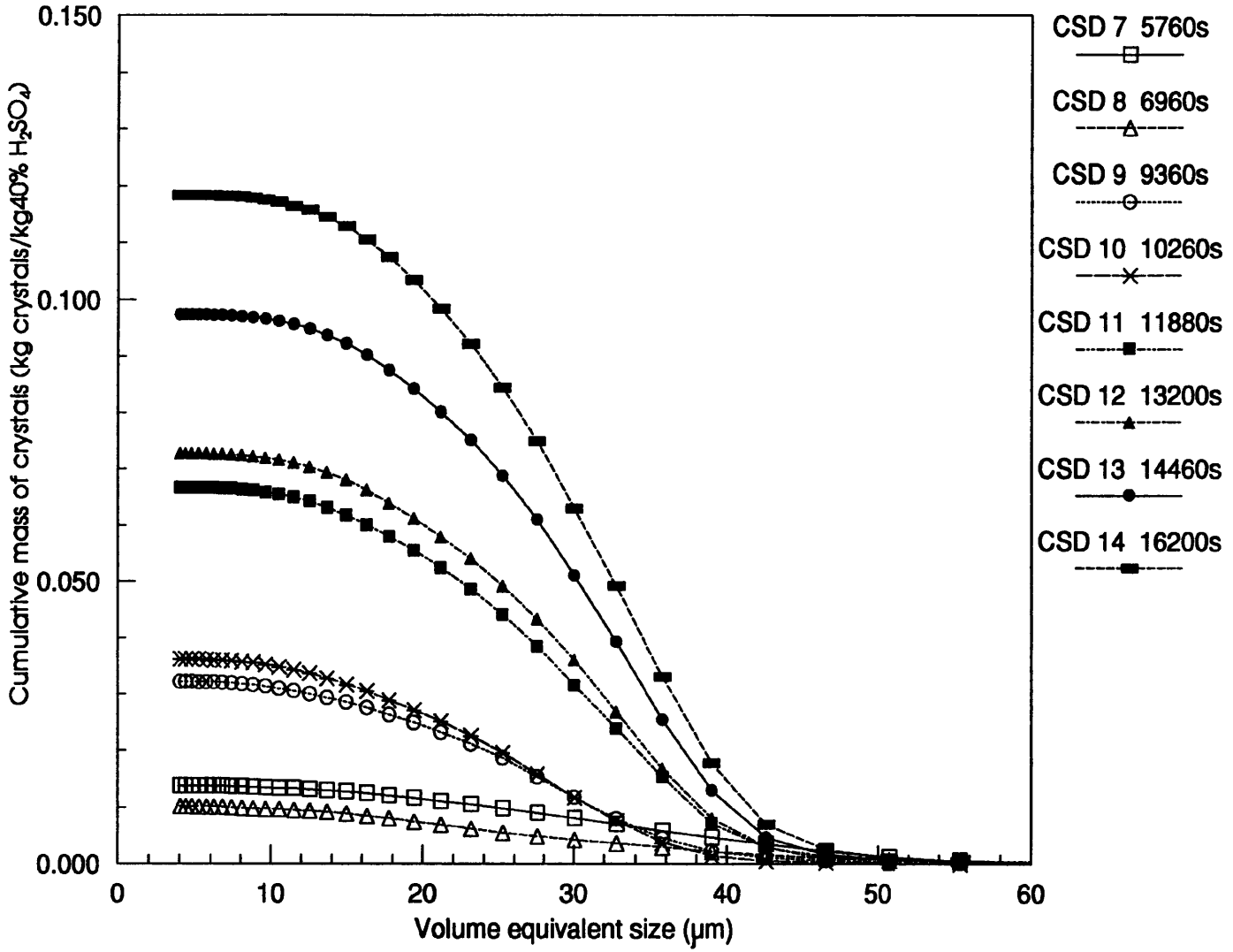

5.4.4 Evaluation of the crystallization kinetics

The crystal size distributions measured by the Elzone 80XY particle size analyser are truncated both at low and high sizes. The loss of data at small size is due the difficulty resolving small crystals from background noise, in this study the cut off point is around 5μm. The screening procedure described in Section 5.3 results in the loss of data concerning the largest crystals in the distributions measured during the latter stages of the experiments.

The weighted moments based procedure was chosen in preference to a graphical procedure to determine the crystallization kinetics because the use of weighting reduced the contribution of the extremities of the crystals size distribution made to the determined kinetics. Growth and nucleation kinetics were obtained from the measured crystal size distributions using the moments method outlined in Section 5.2.2. The graphical procedure described in Section 5.2.1 was used to estimate kinetics from one experiment to provide data for comparison.

Despite the evidence for growth rate size dependency or growth rate disperison discussed in Section 5.4.3 practical difficulties prevented any attempt to quantify the effect of crystal size on the growth kinetics. The weighted moments based procedure yields a single size independent growth rate for the whole size distribution, providing no information on the effect of crystal size. The graphical procedure could in principle be employed to evaluate the growth rate at several sizes. However several practical considerations prevented the pursuit of this course of action:

The experimental errors associated with the measurement of crystal size at high and low size would yield erroneous growth rates from size measurements at the ends of the size distribution, whereas measurements over the central portion of the size distribution would yield more accurate growth rate values but the variation in growth rate with size and the size range covered would be smaller.

The screening procedure required to measure the size distributions in the later stages of the experiments has been shown to mask the evidence for size dependent growth or growth rate despersion. Excluding the size distributions measured after screening was employed drastically reduces the number of distributions from which growth

rate measurements could be made at a range of sizes. Consequently only a small amount of data could be gathered. Excluding the data during the later stages of the experiments would also reduce the range of conditions, especially magma density over which kinetic data were obtainable.

The addition of another variable to the growth rate equation would further complicate the fitting procedure, and since the data expected from such an approach would be subject to significant errors the resulting correlation could be expected to be very poor.

5.4.4.1 The moments method

A computer program for determination of growth and nucleation rates from successive pairs of crystal size distributions using the weighted moments procedure was developed from an earlier program written by Dr. N. S. Tavare. Tavare's original program was designed to extract growth and nucleation kinetics from crystal size distributions measured with a Coulter Counter and ran on an Apple IIe microcomputer. The Coulter counter divided the measured crystal size distribution into 16 size ranges whereas the Elzone 80XY Particle Size Analyser used in this study divided the distribution into 128 size ranges, greatly increasing the computational requirement. The original programme was therefore adapted to run on the Kaypro 10 microcomputer interfaced with the Elzone Particle Size Analyser using the measured 128 channel particle size distributions. A listing of this modified programme is included in Appendix 3. The computational analysis was performed on the pairs of successive size distributions measured during each experiment and in this way estimates of the mean growth and nucleation rates prevailing over the various conditions during each of the batch crystallization experiments were produced. All the successful evaluations are included in Table 5.6.

Table 5.6 Growth and nucleation kinetics estimated from successive pairs of crystal size distributions using the method of moments analysis procedure developed by Tavare. The mean values of important parameters are also tabulated.

Temperature	Supersatn.	Magma density	Stirrer speed	Nucleation rate	Growth rate
(°C)	(kgG-acid.K_2.H_2O/kgF.S.)		(/s)	(#/kgF.S.s)	(μm/s)
52.2	0.024927	0.056	4.17	263440	0.00644
49	0.024605	0.0635	4.17	142310	0.004504
45.75	0.020831	0.0743	4.17	6610	0.00153
39.25	0.017884	0.0905	4.17	159490	0.00492
30.2	0.012866	0.1122	4.17	9720	0.004504
30.1	0.009839	0.1154	4.17	41610	0.004504
54.7	0.033940	0.0406	5.00	297830	0.00897
51.6	0.022093	0.0596	5.00	335610	0.00768
29.15	0.010468	0.1158	5.00	47000	0.00656
78.1	0.012944	0.00005	5.00	39930	0.005944
76.4	0.016798	0.00157	5.00	27570	0.004045
74.45	0.022191	0.00177	5.00	6810	0.002621
71.85	0.029299	0.00197	5.00	18150	0.006658
66.5	0.031902	0.01387	5.00	44550	0.003397
60.3	0.024706	0.03697	5.00	174340	0.006561
56.5	0.021576	0.04937	5.00	13280	0.00667
53.25	0.019916	0.05867	5.00	192300	0.00446
40.15	0.014713	0.09197	5.00	39170	0.00363
35.25	0.013312	0.10277	5.00	43520	0.00217
76.25	0.022632	0.00198	5.00	28080	0.01022
68.2	0.032171	0.01486	5.00	1530	0.00621
64.9	0.030899	0.02488	5.00	174620	0.0127
70.6	0.038352	0.00067	6.67	42210	0.0144
66.8	0.037907	0.01137	6.67	144070	0.004645
56.65	0.021517	0.05337	6.67	77680	0.0025
50.35	0.020108	0.06937	6.67	10940	0.00714
38	0.016811	0.09837	6.67	22500	0.000812
33.15	0.014225	0.11000	6.67	31190	0.000006
76.7	0.008829	0.00425	6.67	98730	0.001916
69.2	0.011773	0.02235	6.67	38700	0.000729
61.75	0.003273	0.05035	6.67	10350	0.001165
50.91	0.003752	0.07575	6.67	1860	0.000241
Continued					

Table 5.6 Continued

Temperature	Supersatn.	Magma density	Stirrer speed	Nucleation rate	Growth rate
(°C)	(kgG-acid.$K_2.H_2O$/kgF.S.)		(/s)	(#/kgF.S.s)	(μm/s)
66.5	0.025702	0.01535	5.00	74040	0.004356
52.8	0.022153	0.05275	5.00	22770	0.002427
47	0.016860	0.07095	5.00	89030	0.005258
43	0.015168	0.08105	5.00	229320	0.01041
36	0.011982	0.09798	5.00	50880	0.00133
66.55	0.021169	0.01431	5.83	21650	0.001795
56.15	0.020212	0.04141	5.83	43030	0.001946
49.75	0.016446	0.05991	5.83	25040	0.001857
45.2	0.015453	0.07075	5.83	153560	0.006579
40.38	0.013227	0.08284	5.83	164660	0.006509
35.75	0.011831	0.09316	5.83	168720	0.002675
74.6	0.015464	0.00404	1.67	9000	0.00215
72.55	0.018248	0.00704	1.67	94470	0.00634
67.45	0.028779	0.01044	1.67	36900	0.00279
63.05	0.029771	0.02094	1.67	169820	0.00392
73.55	0.017340	0.00385	3.33	52510	0.002857
76.9	0.010849	0.00214	1.67	5940	0.000495
74.75	0.016837	0.00234	1.67	55820	0.005402
71.85	0.022999	0.00434	1.67	39620	0.002147
69.7	0.027614	0.00564	1.67	154000	0.01213
74.9	0.014609	0.00455	1.67	35650	0.002516
69.55	0.023322	0.01075	1.67	78790	0.004293
68.4	0.025934	0.01125	1.67	9260	0.001062

Occasionally negative growth and nucleation rates were calculated. In such cases the two size distributions were compared with the ones on either side of them and the one which appeared to be most in error was omitted. Then the kinetics were re-calculated over the increased time interval wherever this was possible.

In those experiments which were not seeded the kinetic data corresponding to the interval between the last size distribution before primary nucleation occurred and the first one after nuclei were detected was excluded from the kinetics correlations. This was necessary for two reasons; Both primary and secondary nucleation

mechanisms would have to be considered in the nucleation correlation which would require the use of a more complex nucleation equation than Equation 5.25. Secondly more observations would be required to obtain a satisfactory correlation.

The kinetic data extracted from the size distributions measured before primary nucleation in the unseeded experiments simply reflect the differences between different measurements of background count. Whilst they cannot be used to describe the kinetics of the crystallizing system they provide an indication of the relatively small errors in sampling and measurement of crystal size distribution when few crystals are present. This is discussed further in Section 5.5.6.

The growth and nucleation kinetics which correspond to the seeded desupersaturation profile shown in Figure 5.9, (seeded run 3), are plotted against supersaturation in Figures 5.16 and 5.17.

- Correlation of the derived crystallization kinetics with the experimental conditions.

The growth and nucleation rates evaluated by the s-plane analysis procedure were correlated with the mean values of the experimental parameters corresponding to the intervals over which they were determined. The data in Table 5.6 formed the input file to a commercially available multivariable non-linear regression program.

Equations based on Equations 5.23 and 5.24 describing the growth and nucleation kinetics respectively were obtained and are shown in Table 5.7. The standard errors for the 95% confidence limits on each parameter and the overall correlation coefficient r^2 are also shown in the table.

Figure 5.16 The dependence of growth rate evaluated by s-plane analysis on supersaturation during a typical seeded batch crystallization. (Seeded batch experiment 3)

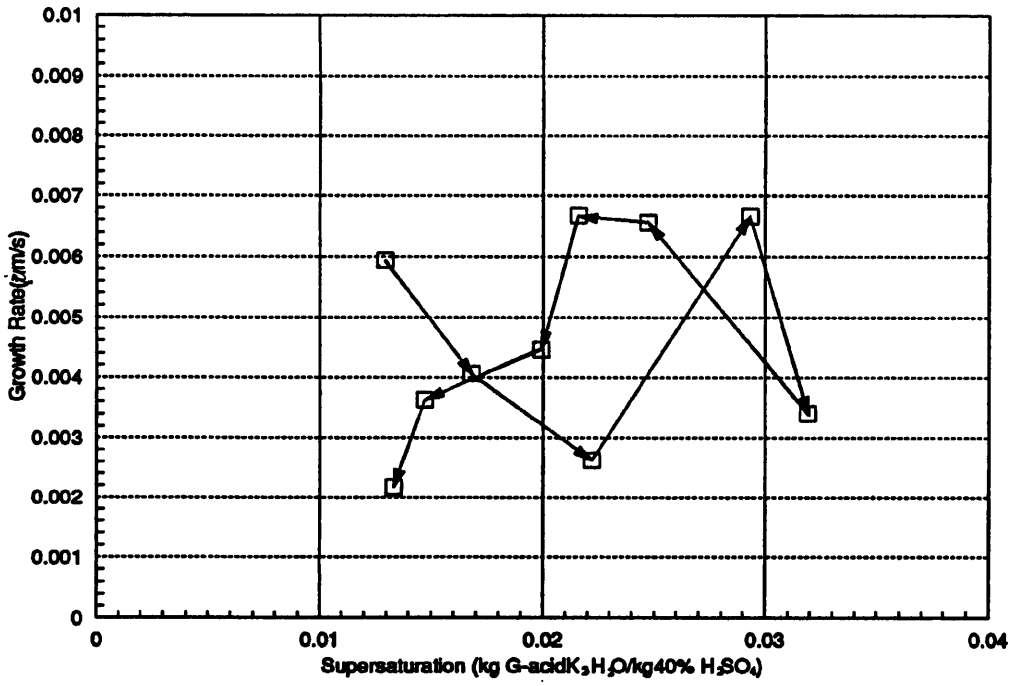

Figure 5.17 The dependence of nucleation rate evaluated by s-plane analysis on supersaturation during a typical seeded batch crystallization. (Seeded batch experiment 3)

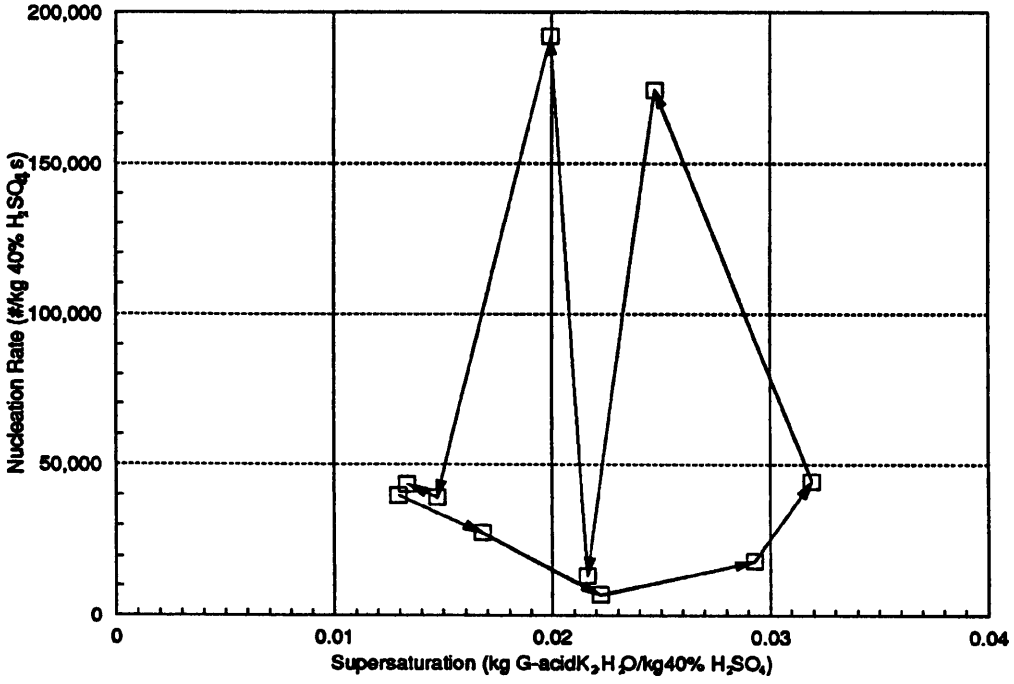

Table 5.7 The growth and nucleation kinetic equations fitted to the growth and nucleation rates determined by the s-plane analysis procedure.

Growth: $\overline{G} = K_g \Delta C^g e^{-E_g/RT}$			
K_g (m/[s (kg/kg)^g])	g	E_g (J/mol)	r^2
5.16×10^{-8}	0.96	-3660	0.245
$\pm 1.13 \times 10^{-7}$	± 0.29	± 6930	

Nucleation: $\overline{B} = K_b \Delta C^b M_T^j N^m e^{-E_b/RT}$					
K_b (#/[kg40%H_2SO_4 s (kg/kg)^j (kg/kg)^b])	b	E_b (J/mol)	j	m	r^2
1.21×10^9	1.74	778	0.61	-0.29	0.287
$\pm 1.18 \times 10^{10}$	± 0.61	± 2660	± 0.37	±0.31	

The correlation coefficients r^2 for the fitted growth and nucleation rate equations are very low, 0.245 for the growth rate equation and 0.287 for the nucleation rate equation. This implies that there is considerable scatter amongst the data and this is seen in the width of the 95% confidence limits. The scatter amongst the data are seen in Figures 5.18 and 5.19.

With such scattered data there is a danger that a multivariable correlation procedure will either find a local minimum on the fitted surface or alternatively it may flex variables which alter the values of the fitted parameter in opposite directions and assign physically unrealistic vales to the variables. To combat the first problem of finding local minima the correlation procedure was performed with different starting values for each variable and left to iterate to a common end point.

Figure 5.18 A plot of growth rate predicted by Equation 5.23 using the values in Table 5.7 against observed growth rate for the kinetic data obtained from the moments analysis.

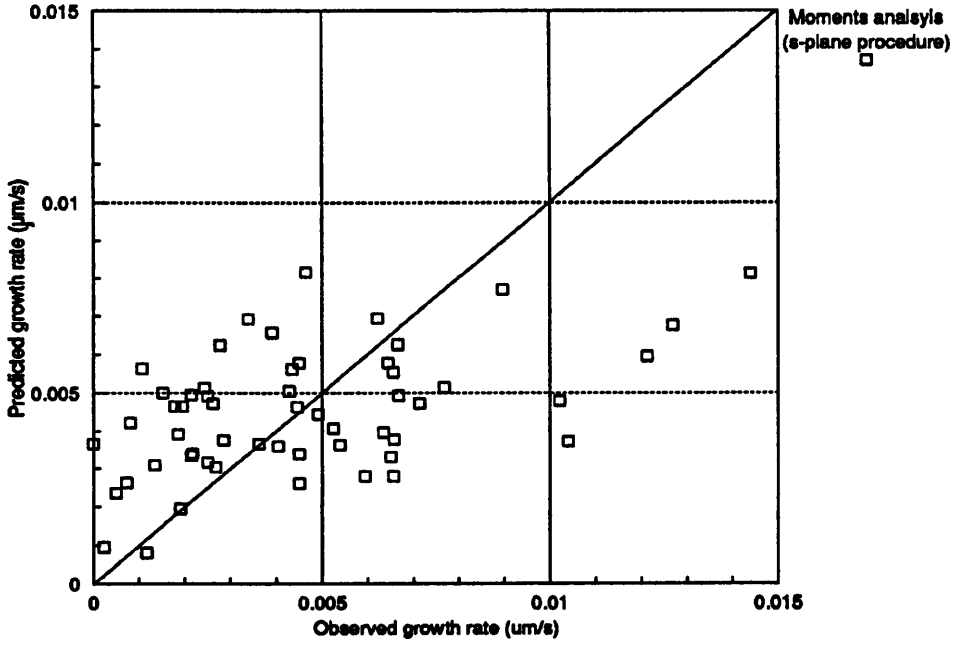

Figure 5.19 A plot of nucleation rate predicted by Equation 5.24 using the values in Table 5.7 against observed nucleation rate for the kinetic data obtained from the moments analysis.

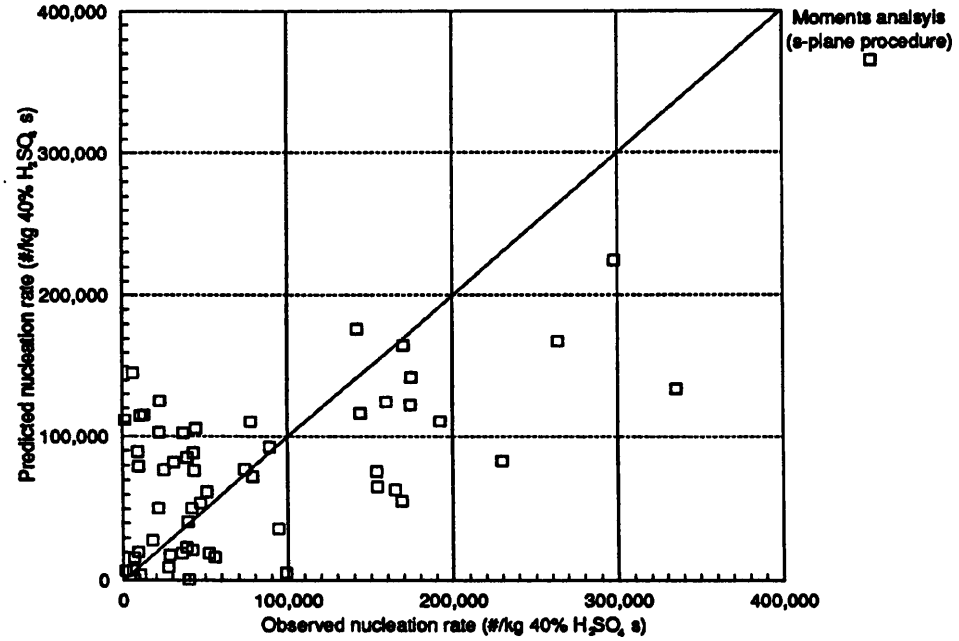

Tavare and Garside (1986) suggest an alternative correlation for nucleation rate data where the correlation between nucleation rate and supersaturation may be poor. Their correlation involves replacing the supersaturation term in Equation 5.24 with the growth rate given by equation 5.23 which is itself a supersaturation dependent term to give Equation 5.26.

$$B = K_r.M_t^j.\exp\left(\frac{-E_r}{RT}\right).N^m.G^i \qquad 5.26$$

Where B is the nucleation rate, K_r is the relative nucleation rate constant, M_t is the magma density and j is the exponent on magma density. E_r is the relative activation energy, R is the gas constant and T is the absolute temperature. G is the measured growth rate and i is the relative kinetic order which is equal to b/g, N is the stirrer speed and m is the exponent on stirrer speed.

A correlation based on Equation 5.26 has been performed using the data obtained by the moments procedure, the resulting correlation is shown in Table 5.8

Table 5.8 Values of parameters in Equation 5.26 determined by correlation using the kinetic data obtained by s-plane analysis.

$B = K_r.M_t^j.\exp\left(\frac{-E_r}{RT}\right).N^m.G^i$					
K_r (#/[kg40%H_2SO_4 s (kg/kg)^j (m/s)^i (rev/s)^m])	j	E_r (j/mol)	i	m	r^2
9.42×10^{10}	0.535	18,350	0.867	-0.422	0.492
$\pm 5.12 \times 10^{11}$	± 0.225	± 14,110	± 0.191	± 0.289	

The correlation co-efficient, r^2 for Equation 5.26 is 0.492 which is higher than the value of 0.287 obtained from Equation 5.24 which included a direct supersaturation dependency. Figure 5.20 is a plot of log $B/M_t^j.\exp\left(\frac{-E_r}{RT}\right).N^m$ against log G, the slope of the line is the relative kinetic order i and the intercept is K_r.

Figure 5.20 A plot of log $B/M_t^j.\exp\left(\frac{-E_r}{RT}\right)N^m$ against log G. The line fitted through the data corresponds to Equation 5.26 using the values of the variables listed in Table 5.8.

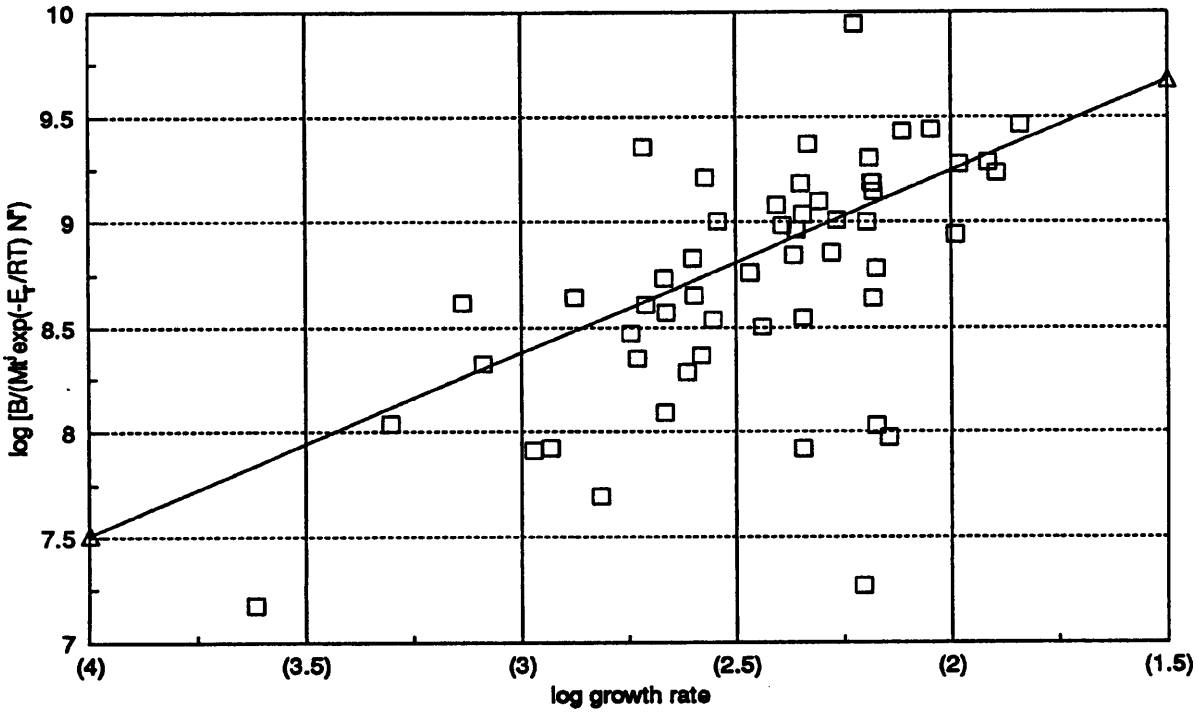

The values of nucleation rate predicted by Equation 5.26 are plotted against the observed values in Figure 5.21. The nucleation rates predicted by Equation 5.24 are included for comparison. Figure 5.21 reveals that the values of the nucleation rates determined by Equations 5.24 and 5.26 are broadly similar.

Figure 5.21 A plot of nucleation rates predicted using Equations 5.24 and 5.26 against the observed nucleation rates.

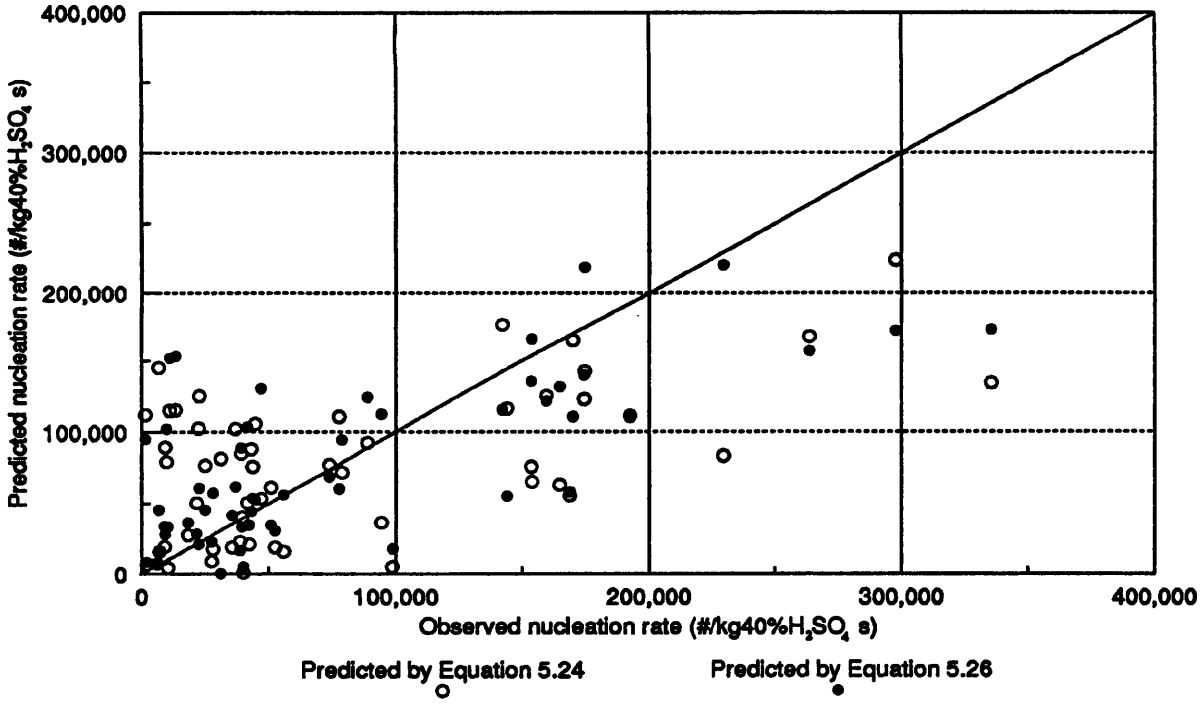

5.4.4.2 The graphical method

A graphical procedure for determining the growth and nucleation kinetics was used to obtain some data for comparison with the calculated kinetic data reported in Table 5.6. and the correlations reported in Tables 5.7. and 5.8. This procedure is based on plotting the cumulative number of crystals oversize against crystal size as described in Section 5.2.1. A typical example of the application of the technique is shown in Figures 5.22. and 5.23. The nucleation rates are estimated from the increase in cumulative number oversize at zero size determined by extrapolation the ln cumulative number oversize to zero size as indicated in Figure 5.22. The growth rates are evaluated at approximately 10μm by selecting a suitable value of ln cumulative number oversize on the y axis and determining the increase in size corresponding to that cumulative number oversize between successive size distributions. The region of the size distribution around 10μm was selected to take advantage of the most accurately measured portion of the crystal size distributions. This is shown in Figure 5.23.

Figure 5.22a Graphical estimation of nucleation kinetics from cumulative number oversize against size plots.

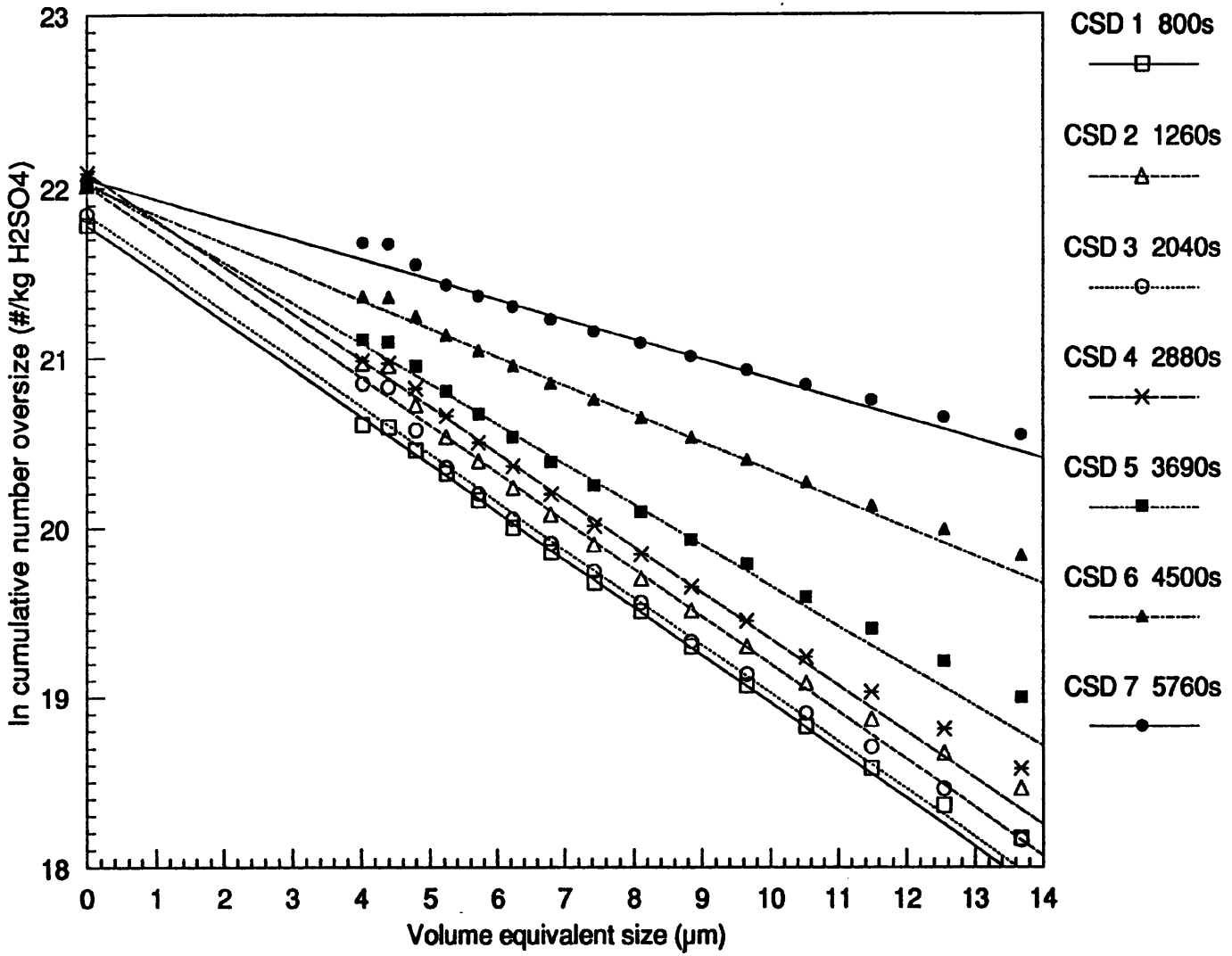

Figure 5.22b Graphical estimation of nucleation kinetics from cumulative number oversize against size plots.

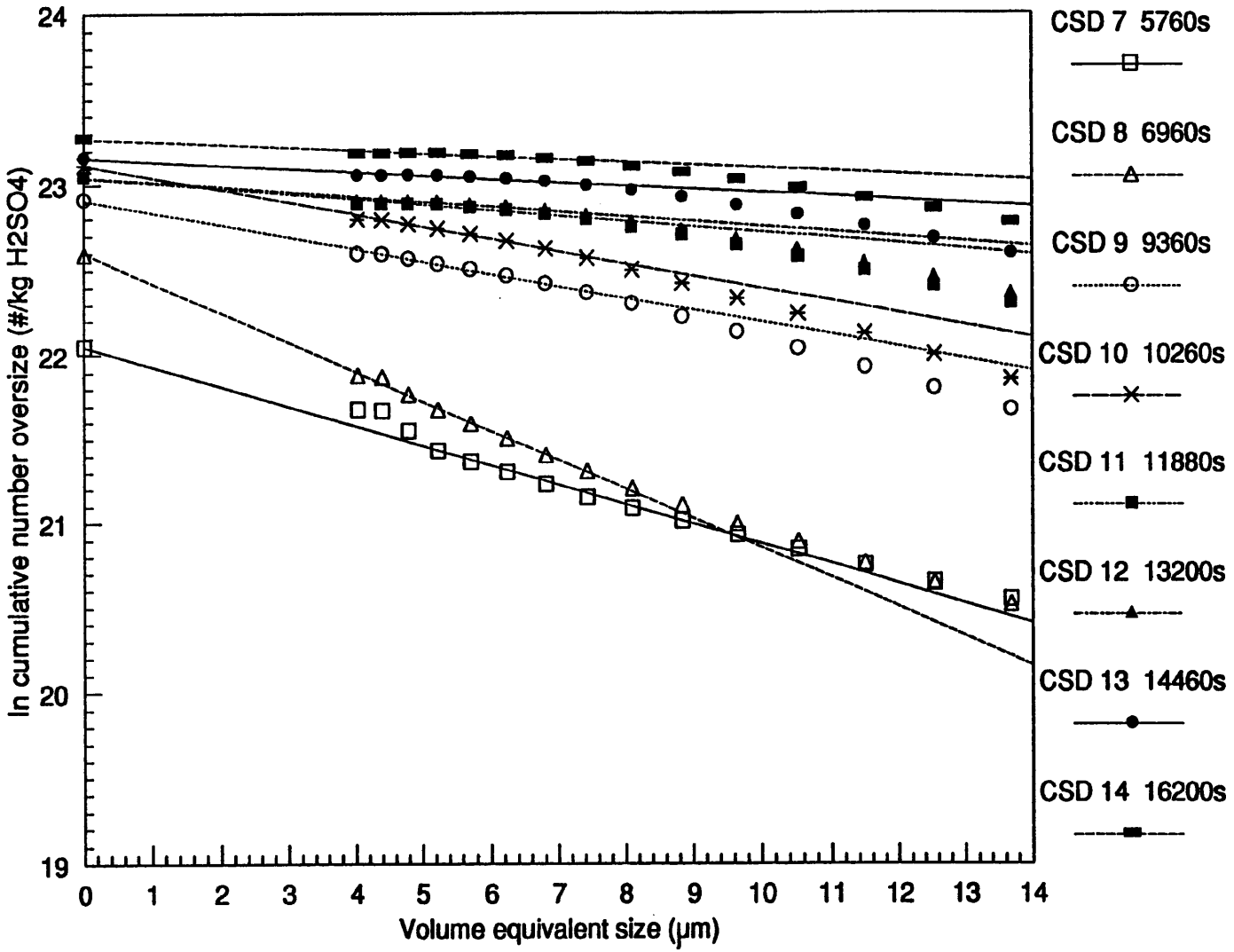

Figure 5.23a Graphical estimation of growth kinetics from cumulative number oversize against size plots.

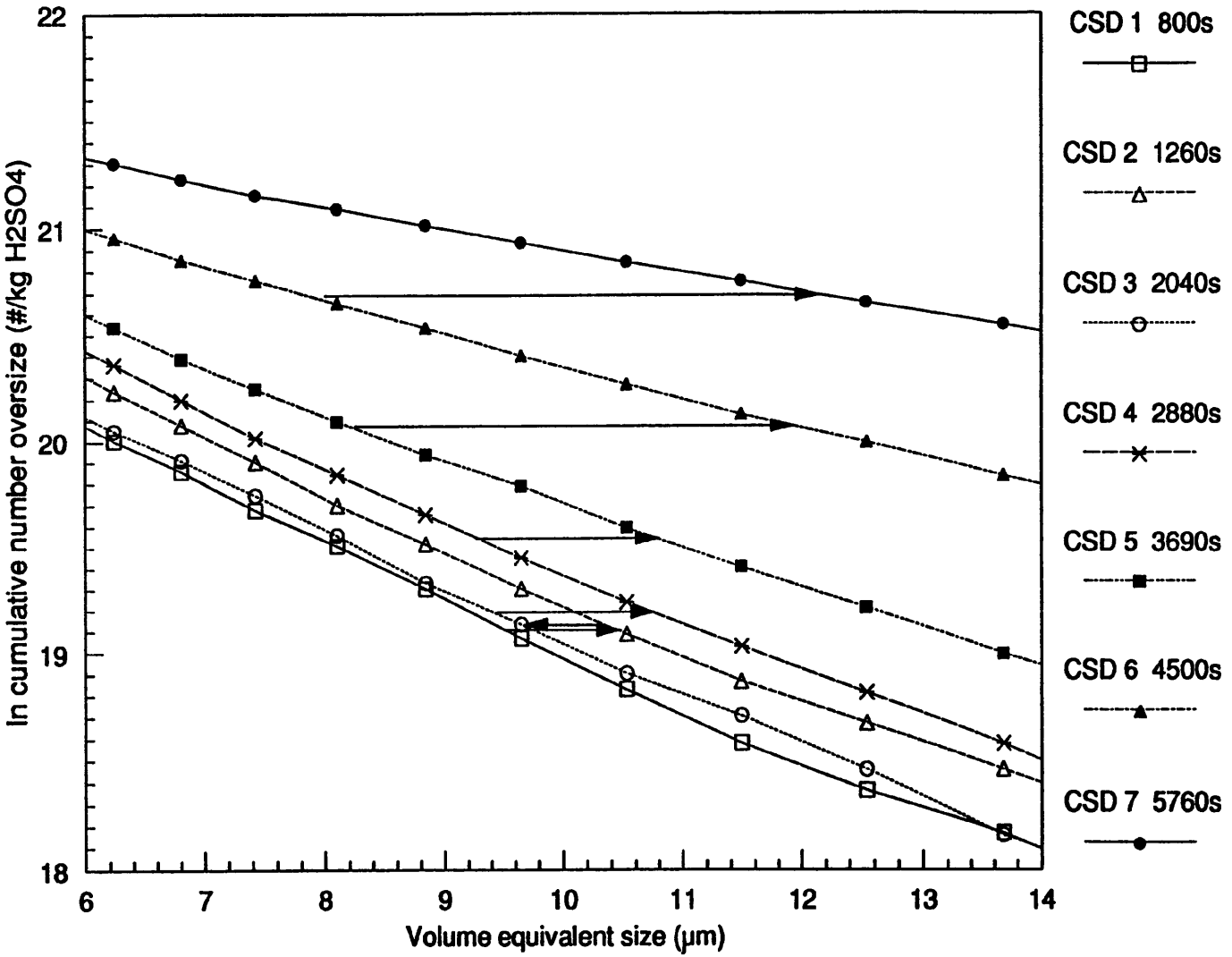

Figure 5.23b Graphical estimation of growth kinetics from cumulative number oversize against size plots.

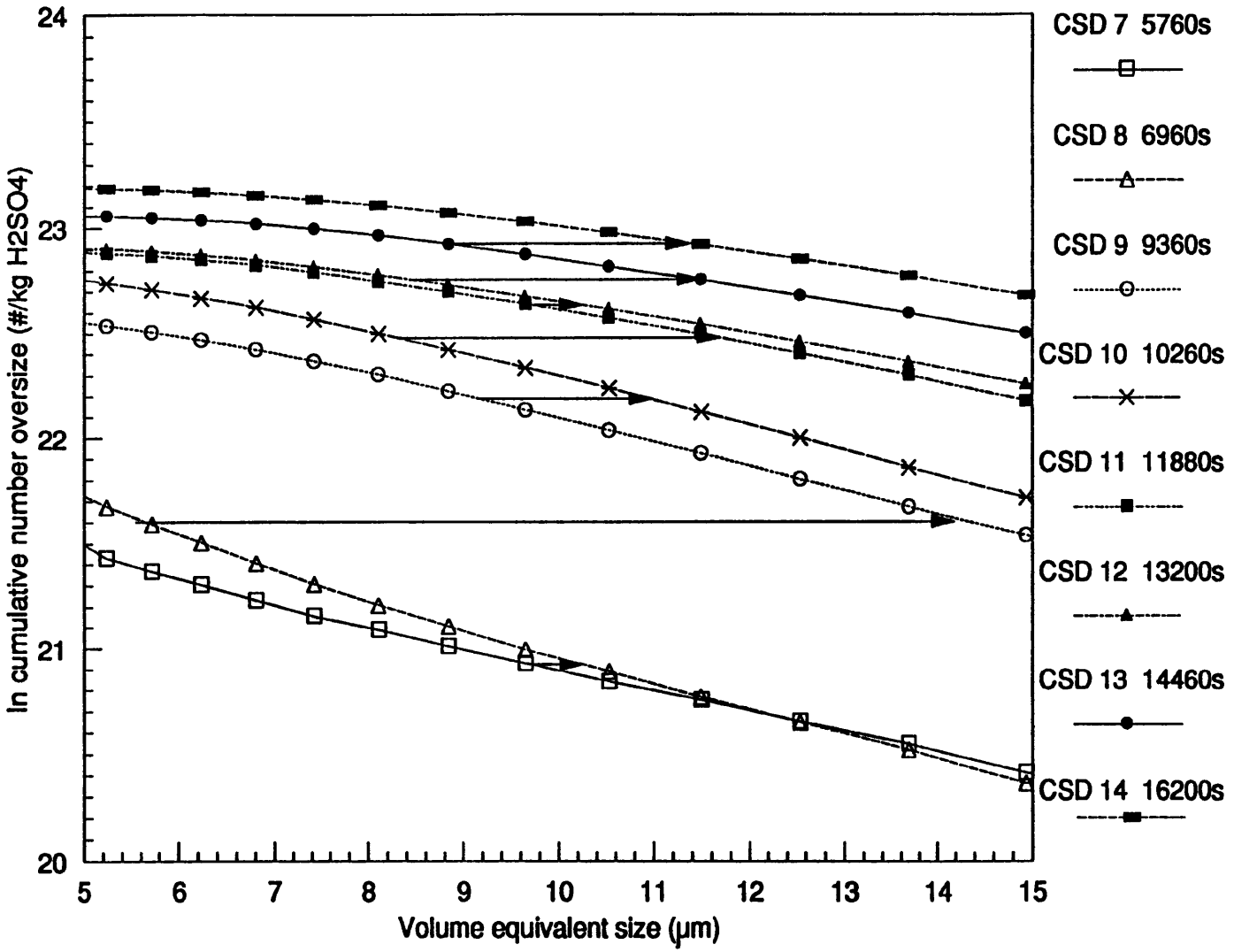

Table 5.9 The growth and nucleation kinetics estimated from a single cooling crystallization experiment (seeded run 3) using the graphical procedure (the data obtained by s-plane analysis of the same experimental data are included for comparison).

Mean values of experimental parameters during the increments over which the kinetics were estimated						Experimentally determined kinetics			
						Graphical method		S-plane method	
Mean Time	Mean Temp	Equilib. Conc.	Expt. Conc.	Supersat.	Magma density	Growth rate	Nucln. rate	Growth rate	Nucln. rate
(s)	(°C)	(kg G-acid.K_2.H_2O/kg 40% H_2SO_4 soln.)				um/s	#/kgFS/s	um/s	#/kgFS/s
1030	78.1	0.1866	0.1996	0.01294	0.00047	0.00193	76010	0.00594	39930
2460	76.4	0.1817	0.1985	0.01680	0.00157	0.00146	341510	0.00405	27570
3285	74.45	0.1761	0.1983	0.02219	0.00177	0.00178	140290	0.00262	6812
4095	71.85	0.1688	0.1981	0.02930	0.00197	0.00439	395340	0.00666	18150
5130	69.05	0.1611	0.1915	0.03038	0.00857	0.00343	612550		
5730	66.5	0.1543	0.1862	0.03190	0.01387			0.0034	44550
6360	65.05	0.1505	0.1785	0.02801	0.02157	0.00062	1115940		
7650	60.3	0.1384	0.1631	0.02471	0.03697			0.00656	174340
8160	58.7	0.1344	0.1578	0.02335	0.04227	0.00385	392960		
8850	56.5	0.1291	0.1507	0.02158	0.04937			0.00667	13280
9810	53.25	0.1215	0.1414	0.01992	0.05867	0.00215	1391770	0.00446	192300
11070	49.15	0.1122	0.1276	0.01534	0.07247	0.00225	435560		
12540	44.45	0.1021	0.1171	0.01497	0.08297	0.00045	69870		
13830	40.15	0.0934	0.1081	0.01471	0.09197	0.00251	1105530	0.00363	39170
15330	35.25	0.0840	0.0973	0.01331	0.10277	0.00145	712540	0.00217	43520

Note; FS = free solvent, in this case 40% sulphuric acid solution.

Figure 5.24 The dependence of growth rates determined by the graphical procedure on supersaturation in a typical seeded crystallization (seeded run 3).

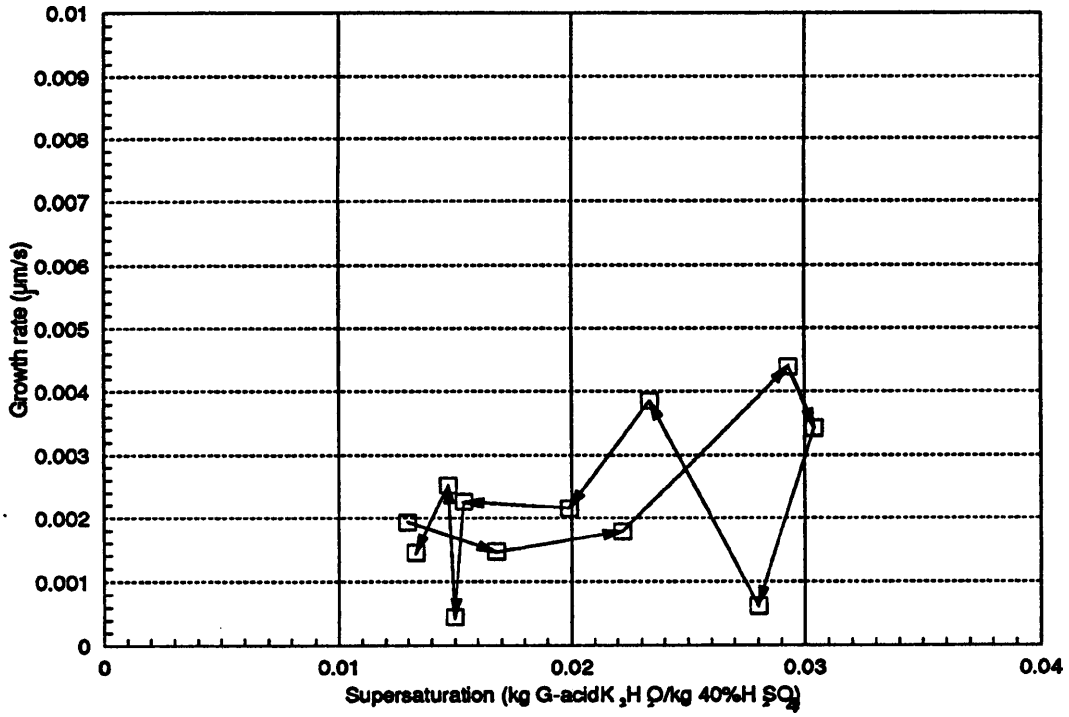

Figure 5.25 The dependence of nucleation rates determined by the graphical procedure on supersaturation in a typical seeded crystallization (seeded run 3).

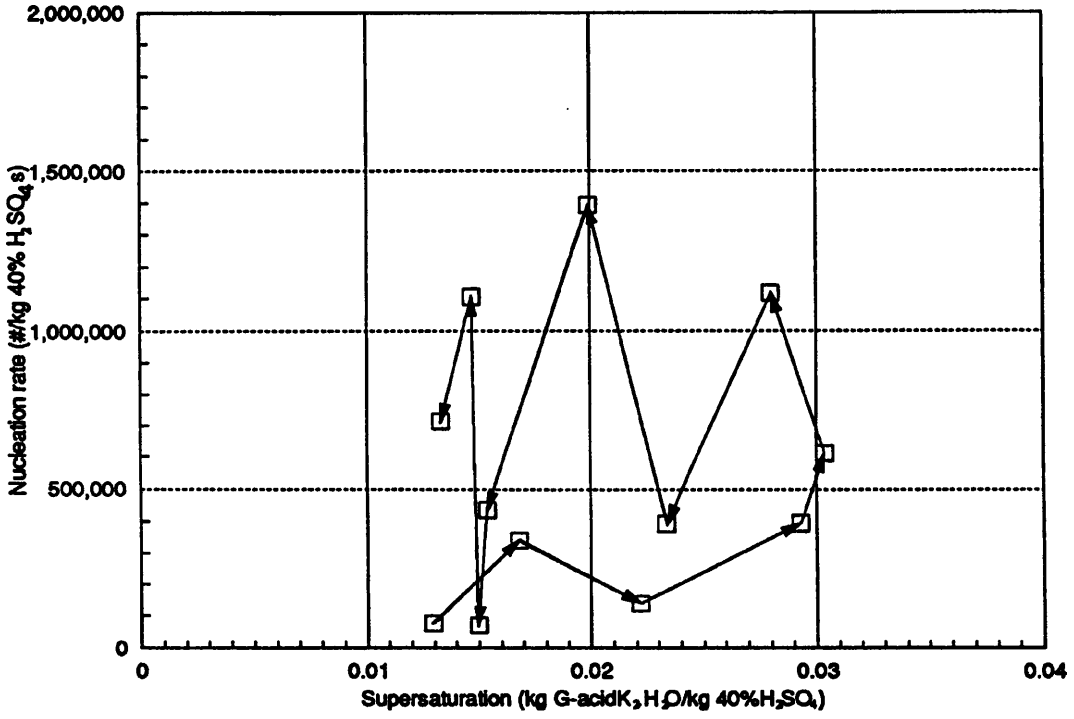

The growth and nucleation rates estimated from Figures 5.22 and 5.23 are included in Table 5.9. The values determined by the method of moments analysis are included for comparison. Table 5.9 also includes the mean values of the measured experimental variables corresponding to the intervals over which the kinetic data were evaluated. The growth rates are plotted against supersaturation in Figure 5.24 and the nucleation rates in Figure 5.25.

The growth and nucleation rates evaluated by the graphical procedure were correlated with the mean values of the experimental parameters corresponding to the intervals over which they were determined. The correlation procedure used was identical with that used for the data obtained by s-plane analysis though there were rather fewer data points. Equations 5.23 and 5.24 were used to describe the growth and nucleation kinetics respectively. The resulting values for the parameters in these equations are shown in Table 5.10 along with the standard errors for the 95% confidence limits on each parameter and the overall correlation coefficient r^2

Table 5.10 The growth and nucleation kinetic equations based on Equations 5.23 and 5.24 fitted to the growth and nucleation rates determined by the graphical procedure.

Growth: $\overline{G} = K_g \Delta C^g e^{E_g/RT}$			
K_g (m/[s (kg/kg)^g])	g	E_g (J/mol)	r^2
5.28×10^{-8}	0.86	-516	0.234
$\pm 2.18 \times 10^{-7}$	± 0.65	± 14000	

Nucleation: $\overline{B} = K_b \Delta C^b M_T^j e^{E_b/RT}$				
K_b (#/[kg40%H_2SO_4 s (kg/kg)^j (kg/kg)^b])	b	E_b (J/mol)	j	r^2
2.37×10^5	2.45	-31875	0.32	0.440
$\pm 3.465 \times 10^6$	± 2.71	± 55710	± 0.38	

The correlation coefficients r^2 for the fitted growth and nucleation rate equations are low, 0.234 for the growth rate equation and 0.440 for the nucleation rate equation.

This suggests that there is considerable scatter amongst the data, this is also seen in the width of the 95% confidence limits on the fitted parameters. The scatter amongst the data are seen in Figures 5.26 and 5.27.

Figure 5.26 A plot of growth rate predicted by Equation 5.23 using the values in Table 5.10 against observed growth rate for the kinetic data obtained by the graphical analysis. The data from the moments analysis procedure are included for comparison.

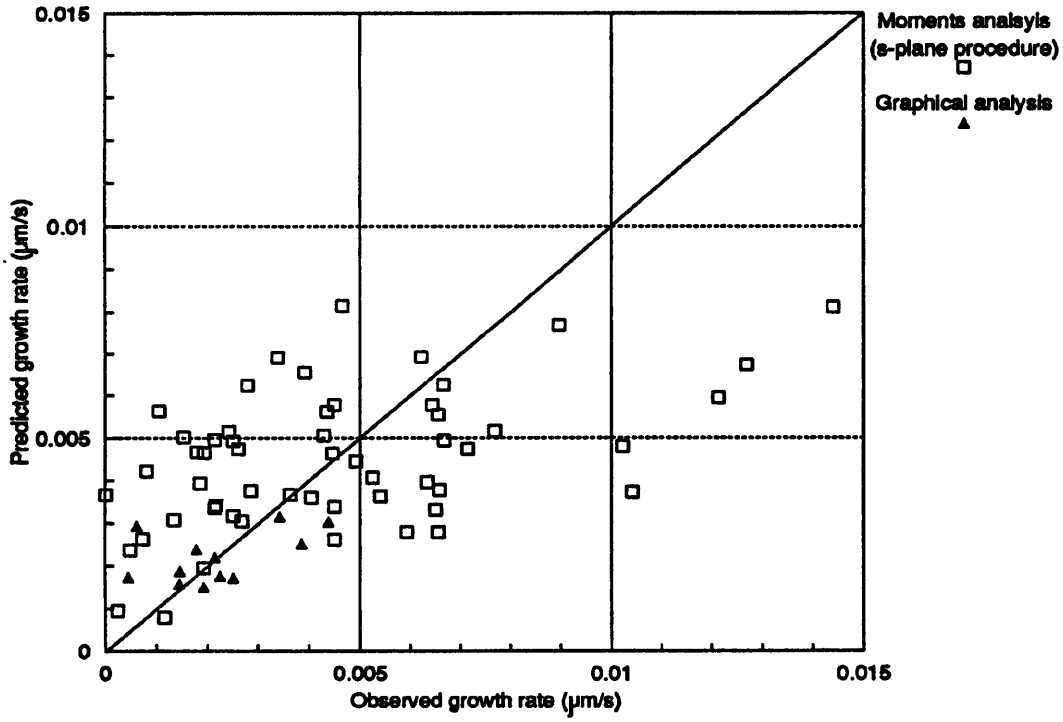

Figure 5.27 A plot of nucleation rate predicted by Equation 5.24 using the values in Table 5.10 against observed nucleation rate for the kinetic data obtained by the graphical analysis. The data from the moments analysis procedure are included for comparison.

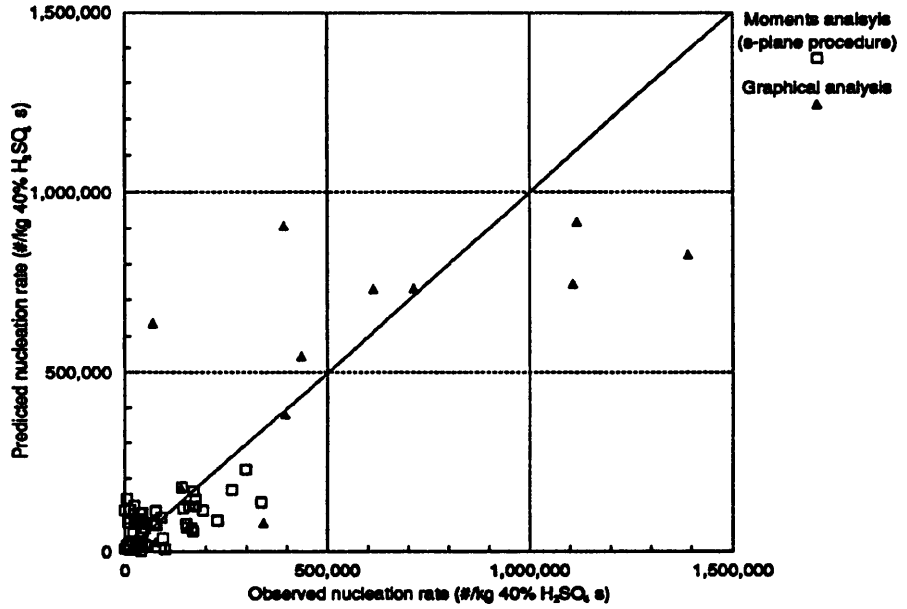

A correlation based on Equation 5.26 was performed using the nucleation rate data obtained by the graphical procedure. The resulting correlation is shown in Table 5.11.

Table 5.11 Values of parameters in Equation 5.26 determined by correlation using the kinetic data obtained by graphical analysis procedure.

$B = K_r M_t^j \exp\left(\frac{-E_r}{RT}\right) G^i$				
K_r (#/[kg40%H_2SO_4 s ([kg/kg)^j (m/s)^i])	j	E_r (j/mol)	i	r^2
7.26×10^8	0.33	13,770	0.13	0.295
9.19×10^9	0.34	32,840	0.32	

The correlation co-efficient, r^2 for Equation 5.26 is 0.295, lower than the value of 0.440 obtained from Equation 5.24 which included a direct supersaturation dependency. Figure 5.28 is a plot of log $B/\left(M_t^j.\exp\left(\frac{-E_r}{RT}\right)\right)$ against log G, the slope of the line is the relative kinetic order, i, and the intercept is K_r, the rate constant.

Figure 5.28 A plot of log $B/\left(M_t^j.\exp\left(\frac{-E_r}{RT}\right)\right)$ against log G. The line fitted through the data corresponds to Equation 5.26 using the values of the variables listed in Table 5.11.

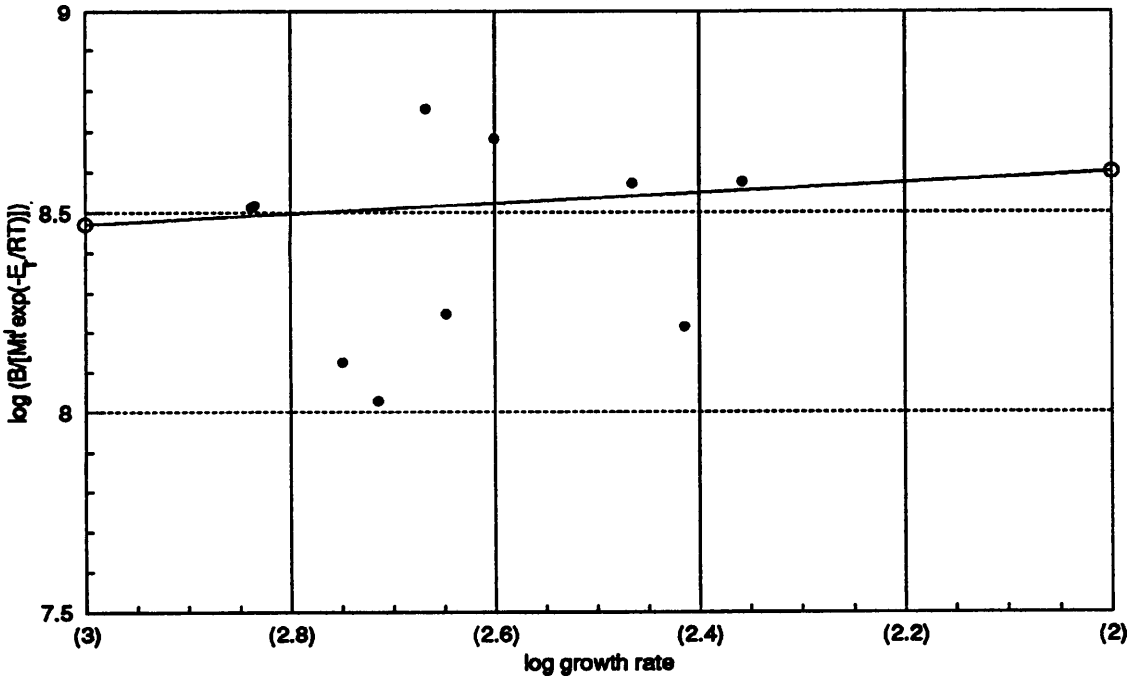

The poor fit of the line to the measured nucleation rate data in Figure 5.28 indicates that the values of i, the gradient, and K_r, the intercept, are inaccurate.

The nucleation rates predicted using Equation 5.26 are compared with the nucleation rates predicted using Equation 5.24 in Figure 5.29.

Figure 5.29 A plot of the nucleation rates predicted by Equations 5.24 and 5.26. against the nucleation rates derived by the graphical procedure.

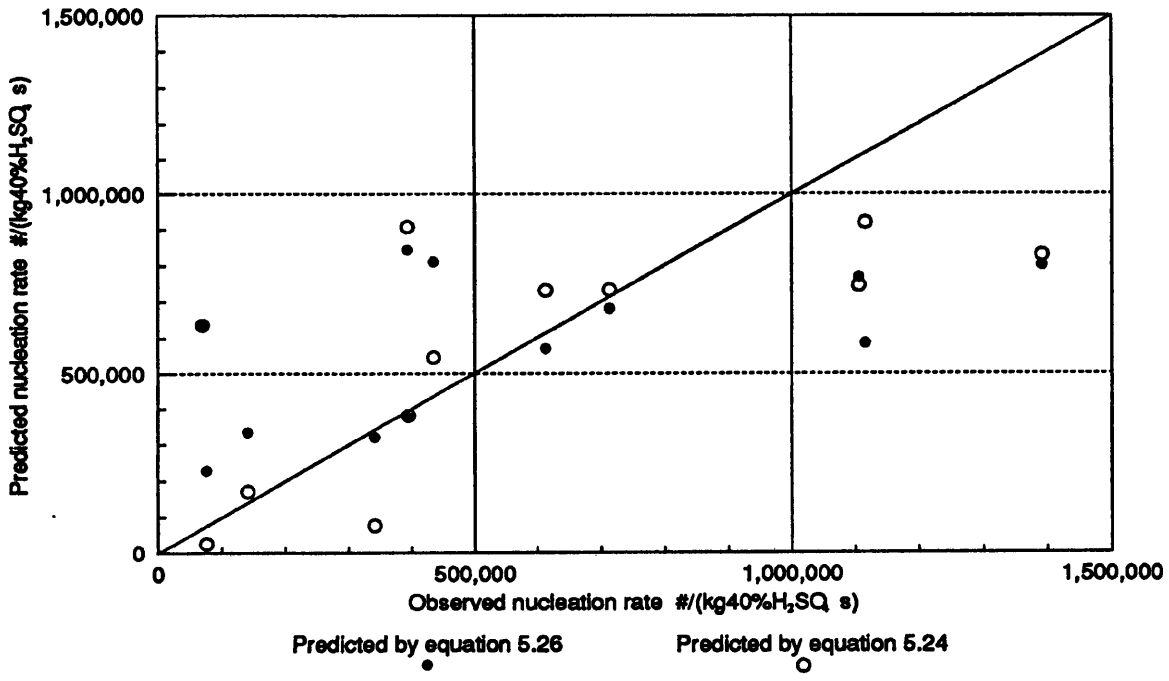

5.5 Discussion of the results

In this section the experimental results are examined critically. Greatest attention is paid to the growth and nucleation kinetics determined using the two analytical procedures employed to extract kinetic information from the size distribution data. The causes of problems associated with the measurement of crystallization kinetics in this system are discussed and suggestions of how these might be overcome are made.

5.5.1 Sources of experimental error

Determination of the dependence of the crystallization kinetics on the experimental variables examined requires that a number of parameters are measured accurately. In this section each measurement is examined and the sources of error are considered. Clearly the accuracy of the experimental data must be considered carefully when discussing the crystallization kinetics evaluated from the

experimental measurements. In all cases efforts were made to minimise the experimental error but the results are likely to have been influenced by such errors. The most important sources of error are discussed below.

- Experimental variables.

The values of experimental variables with which the crystallization kinetics are correlated must be measured accurately. The errors in the measurement of time, temperature and agitation rate were relatively small. However control of the temperature - time profiles was subject to some error due to the thermal inertia of the crystallizer. This shows up most in Tables 5.3 and 5.4. where the time at which the peak supersaturation occurs differs slightly from experiment to experiment between nominaly identical experiments. The measurement of solution concentration and hence supersaturation was subject to rather larger errors. The error on the measurement of G-acid concentration in solution is estimated to be less than 0.005kg G-acid dipotassium salt monohydrate per kg of 40% sulphuric acid solution. This corresponds to less than 5% of the solution concentration but could amount to a 20% error on the supersaturation level. This represents an upper limit on the error on individual determinations, however a series of solution samples were taken during each experiment and so a smooth curve could be drawn through the data reducing the reliance placed on an individual concentration determination.

- Crystal size distributions

The accurate measurement of crystal size distributions is vitally important for the success of both the procedures used to determine crystallization kinetics. There are a number of experimental procedures which are potential sources of errors that are likely to have a significant effect on the measured crystal size distributions.

Sampling from the crystallizer:

The size of the samples from the crystallizer (200 to 1000µl) was rather small though the samples were likely to have been representative, since they contained around 1,000,000 crystals. In the later stages of the experiments where the magma density was quite high and the crystals were nearing their maximum size the crystallizer may not have been well mixed resulting in a biasing of the size distribution to small

size as larger crystals settled. However the slurry in the crystallizer appeared well suspended. The plate like shape of the crystals and the relatively low density difference between the crystals (1837kg/m^3) and the solution (around 1315kg/m^3 towards the end of an experiment) would tend to support the view that the crystals were well suspended. There may have been segregation during the sampling procedure though care was taken to minimise this by increasing the aperture size of the pipette tip and controlling the rate at which the slurry sample was drawn into the pipette tip.

Dilution of the slurry sample:

The slurry sample from the crystallizer was diluted significantly (to around 1/200th of its original concentration). This may have resulted in alteration of the crystal size distribution by dissolution if the electrolyte was undersaturated and the time between sample dilution and analysis was long. The sample volume and the extent of the dilution were carefully chosen and the time between diluting the slurry sample and determining the size distribution was minimised to limit the extent of any dissolution. There were occasions when dissolution of the crystal samples was suspected, in these cases the experiment was terminated and the results discarded. Even after dilution the number of crystals sampled by the Elzone Particle Size Analyser was still statistically valid, in most cases exceeding 5,000 crystals

Screening:

A screening procedure was used to prevent the orifice blocking during the later stages of the experiments when the crystals had grown sufficiently large to block the orifice tube. The screening procedure was presumed to distort the crystal size distribution, both by truncating it at high size and retaining some crystals smaller than the mesh size thus reducing the number of crystals at all sizes. Truncating the size distribution affects the cumulative number oversize plots as the loss of the larger crystals from the distribution cannot be compensated for. The extent of the truncation of the size distribution may be seen from the plots of ln cumulative number oversize against ln Figure 5.13 where at high sizes the distributions measured later in the experiment dip below those measured prior to screening. An attempt was made to quantify this effect by comparing the magma density determined from the concentration

measurements with the magma density determined from the measured crystal volume. The results are shown in Figure 5.30. The magma density data determined from the crystal size distribution measurements show much more scatter than the data obtained from the concentration measurements. The scatter in the results form the measured size distributions indicate the greater errors in these measurements than in the measurements of solution concentration. The discrepancy between the two sets of data became apparent after the screening procedure was employed 6000s after seeding. After screening was employed the magma density determined from the size distribution began to lag behind the data from the concentration measurements. This is in agreement with the suggestion that screening would reduce the measured magma density. It would be expected that the gap between the two measurements of magma density would widen towards the end of the experiment. The last two data points are however at odds with this suggestion and cast some doubt on it, though the accuracy of the measurement of these size distributions may be questioned (see later comments on coincidence and orifice tube blockage).

Figure 5.30 A plot showing magma density determined from both solution concentration measurements and crystal size distribution measurements during a typical seeded cooling crystallization. (seeded run 3).

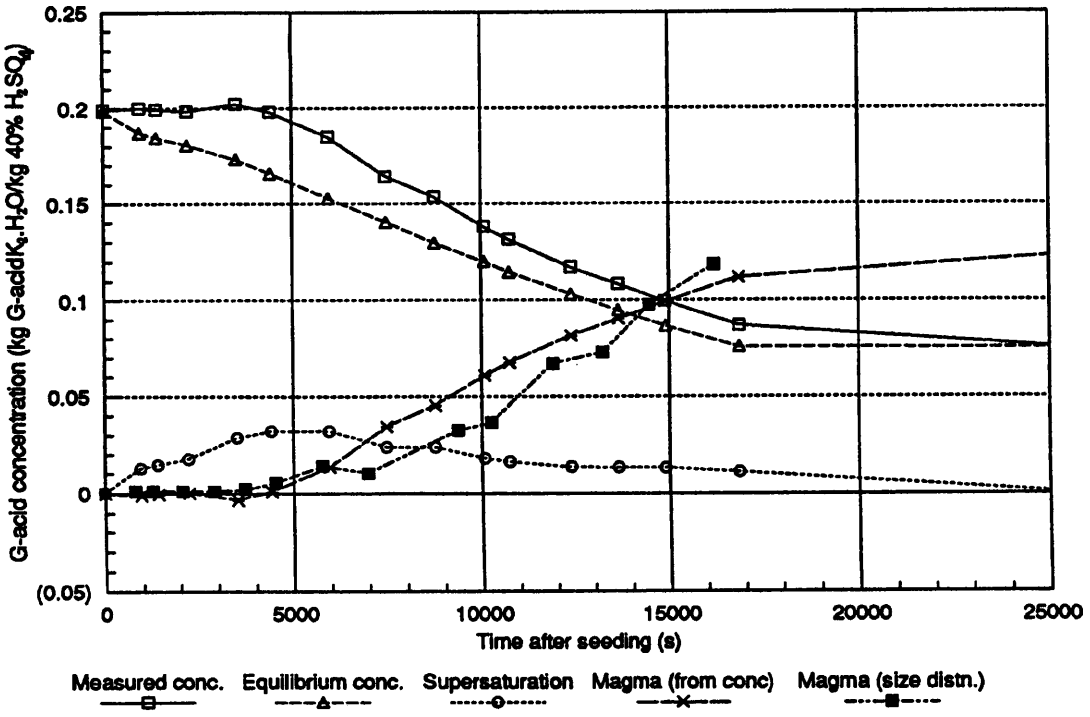

Mixing:

The Elzone instrument relies on the suspension to be analysed being well mixed. The stirrer speed in the Elzone sampling vessel was always set at the same level, a little less than the level at which a vortex began to be formed, but sufficiently high to ensure rapid mixing. The choice of around 5 seconds agitation prior to sampling the slurry was an attempt to minimise the delay between dilution and sampling and was thought not to have caused any problems due to incomplete mixing.

Coincidence:

The high solids concentration towards the end of the experiments meant that even after dilution the particle concentration in the slurry sampled by the Elzone instrument was rather high and coincidence effects may have been significant in some of these measurements towards the end of the experiments. This would lead to an overestimate of the size of the crystals and an underestimate of their number.

Orifice tube blockage:

Some attempts to determine the crystal size distribution were unsuccessful due to blockage of the sizing orifice. The blockage of the orifice was observed using the microscope attachment on the instrument to watch the orifice during sizing. The orifice became blocked as a result of one crystal fouling the edge of the orifice and being held their by the flow of slurry through the orifice, other crystals then accumulated until the orifice became blocked. Sometimes this occurred despite the use of the screening technique. Blockage of the orifice in this way resulted in an increase in the time required to draw the correct sample volume through the orifice. This showed up as an over-time error. It is likely that momentary blockage of this kind could adversely affect the size measurement for a fraction of a second during the count without showing up as an over-time error. The result of such an incident would be to generate a significant number of spurious pulses.

Crystal Shape:

It is difficult to assess the aspect ratio of the crystals accurately as it can vary depending on the growth conditions. This was shown in Plates 5.3 and 5.4. The relationship between the crystal size determined by sieving and by the Elzone Particle Size Analyser is influenced by the aspect ratio which is assumed for the crystals. The volume equivalent diameter determined by the Elzone Particle Size Analyser (that is the diameter of a sphere of the same volume as the measured crystal) is used in all the calculations of the crystallization kinetics. The volume equivalent diameter is convenient for describing a mass balance and does not rely on a subjective assessment of the aspect ratio of the crystals. The reported growth kinetics represent the rate of change in this volume equivalent diameter. It has been reported Lloyd (1979) that the electrical zone sensing procedure used by the Elzone instrument yields an accurate measure of the volume of plate-like and other non-spherical particles.

Seed Crystals:

The seed crystal size distribution is rather broad and contains a significant number of fine particles, the smallest of which were difficult to characterise until they had grown above the threshold size into the measured part of the size distribution. This delay in detection may affect the initial estimate of the nucleation rate as fine crystal fragments adhering to the seed crystals are released and are detected later as additional nuclei.

- Overall effect:

The combined effect of each of these sources of potential error is to highlight the difficulty of accurately determining the crystal size during a crystallization process of this kind. This in turn indicates the principle obstacle in determining crystallization kinetics from crystal size distributions. Both techniques used in this study are based on comparing crystal size distributions measured at intervals during the crystallization process. The techniques require that subsequent size distributions are sufficiently different to allow the difference to be used to describe the process which is taking place. Yet the interval between them must be short enough to allow

sufficiently many observations to be made during an experiment to build-up a picture of the crystallization. The change in the experimental variables during the intervals over which the kinetics are estimated must not be too large otherwise the mean values of the experimental variables could not be used to describe the behaviour of the system. If the distributions are subject to errors of a similar magnitude to the difference between them the technique is likely to yield poor results.

5.5.2 Discussion of the measured growth kinetics

The growth rates determined by both the graphical and the s-plane analysis procedures for the selected seeded batch crystallization (seeded run 3) are shown in Figure 5.31. and are listed in Table 5.12

Figure 5.31 Growth rates determined by the graphical and the s-plane analysis procedures for a seeded batch crystallization experiment.

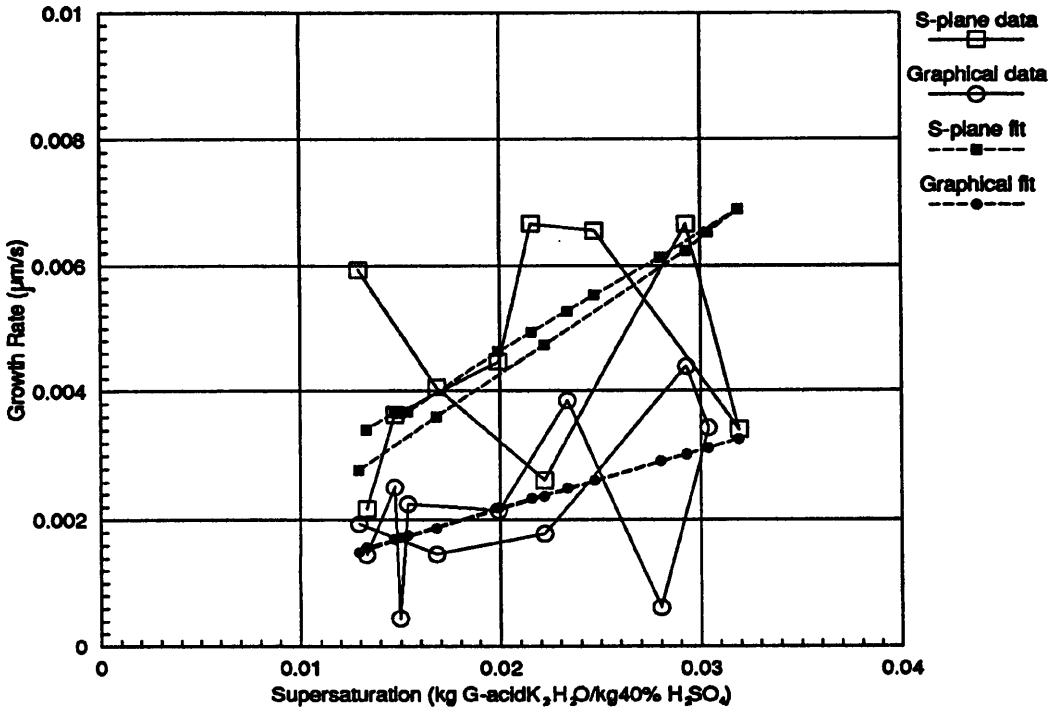

Examination of Figure 5.31 reveals that the growth rate determined graphically is approximately half that determined by the moments method.

In Table 5.12 the growth rates determined by both procedures have for each increment been multiplied by the increment length and summed over the whole experiment to give an estimate of the increase in size of a seed crystal. According to the kinetic data derived by the graphical method a 20μm seed crystal would grow to about 55μm during the 16000 s over which measurements were made. According to the moments method it would grow to 85μm over the same period.

As the 150μm orifice tube was used to measure the size distribution to small sizes so that the nucleation rate could be determined no data on the largest crystal sizes reached was obtained. However the time at which screening became necessary to prevent the orifice tube blocking provides an approximate reference point.

Extending the geometrical arguments of Figure 5.5 it is possible to calculate the volume equivalent size of a crystal with a diagonal length equal to the orifice diameter. This is shown schematically in Figure 5.32. The smallest volume equivalent size of a crystal which could lodge in the orifice tube would be around 55μm. If the largest seeds are presumed to have a volume equivalent size of 20μm the time interval before screening would be required can calculated from the growth rates determined by the two methods. According to the moments method screening would become necessary after about 8500s whereas the growth rates determined graphically indicate that screening would only become necessary towards the end of the experiment after perhaps 16500s. In fact screening was required after 5500s. This crude assessment is very dependent on the aspect ratio which is assumed for the crystal. Reducing the crystal thickness will serve to reduce the volume equivalent size a crystal must attain before it is capable of blocking the orifice tube. Despite the uncertainty over the aspect ratio of the crystals this argument appears to give greatest credibility to the growth rates determined by the moments method. The growth of a 20μm (volume equivalent size) seed crystal is predicted by both of the procedures used to estimate growth kinetics in Figure 5.33.

Table 5.12 Estimations of the increase in crystal size of 20μm seed crystals during a batch cooling crystallization (seeded run 3).

Time (s)			S-plane analysis			Graphical analysis		
Initial t_s	Final t_f	Step Δt	Rate μm/s	Increase μm	Seed size μm	Rate μm/s	Increase μm	Seed size μm
800	1260	460	0.00594	2.7324	22.7324	0.00193	0.8878	20.8878
1260	2880	1620	0.00405	6.561	29.2934	0.00146	2.3652	23.253
2880	3690	810	0.00262	2.1222	31.4156	0.00178	1.4418	24.6948
3690	4500	810	0.00666	5.3946	36.8102	0.00439	3.5559	28.2507
4500	5760	1260			36.8102	0.00343	4.3218	32.5725
4500	6960	2460	0.0034	8.364	45.1742			
5760	6960	1200				0.00062	0.744	33.3165
6960	8340	1380	0.00656	9.0528	54.227			
6960	9360	2400				0.00385	9.24	42.5565
8340	9360	1020	0.00667	6.8034	61.0304			
9360	10260	900	0.00446	4.014	65.0444	0.00215	1.935	44.4915
10260	11880	1620				0.00225	3.645	48.1365
11880	13200	1320				0.00045	0.594	48.7305
10260	14460	4200	0.00363	15.246	80.2904			
13200	14460	1260				0.00251	3.1626	51.8931
14460	16200	1740	0.00217	3.7758	84.0662	0.00145	2.523	54.4161

Figure 5.32 The relationship between volume equivalent crystal size and blockage of the Elzone orifice tube.

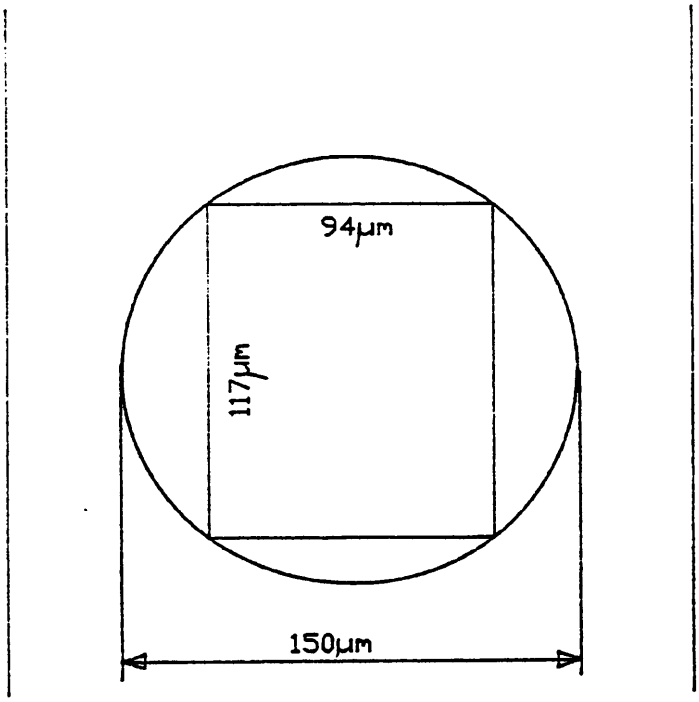

Figure 5.32 The increase in seed crystal size predicted by the graphical and s-plane analysis procedures.

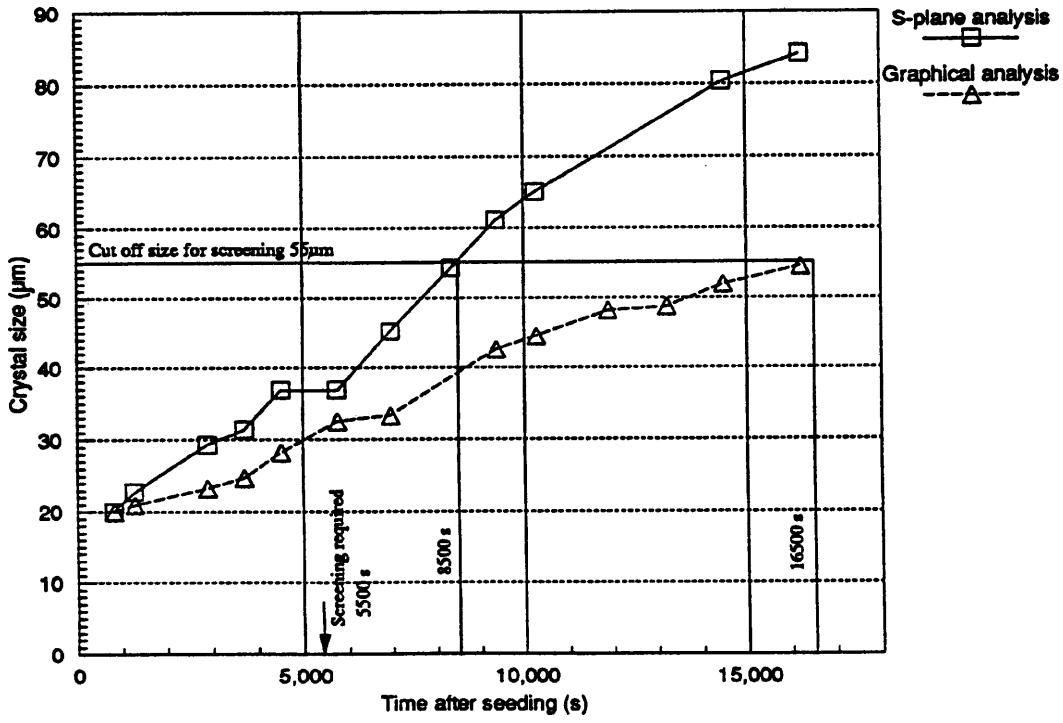

5.5.3 Discussion of the fitted growth rate equations

The equations fitted to the two sets of growth rate data are similar, the differences lying in the exponent on supersaturation and the activation energy. The constant terms in the two equations differ by less than 3%.

- Activation energies, E_g

The activation energies E_g reported for growth in Tables 5.7 and 5.9 are negative. In the case of the s-plane analysis -3660 ± 6920 J/mol, and for the graphical procedure -516 ± 14000 J/mol. The effect of these differences in activation energy over the temperature range 30 to 80°C are examined in Table 5.13

Table 5.13 The effect of the difference in the values of the activation energies for the graphical and moments based growth kinetics.

Estimation technique	Temperature °C	$e^{-E_g/RT}$
Moments analysis (S-plane)	80	3.480
Moments analysis (S-plane)	30	4.275
Graphical analysis	80	1.192
Graphical analysis	30	1.227

The temperature dependence incorporated in the growth rate equations by the activation energy term indicates an increase in growth rate as the temperature decreases. In the case of the equation fitted to the growth rate data obtained by the moments procedure the effect of temperature is noticable; the growth rate increases by almost 23% as the temperature is lowered from 80 to 30°C. This is the cause of the "dog-leg" in the fitted line for the s-plane data in Figure 5.31. The effect of temperature on the growth rate determined by the graphical procedure is much less. The increase in growth rate as the temperature decreases form 80 to 30°C is around 3%. The 95% confidence limit on both the activation energies for growth are much greater than the activation energies themselves indicating that great caution should be used in interpreting these observations. A negative activation energy for growth is unusual, growth rates usually increase with increasing temperature. It is likely

that the negative activation energy for growth in the derived kinetics is a result of the significant degree of scatter amongst the experimental data leading to an equation which contains unrealistic values for temperature dependence. The range of temperatures examined is relatively narrow when considered as absolute temperature (303-353K). It should be noted that the temperature dependence of the growth rates of the different crystal faces is likely to be different, and the crystal shape could change with temperature. This could lead to a complex temperature dependence of the overall growth rate. However this suggestion is difficult to substantiate in this system where it is difficult to measure growth kinetics accurately.

- Exponent on supersaturation, *g*.

The exponents on supersaturation are similar, 0.86 for the data obtained by the graphical procedure and 0.96 for the data obtained by the s-plane analysis procedure. The effect of the difference between the fitted exponents is considered in Table 5.14 assuming typical supersaturation levels of 0.01 and 0.025kg G-acid dipotassium salt monohydrate per kg 40% H_2SO_4 solution.

Table 5.14 The effect of the difference in exponent on supersaturation for typical supersaturation levels.

Estimation technique	Supersaturation kg G-acid/ kg H_2SO_4 soln.	ΔC^g
Moments analysis (S-plane)	0.025	0.02897
Moments analysis (S-plane)	0.010	0.01202
Graphical analysis	0.025	0.04190
Graphical analysis	0.010	0.01905

The supersaturation dependency of the growth rate is slightly greater for the kinetics determined by the moments procedure than those determined by the graphical procedure. The moments method suggests that the growth rate increases 2.4 times over the supersaturation range 0.01 to 0.025, whilst the increase predicted by the graphical procedure is 2.2 times.

5.5.4 Discussion of the measured nucleation kinetics

The nucleation rates determined for the chosen seeded batch cooling crystallization using the two analytical techniques differ greatly. This is shown in Figure 5.34. The numerical data are given in Table 5.15

Figure 5.34 A comparison of the nucleation rates estimated by the graphical and s-plane analysis procedures.

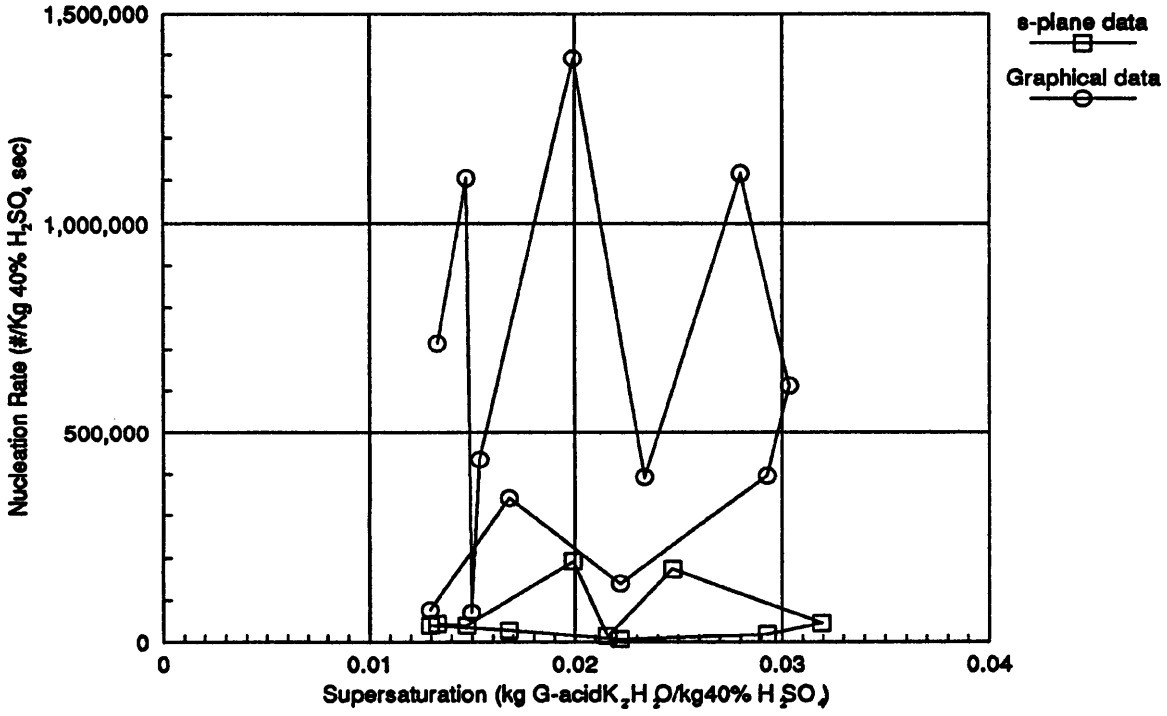

Examination of Figure 5.34 reveals that the nucleation rate determined graphically is substantially greater than that determined by the moments method. It is possible to use the measured nucleation kinetics to calculate the number of crystals which would be in the crystallizer and compare this with the number of crystals measured during the experiment. This has been done by extending the ln cumulative number oversize graphs of the measured crystal size distributions to zero size. The results are plotted in Figure 5.35 and are included in Table 5.15.

Table 5.15 Comparison of the nucleation rates determined by the two procedures for elucidating kinetics with the data obtained by extension of the ln cumulative number over size plot to zero size.

Time (s)			Nucleation (s-plane analysis) (#/kg40%H_2SO_4)				Nucleation (Graphical analysis) (#/kg40%H_2SO_4)				Extended CSDs
Initial t_s	Final t_f	Step Δt	Rate (/s)	Number	CNOS	ln CNOS	Rate (/s)	Number	CNOS	ln CNOS	ln cnos
800	800	0	-	-	2.9E+09	21.78348			2.9E+09	21.78452	21.78452
800	1260	460	39932	18368720	2.9E+09	21.78982	76009	34964140	2.9E+09	21.79654	22.0164
1260	2880	1620	27566	44656920	3.0E+09	21.80507	341511	5.5E+08	3.5E+09	21.96978	22.0859
2880	3690	810	6812	5517720	3.0E+09	21.80694	140286	1.1E+08	3.6E+09	22.00193	22.0151
3690	4500	810	18155	14705550	3.0E+09	21.81191	395340	3.2E+08	3.9E+09	22.08733	22.0116
4500	5760	1260					612546	7.7E+08	4.7E+09	22.26739	22.0497
4500	6960	2460	44547	1.1E+08	3.1E+09	21.84814					
5760	6960	1200					111594o	1.3E+09	6.0E+09	22.51885	22.5958
6960	8340	1380	174340	2.4E+08	3.3E+09	21.92335					
6960	9360	2400					392960	9.4E+08	7.0E+09	22.66432	22.9151
8340	9360	1020	13276	13541520	3.3E+09	21.92742					
9360	10260	900	192303	1.7E+08	3.5E+09	21.97803	139177o	1.3E+09	8.2E+09	22.82967	23.1223
10260	11880	1620					435564	7.1E+08	8.9E+09	22.91204	23.051
11880	13200	1320					69874	92233680	9.0E+09	22.92232	23.0536
10260	14460	4200	39175	1.6E+08	3.7E+09	22.02388					
13200	14460	1260					110553o	1.4E+09	1.0E+10	23.06598	23.1631
14460	16200	1740	43520	75724800	3.7E+09	22.04430	712538	1.2E+09	1.2E+10	23.17851	23.2756

Figure 5.35 Nucleation rates determined by the graphical and the s-plane analysis procedures for a seeded batch crystallization experiment. The data from the extrapolation of the ln cumulative number oversize plots are included for comparison.

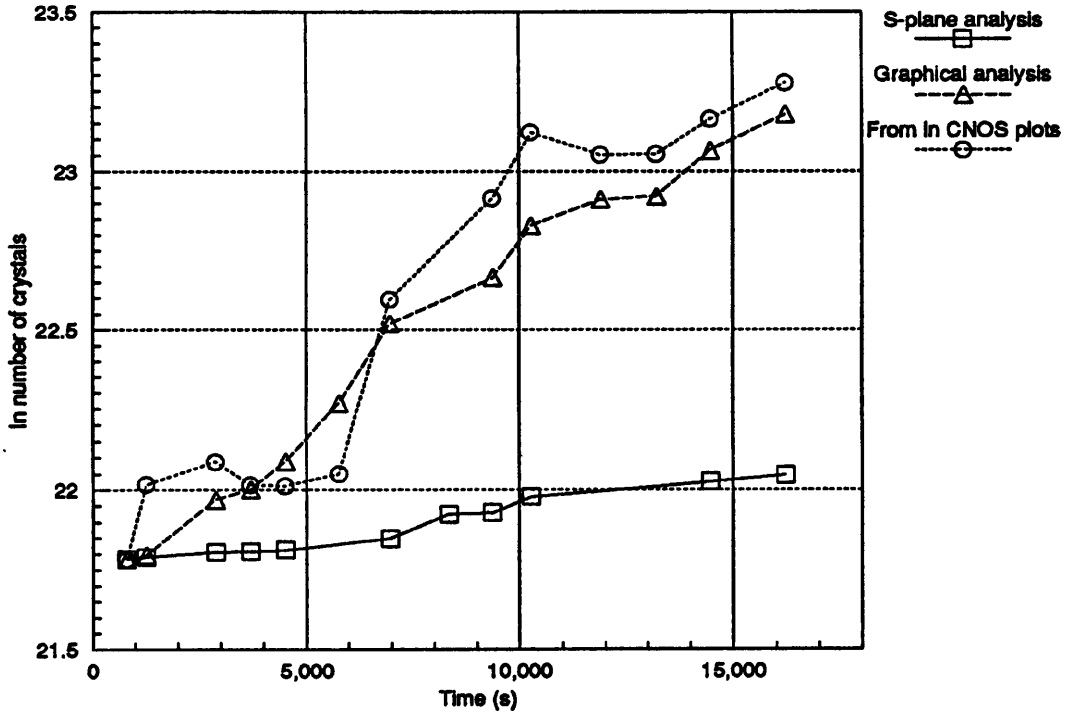

Figure 5.35 reveals that the moments analysis procedure under-predicts the nucleation rate very seriously. The number of crystals present at the end of the experiment being about an order of magnitude lower than the number predicted by the graphical procedure and estimated from the ln cumulative number oversize plots.

A possible reason for the under prediction of the nucleation rate by the moments procedure is that the weighting of the moments to reduce the contribution of the extremes of the size distributions leads to prediction of the nucleation rate from a part of the size distribution which is significantly influenced by the presence of the seed crystals.

The graphical method is in better agreement with the experimental data but it may also be subject to considerable error. The main source of error lies in the extrapolation from the smallest measured crystal size to zero size. The procedure is very dependent upon the subjective judgement of the experimentalist or the use of a curve fitting

procedure used to describe another part of the ln cumulative number oversize curve. Additionally the data at the smallest sizes is likely to be less reliable than that at slightly larger size.

5.5.5 Discussion of the equations fitted to the nucleation rate data

The pairs of equations fitted to the two sets of nucleation rate data differ significantly due to the difference in the estimates of the nucleation rates described in Section 5.5.4. The values of the terms fitted in the nucleation equations are discussed in the sections that follow. Where they are directly comparable the values fitted to Equations 5.24 and 5.26 are compared, when this is not appropriate they are considered separately.

- Exponent on Supersaturation, *b*.

The exponents on supersaturation fitted to Equation 5.24 are 2.45 ± 2.71 for the data obtained by the graphical procedure and 1.74 ± 0.61 for the data obtained by the s-plane analysis procedure. In both cases the nucleation rate shows a strong dependence on the supersaturation level. The effect of the difference between the fitted exponents is considered in Table 5.16 assuming typical supersaturation levels of 0.01 and 0.025kg G-acid dipotassium salt monohydrate per kg 40% H_2SO_4 solution.

Table 5.16 The effect of the difference in exponent on supersaturation for typical supersaturation levels.

Estimation technique	Supersaturation kg G-acid/ kg H_2SO_4 soln.	ΔC^i
Moments analysis (S-plane)	0.025	0.001631
Moments analysis (S-plane)	0.010	0.000331
Graphical analysis	0.025	0.000119
Graphical analysis	0.010	0.0000126

The supersaturation dependency of the nucleation rate determined by the moments procedure is about half that determined by the graphical procedure. The moments

method suggests that the nucleation rate increases almost 5 times over the supersaturation range 0.01 to 0.025, whilst the increase predicted by the graphical procedure is about 9.5 times.

- Exponent on growth rate, the G^i term in Equation 5.26

The G^i term in Equation 5.26 links the nucleation rate with supersaturation via the growth rate. The values of i, the overall kinetic order, fitted to Equation 5.26 were 0.87 ± 0.19 for the nucleation kinetics derived by the moments procedure and 0.13 ± 0.32 for to the kinetics derived by the graphical procedure. According to Tavare and Garside (1986a) i is equal to b/g, the nucleation order divided by the growth order. The resulting values of b/g from the correlations fitted to Equations 5.23 and 5.24 are 1.81 for the kinetic data extracted by the moments procedure and 2.85 for the kinetic data obtained by the graphical procedure. Thus there is a considerable discrepancy between the values of b/g and i. In the case of the kinetic correlations obtained by the moments based procedure i is approximately 50% of b/g. In the case of the kinetic correlations obtained by the graphical procedure i is less than 5% of b/g. The very low value of i fitted to the nucleation rates derived graphically suggests an unrealistically low dependence of the nucleation rate on supersaturation.

- Activation energy, E_b and E_r.

The activation energies fitted to Equations 5.24 and 5.26, E_b and E_r are not directly comparable. The activation energy term, E_r, fitted to Equation 5.26 operates in conjunction with the activation energy term, E_g, used to describe the temperature dependence of the growth kinetics via the growth rate Equation 5.23. The effect of this link to the activation energy for growth, E_g, is taken into account in the calculated effect of temperature on nucleation kinetics derived from Equation 5.26 in Table 5.17.

Table 5.17 The effect of the relative activation energy term fitted to Equation 5.26 on the nucleation kinetics derived by the graphical and moments methods.

Evaluation technique	Moments		Graphical	
Temperature °C	80	30	80	30
$e^{-E_r/RT}$	0.00193	.000686	.00917	.00423
G^i	2.95	3.52	1.023	1.027
Combined effect on nucleation rate	0.00569	0.00241	0.00938	0.00434
Ratio of nucleation rate at 80°C to nucleation rate at 30°C	2.36		2.16	

The combination of the growth rate term, G^i, and the relative activation energy term, E_r, reported in Table 5.17 indicates that the nucleation rates derived by both the moments and graphical procedures increase significantly over the temperature range 30 to 80°C

The activation energies for nucleation, E_b, fitted to Equation 5.24 differ substantially between the two techniques employed to determine the nucleation rates, the values for E_b are reported in Tables 5.7 and 5.10. In the case of the s-plane analysis the activation energy is 780 ± 2660 J/mol, and for the graphical procedure -31870 ± 55710 J/mol. The effect of these differences in activation energy are examined in Table 5.18

Table 5.18 The effect of the difference in the values of the activation energies, E_b for the graphical and moments based nucleation kinetics according to Equation 5.24.

Estimation technique	Temperature °C	$e^{-E_b/RT}$
Moments analysis (S-plane)	80	52098
Moments analysis (S-plane)	30	312737
Graphical analysis	80	0.767
Graphical analysis	30	0.734

The temperature dependence of the nucleation rate described by the activation energy term fitted to the data from the moments method indicates a six fold increase in the nucleation rate as the temperature decreases from 80 to 30°C. This is a very substantial negative dependence on temperature. In the case of the equation fitted to the nucleation rate data obtained by the graphical procedure the effect of temperature is minimal; the nucleation rate decreases by less than 5% as the temperature is lowered from 80 to 30°C. The 95% confidence limit on both the activation energies for nucleation are larger than the activation energies themselves indicating that caution should be used in interpreting these observations. The negative activation energy for nucleation is unexpected, the induction time usually decreases with increasing temperature whilst the nucleation rate usually increases with increasing temperature. This is probably a result of the significant degree of scatter amongst the experimental data allowing the numerical fitting procedure to fit an equation which contains unrealistic value for temperature dependence. The range of temperatures examined is relatively narrow when considered as absolute temperature (303-353K).

- **Exponent on magma density, *j*.**

The effect of magma density on the nucleation rate is described by an exponent on the magma density. Four values for the exponent on magma density have been determined. In the case of the s-plane analysis the fitted exponents were 0.32 ± 0.38, according to Equation 5.24 and 0.53 ± 0.22 according to Equation 5.26. The values of the exponent on magma density fitted to the nucleation rates determined by the graphical procedure were 0.61 ± 0.37 according to Equation 5.24 and 0.33 ± 0.34 according to Equation 5.26. The effect of these differences in exponent on magma density are examined in Table 5.19

According to Equation 5.24 the dependence of the nucleation rate on the magma density is much greater using the kinetics determined by the graphical procedure than using the kinetic equation determined by the moments method. According to the graphical procedure the nucleation rate increases about 2.7 times over the magma density range 0.02 to 0.1 kg G-aid / kg solvent (a five fold increase in magma density). The increase in the nucleation rate over the same magma density range is about 1.7

Table 5.19 The effect of the difference in the fitted exponents on magma density for typical magma densities using the graphical and moments based nucleation kinetics.

Evaluation technique	Moments		Graphical	
Equation fitted	5.24	5.26	5.24	5.26
Magma density 0.02 kg G-acid/kg solvent	0.286	0.125	0.092	0.275
Magma density 0.10 kg G-acid/kg solvent	0.479	0.292	0.245	0.486
Increase in nucleation rate with magma density	1.67	2.34	2.66	1.76

times according to the kinetics derived by the moments method. Thus equation 5.24 suggests the nucleation rate determined by the graphical procedure is about 60% more sensitive to magma density that determined by the moments procedure over the magma density range considered. The values of the exponents of magma density fitted to Equation 5.26 suggest the reverse of the behaviour suggested by Equation 5.24 and suggest that the nucleation rate determined by the moments procedure is about 30% more sensitive to magma density that determined by the graphical procedure over the same magma density range.

- Exponent on agitation rate, *m*.

The effect of the agitation rate could not be considered in the graphical procedure for determination of the nucleation kinetics since the agitation rate was constant throughout the experiment from which the kinetics were derived. The values of *m* fitted to Equations 5.24 and 5.26 using the nucleation kinetics derived by the moments procedure were -0.29 ± 0.31 and -0.42 ± 0.29 respectively. The effect of these values of *m* on the nucleation kinetics is indicated in Table 5.20.

The negative values of *m* indicate that the nucleation rate decreases with increasing agitation rate which is the reverse of what would normally be expected. However the magnitude of this inverse dependence of the nucleation rate on agitation rate is rather low. In the case of the value of *m* in Equation 5.24 the nucleation rate is predicted to fall by 30% with a 150% increase in stirrer speed, the corresponding decline in

Table 5.20 The effect of the difference in the fitted exponents on stirrer speed for typical stirrer speeds on moments based nucleation kinetics according to the values of m fitted to Equations 5.24 and 5.26.

Fitted Equation	Stirrer speed s^{-1}	N^m
5.24	2	0.82
5.24	6	0.59
5.26	2	0.75
5.26	6	0.47

nucleation rate predicted by equation 5.26 is approximately 40%. The effect of stirrer speed on nucleation rate was quite low and so it is feasible that an unrealistic value of m could be fitted through the scattered nucleation rate data.

5.5.6 Primary nucleation

The nucleation rate data from the unseeded experiments illustrates the major difference between a seeded and an unseeded crystallization. The magnitude of the peak primary nucleation rate in the unseeded crystallization is approximately 5 times the maximum nucleation rate observed in the seeded crystallization experiments. The nucleation rates are shown in Figure 5.36.

In the crystallization experiment shown in Figure 5.36 the nucleation rate was initially very low, then once a critical supersaturation was exceeded the nucleation rate increased very rapidly. Subsequently the nucleation rate declined as the supersaturation level decreased because the supersaturation was consumed by the growing crystals. The "nucleation rates" reported for the initial phase of the experiment before primary nucleation had occurred are in fact the result of comparing similar background readings. This provides a useful measure of the variation between nominaly identical crystal free samples. In comparison with the very high nucleation rates seen later in the experiment these differences between "background" counts are insignificant.

Figure 5.36 A plot of the nucleation rates determined during an unseeded cooling crystallization experiment (unseeded run 2).

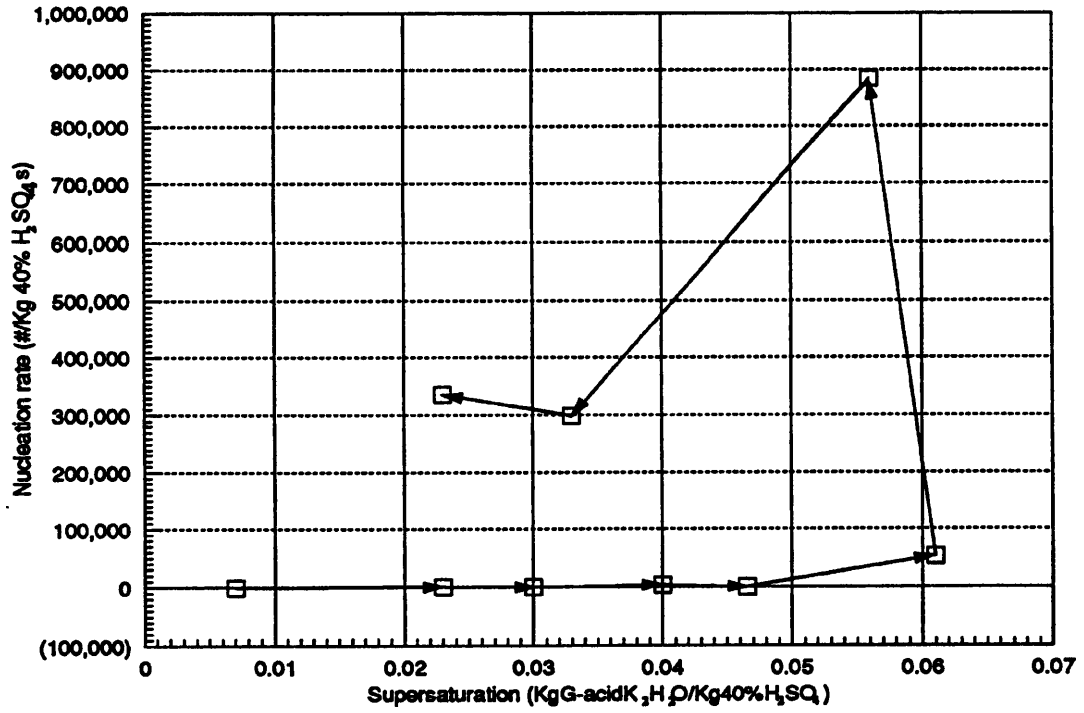

In the same way the "growth rate" data covering the period before primary nucleation occurred allows the variation between nominaly identical background counts to be compared. This is shown in Figure 5.37. Initially the variation was around ±0.015μm/s, around 30% of the average growth rates determined in typical seeded experiments. The growth rate began to rise before the vast increase in the number of crystals seen in Figure 5.36 and linked with primary nucleation took place. This was probably due to the growth of a small number of crystals in the crystallizer which appeared before the main burst of nuclei seen a little later in the experiment. Such "seed" crystals may have formed from droplets of solution which may have splashed on to the vessel walls and from which some of the solvent evaporated causing crystals to form.

These unseeded cooling crystallizations provide an indication of the metastable zone width of the system under these conditions and compare well with the metastable zone width for cooling reported in Chapter 4. In the two unseeded cooling crystallizations the supersaturation ratio at the time of nucleation was estimated to

Figure 5.37 A plot of the growth rates determined during an unseeded cooling crystallization experiment (unseeded run 2).

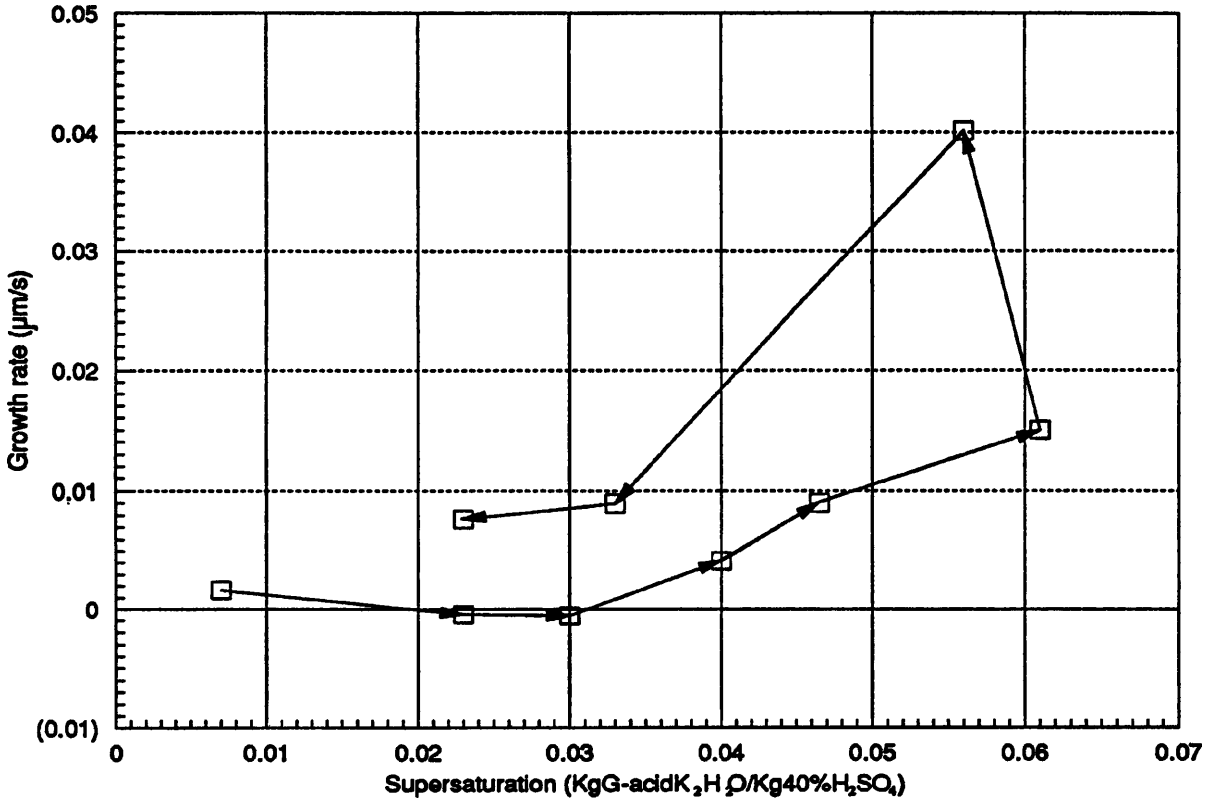

be 1.44 at 57°C and 1.48 at 57.5°C. This agrees well with the value of 1.44 reported in Chapter 4 for cooling a solution saturated at 70°C at 1°C/min until it nucleated at approximately 50°C.

5.5.7 Overall comments on the determination of crystallization kinetics in non-steady state suspension crystallizers.

The two techniques used in this study are the two most suitable procedures to obtain crystallization kinetics from batch crystallization experiments. Both procedures require the evolving crystal size distribution to be measured with reasonable precision. However in the G-acid / sulphuric acid / water system examined here the largest experimental uncertainty concerned the measurement of the crystal size distributions. The particle sizing procedure was pushed to the limit of its performance. The low accuracy with which the crystal size distributions were measured contributed significantly to the uncertainty in the parameters in the fitted kinetic equations.

These procedures are likely to be more successful when applied to a system which is easier to characterise, where the crystal habit is prismatic, ideally where all the crystal faces are equivalent. However it is likely that the majority of industrial crystallization processes are far from this ideal and possess characteristics similar to the G-acid system.

From the discussion it is apparent that these procedures for determination of crystallization kinetics are limited by accuracy of currently available size measurement techniques. As new instruments are developed it is likely that crystallization kinetics may be determined more accurately from batch crystallization experiments.

6 Simulation of G-acid Crystallization using Derived Growth and Nucleation Kinetics

6.1 Objectives

Simulation is often a useful aid to understanding the effect of changing the values of important variables in complex systems. The crystallization of G-acid dipotassium salt monohydrate reported in this study is a process which appeared to be well suited to such an approach. Considerable benefit could be derived from a successful simulation procedure especially if the simulation could be used to optimise the crystallization process in terms of seed loading, temperature - time profile etc. Performing such an optimisation by experimental means would involve a large number of complex experiments and take a considerable time.

The first stage on the way to developing a simulation procedure to describe the crystallization of G-acid was to use the derived kinetic expressions to simulate one of the experiments from which the kinetics were derived. The work reported in this chapter concerns an attempt to simulate a seeded G-acid crystallization experiment using the crystallization kinetics derived in Chapter 5.

The seeded batch cooling crystallization, seeded run 3, which was singled out for discussion in Chapter 5 has been simulated. The simulation was performed in a manner which generated data equivalent to the experimentally measured values to allow the two sets of derived kinetics to be compared with the experimental data from which they were derived.

6.2 Calculation procedure

The procedure used for the simulation of the crystallization process is shown schematically in Figure 6.1. The experimental data included a series of crystal size distributions measured at intervals during the seeded cooling crystallization. The time intervals between the measured size distributions varied slightly as did the cooling rate over the increments. For convenience of comparison of the simulation and the experimental results the crystallization process was divided into 13 steps

Figure 6.1 A schematic diagram of the simulation procedure.

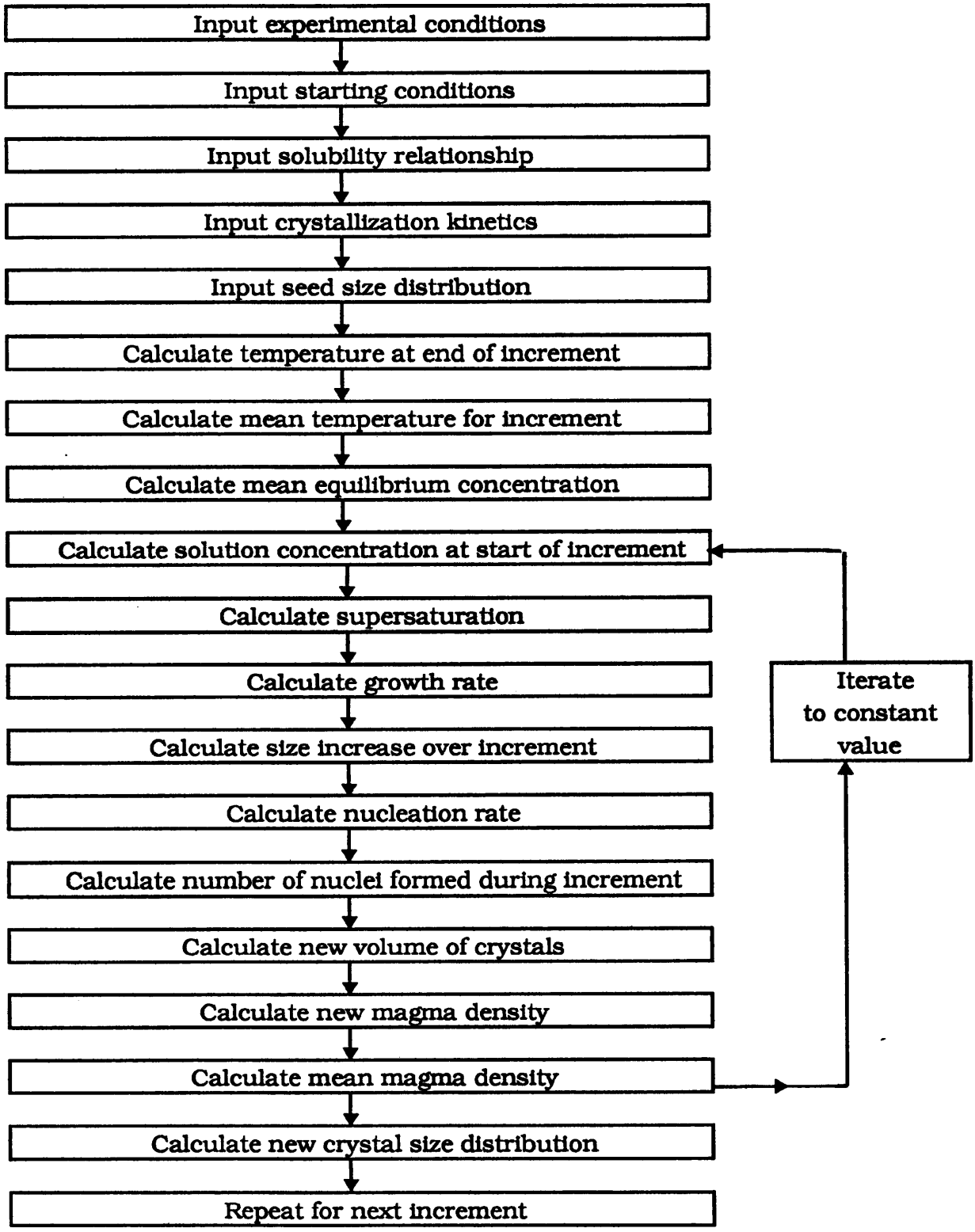

coinciding with the times at which the size distributions were determined. Each of these steps was subdivided into a series of increments of around 200s, their duration being adjusted to allow a whole number of increments to match the interval between the measurements of the crystal size distributions. For each increment the mean values of all the experimental parameters were calculated, the growth and nucleation rates were determined, and the size distribution revised as existing crystals grew and nuclei formed.

The equations and assumptions used in the simulation procedure are discussed block by block following the breakdown of the procedure shown schematically in Figure 6.1.

Experimental conditions:

Time increment duration	Δt	s
Cooling rate	dT/dt	°C s^{-1}
Agitation rate	N	s^{-1}
Crystal density	ρ_c	kg m^3

Starting conditions:

Initial temperature	T_0	°C
Solution concentration	C_0	kg(kg40% H_2SO_4 soln.)$^{-1}$
Solution mass	M_{sol}	kg
Seed mass	M_{seed}	kg

The mass of free solvent as 40% H_2SO_4 soln is calculated from the solution mass and concentration:

$$MFS = \frac{M_{sol}}{1+C_0} \qquad \text{kg40\% } H_2SO_4 \text{ soln.} \qquad 6.1$$

The seed loading is calculated from the mass of seed and the solution mass:

$$MS = \frac{m_{seed}}{MFS} \qquad \text{kg(kg40\% } H_2SO_4 \text{ soln.)}^{-1} \qquad 6.2$$

Solubility:

The solubility is calculated from the solubility equation Equation 5.25 given in chapter 5:

$C = a + (b.T) + (c.T^2)$

Constant a	a	kg (kg40% H_2SO_4 soln.)$^{-1}$
Constant b	b	kg (kg40% H_2SO_4 soln.)$^{-1}$°C^{-1}
Constant c	c	kg (kg40% H_2SO_4 soln.)$^{-1}$°C^{-2}

Crystallization kinetics:

The growth rate is given by Equation 5.23

$G = K_g \Delta C^g \exp\left(\frac{-E_g}{RT}\right)$

Growth rate constant	K_g	m s^{-1} (kg/kg)$^{-g}$
Exponent on supersaturation	g	-
Activation energy	E_g	J mol^{-1}
Gas constant	R	J mol^{-1} K^{-1}

The nucleation rate is given by Equation 5.24

$B = K_b \Delta C^b \exp\left(\frac{-E_b}{RT}\right) M_t^j N^m$

Nucleation rate constant	Kb	#(kgFS)$^{-1e-1}$(kg/kg)$^{-b}$ (kg/kg)$^{-j}$ (rev/s)$^{-m}$
Exponent on supersaturation	b	-
Activation energy	E_b	J mol^{-1}
Gas constant	R	J mol^{-1} K^{-1}
Exponent on magma density	j	-
Exponent on agitation rate	m	-

Seed size distribution:

The first experimentally measured crystal size distribution determined after the seed crystals had been added to the crystallizer was taken to be the seed size distribution. The seed size distribution was divided in to a number of size bands in the manner of the size distribution determined by the Elzone 80XY Particle Size Analyser. For each size band the number of seeds in that band was entered

along with the mean size of the band. The number of seeds in each size band was then normalised to give the number per kg 40% sulphuric acid solution (free solvent). The calculation took into account the dilution of the slurry from the crystallizer before analysis by the Elzone instrument. This was achieved using the calculational procedure reported in Table 5.5 The form of the seed distribution entry is shown in Table 6.1.

Table 6.1 The seed size distribution input to the simulation

Seed band	Mean size (m)	Number in band (#/kg FS)
S_a	$l_{seed\,a\,0}$	NS_a
S_b	$l_{seed\,b\,0}$	NS_b
---	---	---
S_z	$l_{seed\,z\,0}$	NS_z

Temperature at end of increment n:

$$T_n = T_0 - \left(n_n . \Delta t . \frac{\delta T}{\delta t}\right) \qquad ^{\circ}C \qquad 6.3$$

Mean temperature during increment n:

$$\overline{T_n} = \frac{T_n + T_{n-1}}{2} \qquad ^{\circ}C \qquad 6.4$$

Mean (equilibrium) solubility during increment n:

$$\overline{C_{Eq_n}} = a + (b.\overline{T_n}) + (c.\overline{T_n}^2) \qquad \text{kg (kg40\% } H_2SO_4 \text{ soln.)} \qquad 6.5$$

Solution concentration at start of increment n:

$$C_{S_{n-1}} = C_0 - (M_{t_n} - SL) \qquad \text{kg (kg40\% } H_2SO_4 \text{ soln.)}^{-1} \qquad 6.6$$

Note: The seed loading, SL, is subtracted from the magma density as the concentration, C_0, represents the solution concentration when the seeds were added.

Mean supersaturation during increment n:

$$\overline{\Delta C_n} = C_{n-1} - C_{Eq_n} \qquad \text{kg (kg40\% } H_2SO_4 \text{ soln.)}^{-1} \qquad 6.7$$

Mean growth rate during increment n:

$$\overline{G_n} = K_g \overline{\Delta C_n}^g \exp\left(\frac{-E_g}{RT_n}\right) \qquad \text{m s}^{-1} \qquad 6.8$$

Size increase during increment n:

$$\Delta l_n = \overline{G_n}.\Delta t \qquad \text{m} \qquad 6.9$$

Mean nucleation rate during increment n:

$$\overline{B_n} = K_b \overline{\Delta C_n}^b \exp\left(\frac{-E_b}{RT_n}\right) \overline{M_{t_n}}^j N^m \qquad \text{\# (kg40\% } H_2SO_4 \text{ soln.)}^{-1} \text{ s}^{-1} \qquad 6.10$$

Number of nuclei formed during increment n:

$$NN_n = \overline{B_n}.\Delta t \qquad \text{\# (kg40\% } H_2SO_4 \text{ soln.)}^{-1} \qquad 6.11$$

Volume of crystals:

The volume of crystals after the size increase for the current increment is calculated by summation of the volume of crystals in each size band. The calculation of the volume of crystals in each size band is shown in Table 6.2.

The total crystal volume is given by the summation:

$$VC_n = \sum_{x=a}^{z} \frac{\Pi}{6}.(l_{seedx_n})^3.NS_x + \sum_{n=1}^{n} \frac{\Pi}{6}.(l_{nuc\,n_n})^3.NN_n \qquad \text{m}^3 \qquad 6.12$$

Table 6.2 Calculation of the evolving crystal size distribution.

Seed/ nuclei band	Size (m)	Number (#/kg FS)	CNOS (#/kgFS)	Size at end of last increment (m)	Size at end of current increment (m)	Volume of crystals in size band (m^3)
S_a	$l_{seed\ a\ 0}$	NS_a	$\sum_{x=a}^{a} NS_x$	$l_{seed\ a\ n-1}$	$l_{seed\ a\ n-1} + \Delta l_n$	$NS_a\pi(l_{seed\ a\ n})^3/6$
S_b	$l_{seed\ b\ 0}$	NS_b	$\sum_{x=a}^{b} NS_x$	$l_{seed\ b\ n-1}$	$l_{seed\ b\ n-1} + \Delta l_n$	$NS_b\pi(l_{seed\ b\ n})^3/6$
---	---	---	---	---	---	---
S_y	$l_{seed\ y\ 0}$	NS_y	$\sum_{x=a}^{y} NS_x$	$l_{seed\ y\ n-1}$	$l_{seed\ y\ n-1} + \Delta l_n$	$NS_y\pi(l_{seed\ y\ n})^3/6$
S_z	$l_{seed\ z\ 0}$	NS_z	$\sum_{x=a}^{z} NS_x$	$l_{seed\ z\ n-1}$	$l_{seed\ z\ n-1} + \Delta l_n$	$NS_z\pi(l_{seed\ z\ n})^3/6$
N_1		NN_1	$\sum_{x=a}^{z} NS_x + \sum_{n=0}^{1} NN_n$	$l_{nuc\ 1\ n-1}$	$l_{nuc\ 1\ n-1} + \Delta l_n$	$NN_1\pi(l_{nuc\ 1\ n})^3/6$
N_2		NN_2	$\sum_{x=a}^{z} NS_x + \sum_{n=0}^{2} NN_n$	$l_{nuc\ 2\ n-1}$	$l_{nuc\ 2\ n-1} + \Delta l_n$	$NN_2\pi(l_{nuc\ 2\ n})^3/6$
---	---	---	---	---	---	---
N_{n-1}		NN_{n-1}	$\sum_{x=a}^{z} NS_x + \sum_{n=0}^{n-1} NN_n$	$l_{nuc\ n-1\ n-1}$	$l_{nuc\ n-1\ n-1} + \Delta l_n$	$NN_{n-1}\pi(l_{nuc\ n-1\ n})^3/6$

where:
$l_{seed\ x\ n}$ is the size of seed crystals in size band x at the end of the current iteration during time increment n.
NS_x is the number of seed crystals in size band x.
$l_{nuc\ n\ n}$ is the size of seed crystals in size band n at the end of the current iteration during time increment n.
NN_n is the number of seed crystals in size band n.

Magma density at end of increment n:

At the start of the simulation the magma density is determined from the seed loading, *MS*, and the mass of free solvent *MFS*:

$M_t = MS/MFS$ kg(kg40% H_2SO_4 soln.)$^{-1}$ 6.13

This value was used for the first iteration of the first time increment. In all subsequent iterations the mass of crystals per kg free solvent was calculated from the total volume of crystals in the size distribution.

$M_{t_n} = \rho_c . VC_n$ m^3 6.14

Mean magma density:

The mean magma density is calculated from the magma density at the end of the previous increment, $M_{t_{n-1}}$, and the value at the end of the current increment, M_{t_n}.

$\overline{M_{t_n}} = \frac{M_{t_{n-1}} + M_{t_n}}{2}$ kg(kg40% H_2SO_4 soln.)$^{-1}$ 6.15

Iteration:

The iteration around the loop from solution concentration at start of increment to mean magma density was repeated until all the displayed values had stabilised.

New crystal size distribution at end of increment n:

The new size distribution was recorded in two stages, the crystal sizes at the end of the increment $l_{seed\,x\,n}$ and $l_{nuc\,n\,n}$ were stored as the input sizes for the subsequent increment. The number of nuclei formed during the increment, NN_n are added to the end of the size distribution and their size is entered as half the size increase, $\Delta l_n/2$, for the time increment *n*.

Also at the end of the increment the calculated values for the variables are stored as those for the previous increment in readiness to calculate mean temperature, equilibrium concentration and magma density.

6.2.1 Operation of the simulation procedure

The simulation was performed using a commercially available spreadsheet package called Quattro. The advantages associated with the use of a spreadsheet based procedure were considerable in terms of ease of development, flexibility in use and ease of data handling, especially in the generation of graphical output. The principle disadvantages concerned the speed of the operation and the size of the spread sheets produced. To limit these disadvantages the duration of the time increments used in the simulation were relatively long. The durations of around 200s resulted in the entire simulation taking place in 80 increments. The accuracy of the simulation could have been improved by shortening the increment duration and increasing the number of increments. However in this case increasing the number of time increments would have yielded little advantage as the errors associated with the determination of the crystallization kinetics are large. Doubling the number of increments for one step had no significant effect on the results. If the number of increments were doubled for the whole of the simulation the memory limitations on the computer used to run the simulations may have been exceeded. Since doubling the number of increments for one step in the simulation had no significant effect on the result of the simulation it was clear that the uncertainties in the kinetic data far outweigh the errors occurring because the conditions at the start and end of a time increment differed slightly from the mean conditions assumed for the increment. If more accurate kinetic estimates were available reducing the increment duration may have offered advantages. However this would have involved moving away from a spreadsheet based approach to a more sophisticated dedicated programme. Production of such a dedicated program to achieve this would involve considerable effort. A sample worksheet from the spreadsheet based programme is shown in Figure 6.2

Figure 6.2 A sample of the spreadsheet simulation procedure.

START TEMP °C	77.1	STIRRER SPEED rps	5
TIME INCREMENT s	168	CRYSTAL DENSITY kg/m³	1837
COOL RATE °C/s	0.001666	SEED MASS kg	0.000294
SOLUTION MASS kg	0.685	SOLUTION CONC, kg G-acid$K_2.H_2O$ /kg40%H_2SO_4soln	0.1997
FREE SOLVENT MASS kg	0.571	SEED MASS kg/kgFS	0.000294
SOLUBILITY EQUATION (EQUILIBRIUM)		$C = a + (b.t) = (c.t^2)$	
a		0.03419	
b		0.000968	
c		0.000012	
GROWTH RATE EQUATION		$G = K_g.\Delta C^g.\exp\left\{\frac{-E_g}{R.t}\right\}$	
K_g		5.28×10^6	
g		0.86	
E_g		-516	
NUCLEATION RATE EQUATION		$B = K_b.\Delta C^b.\exp\left\{\frac{-E_b}{R.t}\right\}.M_t^j.N^m$	
K_b		237000	
b		2.45	
E_b		-31875	
j		0.32	
m		0	

PROPERTY	UNITS	START	INPUT	RESULT
INCREMENT		0	5	5
TEMP	°C	78.7	75.69997	75.69997
MEAN TEMP	°C		75.83997	75.83997
TIME	s	0	840	840
MEAN EQ SOL	kg/kgFS	0.188420	0.180085	0.180085
INIT ACT CONC	kg/kgFS	0.1997	0.197831	0.197831
SSAT	kg/kgFS	0.011279	0.017746	0.017746
GROWTH RATE	m/s	0	1.97E-9	1.97E-9
SIZE INCREASE	m	0	3.31E-7	3.31E-7
NUCLEATION RATE	#/kgFS.s	0	89432.27	89432.27
NUMBER OF NUCLEI IN TIME INCREMENT	#/kgFS	0	15024622	15024622
MAGMA DENSITY	kg/kgFS	0.000294	0.002163	0.002163
MEAN MAGMA DENSITY	kg/kgFS	0.000294	0.002141	0.002141

SEED/ NUCLEI	SIZE (m)	NUMBER (#/kg FS)	CNOS (#/kgFS)	SIZE AT END OF LAST INCREMENT (m)	SIZE AT END OF CURRENT INCREMENT (m)	VOLUME OF CRYSTALS IN SIZE BAND (m^3)	LNCNOS (#/kgFS)
Seeds	3.28E-5	551464	551464	3.76E-5	3.76E-5	1.54E-8	13.22033
Seeds	3.00E-5	798171.3	1349635.	3.94E-5	3.94E-5	1.77E-8	14.11534
Seeds	2.75E-5	1596342.	2945977.	3.24E-5	3.24E-5	2.83E-8	14.89595
---	---	---	---	---	---	---	---
Seeds	4.8E-6	98791841	7.7E+08	9.64E-6	9.64E-6	4.63E-8	20.45930
Seeds	4.4E-6	1.1E+08	8.8E+08	9.24E-6	9.24E-6	4.63E-8	20.59559
Seeds	4.0E-6	12509521	8.9E+08	8.82E-6	8.82E-6	4.57E-9	20.60970
Nuclei		3922502.	9.0E+08	3.43E-6	3.43E-6	8.3E-11	20.61409
Nuclei		2058097.	9.0E+08	3.31E-6	3.31E-6	3.9E-11	20.61638
Nuclei		2456581.	9.0E+08	3.18E-6	3.18E-6	4.1E-11	20.61911
---	---	---	---	---	---	---	---
Nuclei		13201065	9.9E+08	4.9E-7	4.9E-7	8.2E-13	20.71228
Nuclei		15024622	9.9E+08	1.6E-7	0	0	20.71228
Nuclei			9.9E+08	0	0	0	20.71228
					VOL	1.18E-6	
					MASS	0.002163	

6.3 Results and Discussion

A seeded batch crystallization, seeded run 3, was simulated using the kinetic expressions derived in Chapter 5 by both the moments and graphical procedures. The results of these simulations are recorded here.

It was decided that the kinetic description of Equation 5.24 rather than Equation 5.26 would be used to describe the nucleation kinetics determined by the moments procedure in this simulation. This permitted a direct link between the experimental conditions and the kinetic expressions to be maintained. This was considered to be important since large errors are associated with determination of the growth rate evidenced by the low value, 0.245, of r^2, for correlation with Equation 5.23 in Table 5.7. These errors could be transferred in to the nucleation rate estimates made during the simulation procedure by use of the data fitted to Equation 5.26 to describe the nucleation kinetics determined by the moments procedure.

The results of the simulation include the predicted values of properties such as concentration, supersaturation, magma density and crystal size distribution at a series of time intervals during the crystallization process. The variation in the scalar properties (concentration, supersaturation and magma density) are shown by plotting them against time. The evolution of the crystal size distribution is presented as a series of size distributions predicted at different times during the crystallization. In all cases the results from the two simulations are presented along with the experimentally measured values to allow easy comparison. For convenience in presenting the results the discussion is integrated within this section.

The simulation has allowed the kinetic expressions obtained in Section 5 to be expressed in a form comparable with the experimental data from which they were derived. When the results of the simulations were displayed along with the experimental data it became apparent that some basis for making comparisons between the predicted and observed data would be required. This is made difficult by the magnitude of the errors to which both the measured and simulated values are subject. It has been reported earlier, in Chapter 5, that the experimental error on some of the measured parameters is quite large and that the derived kinetic

expressions are subject to large uncertainties. Under such circumstances identifying what constitutes good agreement and what is a significant deviation is difficult to assess. This is considered in each of the subsequent subsections dealing with concentration and supersaturation, magma density and crystal size distributions.

6.3.1 Concentration and supersaturation

In Figure 6.3 the measured concentration dependence on time is plotted along with the values predicted by both the moments and graphical procedures used to estimate the kinetics.

Figure 6.3 Predicted and observed concentration and supersaturation time profiles.

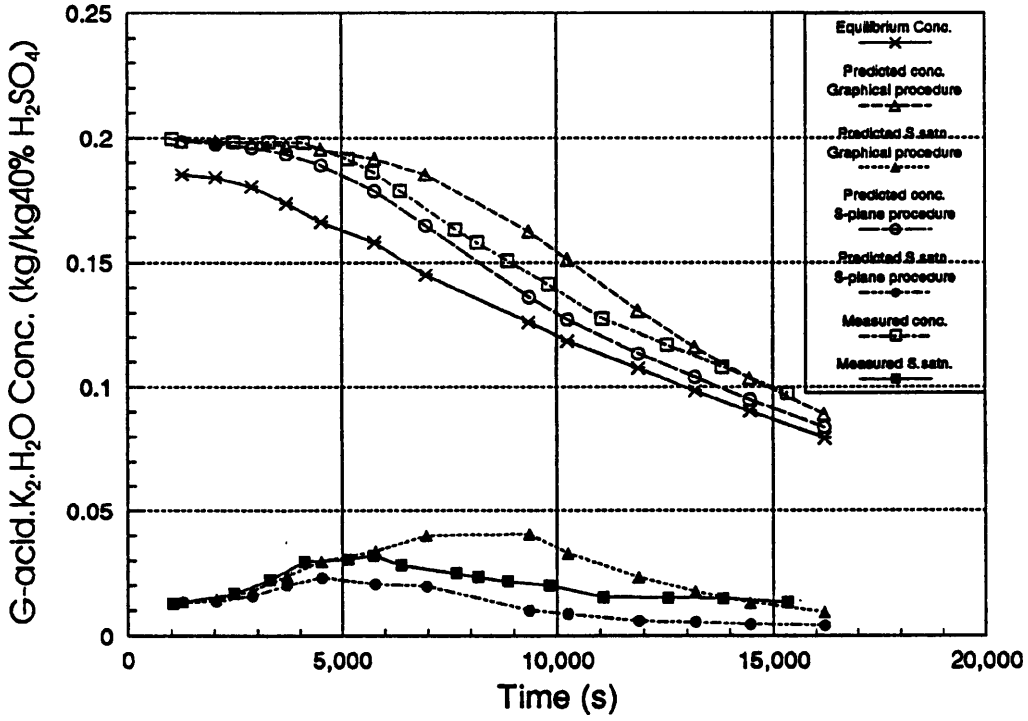

The experimentally determined values of concentration and supersaturation show little scatter; the experimental error was estimated to be around ± 0.005 kg G-acid $K_2.H_2O$ /kg 40% H_2SO_4. Thus comparisons between the experimentally measured values and the simulations was straightforward. The simulation employing the kinetic data determined by the s-plane procedure predicts that supersaturation is consumed from the beginning of the experiment. Depletion is linked with rapid growth (see the comment in Section 6.3.3), the predicted peak supersaturation is around

0.02 kg G-acid $K_2.H_2O$ per kg 40% H_2SO_4. The kinetic expression obtained by the graphical procedure suggests that initially supersaturation builds up until a peak of around 0.04 kg G-acid $K_2.H_2O$ /kg 40% H_2SO_4 is achieved. Depletion gradually increases reaching a significant rate when the supersaturation reaches 0.03 kg G-acid $K_2.H_2O$ /kg 40% H_2SO_4. The measured supersaturation profile behaves differently to both simulations. Initially, for the first 5000s of the experiment, the measured supersaturation agrees with the predictions of the graphically based simulation. After this it begins to decline whilst the supersaturation based on the graphical procedure continues to rise. If it is assumed that the main way of relieving supersaturation in the early stages of the experiment is deposition of solute on the seed crystals the behaviour over the first 6000s of the experiment could be taken to indicate that the growth rate used in the graphically based simulation is an under estimate whilst the growth rate for the moments based simulation is an over estimate. The behaviour over the remainder of the simulation is particularly interesting, the three supersaturation profiles differing considerably. Both the moments based simulation and the experimental profiles decline to a steady supersaturation value which is maintained for the remainder of the experiment. The experimentally measured steady value is approximately 0.015 kg G-acid $K_2.H_2O$ /kg 40% H_2SO_4 where as the value for the moments based simulation is approximately 0.005 kg G-acid $K_2.H_2O$ /kg 40% H_2SO_4. The steady values correspond to a region where the rate of supersaturation generation by cooling is matched by the rate of deposition on the growing crystals. The behaviour of the graphically based simulation is rather different. A much higher peak supersaturation is reached rather later in the experiment, at around 8000s compared with 5000s in the other supersaturation profiles. After the peak is reached the supersaturation level declines quite rapidly and does not attain a steady value before the end of the experiment.

6.3.2 Magma density

The magma density is a measure of the mass of crystals in the solution and serves to describe the extent of the crystallization. The predicted variation of magma density with time during the course of the crystallization is shown in Figure 6.4.

Figure 6.4 Predicted and observed magma density dependence on time.

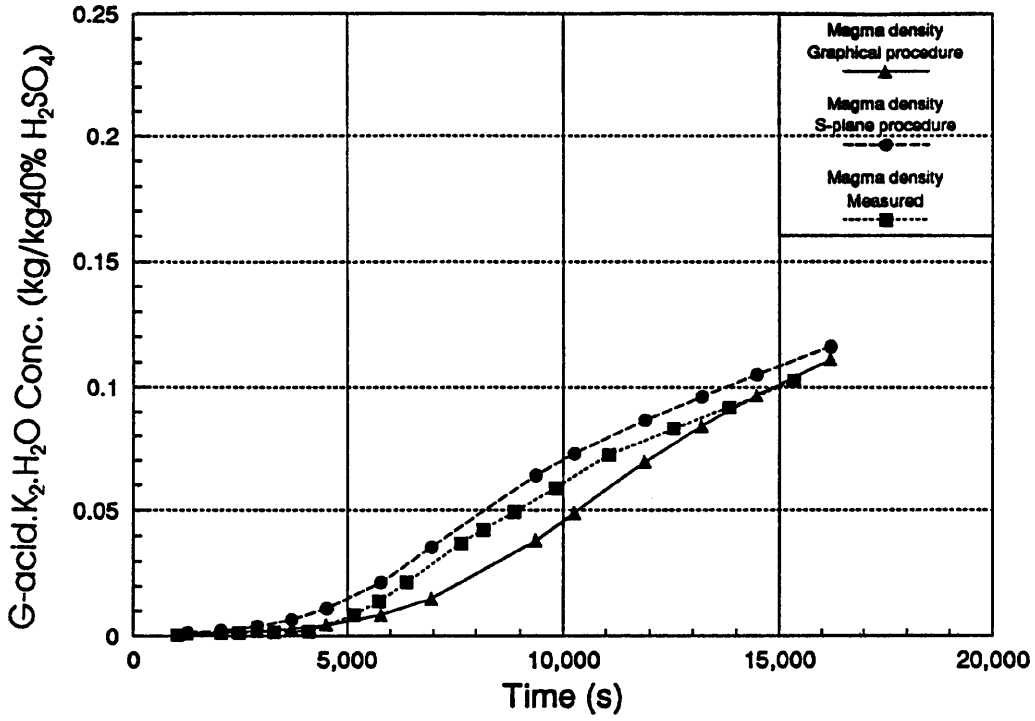

The experimentally determined magma density shown in Figure 6.4 is that determined from the solution concentration measurements rather than from the measured crystal size distributions. The concentration based magma density fluctuates less and is subject to smaller errors than the magma density calculated from the size distribution data. The magma density calculated from the measured crystal size distribution is subject to errors due to inaccuracies in the measurement of the size distribution. In particular the truncation of the size distribution by the screening procedure causes large errors towards the end of the experiment, this is reported in Section 5.5.1. At the start and end of the crystallization the magma density predicted by the graphical kinetic expressions show very good agreement with the measured magma density. In the middle of the crystallization the magma density predicted by the graphical kinetics lags behind the measured magma density. The magma density predicted by the s-plane procedure is a little higher than the measured values throughout the whole experiment. Conservation of mass requires

that the magma density plus the residual supersaturation sum to the same value for the simulations and the experimental measurement; this was found to be the case.

6.3.3 Crystal size distributions

During the course of the simulations crystal size distributions were recorded to coincide with those determined during the experiment that was being simulated. The resulting series of size distributions are plotted in Figures 6.5 to 6.15. In each plot the seed size distribution is shown along with the measured crystal size distribution and the size distributions predicted by the two kinetic expressions derived from the experimental data. The experimentally measured size distributions are subject to considerable error as has already been discussed in Section 5.5.1. This is particularly apparent in Figure 5.13 which shows the overlapping and crossing of the experimentally measured crystal size distributions. The error associated with the experimentally measured crystal size distributions becomes worse as the experiment progresses. The most significant factor in the increase in the experimental error was the screening of the sample to remove large crystals prior to sizing the crystal slurry sample. In consequence the comparison between the measured and simulated size distributions becomes somewhat speculative towards the end of the experiment.

Figure 6.5, elapsed time 1260s:
The seeds were added 800s into the cooling schedule after initial supersaturation had been generated. Thus the first comparison shows the situation after 460s of growth. The measured and two simulated size distributions lie very close together and appear to cross at several points.

Figure 6.5 Observed and predicted crystal size distributions after 1260s.

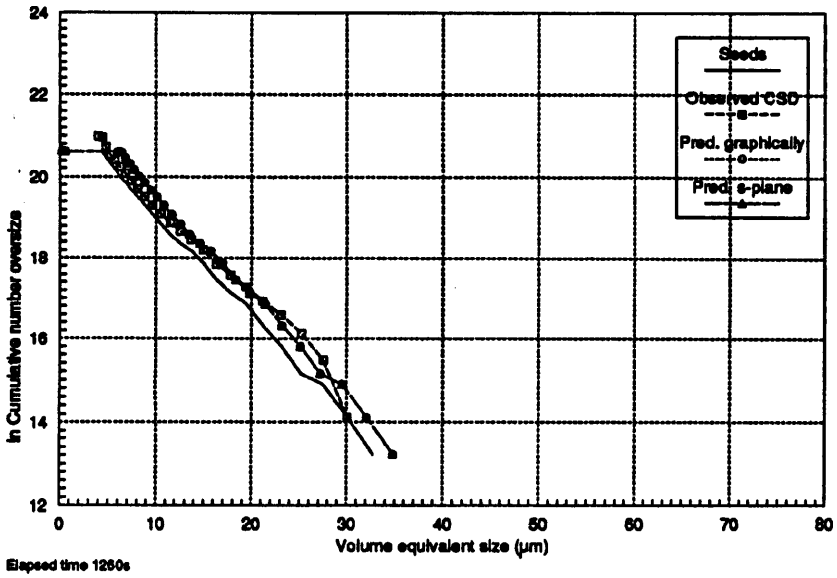

Figure 6.6 Observed and predicted crystal size distributions.

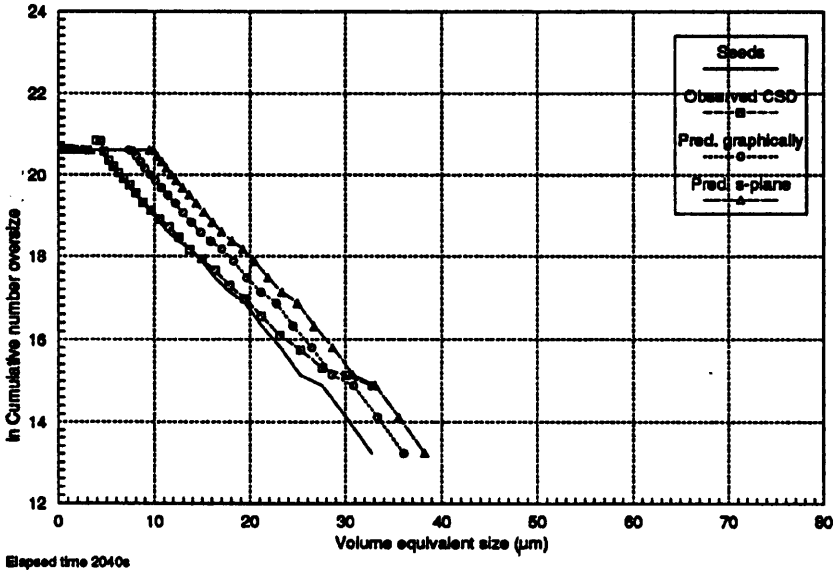

Figure 6.6, elapsed time 2040s:

The distributions are now quite distinct. The measured distribution appears to have moved to the left, probably due to experimental errors in determining the distribution. (Negative growth and nucleation rates was determined for the increment between 1260 and 2040s during the estimation of the crystallization kinetics reported in

Chapter 5). The simulation using the moments based kinetics shows considerable crystal growth, the size distribution having moved to the right. The graphical simulation shows rather less growth.

Figure 6.7 Observed and predicted crystal size distributions.

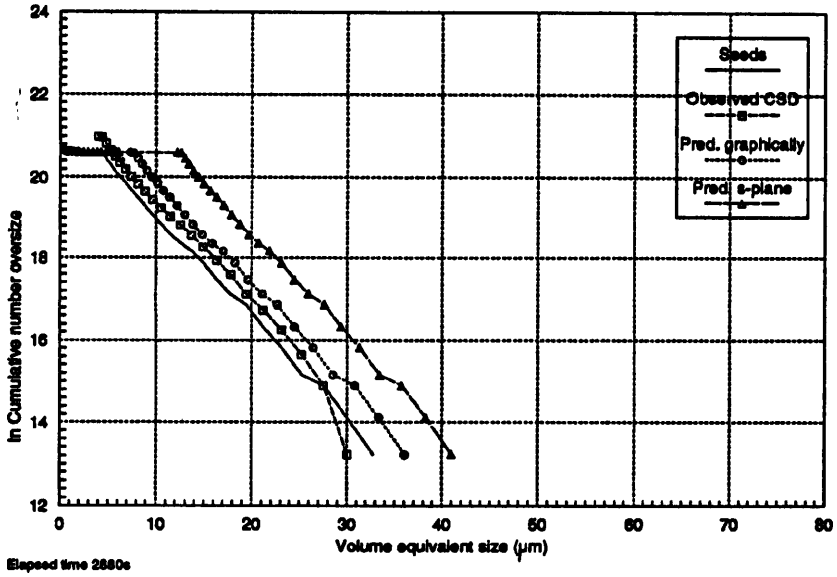

Figure 6.7, elapsed time 2880s:

The measured size distribution shows a little growth from the distribution shown in Figure 6.5 (after 1260s). Both the simulated distributions show rather more growth. The size distribution simulated using the graphical kinetics lies a little to the right of the experimental simulation indicating the size is over estimated by around 2μm. The simulation employing the moments based kinetics lies at larger size still, exceeding the measured size by around 7μm.

Figure 6.8, elapsed time 3960s:

Differences between the nucleation seen in the experimentally measured size distribution and the two simulations are becoming apparent. The experimentally observed size distribution shows a smooth increase in number of crystals whereas there is a discontinuity in both the simulated size distributions. This discontinuity between the seeds and the subsequently formed nuclei can be considered in two parts. The upper 4μm of the discontinuity is due to the inability of the Elzone sizing instrument to measure below about 4μm under these conditions. This could be

Figure 6.8 Observed and predicted crystal size distributions.

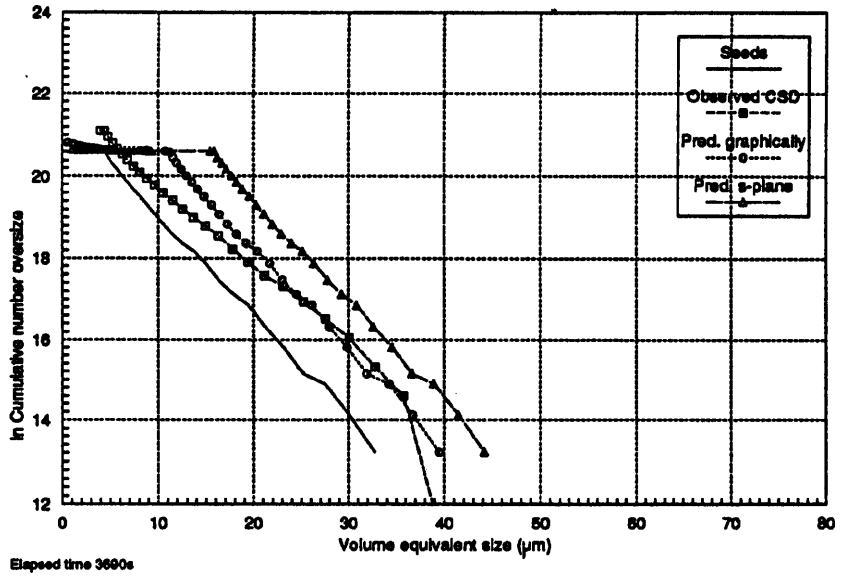

overcome by extrapolating the seed size distribution to zero size. The cause of the second part of the discontinuity lies with the derived nucleation kinetics both of which appear to under predict the nucleation rate during these early stage s of the simulation. Fewer nuclei appear in the moments based simulation than the one employing the graphical kinetics.

The measured size distribution curve has changed shape, the gradient having decreased at larger sizes, indicating greater growth at larger size. This is probably due to growth rate size dependency. It is difficult to quantify any growth rate size dependency in this system due to the truncation of the size distribution at large size by the screening procedure which was employed. The truncation of the size distribution at large size serves to oppose the effect of greater growth at higher size by screening out a proportion of these larger crystals.

The simulation based on the graphical procedure is coincident with the experimentally measured distribution over the size range 25 to 40μm. Below this size the simulated size distribution over estimates the crystal size until the discontinuity at the link between seeds and the nuclei. The moments based simulation over estimates the crystal size by between 5 and 10μm.

Figure 6.9 Observed and predicted crystal size distributions.

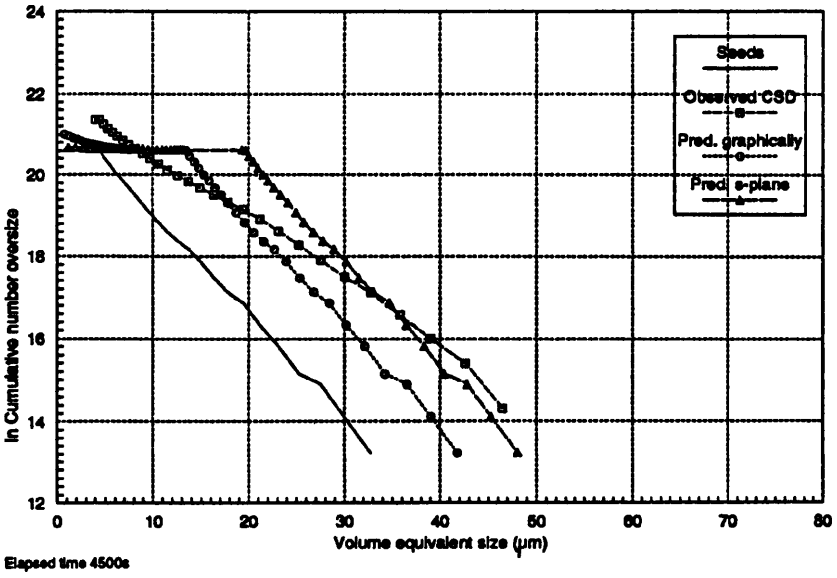

Figure 6.9, elapsed time 4500s:

Here there is much stronger experimental evidence for growth rate size dependency. The size increase over the seed size distribution is about 6μm at an ln CNOS value of 20, whereas, at an ln CNOS value of 16, the size increase is around 16μm. The experimental size distribution crosses both the simulated distributions twice. It crosses them both together at 8μm, due to the discontinuity between the seeds and the nuclei in the simulations. The measured size distribution then crosses the graphical simulation at around 17μm and the moments based simulation at around 35μm. At sizes greater than 35μm it curves down to follow the shape of the moments based simulation ending 2 to 3μm larger than the moments based simulation.

Figure 6.10, elapsed time 5760s:

The screening procedure was employed for the first time in this experiment for the measurement of this size distribution. The higher growth rate at the larger sizes is still apparent in the experimentally measured growth kinetics despite the screening, providing further evidence for growth rate size dependency. The size increase over the seed size is about 12μm at an ln CNOS value of 20, whereas, at an ln CNOS value of 16, the size increase is around 28μm. Again the experimental size distribution crosses both the simulated distributions twice, both together at 13μm, due to the

Figure 6.10 Observed and predicted crystal size distributions.

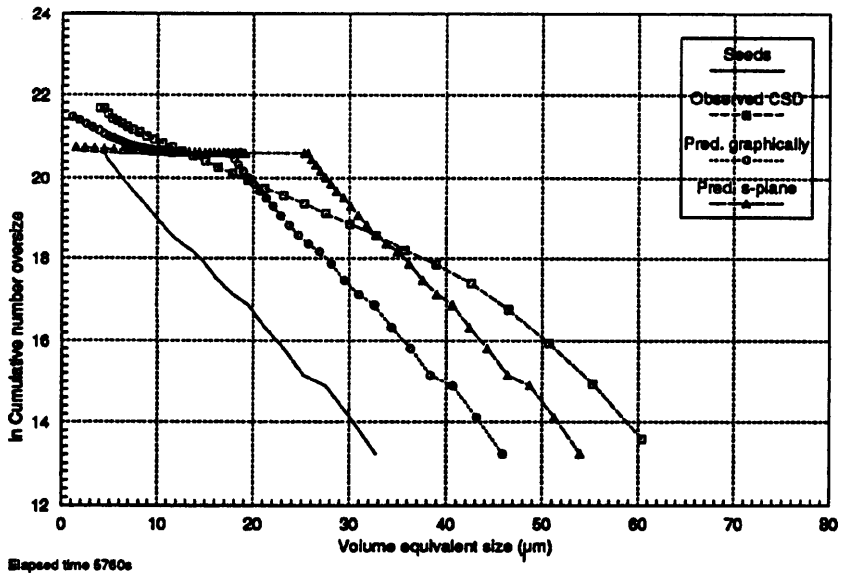

discontinuity between the seeds and the nuclei in the simulations and separately at larger sizes. The measured size distribution crosses the graphical simulation at around 20μm and the moments based simulation at around 33μm. At sizes greater than 50μm it curves down to follow the shape of the moments based simulation ending about 7μm larger than the moments based simulation. The difference between the sizes predicted by the two simulations is approximately 8μm. The nucleation rate predicted by the graphical procedure is much closer to the experimentally observed size distribution at small size than that predicted by the moments based simulation. The gradients of the size distribution simulated using the graphical kinetics and the experimentally measured size distribution are similar at sizes up to 10 μm.

Figure 6.11, elapsed time 6960s:

The experimentally measured size distribution appears to be almost straight. The gradient is still shallower than that of the seed size distribution, again indicating side dependent growth kinetics. The size increase at a value of ln CNOS equal to 20 is approximately 11μm, where as at an ln CNOS value of 16 the size increase is around 24μm. Again the experimental size distribution crosses the distribution from the moments based simulation twice, at the discontinuity between the seeds and the nuclei in the simulation, at 13μm, and then at 53μm, the two distributions both

Figure 6.11 Observed and predicted crystal size distributions.

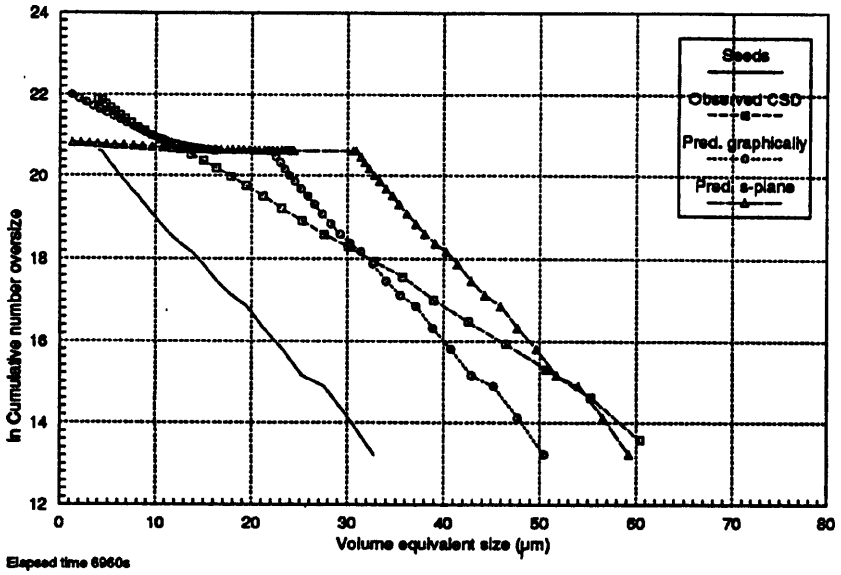

showing maximum sizes of around 60μm. At small sizes the measured size distribution and the graphical simulation lie close together indicating that the simulation predicts the nucleation rate quite well at this stage of the experiment (though the measured size distribution may itself be in error). The measured size distribution then crosses the distribution from the graphical simulation at around 31μm. The size difference between the two simulations is around 9μm, the moments based simulation lying at larger size over the seeded section of the distribution.

Figure 6.12, elapsed time 9360s:

The truncation of the measured size distribution becomes apparent in Figure 6.12. The gradient of the "seeded" part of the experimentally measured distribution corresponding closely to that of the initial seed crystals. The size increase over the seeded part of the distribution is approximately 33μm over the size of the seed crystals. The "seeded" portions of the simulated distributions lie approximately parallel with the "seeded" portion of the measured size distribution, the graphical kinetics over predicting the measured size by 4 to 5μm and the moments based simulation over predicting the size by around 11 or 12μm. The moments based

Figure 6.12 Observed and predicted crystal size distributions.

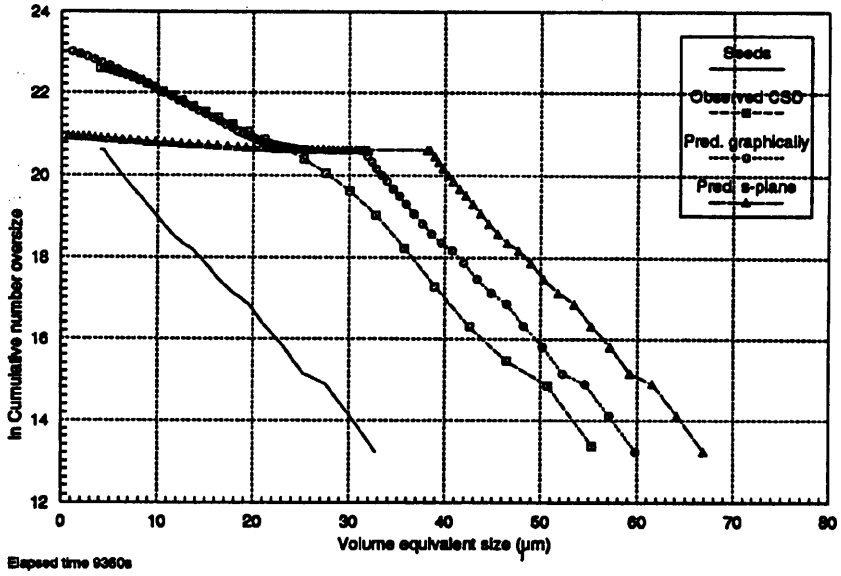

simulation drastically under predicts the number of nuclei formed during the crystallization to this stage where as the graphical procedure shows good agreement with the measured size distribution.

Figure 6.13 Observed and predicted crystal size distributions.

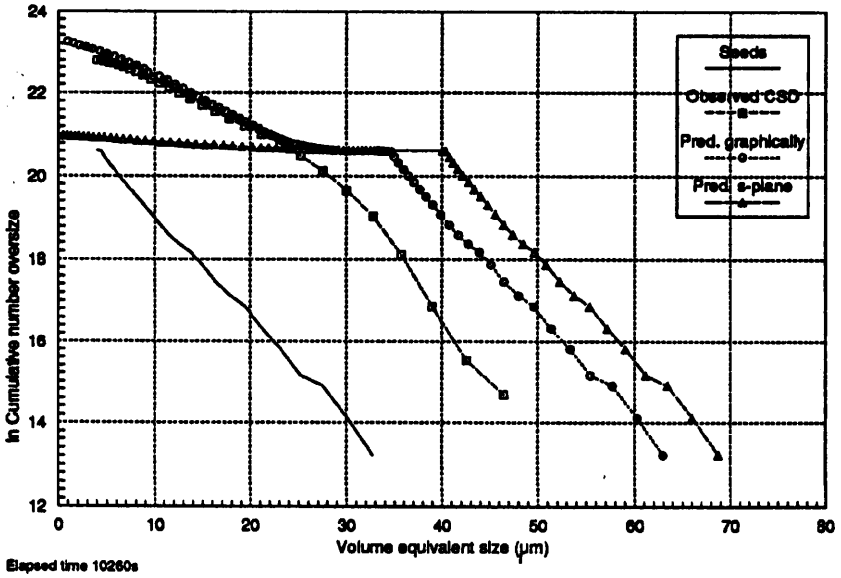

Figure 6.13, elapsed time 10260s:

The truncation of the measured size distribution continues to be apparent. After 5760s the size corresponding to a ln cumulative number over size value of 16 was 51μm, after 10260s the corresponding size is approximately 42μm. As before, in Figure 6.12, the "seeded" portions of the measured and both simulated distributions are approximately parallel. The graphical kinetics lead to an apparent over estimate of around 10μm, and the moments based kinetics yield an apparent overestimate of 15μm. These overestimates are only apparent. It is not possible to asses the real situation due to the truncation of the measured size distribution. It is noticeable that the interval between the two simulated size distributions is narrowing. Examination of the supersaturation time plot in Figure 6.3 suggests the reason for this is that in the moments based simulation more of the supersaturation has been consumed than in the graphical simulation. This results in a narrowing of the size difference between the two simulations as the growth rate declines more rapidly in the moments based simulation than in the graphical simulation.

Figure 6.14 Observed and predicted crystal size distributions.

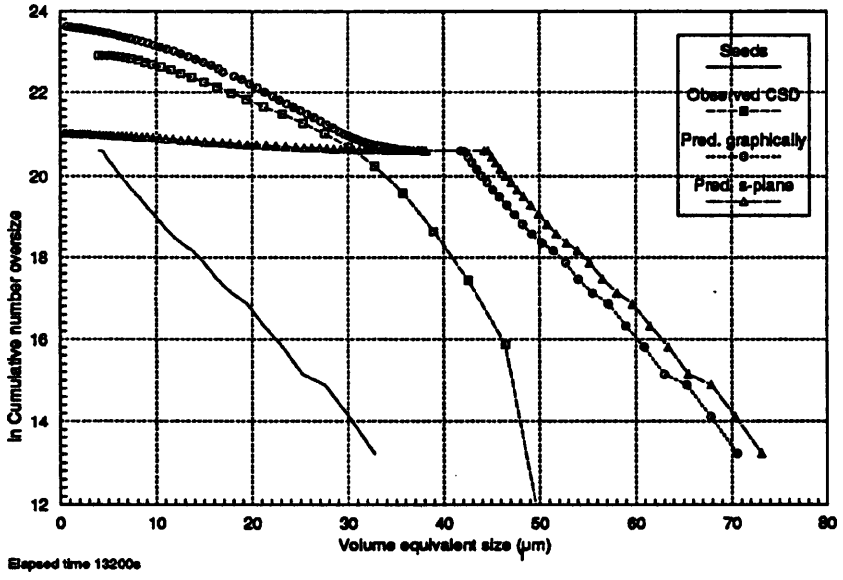

Figure 6.14; elapsed time 13200s.

The comments concerning Figure 6.13 can be extended to Figure 6.14 and the distributions measured before and after it at 11880 and 14460s. There are three

main trends: The gap between the seeded portions of the simulated distributions continues to decline. The number of nuclei predicted by the graphical simulation begins to exceed the number in the measured size distribution. This may be in part a result of the truncation of the size distribution at high size shifting the measured size distribution downwards on the ln cumulative number oversize axis. The measured size distribution shows very little variation at small sizes but shows more substantial variations at higher sizes. This is probably due to the effects of the screening procedure employed prior to sizing the crystals.

Figure 6.15 Observed and predicted crystal size distributions.

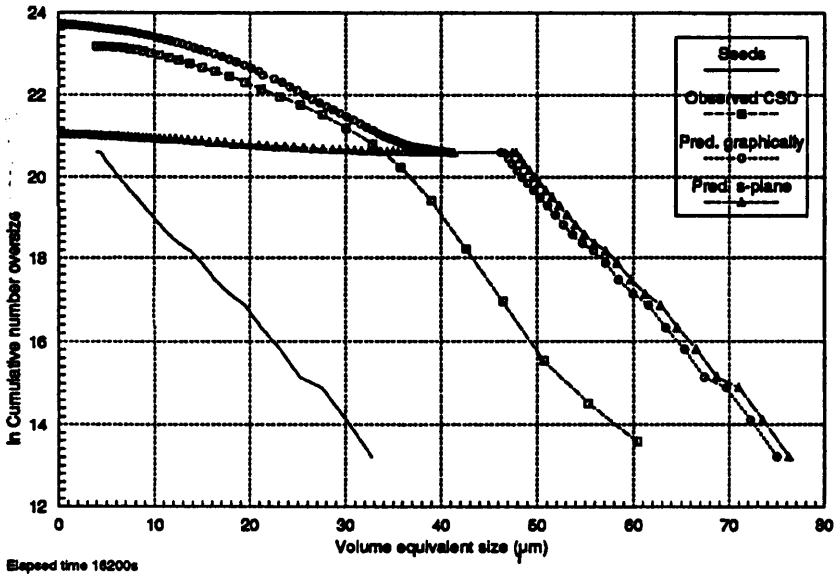

Figure 6.15, elapsed time 16200s:

The size difference between the "seeded" portion of the two simulated distributions is less than 2μm, the graphical procedure predicting the lower sizes. The much higher number of nuclei formed during the graphical simulation accounts for this small difference in the upper predicted sizes. The measured size distribution is likely to be subject to large error due to the effects of the screening procedure and other experimental errors discussed in Chapter 5. The real size distribution is likely to lie above and to the right of the measured distribution shown in Figure 6.15. It may be speculated that the portion up to 40μm would lie in the region of the distribution predicted using the graphical procedure. The location of the portion of the measured

distribution over 40μm is more difficult to assess, though mass balance constraints place an upper size limit. It probably has a shallower gradient than the seeded portions of the two simulated distributions and could cross them at around 60μm perhaps ending just over 80μm.

6.4 Conclusions

This simulation has provided a useful method to compare the kinetics derived from the experimental data using the two different techniques. The differences between the experimentally measured values and the ones predicted by the two sets of kinetics reveal the shortcomings of both the experimental data and the kinetics derived from them. Though only one experiment has been simulated it is reasonable to presume that similar observations could be drawn from simulations of the other seeded experiments. Simulation of an unseeded experiment would necessitate measurement of primary nucleation kinetics which would require different experimental procedures to those employed in this study.

The detailed conclusions in Sections 6.4.1 to 6.4.3 cover the simulation procedure, the comparisons of the simulated and measured values and the significance of these comparisons for the determination of the crystallization kinetics of G-acid dipotassium salt monohydrate. Finally in Section 6.4.4 the use of simulation techniques to asses the effect of changing crystallization conditions on the crystallization process is discussed.

6.4.1 The simulation procedure

The simulation procedure appears to have functioned successfully providing a mechanism to test the derived kinetics against experimental measurements. It has yielded all the information necessary to allow comparison of the experimental data with equivalent values derived from the kinetic data extracted from the experimental data.

6.4.2 Comparison of simulation and experiment

The comparison of the experimental values with values obtained by the simulation procedure has been illuminating. It has revealed shortcomings both in the derived kinetic expressions and the experimental data. The conclusions to be drawn from these comparisons are discussed below:

- Concentration, supersaturation and magma density

These comparisons are particularly useful indicators of the degree of completion of the crystallization process. They appear to be reliable indicators of significant differences between the crystallization followed in the experiment and the two simulations. However their information is incomplete; for example the magma density represents the mass of crystals suspended in the slurry but it cannot provide information about the crystal size distribution. Thus it is clear that this information is best used alongside the size distribution information.

- Crystal size distributions

Comparisons between the measured and predicted size distributions were particularly useful. There are five main conclusions to be drawn;

Considerable differences between the nucleation rates arising from the two sets of derived kinetics have been revealed.

The discontinuity between the seed crystals and the nuclei born subesquently was shown to have a considerable influence on the size distributions.

The CSD simulations revealed a surprisingly small difference between the predicted maximum size attained at the end of the experiment despite considerable differences in the growth kinetics used in the two simulations.

The errors associated with the experimentally measured data have been shown to cause considerable problems in evaluating the two sets of kinetics. The aim of confronting the derived kinetics with the experimental data has only been achieved in part.

Presenting the experimental results in this way has usefully demonstrated the evidence for growth rate size dependency in the G-acid dipotassium salt monohydrate system. The effect of screening in the apparent growth rate size dependency was shown to be substantial during the later stages of the experiment.

6.4.3 Crystallization Kinetics

The results he simulation procedure has revealed defects in the kinetic data derived both by the moments and the graphical procedures.

- Nucleation

The most significant discrepancy between simulations and the experimental data was between measured size distributions and the size distributions predicted using the moments based kinetics at small crystal sizes. The nucleation rate which was apparent from the measured crystal size distributions was much greater than the nucleation rate predicted from the moments based nucleation kinetics. The reason for the moments based kinetics severe under prediction of the nucleation rate is not clear. It is possible that the weighting of the moments used to reduce errors associated with measurement of the extremes of the crystal size distributions lead to the derived kinetics being strongly influenced by the presence of the seed crystals.

In contrast the graphically derived nucleation kinetics showed a measure of agreement with the experimental results. However there was evidence that this agreement only covered part of the experimental regime. In particular the discontinuity between the seeds and the subsequent nuclei was in part a result of the under prediction of the nucleation rate during the initial stages of the experiment. (The omission of the sub 4μm part of the seed size distribution which could not be measured by the Elzone instrument also contributed to the discontinuity in the predicted crystal size distributions).

- Growth

It has been shown that the growth kinetics derived by both procedures are in poor agreement with the experimentally observed growth kinetics. The importance of growth rate size dependency has been demonstrated. However practical difficulties

arose when attempts were made to fit size dependent growth kinetics. The moments based procedure yields a single size independent growth rate for the whole size distribution, providing no data to which size dependent kinetics could be fitted.

The graphical procedure could in principle have been extended to take account of growth rate size dependency by estimating the growth rate at several sizes. However several practical considerations influenced the decision not to pursue this course of action.

The presentation of the experimental data along with the simulation has shown the apparent significance of growth rate size dependency in this system and has shown the inadequacy of using size independent growth kinetics to characterise crystal growth in this system. Re-examination of the experimental data using the graphical procedure to take account of the growth rate size dependency coupled with further experimental work could yield a better description of the growth kinetics in this system.

6.4.4 The simulation procedure as a tool in process development

The results reported in this chapter highlight the difficulties of performing a successful simulation of an industrial crystallization process. The principle difficulties lie with the inputs to the simulation rather than the simulation procedure itself. The derived kinetic expressions have been shown to be subject to considerable errors and the obstacles to reducing these errors have been discussed. Similarly the seed size distribution at small size can have an important effect on the predicted size distributions.

The poor agreement between the predictions and experimental observations of the crystallization examined in this study indicate that the simulation should be used with great caution. It could possibly be used for qualitative prediction of the consequences of large changes in important parameters but the magnitude of the predicted effect would be subject to considerable error.

Clearly optimisation of an industrial crystallization process could be of commercial advantage if it could yield significant improvements to the product quality or reduce the crystallization time. Simulation appears to offer a useful stepping stone towards this goal, reducing the number of time consuming and expensive experiments necessary to gather the data required to optimise the process. However to be successful the simulation must yield results which agree with those found by experiment. In the case of the material used in this study the difficulty in obtaining reliable kinetic expressions has been shown to severely limit the usefulness of the simulation technique. The G-acid dipotassium salt monohydrate - sulphuric acid - water system is probably typical of many industrially important crystallizing systems for which the determination of crystallization kinetics under industrially important conditions is likely to present similar problems. In other systems where more precise kinetic expressions can be obtained simulation may be a much more useful aid to process development and optimisation.

7 Conclusions and Recommendations for Further Work

The conclusions which have been drawn from this study are discussed in this chapter. They fall into two categories; those which pertain to specific topics examined during the study, and those which are of wider application. The conclusions which pertain mainly to a specific aspect of the work are considered chapter by chapter in Sections 7.1 to 7.4 whilst those which have a wider relevance are considered in Section 7.5, the overall conclusions. Recommendations for further work are listed in Section 7.6

7.1 Solubility determinations

The solubility of G-acid dipotassium salt monohydrate in aqueous sulphuric acid in the presence of potassium ion has been determined over a range of temperatures, sulphuric acid concentrations and potassium ion concentrations which span the conditions used during the industrial crystallization of this material.

The experimental procedures employed to determine the solubility of G-acid dipotassium salt monohydrate in aqueous sulphuric acid solution performed well.

A solubility expression, Equation 3.10, has been developed which can be used to predict the solubility of G-acid dipotassium salt monohydrate over the range of conditions investigated.

The solubility expression involved extension of ideal solution theory to solutions of moderately high ionic strength. It is often assumed that ideal solution theory can only be applied to dilute solutions with low ionic strengths.

7.2 Determination of the metastable zone width.

The metastable zone width of G-acid dipotassium salt monohydrate in aqueous sulphuric acid solution has been determined for supersaturation generated by cooling and salting out by addition of excess potassium ion.

The metastable zone width corresponds to the maximum permissible supersaturation attainable prior to primary nucleation and is a useful limit in considering the operation of a crystallizer.

The experimental procedures employed performed satisfactory. However the induction times for salting out were found to be either very short or quite long. This left only a narrow band where the induction time could be measured with adequate precision using the experimental apparatus.

The metastable zone width determined for supersaturation generated by the addition of potassium sulphate was much narrower than that determined for supersaturation generated by cooling. A possible cause of this discrepancy may have been the generation of high local supersaturations around the dissolving potassium sulphate crystals. This would lead to nucleation in the regions of high localised supersaturation whilst the overall supersaturation was quite low. In contrast supersaturation generated by cooling would be a much less localised process leading only to quite small variations in supersaturation levels throughout the solution.

Detection of the nuclei was only possible after they had grown to measurable size. Estimation of this growth period lead to the unexpected inference that the initial growth rate was more rapid than would be expected from the growth kinetics derived later in the study. This finding lends weight to the suggestion that the localised regions of high supersaturation existed in the crystallizing solutions, higher growth rates being due to locally elevated supersaturation.

An attempt was made to assess interfacial tension between the G-acid dipotassium salt monohydrate crystals and the solution phase. The procedure used to determine interfacial tension involved a number of assumptions some of which may have been invalid. The calculated value was quite low and its physical significance is doubtful.

Determination of metastable zone widths and induction times provide useful information concerning primary nucleation and growth at supersaturations higher than those normally employed in seeded crystallizations.

7.3 Kinetics

A knowledge of the crystallization kinetics of a system is of great importance in any systematic attempt to optimise a crystallization process.

Some success has been achieved in an attempt to determine the kinetics of the crystallization of G-acid dipotassium salt monohydrate from aqueous sulphuric acid solution under conditions similar to those used industrially.

The experimental procedures employed were complex and a number of problems were encountered. Some of the problems were solved completely, others partially and some remained.

The principle difficulties lay in the measurement of crystal size distributions during the crystallization process. Electrical zone sensing was the most suitable of the crystal sizing procedures available to study this system. Even so the experimental procedures involved pushing the technique to its limits. As a consequence of this the experimental error associated with the measured size distributions was in some instances almost as great as the differences between size distributions from which the kinetic expressions were derived.

The growth kinetics derived by the moments based procedure were approximately twice those predicted for the same conditions using the graphical procedure.

The growth rates derived by both procedures appear to be plausible under some of the experimental conditions examined as was demonstrated by the simulation procedure.

There was evidence of growth rate size dependency or growth rate dispersion in the early stages of the experiments. However the screening procedure required prior to crystal sizing masked growth rate size dependence during the later stages of the experiments. This apparent growth rate size dependence diminished the usefulness of the derived kinetics.

The moments based procedure is not well suited to the determination of growth kinetics where there is growth rate size dependency.

The graphical procedure could be adapted to take account of the apparent growth rate size dependency. However problems were anticipated in obtaining sufficient data to derive a size dependent growth rate equation.

The moments based procedure substantially underestimated the nucleation rate whereas the graphical procedure yielded more plausible nucleation kinetics.

7.4 Simulation

Simulation has provided a useful method to compare the kinetics derived from the experimental data using the two different techniques. The spreadsheet based simulation procedure worked well.

The differences between the experimentally measured values and the ones predicted by the two sets of kinetics reveal the shortcomings of both the experimental data and the kinetics derived from them.

The lack of precision in the derived kinetic expressions makes the simulation an inadequate tool to aid process development for this system.

7.5 Overall conclusions

One important feature of this study has been the attempt to obtain the information necessary to model and hence optimise an industrial crystallization process. This study has served to highlight the difficulties in this endeavour. The principle obstacle in the case of G-acid dipotassium salt monohydrate was the accurate measurement of the crystallization kinetics under conditions close to those used industrially. The study may serve as a useful guide to other researchers investigating similar industrial crystallization processes. It provides examples of some experimental procedures which may be employed, indicating the nature of the results that may be obtained using them and identifies areas where difficulties may be encountered.

7.6 Recommendations for further work

Recommendations specific to the G-acid dipotassium salt monohydrate - sulphuric acid - water system

The discrepancy between the measured metastable zone widths determined by salting out and cooling could be investigated further. It would be useful to examine the suggestion that localised high supersaturation levels are responsible for the different

nucleation behaviour. A greater understanding of the distribution of supersaturation in solutions could be of benefit in many industrial crystallization processes where salting out is employed.

It would be useful to obtain more evidence of growth rate size dependency in the G-acid dipotassium salt monohydrate - sulphuric acid - water system. If a size dependent growth rate equation could be derived it could be tested against the experimental data using the simulation procedure.

If more reliable kinetic data could be obtained it would be valuable to validate the model of the crystallization of the G-acid dipotassium salt monohydrate by simulating some of the other experiments, attempting to use the simulation predictively and optimising the crystallization of this material.

Recommendations appropriate to the study of industrial crystallization in general.

The practical difficulty associated with accurate measurement of crystal size distributions down to small size is a major obstacle to the determination of crystallization kinetics. Development of new particle sizing techniques which can count and size crystals accurately would be very valuable. Of special interest would be techniques which could make *in-situ* measurements in dense crystal suspensions.

The problems encountered in the accurate determination of crystallization kinetics have been highlighted. It would be useful to devise new procedures for extraction of crystallization kinetics from experimental data. The measurement of nucleation kinetics is an area of particular difficulty.

Appendix 1

Correction factors for the absorption contribution of impurities in industrial G-acid at 236nm.

The G-acid dipotassium salt monohydrate used in the experimental work reported in this thesis contained small traces of other hydroxynaphthalene sulphonic acids which absorb UV light at 236nm, the wave length used in the spectrophotometric determination of G-acid dipotassium salt concentration. The effect of these impurities was to increase the apparent G-acid concentration therefore a correction factor was calculated in the manner reported elsewhere, Price (1985), from compositional data for G-acid determined by HPLC and the UV absorbance data recorded in Table A1.

Table A1.1 Absorption Coefficients of Sulphonic Acid s at 236nm Determined on a Pye Unicam PU8600 Spectrophotometer (Reproduced from Price (1985)).

	G-acid^{2-}	R-acid^{2-}	S-acid^{-}	T-acid^{3-}
λ max (nm)	236	237	232	239
Sample conc (mol free acid. L^{-1})	1.52×10^{-5}	7.99×10^{-6}	9.38×10^{-6}	2.09×10^{-5}
Absorbance (236nm)	0.776	0.600	0.572	1.047
Molar extinction coef. (ε_o)	51221	75056	60981	50074
Free acid as $(g.(100gsol)^{-1}) \equiv 1$ Abs	5.94×10^{-4}	4.05×10^{-4}	3.67×10^{-4}	7.67×10^{-4}

Calculation of the correction factor was based on the absorbance contribution of each component contained in a 1g sample of the G-acid dipotassium salt monohydrate made up to 100g of solution. Two batches of material were examined, the results for both are given below.

Table A1.2 Calculation of the absorbance correction factor for Batch 366 85 B

Substance (expressed as ionic species)	Composition (%) of dry G-acid di-potassium salt as the monohydrate	Concentration in solution g per 100g solution	Sulphonic acid mass g per 100g solution equivalent to 1 Abs.	Contribution to solution absorbance
G-acid^{2-}	75.1	0.751	5.94×10^{-4}	1264.3
R-acid^{2-}	0.22	0.0022	4.05×10^{-4}	5.4
S-acid^{-}	0.04	0.0004	3.67×10^{-4}	1.1
T-acid^{3-}	0.50	0.0050	7.67×10^{-4}	6.5
Total absorbance of impurities (Abs.) Total absorbance (Abs.) Contribution of impurities to total (%) Correction factor				13.0 1277.3 1.02 0.9899

Table A1.3 Calculation of the absorbance correction factor for Batch 5069 A

Substance (expressed as ionic species)	Composition (%) of dry G-acid di-potassium salt as the monohydrate	Concentration in solution g per 100g solution	Sulphonic acid mass g per 100g solution equivalent to 1 Abs.	Contribution to solution absorbance
G-acid^{2-}	75.3	0.753	5.94×10^{-4}	1267.7
R-acid^{2-}	≈0.3	0.003	4.05×10^{-4}	7.4
S-acid^{-}	<0.1	0.001	3.67×10^{-4}	2.7
T-acid^{3-}	≈0.2	0.002	7.67×10^{-4}	2.6
Total absorbance of impurities (Abs.) Total absorbance (Abs.) Contribution of impurities to total (%) Correction factor				12.7 1280.4 0.99 0.99

Appendix 2

Table A2.1 Solubility data for G-acid dipotassium salt monohydrate in 9% sulphuric acid solution. Values are expressed per 100g solution. Values calculated using equation 3.9 are included for comparison.

Equation 3.9 $$\ln[G-acid^{2-}]_{Eq} = -1.6160.\ln[K^{+}]_{Eq} - 0.47284.\ln[H_2SO_4]_{Eq} - \frac{4969.9}{T} + 6.3974$$

Temp (K)	$[H_2SO_4]$ g/100g	$\ln[H_2SO_4]$ mol/100g	$[K^+]$ g/100g	$\ln[K^+]$ mol/100g	[G-acid^{2-}] g/100g	ln[G-acid^{2-}] mol/100g	Plot marker	Calc from Equation 3.9 [G-acid^{2-}] g/100g	Calc from Equation 3.9 ln[G-acid^{2-}] mol/100g
302.6	8.2121	-2.4793	1.9141	-3.0143	7.0035	-3.7640	o	5.6255	-3.9831
302.6	8.1979	-2.4811	2.2818	-2.8386	4.4462	-4.2184	o	4.2383	-4.2662
302.5	8.1261	-2.4899	2.7911	-2.6371	2.5794	-4.7629	o	3.0567	-4.5931
302.6	7.9608	-2.5104	3.5422	-2.3988	1.8704	-5.0843	o	2.1114	-4.9631
302.6	7.6283	-2.5531	5.0452	-2.0451	1.2224	-5.5096	o	1.2165	-5.5145
321.2	8.1152	-2.4912	2.1257	-2.9094	8.3632	-3.5866	x	12.3611	-3.1959
321.2	8.1076	-2.4922	2.4923	-2.7504	5.6161	-3.9848	x	9.5631	-3.4525
321.1	8.0027	-2.5052	3.1310	-2.5222	3.8303	-4.3675	x	6.6229	-3.8200
321.1	7.9544	-2.5112	3.4647	-2.4209	2.7173	-4.7108	x	5.6392	-3.9807
321.1	7.6485	-2.5504	4.8856	-2.0773	1.7888	-5.1289	x	3.2966	-4.5175
325.5	7.9355	-2.5136	2.5108	-2.7429	11.144	-3.2995	•	11.7101	-3.2500
325.3	7.9701	-2.5093	2.7142	-2.6651	8.3195	-3.5918	•	10.2079	-3.3873
325.3	7.8744	-2.5213	3.3788	-2.4460	6.1299	-3.8972	•	7.2062	-3.7355
325.2	7.7752	-2.5340	3.9540	-2.2888	4.8732	-4.1267	•	5.5966	-3.9883
324.8	7.5938	-2.5576	4.9350	-2.0672	3.3839	-4.4914	•	3.8820	-4.3541
339.9	7.7055	-2.5430	3.1058	-2.5303	14.271	-3.0522	+	16.0800	-2.9328
340.1	7.6894	-2.5451	3.5050	-2.4094	11.587	-3.2606	+	13.3536	-3.1186
339.4	7.6750	-2.5470	3.9104	-2.2999	8.7950	-3.5362	+	10.8659	-3.3248
339.0	7.3822	-2.5859	5.6533	-1.9313	5.5334	-3.9995	+	5.9959	-3.9193
352.8	7.4449	-2.5774	4.2779	-2.2101	14.344	-3.0471	#	16.6270	-2.8994
351.9	7.4091	-2.5822	4.7746	-2.1005	11.665	-3.2538	#	13.4608	-3.1106
351.7	7.3404	-2.5916	5.2690	-2.0012	10.312	-3.3771	#	11.4379	-3.2735
351.2	7.2499	-2.6040	5.9920	-1.8731	8.0170	-3.6289	#	9.1603	-3.4955

Table A2.2 Solubility data for G-acid dipotassium salt monohydrate in 18% sulphuric acid solution. Values are expressed per 100g solution. Values calculated using equations 3.9 and 3.10 are included for comparison.

Equation 3.9 $$\ln[G-acid^{2-}]_{Eq} = -1.6160.\ln[K^{+}]_{Eq} - 0.47284.\ln[H_2SO_4]_{Eq} - \frac{4969.9}{T} + 6.3974$$

Equation 3.10 $$\ln[G-acid^{2-}]_{Eq} = -1.9736.\ln[K^{+}]_{Eq} - 1.1873.\ln[H_2SO_4]_{Eq} - \frac{5287}{T} + 5.5957$$

Temp (K)	$[H_2SO_4]$ g/100g	$\ln[H_2SO_4]$ mol/100g	$[K^+]$ g/100g	$\ln[K^+]$ mol/100g	$[G\text{-}acid^{2-}]$ g/100g	$\ln[G\text{-}acid^{2-}]$ mol/100g	Plot mark	Calc from Equation 3.9 $[G\text{-}acid^{2-}]$ g/100g	Calc from Equation 3.9 $\ln[G\text{-}acid^{2-}]$ mol/100g	Calc from Equation 3.10 $[G\text{-}acid^{2-}]$ g/100g	Calc from Equation 3.10 $\ln[G\text{-}acid^{2-}]$ mol/100g
297.4	16.5410	-1.7791	1.8541	-3.0462	5.6677	-3.9756	o	3.1915	-4.5499	5.2225	-4.0574
297.6	16.3817	-1.7888	2.5103	-2.7431	2.8048	-4.6791	o	1.9870	-5.0238	2.9400	-4.6320
297.6	15.4416	-1.8479	4.6750	-2.1213	0.9075	-5.8074	o	0.7480	-6.0007	0.9243	-5.7891
297.7	14.9783	-1.8784	5.7485	-1.9146	0.6490	-6.1427	o	0.5464	-6.3147	0.6411	-6.1549
311.7	16.1615	-1.8023	2.3615	-2.8042	7.5516	-3.6887	x	4.6983	-4.1632	7.5283	-3.6917
311.7	16.0263	-1.8107	2.9761	-2.5729	4.7501	-4.1522	x	3.2458	-4.5330	4.8169	-4.1383
311.5	15.7890	-1.8256	3.6994	-2.3554	2.8250	-4.6719	x	2.2765	-4.8878	3.1570	-4.5608
311.6	15.4451	-1.8477	4.5581	-2.1466	1.8008	-5.1222	x	1.6501	-5.2096	2.1581	-4.9412
311.5	15.0896	-1.8710	5.4215	-1.9732	1.2282	-5.5049	x	1.2541	-5.4840	1.5669	-5.2613
326.0	15.6687	-1.8333	3.0553	-2.5467	10.1500	-3.3929	•	6.3282	-3.8654	9.8860	-3.4193
326.0	15.5574	-1.8404	3.6376	-2.3722	7.3345	-3.7178	•	4.7899	-4.1439	7.0663	-3.7551
325.7	15.4145	-1.8496	4.2424	-2.2184	4.9257	-4.1159	•	3.6997	-4.4022	5.1955	-4.0626
325.8	15.1286	-1.8684	5.0638	-2.0414	3.4230	-4.4799	•	2.8173	-4.6746	3.7648	-4.3847
325.0	14.5614	-1.9066	6.5180	-1.7890	2.4822	-4.8013	•	1.8374	-5.1021	2.3000	-4.8775
335.7	15.3571	-1.8534	3.5596	-2.3939	11.531	-3.2654	+	7.7537	-3.6622	11.9666	-3.2283
335.7	15.2761	-1.8587	4.0684	-2.2603	8.8417	-3.5309	+	6.2635	-3.8757	9.2506	-3.4857
334.9	15.2210	-1.8623	4.5182	-2.1554	6.1751	-3.8899	+	5.1123	-4.0788	7.2748	-3.7260
334.8	14.8903	-1.8842	5.4485	-1.9682	4.7751	-4.1470	+	3.8001	-4.3754	5.1360	-4.0741
334.8	14.5538	-1.9071	6.4169	-1.8046	3.4599	-4.4692	+	2.9491	-4.6289	3.8211	-4.3699
351.8	14.8224	-1.8888	4.3804	-2.1864	14.804	-3.0155	#	11.1019	-3.3033	17.0373	-2.8750
351.8	14.6814	-1.8984	5.0022	-2.0537	12.478	-3.1864	#	8.9995	-3.5133	13.2609	-3.1256
351.1	14.7572	-1.8932	5.2374	-2.0077	9.0705	-3.5054	#	8.1036	-3.6181	11.6821	-3.2524
350.8	14.5388	-1.9081	5.9654	-1.8776	7.4469	-3.7026	#	6.5333	-3.8335	9.0793	-3.5044
350.4	14.2282	-1.9297	6.9248	-1.7284	5.9896	-3.9204	#	5.1037	-4.0805	6.8217	-3.7903

Table A2.3 Solubility data for G-acid dipotassium salt monohydrate in 26% sulphuric acid solution. Values are expressed per 100g solution. Values calculated using equations 3.9 and 3.10 are included for comparison.

Equation 3.9 $$\ln[G-acid^{2-}]_{Eq} = -1.6160.\ln[K^{+}]_{Eq} - 0.47284.\ln[H_2SO_4]_{Eq} - \frac{4969.9}{T} + 6.3974$$

Equation 3.10 $$\ln[G-acid^{2-}]_{Eq} = -1.9736.\ln[K^{+}]_{Eq} - 1.1873.\ln[H_2SO_4]_{Eq} - \frac{5287}{T} + 5.5957$$

Temp (K)	$[H_2SO_4]$ g/100g	$\ln[H_2SO_4]$ mol/100g	$[K^+]$ g/100g	$\ln[K^+]$ mol/100g	$[G\text{-}acid^{2-}]$ g/100g	$\ln[G\text{-}acid^{2-}]$ mol/100g	Plot mark	Calc from Equation 3.9 $[G\text{-}acid^{2-}]$ g/100g	Calc from Equation 3.9 $\ln[G\text{-}acid^{2-}]$ mol/100g	Calc from Equation 3.10 $[G\text{-}acid^{2-}]$ g/100g	Calc from Equation 3.10 $\ln[G\text{-}acid^{2-}]$ mol/100g
297.3	24.3865	-1.3909	1.5444	-3.2289	4.7038	-4.1620	o	3.5491	-4.4437	4.6965	-4.1636
297.4	24.8480	-1.3722	2.2194	-2.8663	2.1529	-4.9436	o	1.9689	-5.0329	2.2590	-4.8955
297.4	24.8814	-1.3708	3.2675	-2.4795	0.9663	-5.7447	o	1.0532	-5.6586	1.0512	-5.6605
297.4	24.7082	-1.3778	4.3778	-2.1870	0.5426	-6.3217	o	0.6586	-6.1281	0.59506	-6.2295
297.4	24.5010	-1.3862	5.3670	-1.9833	0.3897	-6.6528	o	0.4757	-6.4533	0.40206	-6.6216
311.2	23.8678	-1.4124	1.9921	-2.9744	6.4449	-3.8471	x	5.0136	-4.0983	6.4512	-3.8462
311.2	24.3659	-1.3918	2.5834	-2.7145	3.7446	-4.3901	x	3.2621	-4.5280	3.7689	-4.3836
311.1	24.5716	-1.3834	3.4033	-2.4388	2.0756	-4.9802	x	2.0706	-4.9826	2.1540	-4.9431
310.8	24.5043	-1.3861	4.5179	-2.1555	1.2298	-5.5036	x	1.2916	-5.4545	1.2154	-5.5154
310.9	24.4170	-1.3897	5.2668	-2.0021	0.8358	-5.8897	x	1.0150	-5.6956	0.90669	-5.8084
325.8	23.2593	-1.4383	2.4886	-2.7518	8.6406	-3.5539	•	7.2457	-3.7300	9.1802	-3.4934
325.6	23.7193	-1.4187	3.2045	-2.4990	5.8707	-3.9405	•	4.7265	-4.1572	5.3915	-4.0256
325.5	24.0344	-1.4055	3.8376	-2.3187	3.8755	-4.3557	•	3.4935	-4.4595	3.7000	-4.4021
325.3	24.1555	-1.4004	4.7512	-2.1052	2.4440	-4.8168	•	2.4450	-4.8164	2.3892	-4.8395
324.9	24.1657	-1.4000	5.5024	-1.9584	1.6461	-5.2120	•	1.8924	-5.0726	1.7519	-5.1497
341.7	22.5269	-1.4702	3.2520	-2.4843	11.3101	-3.2847	+	9.7090	-3.4374	11.967	-3.2282
341.7	22.9785	-1.4504	3.7737	-2.3355	8.6405	-3.5540	+	7.5624	-3.6872	8.7139	-3.5455
340.9	23.3646	-1.4337	4.3668	-2.1895	6.2760	-3.8737	+	5.7274	-3.9652	6.1762	-3.8897
340.9	23.5201	-1.4271	5.1565	-2.0233	4.7863	-4.1447	+	4.3645	-4.2369	4.4140	-4.2256
340.4	23.649	-1.4216	6.1095	-1.8537	3.2586	-4.5291	+	3.2396	-4.5350	3.0673	-4.5896
353.1	22.0270	-1.4927	3.7736	-2.3355	13.262	-3.1255	#	12.3392	-3.1976	15.100	-2.9957
353.1	22.6054	-1.4668	4.3040	-2.2040	9.8734	-3.4206	#	9.8555	-3.4224	11.295	-3.2860
352.2	23.0079	-1.4491	4.9344	-2.0673	7.3367	-3.7175	#	7.5595	-3.6876	8.1286	-3.6150
352.2	23.1617	-1.4425	5.5005	-1.9587	6.0579	-3.9090	#	6.3228	-3.8663	6.5087	-3.8373
351.8	23.3764	-1.4332	5.9411	-1.8817	4.6401	-4.1757	#	5.4697	-4.0112	5.4359	-4.0174

Table A2.4 Solubility data for G-acid dipotassium salt monohydrate in 33% sulphuric acid solution. Values are expressed per 100g solution. Values calculated using equations 3.9 and 3.10 are included for comparison.

Equation 3.9 $$\ln[G-acid^{2-}]_{Eq} = -1.6160.\ln[K^{+}]_{Eq} - 0.47284.\ln[H_2SO_4]_{Eq} - \frac{4969.9}{T} + 6.3974$$

Equation 3.10 $$\ln[G-acid^{2-}]_{Eq} = -1.9736.\ln[K^{+}]_{Eq} - 1.1873.\ln[H_2SO_4]_{Eq} - \frac{5287}{T} + 5.5957$$

Temp (K)	$[H_2SO_4]$ g/100g	$\ln[H_2SO_4]$ mol/100g	$[K^+]$ g/100g	$\ln[K^+]$ mol/100g	$[G\text{-}acid^{2-}]$ g/100g	$\ln[G\text{-}acid^{2-}]$ mol/100g	Plot mark	Calc from Equation 3.9 $[G\text{-}acid^{2-}]$ g/100g	Calc from Equation 3.9 $\ln[G\text{-}acid^{2-}]$ mol/100g	Calc from Equation 3.10 $[G\text{-}acid^{2-}]$ g/100g	Calc from Equation 3.10 $\ln[G\text{-}acid^{2-}]$ mol/100g
301.9	31.3111	-1.1410	1.8279	-3.0604	3.2629	-4.5278	o	3.0984	-4.5795	3.2819	-4.5220
301.9	31.5924	-1.1320	2.2700	-2.8437	1.9309	-5.0524	o	2.1739	-4.9339	2.1175	-4.9602
301.9	31.6156	-1.1313	3.3288	-2.4609	0.79399	-5.9411	o	1.1707	-5.5529	0.9938	-5.7166
316.3	30.2632	-1.1750	1.9173	-3.0126	6.6238	-3.8197	x	6.1670	-3.8912	6.9020	-3.7786
316.3	30.6611	-1.1620	2.2199	-2.8661	4.9816	-4.1047	x	4.8368	-4.1342	5.0893	-4.0833
316.1	30.9966	-1.1511	2.5966	-2.7094	3.5013	-4.4573	x	3.6983	-4.4025	3.6484	-4.4161
316.1	31.2414	-1.1432	3.4941	-2.4125	1.8100	-5.1171	x	2.2805	-4.8860	2.0118	-5.0114
331.4	29.3743	-1.2048	2.7811	-2.6407	8.8759	-3.5271	•	7.0164	-3.7622	7.3510	-3.7156
331.2	29.7223	-1.1931	3.1303	-2.5224	7.2811	-3.7251	•	5.7115	-3.9679	5.6847	-3.9726
331	29.9868	-1.1842	3.8505	-2.3154	5.6310	-3.9821	•	4.0333	-4.3158	3.7022	-4.4015
330.9	30.6401	-1.1626	4.0368	-2.2681	3.2248	-4.5395	•	3.6821	-4.4069	3.2715	-4.5252
349.1	28.4792	-1.2358	3.3859	-2.4439	11.607	-3.2588	+	11.081	-3.3052	11.613	-3.2583
348.9	28.9749	-1.2185	3.3756	-2.4470	9.7429	-3.4339	+	10.956	-3.3166	11.347	-3.2815
348.2	29.1335	-1.2131	3.8594	-2.3130	8.6701	-3.5505	+	8.5522	-3.5642	8.3951	-3.5828
347.9	29.7056	-1.1936	4.3911	-2.1840	6.0727	-3.9066	+	6.7945	-3.7943	6.2760	-3.8737

Table A2.5 Solubility data for G-acid dipotassium salt monohydrate in 40% sulphuric acid solution. Values are expressed per 100g solution. Values calculated using equations 3.9 and 3.10 are included for comparison.

Equation 3.9 $$\ln[G-acid^{2-}]_{Eq} = -1.6160.\ln[K^{+}]_{Eq} - 0.47284.\ln[H_2SO_4]_{Eq} - \frac{4969.9}{T} + 6.3974$$

Equation 3.10 $$\ln[G-acid^{2-}]_{Eq} = -1.9736.\ln[K^{+}]_{Eq} - 1.1873.\ln[H_2SO_4]_{Eq} - \frac{5287}{T} + 5.5957$$

Temp (K)	$[H_2SO_4]$ g/100g	$\ln[H_2SO_4]$ mol/100g	$[K^+]$ g/100g	$\ln[K^+]$ mol/100g	$[G\text{-}acid^{2-}]$ g/100g	$\ln[G\text{-}acid^{2-}]$ mol/100g	Plot mark	Calc from Equation 3.9 $[G\text{-}acid^{2-}]$ g/100g	Calc from Equation 3.9 $\ln[G\text{-}acid^{2-}]$ mol/100g	Calc from Equation 3.10 $[G\text{-}acid^{2-}]$ g/100g	Calc from Equation 3.10 $\ln[G\text{-}acid^{2-}]$ mol/100g
299.0	37.727	-0.95459	1.2959	-3.40435	4.3943	-4.23012	o	4.2160	-4.27153	4.3757	-4.23435
299.0	38.346	-0.93831	1.6700	-3.15073	2.3999	-4.83500	o	2.7769	-4.68907	2.6018	-4.75421
299.0	38.535	-0.93340	2.1189	-2.91266	1.4640	-5.32925	o	1.8857	-5.07612	1.6169	-5.22991
299.0	38.531	-0.93350	2.2881	-2.83583	1.3059	-5.44353	o	1.6656	-5.20022	1.3896	-5.38141
299.0	38.558	-0.93280	2.3282	-2.81846	1.1968	-5.53077	o	1.6190	-5.22863	1.3416	-5.41653
309.8	37.083	-0.97180	1.6413	-3.16807	5.7891	-3.95445	x	5.1792	-4.06577	5.1894	-4.06381
309.8	38.101	-0.94472	2.5222	-2.73843	2.1778	-4.93211	x	2.5537	-4.77288	2.1523	-4.94390
309.7	38.172	-0.94286	3.1269	-2.52351	1.3856	-5.38429	x	1.7935	-5.12623	1.3974	-5.37577
309.7	38.138	-0.94375	3.3383	-2.45809	1.2612	-5.47836	x	1.6143	-5.23153	1.2295	-5.50383
325.0	36.280	-0.99370	2.0525	-2.94450	7.6325	-3.67801	•	7.7215	-3.66642	7.6105	-3.68089
325.0	36.885	-0.97716	2.3938	-2.79067	5.5805	-3.99115	•	5.9751	-3.92282	5.5086	-4.00412
324.8	37.388	-0.96361	2.8001	-2.63390	3.7908	-4.37785	•	4.5651	-4.19199	3.9385	-4.33962
324.8	37.598	-0.95801	3.4584	-2.42275	2.5641	-4.76882	•	3.2368	-4.53585	2.5790	-4.76300
324.6	37.657	-0.95644	4.1121	-2.24962	1.7496	-5.15104	•	2.4221	-4.82580	1.8109	-5.11658
342.9	34.993	-1.02981	2.8047	-2.63226	10.710	-3.33925	+	10.536	-3.35565	10.028	-3.40504
342.6	35.671	-1.01062	3.0361	-2.55298	8.4249	-3.57923	+	9.0693	-3.50553	8.2700	-3.59779
342.2	36.249	-0.99455	3.3598	-2.45168	6.4067	-3.85308	+	7.5130	-3.69380	6.5245	-3.83485
342.1	36.577	-0.98554	3.9213	-2.29713	4.9068	-4.11980	+	5.8031	-3.95205	4.7368	-4.15507
341.7	36.789	-0.97976	4.6501	-2.12667	3.5781	-4.43559	+	4.3196	-4.24725	3.3002	-4.51645
354.0	34.349	-1.04839	3.2120	-2.49666	12.326	-3.19872	#	13.449	-3.11153	12.721	-3.16714
353.7	34.879	-1.03308	3.4968	-2.41171	10.368	-3.37170	#	11.501	-3.26796	10.431	-3.36565
353.4	35.415	-1.01783	3.8287	-2.32103	8.3947	-3.58283	#	9.7454	-3.43363	8.4571	-3.57541
353.1	35.841	-1.00587	4.2377	-2.21954	6.7130	-3.80638	#	8.1268	-3.61525	6.7382	-3.80263
352.1	36.127	-0.99792	4.9129	-2.07169	5.1989	-4.06198	#	6.1259	-3.89790	4.7781	-4.14638

Table A2.6 The solubility of G-acid dipotassium salt monohydrate from batch BX 5069 A in sulphuric acid solution of initial concentration 40g H_2SO_4 per 100g solution. The solubilities are expressed in Kg G-acid dipotassium salt monohydrate per Kg of solvent. (The solvent was assumed to be 0.4Kg H_2SO_4 per Kg solution.)

Temp °C	Temp K	G-acid $^{2-}$ conc. (MW = 302) g per 100g soln.	G-acid dipotassium salt monohydrate conc. (MW = 398) Kg per Kg solvent. Measured	Predicted by Equation 5.25
82.8	355.8	12.75	0.2004	0.200804
81	354	12.42	0.1947	0.195346
80	353	12.3	0.1919	0.19235
79.8	352.8	12.35	0.1929	0.191753
75.5	348.5	11.67	0.1803	0.179176
72.6	345.6	11.1	0.17	0.170956
71.5	344.5	11.08	0.1697	0.167893
70.5	343.5	10.75	0.1638	0.165136
69.9	342.9	10.82	0.165	0.163493
65.8	338.8	10.11	0.1525	0.152513
65.5	338.5	10.14	0.1531	0.151726
64.3	337.3	9.82	0.1475	0.148601
60.6	333.6	9.38	0.14	0.139194
55.9	328.9	8.74	0.1292	0.127743
55.4	328.4	8.5	0.1252	0.126557
49.7	322.7	7.75	0.1129	0.113487
46.1	319.1	7.37	0.1061	0.105654
45	318	7.13	0.103	0.103325
40.2	313.2	6.52	0.0933	0.093521
38.8	311.8	6.3	0.0899	0.090771
34.6	307.6	5.85	0.0829	0.082817
29.6	302.6	5.26	0.074	0.073926
28.6	301.6	5.15	0.0732	0.072224

Appendix 3

A listing of the computer program used to perform the s-plane analysis procedure using the size distributions measured by the Elzone 80XY particle size analyser. This program was developed from an earlier program written by Dr. N. S. Tavare to perform s-plane analysis on data measured by the Coulter Counter.

```
1 DIM G$(50),H$(50),I$(50),J$(50)
2 PRINT "CRYSTALLISATION KINETICS"
3 INPUT"ENTER RUN NUMBER";R1
4 INPUT"DATE";G$
5 INPUT"MATERIAL CRYSTALLISED";H$
6 INPUT"SOLVENT";I$
7 INPUT"TEMPERATURE PROFILE eg. 80 to 20 in 5 hours.";J$
8 INPUT"SEED LOADING";R5
9 INPUT"AGITATION RATE";R6
10 OPEN"I",#1,"20.8XA"
11 LPRINT"CRYSTALLISATION KINETICS"
12 LPRINT"   RUN NUMBER",R1,"DATE",G$
13 LPRINT"   MATERIAL CRYSTALLISED",H$
14 LPRINT"   SOLVENT",I$
15 LPRINT"   TEMPERATURE PROFILE",J$
16 LPRINT"   SEED LOADING",R5
17 LPRINT"   AGITATION RATE",R6
20 DIM A$(200),L(200),D(200)
22 DIM X(100),Y(100)
25 JM=1:W2=0
26 DIM B$(200),C$(200),X$(200)
30 FOR I=1 TO 156 STEP 1
35 IF EOF(1) THEN GOTO 70
40 INPUT #1,A$(I)
60 NEXT I
70 CLOSE
80 FOR I=0 TO 127
90 A25=VAL(A$(25))
100 L(I)=((A25*(1.0221^I))+(A25*(1.0221^(I+1))))/2
110 D(I)=((A25*(1.0221^(I+1)))-(A25*(1.0221^I)))
130 NEXT I
140 INPUT"ENTER TIME OF SAMPLE,S";W1
150 INPUT"VOLUME OF CELL,ML";VC
160 INPUT"VOLUME OF SAMPLE,ML";VS
170 INPUT"VOLMETRIC SECTION,ML";SV
180 INPUT"NAME OF BACKGROUND COUNT FILE";F$
190 OPEN"I",#1,F$
200 FOR I=1 TO 156
210 INPUT #1,A$(I)
230 IF EOF(1) THEN GOTO 240
235 NEXT I
240 CLOSE
250 INPUT "NAME OF SAMPLE FILE";E$
255 OPEN"I",#1,E$
260 FOR I=1 TO 156
270 INPUT#1,B$(I)
290 IF EOF(1)THEN GOTO 300
295 NEXT I
300 CLOSE
```

Appendix 3 *(continued)*

```
310 FOR I=26 TO 154
320 J=I-26
330 C$(J)=STR$(VAL(B$(I))-VAL(A$(I)))
340 NEXT I
350 ZA=0
355 ZB=0
360 FOR I=0 TO 127
370 ZA=ZA+VAL(C$(I))
380 ZB=ZB+VAL(C$(I))*L(I)
390 NEXT I
400 AL=ZB/ZA
410 IF JM=< 1 THEN GOTO 480
420 GOSUB 7000
440 FOR I=0 TO 127
450 X$(I)=STR$(VAL(C$(I)))
460 NEXT I
480 INPUT "ARE THERE ANY MORE RUNS,Y/N";Z$
485 W2=W1:JM=JM+1
490 IF Z$="Y" THEN GOTO 140
500 IF Z$="N" THEN END
7000 SF=1/AL
7010 NP=50:SN=SF/NP
7020 ZX=0
7030 FOR K=1 TO NP
7040 U20=0:U10=0
7050 FOR I=0 TO 127
7060 U20=U20+VAL(C$(I))/D(I)*(VC/(SV*VS))*EXP(-ZX*L(I))*D(I)
7070 U10=U10+(VAL(X$(I))*(VC/(SV*VS))*EXP(-ZX*L(I)))
7080 NEXT I
7090 W3=W1-W2
7100 Y(K)=(U20-U210)/W3
7110 X(K)=(U20+U10)*.5*ZX
7120 ZX=ZX+SN
7130 NEXT K
7140 S1=0!:S3=0!:S5=0!:T1=0!:T3=0!:T5=0!
7150 FOR K=1 TO NP
7160 S1=S1+X(K)
7170 S3=S3+X(K)^2
7180 S5=S5+X(K)*Y(K)
7190 T1=T1+Y(K)
7200 T3=T3+Y(K)^2
7210 NEXT K
7220 S2=S1/NP
7230 S4=S3-(S1^2)/NP
7240 S6=S5-S1*T1/NP
7250 T2=T1/NP
7260 T4=T3-T1^2/NP
7270 G=-S6/S4
7280 BN=T2-G*S2
7290 R=S6/(S4*T4)^.5
7300 W4=(W1+W2)*.5
7400 PRINT"MEAN GROWTH RATE,UM/S=";G
7410 LPRINT "MEAN GROWTH RATE,UM/S= ";G
7420 PRINT"MEAN NUCLEATION RATE,#/SML";BN
7430 LPRINT "MEAN NUCLEATION RATE,#/SML= ";BN
7450 LPRINT "CORRELATION COEFFICIENT =";ABS(R)
7460 PRINT"CORRELATION COEFFICIENT=";ABS(R)
7470 LPRINT "MEAN TIME,S= ";W4
7480 PRINT"MEAN TIME,S";W4
7500 RETURN
```

Nomenclature

a	constant in equation 5.25	kg (kg40% H_2SO_4 soln.)$^{-1}$
A	constant in equation 4.1	# m^{-3} s^{-1}
b	constant in equation 5.25	kg (kg40% H_2SO_4 soln.)$^{-1}$ $°C^{-1}$
B	constant in equation 4.4	-
B	nucleation rate	# $kgFS^{-1}$ s^{-1}
B_N	nucleation rate	# $kgFS^{-1}$ s^{-1}
c	constant in equation 5.25	kg (kg40% H_2SO_4 soln.)$^{-1}$ $°C^{-2}$
C^*	equilibrium solubility	kg (kg40% H_2SO_4 soln.)$^{-1}$
d	an incremental quantity	-
D	diffusivity	m^2 s^{-1}
E_b	Activation energy (nucleation, 5.24)	J mol^{-1}
E_g	Activation energy (growth, 5.23)	J mol^{-1}
E_r	Activation energy (nucleation, 5.26)	J mol^{-1}
f_A	area shape factor	-
f_V	volume shape factor	-
G	growth rate	m s^{-1}
I	impurity concentration	mol 100gsoln^{-1}
J	nucleation rate	# $kgFS^{-1}$ s^{-1}
k	Boltzman constant	J K^{-1}
K	constant eq 4.3	# m^{-3}
K_b	nucleation rate constant 5.24	# $kgFS^{-1}$ s^{-1} $(kg/kg)^{-b}$ $(kg/kg)^{-j}$ $(s^{-1})^{-m}$
K_g	growth rate constant	m s^{-1} $(kg/kg)^{-g}$
K_r	nucleation rate constant 5.26	# $kgFS^{-1}$ s^{-1} $(m\ s^{-1})^{-i}$ $(kg/kg)^{-j}$ $(s^{-1})^{-m}$
K_{sp}	solubility product	mol l^{-1}
L	characteristic length	m
$\bar{L}$	sum of the characteristic lengths of the crystals in the distribution	m
$l_{nuc\,n\,n}$	size of growing nuclei in size band n at the end of the current iteration during time increment n.	m
$l_{seed\,x\,n}$	size of seeds in band x at time n	m
m	gradient	
MFS	mass of free solvent	kg
MS	mass of seeds	kg
M_{seed}	Seed mass (normalised)	kg
M_{sol}	Solution mass	kg

M_t	magma density	kg (kg40% H_2SO_4 soln.)$^{-1}$
MW	molecular weight	amu
n	population density	# $m^{-1}m^{-3}$
N	agitation rate	s^{-1}
N	Avogadros number	# mol^{-1}
$\overline{\mathcal{N}}$	average total number of crystals in the distribution during a time increment	# $kgFS^{-1}$
NN_n	number of nucleated crystals in size band n.	# $kgFS^{-1}$
n_o	population density at zero size	# m^{-1} m^{-3}
NS_x	number of seeds in band x	# $kgFS^{-1}$
R	gas constant	J mol^{-1} K^{-1}
r_c	radius of a critical sized cluster	m
s	laplace transform variable	-
S	supersaturation ratio	-
S_a	seeds from band a	-
SL	seed loading	kg $kgFS^{-1}$
t	time	s
T	absolute temperature	K
VC_n	volume of crystals in band n	m^3
W_S	weight of seed crystals	kg
[ ]	solution concentration	mol $100gsoln^{-1}$
{ }	solution concentration	g $100gsoln^{-1}$

Subscripts

Eq	equilibrium
Hyd	hydrated
n	nth increment
o	initial
N	nuclei
s	seed crystals

Superscripts

b	exponent on supersaturation
d	exponent on crystal size
g	exponent on supersaturation
i	exponent on growth rate (relative kinetic order)
j	exponent on magma density
m_b	exponent on agitation rate for nucleation
m_g	exponent on agitation rate for growth
-	mean value during time increment

Greek symbols

β	shape factor	
Δl_n	size increase during increment n	m
ΔG^*	Gibbs free energy	J mol^{-1}
ΔC	supersaturation	kg (kg40% H_2SO_4 soln.)$^{-1}$
Δ	an incremental quantity	-
ε_o	molar extinction coefficient	Abs
λ_{max}	wavelength of maximum absorption	nm
μ_j	the jth moment of a function $f(L)$	-
ρ	crystal density	kg m^3
ρ	solution density	kg m^3
σ	interfacial tension	J m^{-2}
τ	induction period	s
τ	residence time	s
Ω	molecular volume	m^3

Anderssen A. S. and White E. T.
"Parameter Estimation by the Weighted Moments Method"
Chem. Eng. Sci. **26** 1203-1221 (1971).

Ang H. M. and Mullin J. W.
"Crystal Growth Rate Determinations from Desupersaturation Experiments: Nickel Ammonium Sulphate Hexahydrate"
Trans. I.Chem.E. **57** 237-243 (1979).

Aquilano D., Rubbo M., Vaccari G., Mantovani G. and Sgualdino G.
"Growth Mechanisms of Sucrose form Face by Face Kinetics and Crystal Habit Modifications from Impurities Effect."
"Industrial Crystallization '84" p91-96. Ed. S. J. Jancic and E. J. de Jong. Elsevier, Amsterdam (1984). The Proceedings of the 9th Symposium on Industrial Crystallization 25-28 Sept 1984 The Hague, Netherlands.

Becker R. and Döring W.
"The Kinetic Treatment of Nuclear Formation in Supersaturated Solutions
Ann. Physik. **24** 719-752 (1935) (See Nielsen 1964)

Benema P.
"Theory and Experiment for Crystal Growth from Solution: Implications for Industrial Crystallization"
Proceedings of the 6th Symposium on Industrial Crystallization Ústí nad Labem Czechoslovakia Sept 1-3 1975. In "Industrial Crystallization" p91-112. Ed. J. W. Mullin. Plenum Press, New York (1976).

Bohm J.
"The History of Crystal Growth"
Acta Physika Hungarica **57**(3-4) 161-178 (1985).

Botasris G. D.
"Secondary Nucleation - A Review"
Proceedings of the 6th Symposium on Industrial Crystallization Ústí nad Labem Czechoslovakia Sept 1-3 1975. In "Industrial Crystallization" p3-22. Ed. J. W. Mullin. Plenum Press, New York (1976).

Bourne J. R. and Davey R. J.
"The role of Solvent - Solute Interactions in Determining Crystal Growth Mechanisms form Solution"
J. Crystal Growth **36**(2) 278-286 (1976)

Bourne J. R. and Davey R. J.
"α Factors for Solution Growth with Special Reference to Glyceryl Tristearate"
J. Crystal Growth **43** 224-228 (1978)

Bucherer H.
"Lehrbuch der Farben Chemie" p128. Otto Spainer, Leipzig (1914).

Burton W. K., Cabrera N. and Frank F. C.
"The Growth of Crystals and the Equilibrium Form of their Surfaces"
Phil. Tran. **243A** 299-358 (1951).

Chianese A., Di Cave S and Mazzarotta B.
"Solubility and Metastable Zone Width of Sodium Chloride in Water - Diethylene Glycol Mixtures."
J. Chem. Eng. Data **31** 329-332 (1986a).

Chianese A., Di Cave S. and Mazzarotta B.
"Main Factors Influencing the Crystal Size Distribution from a Batch Cooling Crystallizer"
Cryst. Res. Technol. **21**(1) 31-39 (1986b).

Chivate M. R. and Tavare N. S.
"Design Parameters of Industrial Crystallizers"
Chemical Industry Developments **9**(2) 19-30 (1975)

Christen M. and Zollinger H.
"Bromierung von 2-Naphthol-6,8-disulfosäure. I Kinetik der Reaktionen mit Br_2 und HOBr"
Helv. Chim. Acta. **45 6** (243-244) 2057-2077 (1962).

Cloutz N. A. and McCabe W. L.
"Contact Nucleation of Magnesium Sulphate Heptahydrate"
Chem. Eng. Prog. Symp. Ser. **67** (110) 6-17 (1971).

Daglish C.
"The Ultraviolet Absorption Spectra of some Hydroxynaphthalenes"
J. Am. Chem. Soc. **72** 4859-4864 (1950).

Davey R. J., Fila W. and Garside J.
"The Influence of Biuret on the Growth Kinetics of Urea Crystals from Aqueous Solution"
J. Crystal Growth **79** 607-613 (1986)

Davey R. J. and Richards J.
"Precipitation of a Reactive Dye"
J. Colloid. Int. Sci. **114**(1) 282-285 (1986).

Daglish C.
"The Ultraviolet Absorption Spectra of Some Hydroxynaphthalenes"
J. Am. Chem. Soc. **72** 4859-4864 (1950)

Denk E. G. and Botsaris G. D.
"Fundamental Studies in Secondary Nucleation from Solution"
J. Crystal Growth **13/14** 493-499 (1972).

Donaldson N.
"The Chemistry and Technology of Naphthelene Compounds"
p250-280, Arnold, London (1958).

Dunning W. J.
"Theory of Crystal Nucleation from Liquid"
"Chemistry of the Solid State", Butterworths, London (1955)

Elwenspoek M. Bennema P. and van der Eerden
"Orientational Order in Naphthalene Crystal - Solution Interfaces"
J. Crystal Growth 83 297-305 (1987)

Ephraim F. and Pfister A.
"Über die Salze einiger aromatisher Sulfonsäuren und deren Löslichket"
Helv. Chem. Acta. **8** 229-241 (1925).

Evans T. W. Sarofim A. F. and Margolis G.
"Mechanisms of Secondary Nucleation in Agitated Crystallizers"
A.I.Ch.E.J. **20**(5) 950-958 (1974).

F.I.A.T. (Field Intelligence Agency - Technical)
Final Report N° 1016 "Miscellaneous Dyestuffs Intermediates at I. G. Farben - Industrie AG. Leverkussen." p 3, 19-24. HMSO, London (1947).

Fierz - David H. E. and Blangey L.
"Fundamental Processes of Dye Chemistry". p 192-198 and 387-393. Interscience, New York (1949).

Forrester S. D. and Bain D.
"The Bromopotentiometric Titration of β-naphtholsulphonic acids in the Presence of Each Other. Part I Schaeffer Acid, R-Acid and G-Acid."
J. Soc. Chem. Ind. **49** 410-412 (1930a).

Forrester S. D. and Bain D.
"The Bromopotentiometric Titration of β-naphtholsulphonic acids in the Presence of Each Other. Part II Mixtures Containing Crocein Acid"
J. Soc. Chem. Ind. **49** 423-425 (1930b).

Forster R. B. and Keyworth C. M.
"Arylamine Salts of the Naphtholsulphonic Acids. I The Salts of 2,6- and 2,7-Naphthalenedisulphonic Acids."
J. Soc. Chem. Ind. **43**(22) 165-168 (1924a).

Forster R. B. and Keyworth C. M.
"Arylamine Salts of the Naphtholsulphonic Acids. II The Salts of α- and β-naphthalenedisulphonic Acids."
J. Soc. Chem. Ind. **43**(40) 301-303 (1924b).

Forster R. B. and Keyworth C. M.
"Arylamine Salts of the Naphtholsulphonic Acids. III Separation of Crocein, Schäeffer, R- and G- Acids and their Arylamine Salts."
J. Soc. Chem. Ind. **46**(22) 25T-35T (1927).

Frank F. C.
"The Influence of Dislocations on Crystal Growth"
Discuss. Farraday Soc. **5** 48-54 (1949).

Garner W.
"Micro-identification of some Naphthol, Naphthylamine and Aminonaphthol Sulphonic Acids"
J. Soc. Dyers and Colourists **52** 302-306 (1936)

Garside J.
"Fundamentals of Industrial Crystallization"
"Industrial Crystallization '84". p 1-7. Ed. S. J. Jancic and E. J. de Jong. Elsevier, Amsterdam (1984). The Proceedings of the 9th Symposium on Industrial Crystallization 25-28 Sept 1984 The Hague, Netherlands.

Garside J.
"Industrial Crystallization from Solution"
Chem. Eng. Sci. **40**(1) 3-26 (1985)

Garside J. and Jancic S. J.
"Growth and Dissolution of Potash Alum Crystals in the Subsieve Size Range"
A.I.Ch.E Journal **22**(5) 887-894 (1976)

Garside J. and Larson M. A.
"Direct Observation of Secondary Nuclei Production"
J. Crystal Growth **43** 694-704 (1978)

Garside J. and Ristic R. I.
"Growth Rate Dispersion Among ADP Crystals Formed by Primary Nucleation"
J. Crystal Growth **61** 215-220 (1983).

Garside J., Rusli I. T. and Larson M. A.
"Origin and Size Distribution of Secondary Nuclei"
A.I.Ch.E. J. **25**(1) 57-64 (1979).

Garside J. and Shah M.B.
"Crystallization Kinetics from MSMPR Crystallizers"
Ind. Eng. Chem. Proc. Des. Dev. **19**(4) 509-514 (1980).

Griess P.
"Uber β-Naphtholdisulfosäuren and Dioxynaphthalin disulfosäure"
Brichte der Bunsengessellschaft **13** 1956-1960 (1880).

Hampton E. M., Shah B. S. and Sherwood J. N.
"The growth and Perfection of Orthorhombic (α) Sulphur Single Crystals."
J. Crystal Growth **22**(1) 22-28 (1974).

Hulburt H. M.
"Perspectives on Crystallization in Chemical Process Technology"
A.I.Ch.E. Symp. Ser. **79**(235) 77-89 (1983).

Jackson K. A.
"Mechanism of Growth"
"Liquid metals and Solidification" p243-275 39th National Metals Congress Chicargo (1958)

Jagganathan R., Sung C. Y., Youngquist G. R. and Estrin J.
"Fluid Sheer Secondary Nucleation of Magnesium Sulphate and Potassium Aluminium Sulphate."
A.I.Ch.E. Symp. Ser. **76**(193) 90-96 (1980).

Jancic S. J., van Rosmalen G. M. and Peeters J. P.
"Growth Dispersion in Nearly Monosize Crystal Populations."
"Industrial Crystallization '84" p43-49. Ed. S. J. Jancic and E. J. de Jong. Elsevier Amsterdam (1984). The Proceedings of the 9th Symposium on Industrial Crystallization 25-28 Sept 1984 The Hague, Netherlands.

Janse A. H. and de Jong E. J.
"The Occurrence of Growth Dispersion and its Consequences."
Proceedings of the 6th Symposium on Industrial Crystallization Ústí nad Labem Czechoslovakia Sept 1-3 1975. In "Industrial Crystallization" p145-155. Ed. J. W. Mullin. Plenum Press, New York (1976).

Janse A. H. and de Jong E. J.
"On the Width of the Metastable Zone"
Trans I.Chem.E. **56** 187-193 (1978).

Jones A. G., Budz J. and Mullin J. W.
"Batch Crystallization and Solid - Liquid Separation of Potassium Sulphate."
Chem. Eng. Sci. **42**(4) 619-629 (1987).

Jones A. G. and Mullin J. W.
"Crystallization Kinetics of Potassium Sulphate in a Draft-tube Agitated Vessel."
Trans. I.Chem.E. **51** 302-308 (1973).

Jones A. G. and Mullin J. W.
"Programmed Cooling Crystallizations of Potassium Sulphate Solutions"
Chem. Eng. Sci. **29** 105-118 (1974)

Karpinski P. H., Budz J. and Larson M. A.
"Influence of Cationic Admixtures on the Kinetics of Crystal Growth from Aqueous Solution."
"Industrial Crystallization '84" p85-90. Ed. S. J. Jancic and E. J. de Jong. Elsevier Amsterdam (1984). The Proceedings of the 9th Symposium on Industrial Crystallization 25-28 Sept 1984 The Hague, Netherlands.

Knox J. H. and Laird G. R.
"Soap Chromatography - A New High-Performance Liquid Chromatographic Technique for Separation of Ionisable Materials: Dyestuff Intermediates."
J. Chromatogr. **112** 17-34 (1976).

Koepernik H. and Borsdorf R.
"Dependence of UV-Spectra of Substituted Naphthalene-Sulphonic Acids upon the pH Value - A Contribution in order to Elucidate the Structure of Acid Azo Dyes."
J. Pract. Chem. **326**(5) 823-828 (1984)

Kossel W.
"The Energy of Surface Processes"
Ann. Physik **21** 457-80 (1934)

Kraak J. H. and Huber J. F. K.
"Separation of Acidic Compounds by High Pressure Liquid Chromatography Involving Ion Pair Formation."
J. Chromatogr. **102** 333-351 (1974)

Lahav M., Leiserowitz L., Shimon L. J. W., Weissbuch I., Addadi L. and Berkovitch-Yellin Z.
"Morphology Engineering of Organic Crystals with the Assistance of Tailor-made Growth Inhibitors."
"Northern Branch Meeting". I.Ch.E. Symp. Papers **3** 1.1-1.22, 7.5.85 Manchester (1985).

Lal P. D., Mason R. E. A. and Strictland-Constable R. F.
"Collision Breeding of Crystal Nuclei"
J. Crystal Growth **5** 1-8 (1969)

La Mer V. K.
"Nucleation in Phase Transformations"
Ind. Eng. Chem. **44**(6) 1270-1277 (1952).

Lange N. A.
"Lange's Handbook of Chemistry" 12th Ed. p 7.290-7.291, McGrawhill, New York. (1979).

Larson M. A. and Garside J.
"Solute Clustering and Interfacial Tension."
J. Crystal Growth **76** 88-92 (1986)

Lee K. S. and Yeh T. L.
"Quantitative High - Performance Liquid Chromatographic Analysis of the Commercial Dyestuff G-acid and Gamma acid."
J. Chromatogr. **260** 97-107 (1983).

Lloyd P. J.
"The response of the Coulter Counter to cylinder and disc shaped particles"
p703 2nd European Symposium on Particle Characterisation, Nuremburg 24-26.9.79

Lo H. H.
M.Sc. thesis, Case Institute of Technology (1965) Cited by Walton (1965)

Lowitz J. T.
"Bemerkungen über das Krystallisiren der Salze, und Anzeige eines sicheren Mittels, regelnäßige Krystallen zu erhalten."
Chem. Ann. v.D.L.v. Crell (Crell's Chem. Ann.) Helmstadt **1** 3-11 (1795).
(Cited by Bohm (1985) and Söhnel (1983)).

Mason R. E. A. and Strictland-Constable R. F.
"Breeding of Crystal Nuclei."
Trans. Farraday Soc. **62** 455-461 (1966).

McArdle B. J. and Sherwood J. N.
"The Growing of Organic Crystals"
p179-215 "Advanced Crystal Growth" Ed Dryburgh P. M, Cockayne B. and Barraclough K. G. ISSCG6 Edinburgh 6-11.7.86. Prentice Hall, London (1977)

McCabe W. L. and Stevens R. P.
"Rate of Growth of Crystals in Aqueous Solutions."
Chem. Eng. Prog. **47**(4) 168-174 (1951)

Mohamed-Kheir A. K. M. Tavare N. S. and Garside J
"Development of a Microcomputer Software Package: Batch Cooling Crystallization"
"Industrial Crystallization '87" Proceedings of the 10th Symposium on Industrial Crystallization" Bechyne Czechoslovakia 21-25.9.87 p333-336 ed Nyvlt J and Zacek S., Elsiver, Amsterdam, (1989)

Mohamed-Kheir A. K. M. Tavare N. S. and Garside J
Crystallization Kinetics of Potassium sulphate in a 1 m^3 Batch Cooling Crystallizer"
"Crystallization and Precipitation" p61-70, Proceedings of International Symposium on Crystallization and Precipitation Processes Saskatoon, Saskatchewan, Canada, 5-7.10.87. Pergamon, Oxford, (1988)

Mullin J. W.
"Crystallization"
2^{nd} ed. Butterworths, London, (1972).

Mullin J. W. and Gaska C.
"The Growth and Dissolution of Potassium Sulphate Crystals in a Fluidised Bed Crystallizer."
Can. J. Chem. Eng. **47** 483-489 (1969).

Mullin J. W. and Jancic S. J.
"Interpretation of Metastable Zone Widths."
Trans I. Chem. E. **57** 188-193 (1979).

Mullin J. W. and Nyvlt J.
"Programmed Cooling of Batch Crystallizers"
Chem. Eng. Sci. **26** 369-377 (1971).

Nes J. N. and White E. T.
"Collision Nucleation in an Agitated Crystallizer"
A.I.Ch.E. Symp Ser **72** *N°* **153** 64-73 (1976).

Nielsen A. E.
"Kinetics of Precipitation"
Pergamon Press, Oxford, (1964).

Nielsen A. E.
"Nucleation in Aqueous solution"
J. Phys. Chem. Solids Supplement **1** 419-426 (1967)

Noyes A. A. and Whitney W. R.
"Über die Auflösungsgeschwindigkeiten von festen Stoffen in ihren eigenen Lösungen."
Z. Phys. Chem. (Leipzig) **23** 689-692 (1897) (See Bohm 1985)

Nyvlt J.
"Kinetics of Nucleation in Solution"
J. Crystal Growth **3/4** 377-383 (1968).

Nyvlt J.
"Evaluation of Experimental Data on the Width of Metastable Zone in Aqueous Solution."
Collect. Czech. Chem. Commun. **37** 3155-3165 (1972).

Pawle B. G., Chivate M. R. and Tavare N. S.
"Growth Kinetics of Ammonium Nitrate Crystals in a Draft Tube Baffled Agitated Batch Crystallizer."
Ind. Eng. Chem. Process Des. Dev. **24** 914-919 (1985).

Prandi C. and Venturini T.
"Retention Behaviour of Aromatic Sulphonic Acids in Ion-Pair Reversed Phase Column Liquid Chromatography"
J. Chromatog. Sci. **19**(6) 308-314 (1981).

Price C. J.
"Characterisation of Hydroxynaphthalene Sulphonic Acids."
M.Sc. thesis, Chemical Engineering Department, UMIST, Manchester. (1985)

Price C. J. and Hazell M.
"Measurement of the Crystallization Kinetics of Industrial Grade Copper Sulphate Pentahydrate"
SPS 1987 Symposium Proceedings, p72-84, 8-10.9.'87, Oxford, Separation Processes Service, Harwell (1987)

Prostakov S. M., Driker B. N. and Rempel S. I.
"Determination of the Nucleation Parameters of Calcium Sulfate by Various Methods."
J. App. Chem. USSR **55** 2333-2337 (1982).

Randolph A. D. and Larson M. A.
"Theory of Particulate Processes"
Academic Press, New York, (1971).

Rodriguez-Hornedo N. and Carstensen J. T.
"Crystallization Kinetics of Oxalic Acid Dihydrate: Nonisothermal Desupersaturation of Solutions."
J. Pharm. Sci. **75**(6) 552-558 (1986).

Rossinelli L., Thies H. and Richarz W.
"High performance Liquid Chromatographic Determination of Naphtholsulphonic Acids."
Chimia **33**(12) 451-452 (1979).

Rusli I., Larson M. A. and Garside J.
"Initial Growth of Secondary Nuclei Produced by Contact Nucleation."
A.I.Ch.E. Symp. Ser. **76** *N°* **193** 52-58 (1980).

Shah B. C., McCabe W. L. and Rousseau R. W.
"Polyethylene vs Stainless Steel Impellers for Crystallization Processes."
A.I.Ch.E.J. **19**(1) 194 (1973).

Smith C.
"Stearic Hindrance in the Naphthalene Series."
J. Chem. Soc. **89**(2) 1505-1512 (1906).

Smith-Harland J., Forrester S. D. and Bain D.
"The Bromopotentiometric Titration of β-Naphtholsulphonic Acids in the Presence of each other. Part III Mixtures Containing Oxy-Tobias Acid, F-acid and Trisulpho-acid."
J. Soc. Chem. Ind. **50** 100-112 (1931).

Söhnel O.
"Metastable Zone of Solutions."
Chem. Eng. Res. Des. **61** 186-190 (1983).

Söhnel O. and Mullin J. W.
"Expressions of Supersaturation for Systems Containing Hydrates, Partially Dissociated Electrolytes and Mixtures of Electrolytes."
Chem. Eng. Sci. **33**(11) 1535-1538 (1978)

Söhnel O. and Nyvlt J.
"Evaluation of Experimental Data on Width of Metastable Region in Aqueous Solutions."
Collect. Czech. Chem. Commun. **40** 511-518 (1975).

Strictland-Contable R. F.
"Method for Production and Growth Inhibition of Collision Crystallites."
J. Chem. Soc. Farraday Trans 1 **75** 921-924 (1979).

Tai C. Y. and Pan R. K.
"Growth Kinetics of Copper Sulphate Pentahydrate Crystals in Pure and Impure Systems."
J. Chin. I. Ch. E. **16**(4) 379-387 (1985).

Tavare N. S.
"Batch Crystallizers: A Review."
Chem. Eng. Commun. **61**(1-6) 259-318 (1987).

Tavare N. S. and Garside J.
"Simultaneous Estimation of Crystal Nucleation and Growth Kinetics from Batch Experiments"
Chem. Eng. Res. Des. **64**(3) 109-118 (1986a)

Tavare N. S. and Garside J.
"Recent progress in Solids Processing: Recent Advances in Industrial Crystallization Research."
Chem. Eng. Res. Des. **64**(3) 77-79 (1986b).

Tengler T. and Mersmann A.
"Influence of Temperature, Supersaturation and Flow Velocity of Solution on Crystal Growth from Solution."
Ger. Chem. Eng. **7** 248-259 (1984).

Thorpe J. F.
"Dictionary of Applied Chemistry" Vol IV p476-483.
Longmans Green and Co., London, (1922).

Timm D. C. and Larson M. A.
"Effect of Nucleation Kinetics on the Dynamic Behaviour of a Continuous Crystallizer."
A.I.Ch.E.J. **14**(3) 452-457 (1968).

Turnball D.
"The Kinetics of Precipitation of Barium Sulphate from Aqueous Solution."
Acta. Metallurgica. **1** 684-691 (1953)

van der Erden J. P. Bennema P. and Cherepanova T. A.
"Survey of Monte Carlo Simulations of Crystal Surfaces and Crystal Growth"
Prog. Crystal Growth Characterisation **1**(3) 219-254 (1978)

Volmer M. and Webber A.
"Nucleus formation in supersaturated systems"
Z. Physik. Chim. **119** 277-301 (1926) (see Nielsen 1964)

Volmer M.
"Kinetik der Phasenbildung"
Steinkopff, Leipzig (1939) (see Hulbert 1983 and Nyvlt 1968)

Vorontsov I. I.
"Hydrolysis of 2-naphthol-6,8-disulphonic acid in the process of sulphonation of 2-naphthol."
J. App. Chem. (USSR) **24** 367-371 (1951). (*Chem. Abs.* **46** 2531h).

Wakao H. Hiraguchi H. and Ishii T.
"A Simulation of Crystallization from Aqueous Supersaturated Solutions in a Batch Isothermal Stirred Tank"
Chem. Eng. J. **35**(3) 169-178 (1987)

Walton A. G.
"Nucleation of Crystals form Solution"
Science **145** 601-607 (1965)

Walton A. G.
in "Nucleation"
p243 Ed. A. C. Zettelmoyer, Dekker, New York (1969).

White E. T. and Wright P. G.
"Magnitude of Size Distribution Effects in Crystallization."
A.I.Ch.E. Chem. Eng. Prog. Symp. Ser. **67** *N°* 110 81-87 (1971).

Whitmore W. F. and Gebhart A. I.
"Microscopic Identification of Some Important Substituted Naphthalenesulphonic Acids."
Ind. Eng. Chem. **10**(11) 654-661 (1938).

Willard H. H., Meritt L. L., Dean J. A. and Settle F. A.
"Instrumental Methods of Analysis"
6th Ed. Wadsworth Publishing Co., Belmont, California, (1981).

Wojciechowski K. and Kibalczyc W.
"Light Scattering Study of KH_2PO_4 and $BaSO_4$ Nucleation Processes."
J. Crystal Growth **76** 379-382 (1986).

Zumstein R. C. and Rousseau R. W.
"Growth rate Dispersion in the Crystallization of Copper Sulphate Pentahydrate."
Paper presented at the 1986 Spring National Meeting of the A.I.Ch.E, New Orleans, April (1986).

Zumstein R. C. and Rousseau R. W.
"Growth Rate Dispersion by Initial Growth Rate Distributions and Growth Rate Fluctuations."
A.I.Ch.E J. **33**(1) 121-129 (1987).